Ocean and land climate dynamics off southeast Africa during the late Pleistocene:

A multi-proxy approach

Margit Hildegard Simon

Thesis submitted for the Degree of Doctor of Philosophy
Cardiff University
May 2014

GATEWAYS
Initial Training Network

MARIE CURIE ACTIONS

CARDIFF UNIVERSITY
PRIFYSGOL CAERDYDD

DECLARATION

This work has not been submitted in substance for any other degree or award at this or any other university or place of learning, nor is being submitted concurrently in candidature for any degree or other award.

Signed …… (candidate) Date ……

STATEMENT 1

This thesis is being submitted in partial fulfillment of the requirements for the degree of …… PhD ……(insert MCh, MD, MPhil, PhD etc, as appropriate)

Signed …… (candidate) Date ……

STATEMENT 2

This thesis is the result of my own independent work/investigation, except where otherwise stated.
Other sources are acknowledged by explicit references. The views expressed are my own.

Signed …… (candidate) Date ……

STATEMENT 3

I hereby give consent for my thesis, if accepted, to be available for photocopying and for inter-library loan, and for the title and summary to be made available to outside organisations.

Signed …… (candidate) Date ……

STATEMENT 4: PREVIOUSLY APPROVED BAR ON ACCESS

I hereby give consent for my thesis, if accepted, to be available for photocopying and for inter-library loans **after expiry of a bar on access previously approved by the Academic Standards & Quality Committee.**

Signed …… (candidate) Date ……

Summary

The Agulhas Current transport of heat and salt from the Indian Ocean into the South Atlantic around South Africa (Agulhas leakage), can affect the Atlantic Meridional Overturning Circulation (AMOC) and, thus, influence global climate.

Upper water column reconstructions in the southwest Indian Ocean over the past 100 kyr based on marine sediments from the core region of the Agulhas Current suggest that surface ocean temperature, salinity and planktonic foraminiferal assemblage records from the Agulhas Current exhibit high variability on orbital to millennial timescales. A high degree of similarity in this variability could also be identified in the Agulhas leakage records in the South Atlantic which suggests that changes in the Agulhas leakage can be partly explained by upstream variability in the Current itself.

The results of a benthic stable isotope record from the southwest Indian Ocean over the past 270 kyr gives evidence that during glacial periods as well as during Northern Hemisphere Cold Stadials Southern Component Waters substituted for North Atlantic Deep Waters. The recorded hydrographic variability in the deep southwest Indian Ocean is explained in terms of a less vigorous AMOC exporting a reduced amount of NADW into the Southern Hemisphere and/or at shallower depth causing the observed changes in the deep water inventory.

A multiproxy data and model integration approach reveals that phases of more humid southeast Africa climate were driven by southward oscillations of the Intertropical Convergence Zone and its associated rain belt over the past two glacial-interglacial cycles. Low-latitude summer insolation changes paced by orbital precession explain the long-term climate variability whereas abrupt climate oscillations in the northern high latitudes are the main driver for the observed millennial-scale wet phases. Southeast African climate variability seems to have been coupled, and anti-phased, with the East Asian Summer Monsoon during the late Pleistocene. Agulhas Current sea surface temperatures changes did not exert a primary control on southeast African hydrology.

Author's Note

Chapter 3 of this thesis has been published as:

Simon, M.H, Arthur, K.L, Hall, I.R, Peeters, F.J.C, Benjamin R. Loveday, Barker, S., Ziegler, M., Zahn, R., (2013): Millennial-scale Agulhas Current variability and its implications for salt-leakage through the Indian–Atlantic Ocean Gateway. *Earth and Planetary Science Letters* 383, 101-112, doi: 10.1016/j.epsl.2013.09.035 (2013).

Chapter 4 of this thesis is in preparation as:

Simon, M.H, Hall, I.R., Ziegler, M., Barker, S., Jonkers, L., : Deep water variability off southeast Africa during the past 270 kyr. *To be submitted to Paleoceanography*

Chapter 5 and 6 build upon collaborative work published as**:**

Ziegler, M., **Simon, M.H**., Hall, I.R, Barker, S., Stringer, C., Zahn, R., (2013): Development of Middle Stone Age innovation linked to rapid climate change. *Nature communication* 4, 1905, doi:10.1038/ncomms2897.

and the following are in preparation as follow up publications:

Simon, M.H, Purcell, C., Hall, I.R., Ziegler, M., Barker, S., Knorr, G., Jonkers, L., van der Meer, M. T. J., Kasper, S., Schouten, S.: Salinity changes in the southern Agulhas Current since the Last Glacial Maximum. *To be submitted to Quaternary Science reviews*

Simon, M.H, Ziegler, M., Hall, I.R., Barker, S.,: A 270 kyr-long record of southeast African climate variability in the context of a global-palaeo-monsoon. *To be submitted to Nature Geosciences*

"Science never solves a problem without creating ten more"
George Bernard Shaw

I could not think of a better quote to start my acknowledgements than with the one above to summarise the experience of my PhD during the last 4 years. In June 2010 I came to Cardiff and joined the Palaeoclimate Research Group as an Early Stage researcher within the Gateways project.

I would like to thank Ian Hall, my main PhD supervisor, for giving me the opportunity to do this study and become part of the Cardiff Research Group moreover to be part of the Gateways project. He has been a great mentor and supported me scientifically as well as personally during the last 4 years. Someone I can't thank enough is Martin Ziegler for all his guidance and support during our past and on-going collaboration. He has been fuelling my scientific motivation, enthusiasm and overall inspiring me with his work. I am grateful that Stephen Barker, my co-supervisor, was part of this journey as well because he always added another point of view to the topic which made me see things from a different angle. It has been really inspirational to work with him.

I thank everyone from the Palaeoclimate Group in Cardiff for providing such a great and friendly working environment.

Being part of the Gateways project was such an amazing experience and I am grateful. Especially I want to mention the other Gateways PhDs and post docs: Conor, Kristina, Emma, Ben, Jonathan, Paolo, Sebastian, Marlen, Juliane, Kerstin, Kristin, Jeroen, Martin, Lukas, Caroline who I have been sharing some fun times during workshops, summer schools, meetings, conferences and road trips together.

There are many special people who have been an important part of my life and inspired me scientifically and socially and I am grateful:

Special thanks go to Paola Moffa Sánchez and Anabel Morte Rodenas for not only all of their scientific and technical help but also for always being so caring and supportive.

My PhD fun office: Milly, Jamie, Scott, Sam, Elaine, Rachel, Miros, Kim and Steph. My lunch group: Xun, Eleanor, Kirsty, Lukas, Paola, Steve, David, Jenny, Sindia, Carrie. My football team "Rock Solid" and coaches: Scott, Jack, Toby, Milly, Tracy, Jules, Eleanor, Kim, Miriam, Rebekah, Anabel, Paola, Kirsty, Anna, Sindia and Bethan.

My family – overall my parents; my siblings: Uwe, Jana; my nieces and nephews: Robert, Luise, Lotte, Levin, Leni and friends of course: Linda, Lotte, Giulia, Lisa, Ihlem, Rosa, Sri, Dee, Heather, Andrea, Claire W., Hannah, Claire M., Barbara, Aldina, Martino, Katia, who always supported me and believed that I can do that.

Commonly used symbols and Abbreviations

AABW	Antarctic Bottom Water
AAIW	Antarctic Intermediate Water
ABR	Agulhas Bank Record
ABS	Agulhas Bank Splice Record
ACC	Antarctic Circumpolar Current
ALF	Agulhas Leakage Fauna
AMOC	Atlantic Meridional Overturning Circulation
ARC	Agulhas Return Current
ASM	Agulhas Salt-leakage Maxima
ASMD	Asian Monsoon Domain
AUC	Agulhas Undercurrent
B/A	Bølling-Allerød Interstadial
BIT	Branched Isoprenoid Tetraether Index
CAB	Congolian Air Boundary
CBR	Cape Basin Record
CDW	Circumpolar Deep Water
CWR	Cold Water Route
D/O	Dansgaard-Oeschger Oscillation
DIC	Dissolved Inorganic Carbon
EASM	East Asian Summer Monsoon
EKE	Eddy Kinetic Energy
EMC	East Madagascar Current
EPICA	European Project for Ice Coring in Antarctica
GCM	General Circulation Model
GDGT	Glycerol Dialkyl Glycerol Tetraether
G-I	Glacial-interglacial
GM	Global Monsoon
GNAIW	Glacial North Atlantic Intermediate Water
GPM	Global-Palaeo-Monsoon
HS	Heinrich Stadial
HTM	Holocene Thermal Maximum
IAOG	Indian-Atlantic Ocean Gateway
IRD	Ice-rafted detritus
ISM	Indian Summer Monsoon
ITCZ	Intertropical Convergence Zone
ka:	Thousand years before present , (kilo annum)
kyr:	Thousand years (duration)
LCDW	Lower Circumpolar Deep Water
LGM	Last Glacial Maximum
LSCW	Lower Southern Component Water
Ma	Million years before present (age), datum
MIS	Marine Isotope Stage

MKE	Mean Kinetic Energy
MOC	Meridional Overturning Circulation
Myr:	Million Years (duration)
NADW	North Atlantic Deep Water
NCW	Northern Component Waters
NHCS	Northern Hemisphere Cold Stadials
NIDW	North Indian Deep Water
OM	Organic matter
PCA	Principal Component Analysis
PF	Polar Front
RSIW	Red Sea Intermediate Water
SAF	Subantartic Front
SAO	South Atlantic Ocean
SASM	South American Summer Monsoon
SCW	Southern Component Waters
SIO	South Indian Ocean
SLP	Surface Level Pressure
SSS	Sea Surface Salinity
SST	Sea Surface Temperature
STF	Subtropical Front
STIOG	Subtropical Indian Ocean gyre
Sverdrup	1 Sv = 1 x 10^6 m^3/s
SWIOSG	Southwest Indian Ocean Sub-gyre
THC	Thermohaline Circulation
TI, TII, …	Termination I, Termination II, etc….
UCDW	Upper Circumpolar Deep Water
USCW	Upper Southern Component Water
VPDB	Vienna Pee Dee Belemnite
WBUC	Western Boundary Undercurrent
WWR	Warm Water Route
XRF	X-ray Fluorescence
YD	Younger Dryas
$\delta^{18}O_{sw}$	$\delta^{18}O$ of Ambient Seawater
δD	Stable Hydrogen Isotope

Contents

Data tables, PDF copy of the thesis as well as author's publications are enclosed as CD at the back of this thesis.

1. Introduction

Increased public and scientific attention has been placed on the understanding of the global climate system, specifically its characteristics, functioning and natural variability. That awareness is arising from the current climate situation, with temperatures likely rising as a consequence of human-induced increase in greenhouse gas concentrations in the atmosphere. The Southern Hemisphere has traditionally been considered as a passive player in the oceanic and climate changes while (palea)oceanographic research and numerical model simulations increasingly are emphasising that it plays an important role, both in global circulation changes and in defining the state of Earth´s climate.

A key region for the global circulation system is found around the southern tip of Africa. There, Indian Ocean surface and thermocline waters are transferred to the South Atlantic by rings and filaments of the strongest western boundary current in the Southern Hemisphere, the Agulhas Current. At depth, the water transfer occurs in the opposite direction, with North Atlantic Deep Water (NADW) leaving the Atlantic Basin entering the Indian. The input of warm, saline Agulhas waters to the South Atlantic is thought to influence the buoyancy of the far distant North Atlantic and be crucial for the mode and stability of the Atlantic Meridional Overturning Circulation (AMOC).

1.1. Late Pleistocene climate variability

Cyclic variations in insolation, caused by the precession and obliquity of Earth's spin axis and variations in the eccentricity of Earth's orbit, have been widely acknowledged as a key driver of Quaternary climate variability since Hays et al. (1976). These orbital changes do not affect the amount of solar energy that reaches the planet but cause differences in the distribution of the incoming energy, which in turn affects the insolation received at a particular location and in a particular season. The Milankovitch theory (Milanković, 1941) describes the collective effects of changes in the Earth's movements upon its climate, named after Serbian geophysicist and astronomer Milutin Milanković. He unravelled the cyclicity of change in the three parameters that characterise the Earth’s orbit around the sun outlined above.

Shackleton and Opdyke (1976) published the stable oxygen isotope and palaeomagnetic records of sediment core V28-179 from the Equatorial Pacific showing variations in the Northern Hemisphere ice volume over the past 870 kyr. They showed that glacial to interglacial cycles, previously identified in ice cores from Antarctica (Johnsen et al., 1972) and other ocean cores were present in marine cores throughout the World's ocean (Broecker et al., 1968; Broecker and van Donk, 1970), not just those close to ice sheets, and could be extended back through 22 glacial and interglacial stages.

Eccentricity is the term used to describe variations in the shape of the Earth's orbit around the sun, which ranges from the high (elliptic) to low (more circular) and affects the distance of the earth relative to the sun (Fig. 1. 1), (Denton and Hughes, 1983). Variations between high and low eccentricity is about 6% resulting in only small effects on insolation which is integrated over all latitudes (Berger, 1989). Eccentricity does play an important role in modulating the amplitude of the precessional cycle (see below). Eccentricity is the longest of the orbital cycles of Milankovitch Theory and was originally calculated to be ~100 kyr (95.8 kyr), although Hays et al. (1976) were the first to suggest that this 100-kyr cycle, present in many palaeo data sets, may be a non-linear climate response to a far longer cycle of eccentricity thought to be ~400 kyr (Rial, 1999).

Obliquity acts over a 41-kyr cycle as the angle of the Earth's rotational axis varies between 21.8 and 24.4 degrees (Fig. 1. 1), (Denton and Hughes, 1983). The angle of tilt affects the incoming radiation on Earth's surface greatest at high latitudes, with less radiation at the poles during periods of low tilt and high levels of solar radiation at high tilt (Ruddiman and McIntyre, 1981). In effect the obliquity cycle controls the strength of the seasons, with amplifications and a greater difference in seasonality occurring during periods of high tilt. Changes in obliquity have little effect at low latitudes, since the strength of the effect decreases towards the equator. Consequently, variations in the Earth's axial tilt affect the strength of the latitudinal temperature gradient. Increased tilt has the effect of raising the annual receipt of solar energy at high latitudes, with a consequent reduction in the latitudinal temperature gradient.

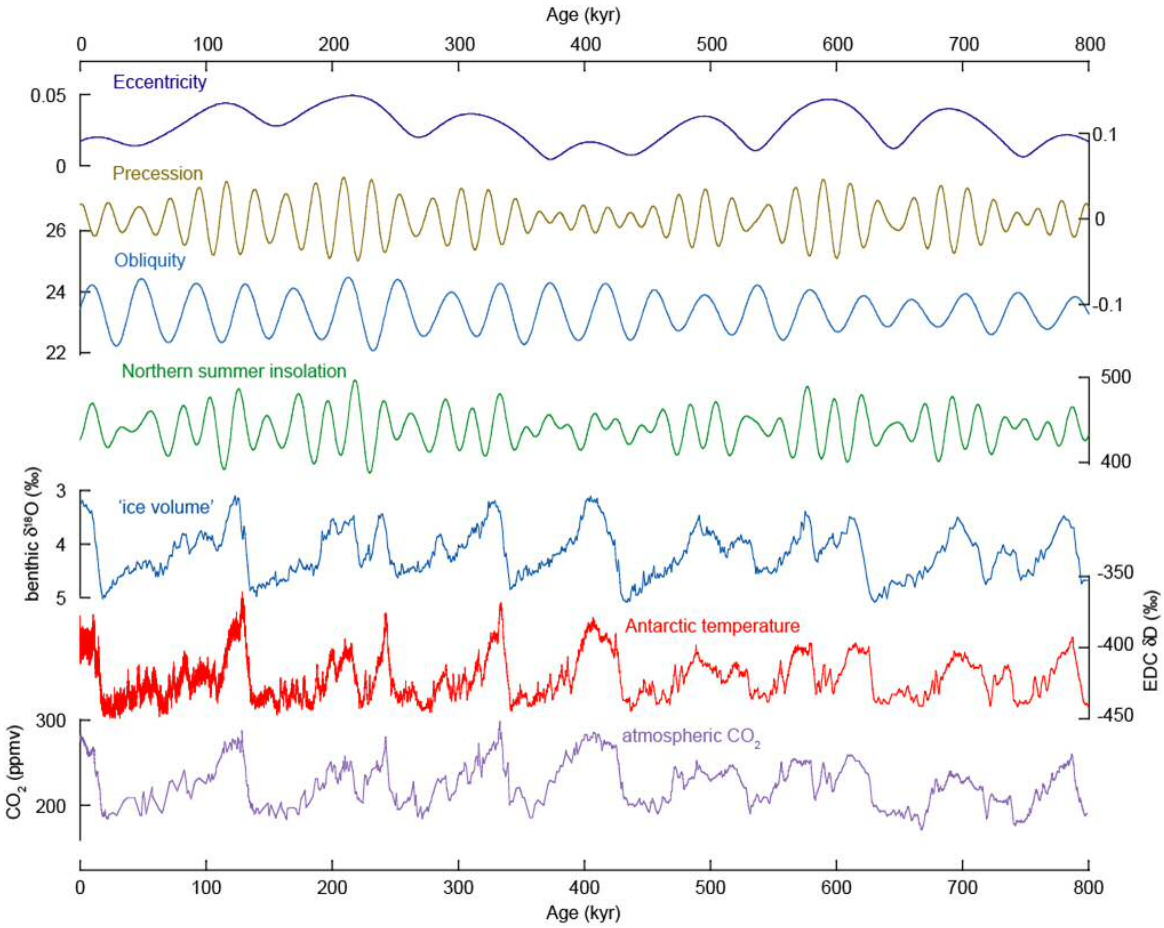

Fig. 1. 1 Late Pleistocene climate variability (Stephen Barker pers. comm). The parameters of the Earth's orbit around the sun, depicted in their temporal evolution for the last 800 kyr. Eccentricity (purple) quantifies the deviation of the orbit from a circle. Precession (brown) parameter indicates the orientation of the rotational axis with respect to the firmament. Obliquity angle (blue) reflects the tilt of the earth's rotational axis with respect to the orbital plane(Berger, 1991). The combination of all of these orbital parameters appear to influence the variations in the Northern Hemisphere summer insolation (green) resulting in the glacial-interglacial cycles, exemplified by ice-volume changes (blue), (Lisiecki and Raymo, 2005); the temperature variation reconstructed from Antarctic ice cores (red); (Jouzel et al., 2007) and atmospheric CO_2 (purple), (Luthi et al., 2008).

Precession is the change in orientation of the Earth's axis of rotation (Fig. 1. 1), referring specifically to the precession of the equinoxes, the position of the solstices and equinoxes in relation to the aphelion (point in the Earth's orbit farthest from the sun) and perihelion (point in the Earth's orbit closets to the sun) (Hays et al., 1976). Precession occurs as a result of the gravitational effects of the sun and moon (and to a lesser extent the other planets) on the Earth's equatorial bulge. Two periodicities are produced by this: the 23-kyr and 19-kyr cycle, which control the direction the Earth spin axis within space at the aphelion or perihelion and which season occurs at both the aphelion and perihelion (Berger, 1977). This acts to dampen or amplify the seasonal climate variability as it effects the distribution of insolation with stronger seasonality in one hemisphere coinciding with

weaker seasonality in the opposite hemisphere (Imbrie, 1985; Berger, 1992). Eccentricity modulates precession by changing the shape of the Earth's orbit and that controls how effective precession is in modulating the seasons by controlling how close to the sun the perihelion is (Milankovitch, 1930; Berger, 1977). As eccentricity moves towards a value of 0 (circular) the effect of precession is reduced. The 23-kyr cycle is produced by a combination of the 27-kyr (axis of rotation of the tilt) and 105-kyr (precession of the Earth's orbit) cycles, whilst the 19- kyr cycle is a combination of the 27-kyr (axis of rotation of the tilt) and the 96-kyr (eccentricity) cycles (Berger, 1977).

Climate during the early Pleistocene varied with a main period of 41-kyr and was related to variations in Earth's obliquity (Lisiecki and Raymo, 2005). About 900 kyr ago, variability increased and oscillated primarily at a period of 100-kyr, the so-called mid-Pleistocene Transition, suggesting a stronger link with the eccentricity of Earth's orbit. The underlying mechanism for this transition remains disputed but has been attributed to a nonlinear response to small changes in external boundary conditions (Crowley and Hyde, 2008). Across glacial to interglacial cycles ice core records show that, air temperature and CO_2 closely followed each other over the last 850,000 years (Fig. 1. 1), (EPICA, 2004). The Milankovtich Cycles are the trigger of glacial-interglacial variations however the classic "sawtooth" structure of glacial cycles (Broecker and van Donk, 1970) is punctuated by rapid increases in sea level, temperature, and CO_2 that require a nonlinear response of the ocean-atmosphere system to solar forcing (Fig. 1. 1).

Additional feedbacks such as from greenhouse gas concentrations, the ice albedo effect but also changes in vertical ocean circulation and productivity are required to supplement or better amplify the rather small changes in orbital forcing (Clark et al., 2009). While CO_2 does not seem to initiate deglaciations (Caillon et al., 2003), its role as a greenhouse gas is one of the most important amplifiers to temperature change during these climate transitions. Increased CO_2 and CH_4 (another greenhouse gas) levels in the atmospheric increase the greenhouse effect and both are inked with changes in climate (Bender et al., 1997). It is widely accepted that CO_2 concentrations are linked to the exchange between the surface ocean and the atmosphere, with 99% of the CO_2 in the ocean/atmosphere system residing in the ocean (Raven and Falkowski, 1999). The modern ocean absorbs about half of the anthropogenic CO_2 (Sabine et al., 2004). Biosequestration or carbon sequestration through biological processes affects the global carbon cycle. By this

mechanism carbon (in the form of CO_2) is sequestered from the atmosphere and moved to the deep water layers, mostly in the form of $CaCO_3$ (Falkowski et al., 2000). Part of that amount is incorporated in the sediments deposited at the ocean's floor, and part remains available to re-enter the carbon cycle, and the atmospheric circulation, under modified oceanographic circumstances (Anderson and Carr, 2010).

Potentially even more important for climate is the high heat capacity of water, compared to other components of the Earth's surface, such as land and the atmosphere. Due to its size (71% of the Earth's surface) large amounts of heat are stored in the ocean. Therefore the ocean acts as an efficient thermal regulator through its ability to redistribute heat from one latitude to another before it is released to the atmosphere or radiated back into space (Clark et al., 2002; Rahmstorf, 2002). The global distribution of oceanic water masses is partly driven by this high heat capacity superficially or in the deep. In particular, the circulation in the Atlantic- the AMOC is a sensitive component of the climate system. AMOC changes seem to play an instrumental role in the mechanism of glacial termination (Barker et al., 2009; Barker et al., 2010; Barker et al., 2011).

1.1.1. Global overturning circulation system

Changes in the ocean thermohaline circulation (THC) have been frequently proposed as one of the most important climatic amplifiers of the external forcings during the Pleistocene as the oceans play a major role in both global and regional aspects of the climate system (e.g., Rahmstorf, 2002). Ocean circulation is driven by a combination of processes comprising wind forcing, density gradients and internal mixing of the oceans by tides (Rahmstorf, 2002). Cold dense waters sink in Polar Regions while warmer less dense waters upwell in equatorial zones and along the Antarctic Circumpolar Current (ACC). While the ocean surface layer is largely driven by atmospheric wind stresses, the THC refers to that part of the ocean circulation which is driven by heat and freshwater fluxes across the surface, and the subsequent interior mixing of heat and salt (Rahmstorf, 1996). A consequence of this combined sinking‑upwelling ocean system is the Meridional Overturning Circulation (MOC), a large-scale slow overturning motion of the ocean. This overturning is characterised by wind driven flow in the near-surface Ekman layer and the density driven thermohaline flow below. This system of global distribution of heat and

water mass is often colloquially referred to as the 'Global Conveyor Belt' (Fig. 1. 2), (Broecker, 1991).

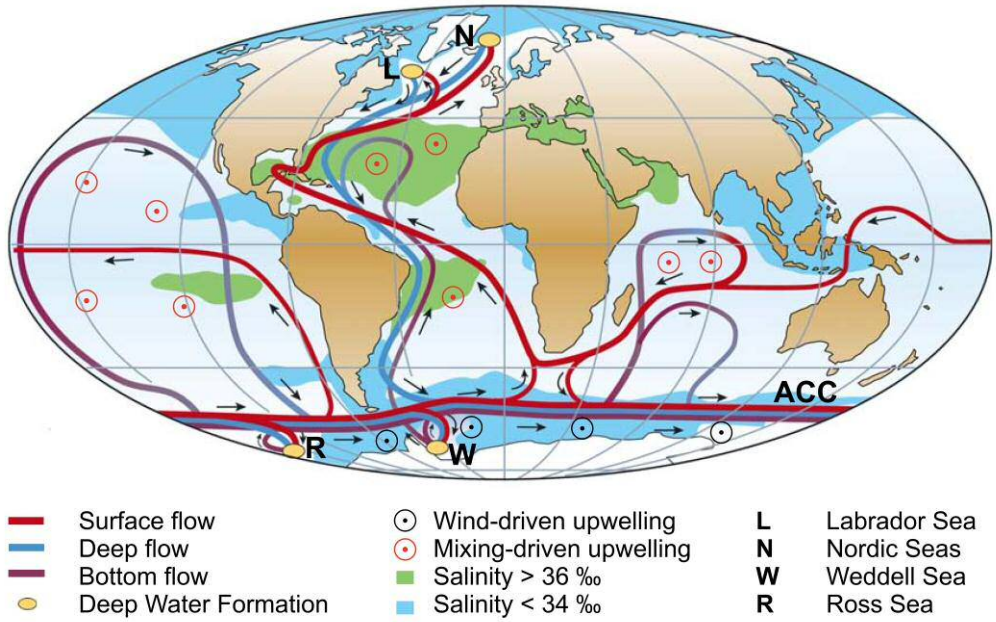

Fig. 1. 2 Strongly simplified sketch of the global overturning circulation system from Rahmstorf (2002). In the Atlantic, warm and saline waters flow northward all the way from the Southern Ocean into the Labrador and Nordic Seas. By contrast, there is no deep water formation in the North Pacific, and its surface waters are fresher. Deep waters formed in the Southern Ocean become denser and thus spread in deeper levels than those from the North Atlantic. Note the small, localized deep water formation areas in comparison with the widespread zones of mixing-driven upwelling. Wind-driven upwelling occurs along the Antarctic Circumpolar Current (ACC).

There are four major areas of deep water formation. In the Northern Hemisphere North Atlantic Deep Water (NADW) formation occurs in the Nordic and Labrador Seas (Fig. 1.2). In the Southern Hemisphere Antarctic Bottom Water (AABW) forms around Antarctica in the Ross and Weddell Seas. Estimates for the rate of the NADW production range between 15 ± 2 Sv (1 Sv = 1 x 10^6 m^3/s) (Ganachaud and Wunsch, 2000) and 18 ±-5 Sv (Talley et al., 2003). AABW production rate has been approximated at 21 ± 6 Sv (Ganachaud and Wunsch, 2000). NADW descends to depths of 2‑3 km where it flows equatorwards via the Deep Western Boundary Current (DWBC) and then polewards in the Southern Hemisphere where it meets the ACC, which acts to distribute NADW water throughout the Indian and Pacific Oceans. Due to its low temperature and high density, AABW descends to greater abyssal depths, where it spreads northwards into the Atlantic basin, over the ocean floors beneath southward flowing NADW. This ventilation of the world's oceans is compensated for by upwelling of deep waters in the Indian and Pacific Oceans as a consequence of

equatorial warming and wind driven uplift around the ACC (Rahmstorf, 2002). These upwelled waters develop into surface currents, which act to bring warm water back into the Atlantic and close the circulation loop (Fig. 1. 2).

The AMOC defines the basin-wide circulation process in the meridional-vertical plane in the Atlantic Ocean (Kuhlbrodt et al., 2007). Two overturning cells stretched out over the entire Atlantic on both Hemispheres to form this circulation system, a deep one with NADW and an abyssal one with AABW (Fig. 1. 3).

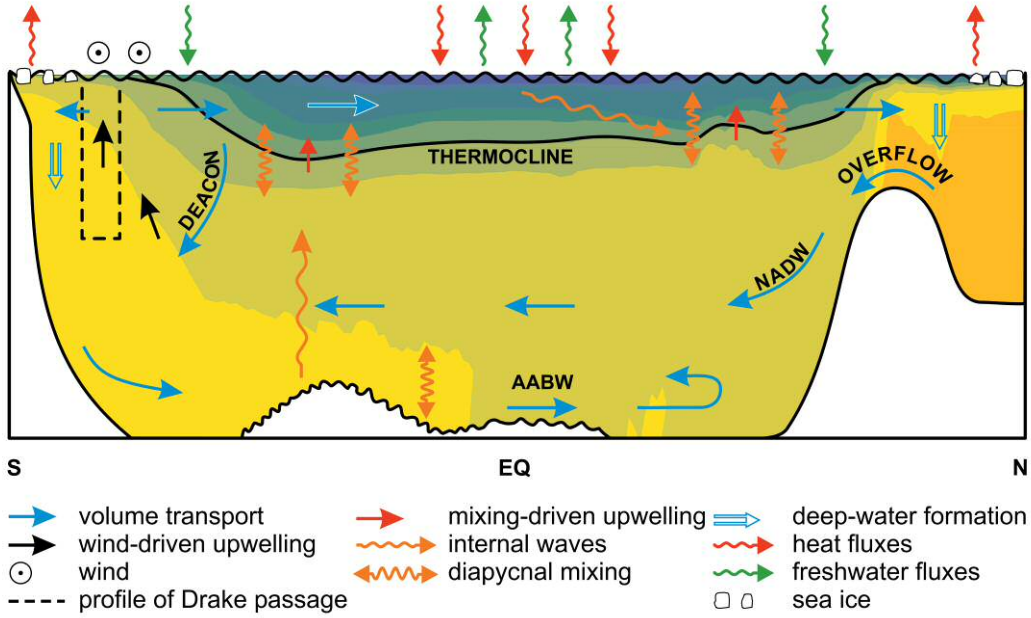

Fig. 1. 3 Idealised meridional section representing a zonally averaged picture of the Atlantic Ocean from Kuhlbrodt et al. (2007). Straight arrows sketch the MOC. Deepwater formation (DWF) occurs in the high northern and southern latitudes, creating North Atlantic Deep Water (NADW) and Antarctic Bottom Water (AABW), respectively. The locations of DWF are tightly linked with the distribution of surface fluxes of heat and fresh water; since these influence the buoyancy of the water, they are subsumed as buoyancy fluxes. The freshly formed NADW has to flow over the shallow sill between Greenland, Iceland, and Scotland. Close to the zone of wind-driven upwelling in the Southern Ocean is the Deacon cell recirculation, visible in the zonally integrated meridional velocity in ocean models.

Four distinct branches determine the processes in these two cells: upwelling processes that transport volume from depth to near the ocean surface, surface currents that transport relatively light water toward high latitudes, deep water formation regions where waters become denser and sink, and deep currents closing the loop (Fig. 1. 3), (Kuhlbrodt et al., 2007). Changes in the strength and structure of the AMOC play a critical role in the Earth's climate variability through the distribution of heat, nutrients and gasses (Rahmstorf, 2002). Therefore, there is a large interest on the direct monitoring and

estimation of the variability of the AMOC strength. Direct transport estimates for AMOC strength are difficult to reconstruct for past climates and equally challenging in the modern because estimates are sparse and difficult to obtain as they show large interannual and decadal variability. However, AMOC strength has been estimated with a mean and standard deviation of ~18.4 ±5 Sv (Bryden et al., 2005b; Cunningham et al., 2007).

1.1.2. Abrupt climate variability during the late Pleistocene

Abrupt sub-orbital millennial timescale climate shifts characterised by "saw-toothed" shaped transitions between cold (stadial) and warm (interstadial) periods were first recognised in Greenland ice cores (Dansgaard et al., 1993; NGRIP, 2004) and became known as Dansgaard-Oeschger oscillations (D/O), (Fig. 1. 4). There are twenty-five of these distinct warming-cooling oscillations during the last glacial cycle with shifts from cold stadials to the warm interstadial intervals occurring in a matter of decades, with air temperatures over Greenland rapidly warming 8 to 15 °C (Huber et al., 2006). They have a cyclicity of 1470 ± 532 years (Bond et al., 1997). Additionally some of the D/O events were associated with increased meltwater and ice-rafted detritus (IRD) influx into the North Atlantic originating from the Iceland and East Greenland ice sheets, apparently associated with D/O cooling (Bond et al., 1993; Bond and Lotti, 1995). These episodes have become known as Heinrich events (Heinrich, 1988).

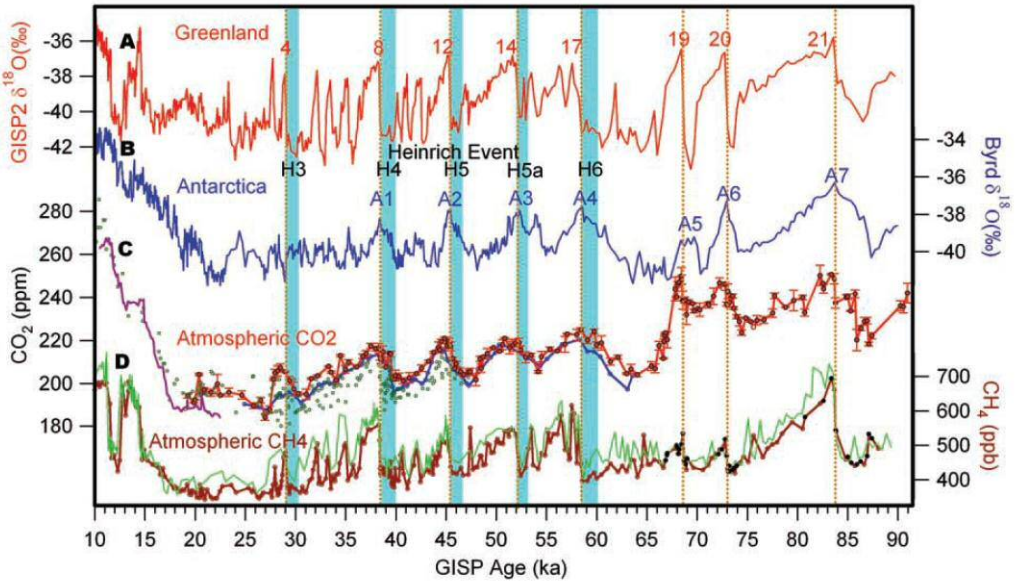

Fig. 1. 4 Atmospheric CO_2 composition and climate during the last glacial period from Ahn and Brook (2008). (A) Greenlandic temperature proxy, $\delta^{18}O_{ice}$. Red numbers denote D-O events (B) Byrd Station, Antarctica temperature proxy, $\delta^{18}O_{ice}$. A1 to A7, Antarctic warming events (C) Atmospheric CO_2 concentrations. (D) CH_4 concentrations from Greenland (green) and Byrd ice cores (brown).

Synchronization of ice core records from both polar regions to a common timescale has shown that these oscillations did not occur synchronously across the hemispheres; that is, the abrupt and high-amplitude temperature shifts in Greenland were out of phase with respect to the gradual changes in Antarctica, which were identified to precede D/O events in Greenland by 1.5-3 ka (Fig. 1. 4), (Blunier and Brook, 2001). The relationship between the two hemispheres suggests that the climate system acted like a seesaw. This (thermal) bipolar seesaw (Broecker, 1998; Stocker and Johnsen, 2003) is consistent with the contrasting response simulated for each hemisphere to reorganisations of the cross-equatorial heat transport dictated by AMOC strength variations and with the notion that the ocean played a pivotal role in millennial-scale climate fluctuations. These abrupt oscillations between cold (stadial) and warm (interstadial) conditions that punctuated the North Atlantic climate were also a prominent component of the last several glacial-interglacial cycles of the late Pleistocene climate dynamics (Martrat et al., 2007; Barker et al., 2011).

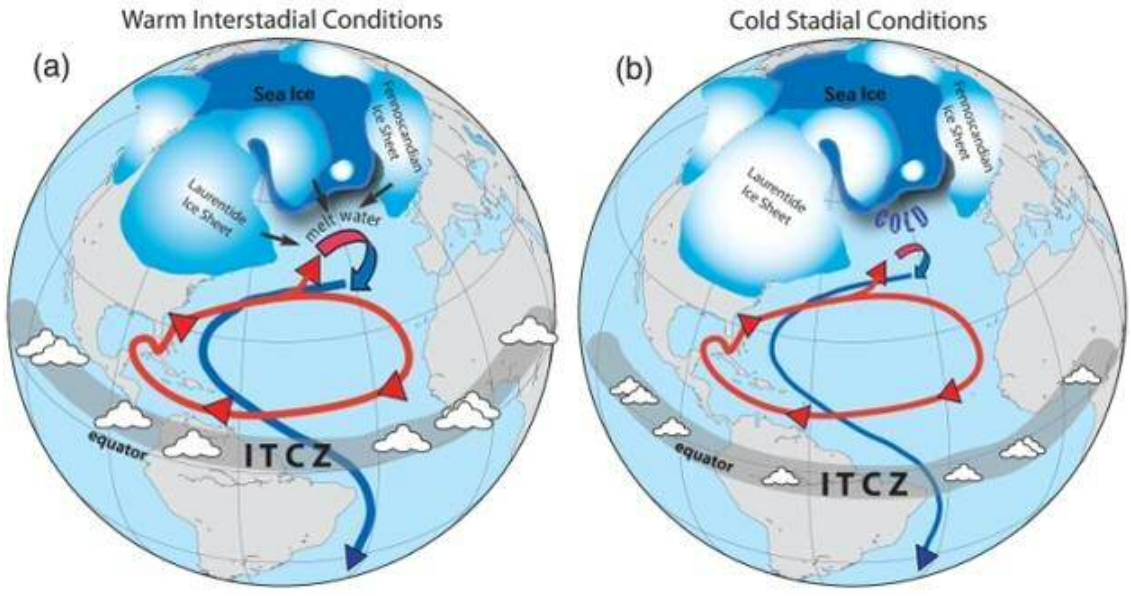

Fig. 1. 5 Mechanism of the salt oscillator hypothesis from Schmidt and and Hertzberg (2011). During warm interstadials, when AMOC is stronger (a) enhanced northward oceanic heat transport results in warmer conditions in the North Atlantic. Warmer conditions in the North Atlantic cause the ice sheets around the North Atlantic to melt, gradually reducing surface water salinity. In addition, the more northerly position of the ITCZ during interstadials results in enhanced freshwater precipitation in the tropical North Atlantic, further reducing surface salinity. Eventually, surface salinity is reduced enough to weaken AMOC, shifting the climate into a cold stadial (b) During stadials, cooler conditions in the

North Atlantic reduce meltwater input from the ice sheets, allowing surface salinity to increase. In addition, the ITCZ shifts southward during stadials, reducing the amount of freshwater input to the tropical North Atlantic. Both mechanisms result in an increase in North Atlantic salinity that eventually causes AMOC to strengthen, returning the climate system to an interstadial.

The underlying controls of these millennial-scale reorganisations of the coupled ocean-atmosphere system remains discussed. Broecker et al. (1990) hypothesized that millennial-scale AMOC changes were modulated by salinity oscillations altering ocean water density (buoyancy) in the proximity of the NADW formation sites (Fig. 1. 5), (Renold et al., 2010). The main drivers of the changes in the North Atlantic salt budget are still thought to be related to freshwater discharge from collapsing circum–North Atlantic ice sheets (Clark et al., 2002) and the Atlantic-to-Pacific moisture transport (Broecker, 1997; Leduc et al., 2007). Others argue that changes in atmospheric circulation were the driver (the wind field oscillation hypothesis) (Clement and and Cane, 1999; Seager and Battisti, 2007). However, new results offer an alternative explanation in which a nonlinear response of the glacial ocean to gradual variations in the Northern Hemisphere ice sheets height can control abrupt transitions from weak to strong AMOC modes (Zhang et al., 2014).

Increasing interest has focussed on the salt transport through the Indian-Atlantic Ocean Gateway (IAOG), via the Agulhas leakage, which can be considered as another potential controlling factor impacting on the North Atlantic salt budget (Lutjeharms, 2006; Beal et al., 2011). The Agulhas leakage of ~5–15 Sv is considered one dominant source of the upper branch of the AMOC, connecting the southern tip of Africa to the North Atlantic (Gordon, 1986; Lutjeharms, 2006; Beal et al., 2011).

1.2. The Agulhas Current present and past – Dynamics, climate and the AMOC

1.2.1. Warm Water Transports and Circulation off southeast Africa and the Indian-Atlantic Ocean Gateway Circulation

The largest surface western boundary current in the Southern Hemisphere, the Agulhas Current, is part of the subtropical Indian Ocean gyre (STIOG) and transports about 70–78 Sv (1 Sv = 10^6 m^3 s^{-1}) of tropical and subtropical waters along the eastern margin of southern Africa (Lutjeharms, 2006). At the southern tip of Africa, between 15 °E and 20 °E, the current retroflects with the majority of its waters, about 70 to 75%, flowing back into

the Indian Ocean as the Agulhas Return Current (ARC) (Feron et al., 1992) and feeding the southwest Indian Ocean sub-gyre (SWIOSG), (Gordon et al., 1987; Stramma and Lutjeharms, 1997; Lutjeharms and Ansorge, 2001), (Fig. 1. 6).

The Agulhas Current carries thermocline waters from the South Indian subtropical gyre with contributions of Red Sea and Arabian Sea waters, and from the Indonesian Throughflow. Driven by the anti-cyclonic wind field over the South Indian Ocean these water types are advected via eddies and meanders from the equatorial Indian Ocean through the Mozambique Channel and the East Madagascar Current (EMC), (Fig. 1. 6), (Song et al., 2004; Beal et al., 2006). When westward travelling Rossby waves derived from the tropical Indian Ocean arrive at Madagascar the interaction between them contributes to the formation of eddies (Schouten et al., 2002a) east of Madagascar (Biastoch and Krauss, 1999). Every year four to five of these up to 350-km wide eddies penetrate southwards through the Mozambique Channel, transporting approximately ~17 Sv (Ridderinkhof et al., 2010). These eddies are responsible for short-term modulation over the whole depth range and width of the channel (de Ruijter et al., 2002) thereby causing an interannual variability of about 9 Sv into the Agulhas Current. At the latitude of Durban (30 °S) the westward flowing southern extension of the EMC converges with the southward flowing train of Mozambique eddies to form the Agulhas Current as a narrow jet-type current that is steered by the steep South African continental margin (Fig. 1. 6). At the tip of Africa the current turns west, driven by its own inertia, and retroflects back into the Indian Ocean forming the ARC (Lutjeharms and Van Ballegooyen, 1988). The eastward flowing ARC forms the final outflow of the system and its volume transport diminishes along its path as Agulhas water leaks into the SWIOSG. The ARC flows along the Subtropical Front (STF) south of Africa.

This front has been shown to exhibit one of the most strongly developed meridional gradients in temperature and salinity (e.g., Lutjeharms and Valentine, 1984) with a 6 °C decrease in temperature over a distance of 20 km.

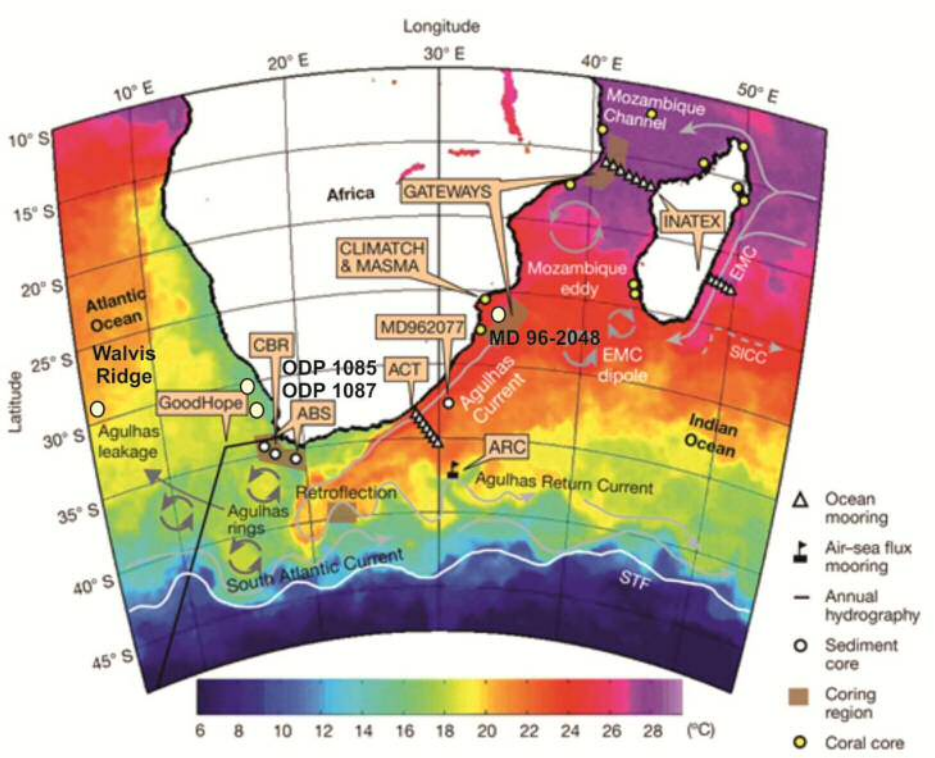

Fig. 1. 6 The Agulhas system and associated flow patterns from Beal et al. (2011). Sea surface temperature (SST) for 23 May 2009, showing water at 23–25 °C in the Agulhas Current and at 20 °C in the Retroflection. Main circulation features and observation programs are highlighted. Monitoring and repeat measurement programmes in the region include Agulhas Current Time-series (ACT), Indian–Atlantic Exchange in Present and Past Climate (INATEX), the Agulhas Return Current (ARC) air–sea flux buoy and the GoodHope repeat-hydrography line. Individual sediment core locations are marked for the Cape Basin record (CBR), (Peeters et al., 2004); MD962077 (Bard and Rickaby, 2009); Agulhas Bank splice (ABS), (Martínez-Méndez et al., 2010; Marino et al., 2013; Kasper et al., 2014); MD962048 (Caley et al., 2011a); ODP 1087 (Caley et al., 2012); ODP 1085 (Dickson et al., 2010); Walvis Ridge 64PE174-P13 (Scussolini and Peeters, 2013; Scussolini et al., 2013); coral cores Madagascar (Zinke et al., 2014).

Eddies from the Mozambique Channel and EMC propagating downstream with the Agulhas Current are strongly barotropic solitary meanders (Bryden et al., 2005a; Biastoch et al., 2009a; Tsugawa and Hasumi, 2010) and therefore destabilize the retroflection to the extent that four to six, up to 400 km wide anticyclonic eddies 'Agulhas Rings' form per year and spin of the retroflection area (Fig. 1. 6). Some indications suggest that Agulhas leakage is linked with interannual modes of Indian and Pacific variability, postulating a connection with the Indian Ocean Dipole and Pacific La Niña/El Niño phases (Schouten et al., 2002a; Palastanga et al., 2006).

1.2.2. Indian-Atlantic water exchanges: Agulhas leakage and the AMOC

At all latitudes the upper ocean transport of the Atlantic Ocean is generally northward with waters originating from the Southern Ocean as well as from the Indian-Pacific Oceans. These two sources are referred as the Atlantic cold- and warm-water routes (Fig. 1. 7), (Speich et al., 2001). Waters from both routes, ultimately, penetrate the subpolar North Atlantic and the Nordic Seas, where deep convection occurs (Fig. 1. 7), (Marshall and Schott, 1999). The contribution from Southern Ocean waters via the Drake Passage is direct where the warm water pathway is more diverse due to its various sources (Fig. 1. 7). Only a relative small proportion of the Agulhas Current's warm and salty waters, approximately 2–15 Sv, are transported into the South Atlantic through the IAOG via the Agulhas leakage (de Ruijter et al., 1999a; Richardson, 2007). The warm and saline Indian Ocean waters that enter the South Atlantic are carry up to 0.38 PW of heat and $38x10^5$ kg s^{-1} of salt (de Ruijter et al., 1999a), causing a salinity anomaly of +0.2 in the South Atlantic thermocline thereby constituting the warm water route of the global overturning circulation that feeds the renewal of NADW in the Northern Hemisphere (Fig. 1. 7), (Gordon, 2001).

Early theoretical studies by Gordon in the 1980's suggested that the inter-ocean salt transport should trigger a response in the AMOC (Gordon, 1985; Gordon, 1986). The impact of Agulhas leakage on the Atlantic circulation is binary: through radiation of planetary waves and through advection. Isotherms and isohalines in the South Atlantic thermocline are depressed when warmer and saltier Agulhas leakage waters entering this basin (Giulivi and Gordon, 2006). The resulting undulations in isopycnals radiate dynamic disturbances that slowly propagate across the South Atlantic as planetary (Kelvin, Rossby) waves that propagate across the Atlantic basin (van Sebille and van Leeuwen, 2007; Biastoch et al., 2008b). These waves, carriers of the dynamical imprint of Agulhas leakage, reach the South American coast within 4–6 years and are subsequently rapidly communicated across the Equator by coastal Kelvin waves (Weijer et al., 2002; Biastoch et al., 2008b). As such, leakage impacts the zonally-integrated flow of the Atlantic, the AMOC, within a decade (Cunningham and Marsh, 2010). In the subtropical North Atlantic short-term variability potentially associated with Agulhas leakage is observed (Tsugawa and Hasumi, 2010), while some of the interannual-to-decadal AMOC variability seen in the

models plausibly stems from the frequency of Agulhas Ring shedding that, in turn, is modulated by the Indian Ocean Dipole and ENSO modes.

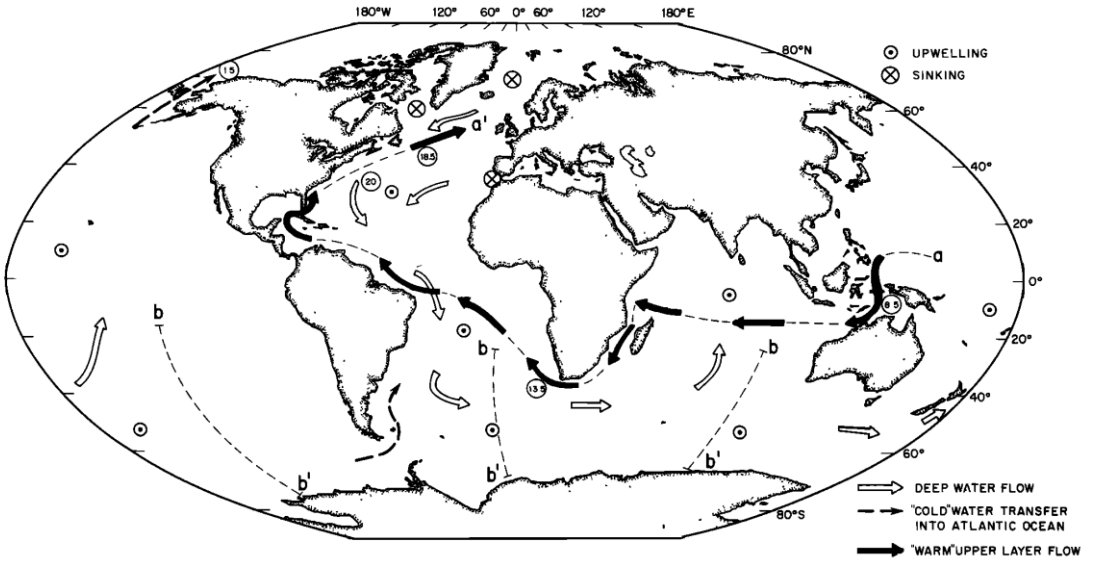

Fig. 1. 7 Global structure of the thermohaline circulation cell associated with NADW production taken from Gordon (1986). The warm water route, shown by the solid arrows, marks the proposed path for return of upper layer water to the northern North Atlantic as is required to maintain continuity with the formation and export of NADW. The circled values are volume flux in 10^6 m^3/s which are expected for uniform upwelling of NADW with a production rate of 20 x $10^6 m^3/s$. These values assume that the return within the cold water route, via the Drake Passage, is of minor significance.

The advection of salt water entering from the Agulhas region to the convection centres in the North Atlantic is another important variable defining the AMOC response to Agulhas leakage. The principal carrier of Agulhas leakage, the Agulhas Rings, decay rapidly in the Cape Basin (Schmid et al., 2003; van Sebille et al., 2010) thereby losing their anomalous surface thermal content fairly quickly to the atmosphere (van Aken et al., 2003). What remains is the salt content, which persists for longer and contributes to the overall densification of the South Atlantic (Biastoch et al., 2008b; Biastoch and Böning, 2013). The advection of salt is communicated north within 2–4 decades (Weijer et al., 2002; van Sebille et al., 2011; Rühs et al., 2013) suggesting a rather fast implication of Agulhas leakage on the AMOC. However, a recent modelling study showed that despite the advective connection between transported salinity anomalies from the Agulhas region into the North Atlantic within 30-40 years no identifiable impact of Agulhas leakage on the strength of the AMOC existed (Weijer and van Sebille, 2013). It was argued that the salinity variations are too weak to significantly modify the stratification in the North Atlantic.

Through the planetary wave propagation and advective mechanisms described above, Agulhas leakage might also play an important role for future climate change. There is evidence that Agulhas leakage is actually increasing (Rouault et al., 2009; Beal et al., 2011) under anthropogenic climate change and may continue to do so in the future. The slow increasing import of additional salt from the Agulhas could be a plausible mechanism to stabilise the AMOC (Biastoch and Böning, 2013) at a time when anthropogenic warming and freshwaters from rapid melting of Arctic sea-ice (Walsh, 2013) and the Greenland ice-sheet (Bamber et al., 2012) is predicted to weaken it. Satellite and hydrographic data show a southward expansion of the Indian Ocean subtropical gyre (Alory et al., 2007) and subsequent warming of the Agulhas system since the 1960s (Rouault et al., 2009).

1.2.3. Influence of variable Agulhas warm water transports on southern African climates and rainfall patterns

African climates depend on low altitude pressure and winds over the continent, which are the surface expression of the upper air circulation (Gasse, 2000). Southern Africa bridges climates of the low-latitude tropical regime that is primarily under the influence of the Intertropical Convergence Zone (ITCZ) and Congo Air Boundary (CAB) and the high southern latitudes that are influenced by the northern extensions of the circum-Antarctic westerly wind belt, determining climates of the Cape Provinces of South Africa (Tyson and Preston-Whyte, 2000; Chase and Meadows, 2007). The junction between the easterly trade wind belts of each hemisphere is the ITCZ and its seasonal migration occurs in response to changes in the location of maximum solar heating which results in northern and southern belts of monsoonal climates with summer rains and winter droughts (Gasse et al., 2008). The CAB, a low pressure area, is part of the discontinuities that divide easterly trades arriving from the Indian Ocean and westerly monsoonal wind systems from the Atlantic over Africa and can be regarded as a southern branch of the ITCZ. The latitudinal position and annual migration of these systems determines the timing and duration of the rainfall seasons. They are associated with the global thermal gradient and the strength and position of the Hadley Cell (Nicholson, 2000). While directly connected with the ITCZ the convergence zone over tropical southern Africa on occasion is decoupled from the divide between dry trade winds in the east and wet monsoon in the west as occurs, for instance, over West Africa in summer (Nicholson, 2000). Terrestrial evidence for the climate evolution of southern Africa is based on a sediment record from Tswaing Crater north of

Pretoria (Partridge et al., 1997) which constitutes the single most important terrestrial record of palaeoclimates in southern Africa that spans several glacial cycles. Clastic particle size variations suggest that cyclic changes in precipitation were linked with orbital precession variations and suggest sensitivity of past precipitation to changes in orbitally modulated insolation (Partridge et al., 1997).

Coastal cave records (Bar-Matthews et al., 2010) from South Africa and marine sediment cores (Schefuß et al., 2011; Ziegler et al., 2013b) along the southeast African margin display recurrent rainfall oscillations that do not seem follow orbital modulation during the past 100 kyr but show a potential link with the timing of millennial timescale Northern Hemisphere cold events and their interhemispheric atmospheric linkage. In summary, climate changes in southern Africa have been linked with changes in ocean and atmospheric circulation, with indications that fluctuating heat budgets of the western Indian Ocean possibly in conjunction with variable ocean-atmosphere heat and moisture transfer in the Agulhas Current region were important (Zonneveld et al., 1997; Dupont et al., 2011).

1.2.4. Palaeoceanographic reconstruction of the Agulhas Current and Agulhas leakage

The interest of the palaeoclimate community in Agulhas leakage arose from the finding that peak Agulhas leakage occurred during glacial terminations (Peeters et al., 2004) and plausibly aided the AMOC to shift to its full-strength interglacial mode (Fig. 1. 8), (Knorr and Lohmann, 2003, 2007). This hypothesis builds on a variety of records from within the Agulhas leakage pathway which inferred fluctuations in the strength of Agulhas leakage over the late Pleistocene epoch based on variety of geochemical proxy reconstructions (Peeters et al., 2004; Franzese et al., 2006; Martínez-Méndez et al., 2010; Rackebrandt et al., 2011; Marino et al., 2013; Scussolini and Peeters, 2013; Scussolini et al., 2013; Kasper et al., 2014)(Fig. 1. 6). The evidences from these studies have been interpreted in terms of less Agulhas water leaking into the South Atlantic during glacial periods. Furthermore, leakage started to increase during late-glacial conditions several thousand years before the glacial ice volume fully disappeared (Peeters et al., 2004; Martínez-Méndez et al., 2010). This maximum during glacial terminations suggests that Agulhas leakage may have had a role in the rapid resumption of interglacial/interstadial climate, presumably through its

influence on the AMOC (Fig. 1. 8), (Knorr and Lohmann, 2003; Peeters et al., 2004; Marino et al., 2013).

The continuous presence of subtropical planktonic foraminifera (e.g., *Globorotalia menardii* and the so-called Agulhas Leakage Fauna (ALF)) has been used to infer persistent Indian-to-Atlantic surface water flow during the last 450 kyr while the transient occurrence of subpolar species (*Neogloboquadrina incompta*) suggests intermittent incursions of cold sub-Antarctic waters in the Agulhas Corridor during glacial periods (Fig. 1. 8; Fig. 1. 6), (Rau et al., 2002; Peeters et al., 2004).

Recent multiple-proxy data from sediment cores in the IOAG have provided the first detailed pictures of the surface ocean climatology in the area during the Pleistocene (Fig. 1. 6). Martínez-Méndez et al. (2010) used planktonic Mg/Ca data from Agulhas Bank Splice (ABS) record located in the Cape Basin to show continuous SST warming across full-glacial stages (Marine Isotope Stages MIS 2 and 6) plausibly indicating an increased influence of warm Agulhas water in the region and/or reduced northward advection of cold subantarctic surface water (Fig. 1. 6). Kasper et al., (2014) applying organic proxies on the same core material as Martínez-Méndez et al. (2010), found relatively high salinities in the IAOG during glacials, with subsequent freshening during glacial terminations.

Marino et al. (2013) recently attributed transient millennial timescale salinity increases within the IAOG during MIS 6, to increased Agulhas salt-leakage coincident with cold stadial conditions in the Northern Hemisphere pointing to the Indian-to-Atlantic salt-leakage as an essential modulator of abrupt climate change (Fig. 1. 6). Provenance studies using $^{87}Sr/^{86}Sr$ and Nd/Sr ratios suggest reduced advection of Agulhas water and possibly even reduced Agulhas leakage volume flux during peak glacial times (Franzese et al., 2006).

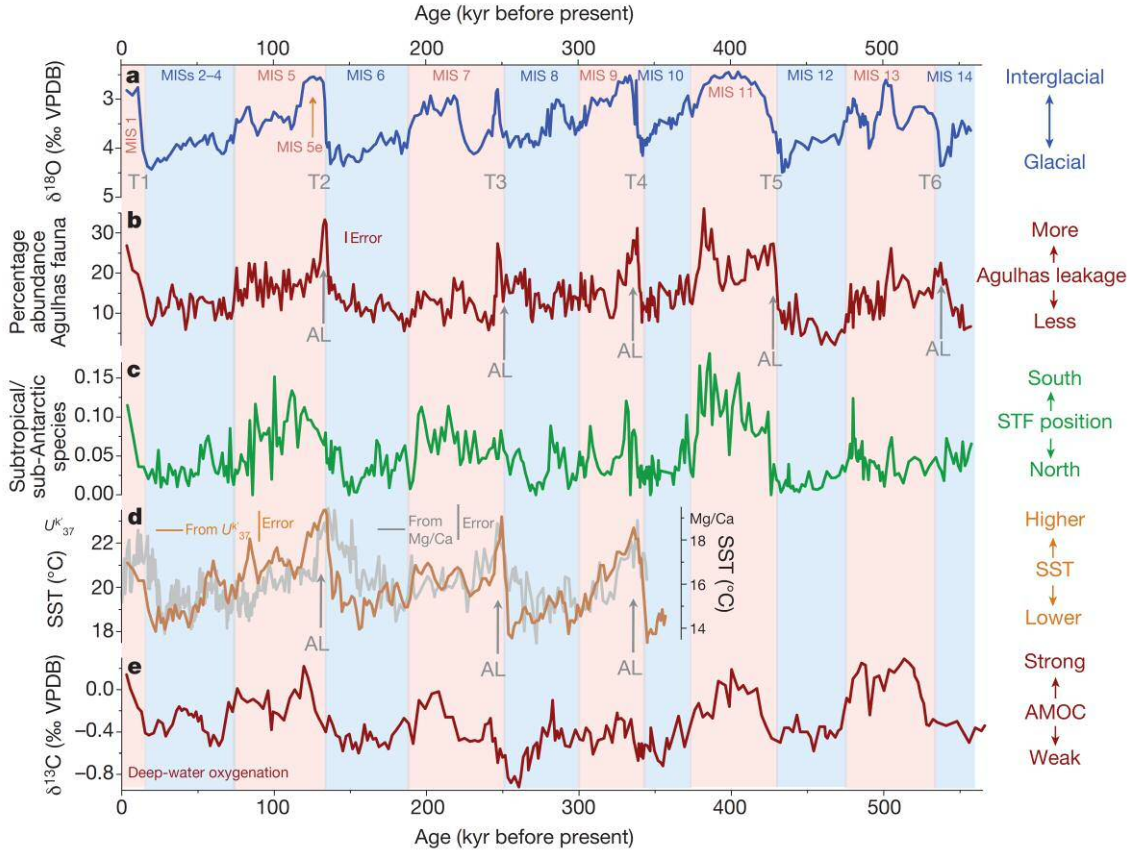

Fig. 1. 8 Palaeoceanographic time series from the Agulhas leakage corridor spanning the last 570 kyr from Beal et al. (2011) (a) Stable oxygen isotope profile of benthic foraminifera from the Cape Basin Record (CBR), (Peeters et al., 2004) represents a proxy for glacial–interglacial variations in global climate (highlighted by vertical blue/ red shading). Marine Isotope Stages (MISs) are labelled. T1–T6 mark terminations of the past six glacial periods (MISs 2, 6, 8, 10, 12 and 14) (b) Abundance of tropical planktonic foraminiferal marker species along the CBR indicate maximum Agulhas leakage during glacial terminations T2–T6. Standard error (1.73%) is illustrated (c) Ratio of subtropical to sub- Antarctic planktonic marker species along the CBR, thought to be related to north–south migrations of the STF (d) SST derived from temperature-sensitive biomarkers (Uk'_{37}) produced by prymnesiophyceae algae along the CBR (brown line), and Mg/Ca ratios in planktonic foraminifera from the ABS record (grey line), (Martínez-Méndez et al., 2010). Both reconstructions show maximum SST during glacial terminations, coinciding with Agulhas leakage events. SST reconstructions diverge during glacial periods, possibly corresponding to changes in seasonality (e) Record of benthic $\delta^{13}C$ from ODP Site 846 in the deep Pacific (Mix et al., 1995) is thought to be linked to ventilation of the deep Pacific (Lisiecki et al., 2008), which is related to the strength of the AMOC. With this interpretation, AMOC strength seems to increase at each glacial termination, leading to the hypothesis that Agulhas leakage may stimulate the AMOC. All records are synchronized using standard oxygen isotope stratigraphy.

With the aim to unravel if Agulhas leakage waters were effectively incorporated into the South Atlantic gyre, or whether they retroflected into the Indian and/or Southern Oceans Scussolini and Peeters (2013) and Scussolini et al. (2013) studied a piston core 64PE-174P13 from the Walvis Ridge (Fig. 1. 6), within the Agulhas leakage pathway, almost 1800 km farther into the Atlantic Basin than previously studied. Based on the upper ocean $\Delta^{18}O$ gradient between shallow and deep dwelling planktonic foraminifera, used as a proxy for

upper ocean density stratification, they concluded that an enhanced passing of Agulhas rings during glacial terminations impacted the upper ocean stratification of the South Atlantic.

Multiple-species stable isotope and alkenone data from ODP Site 1085 further north of the immediate IAOG suggest that Agulhas leakage variability during MIS11 was directly related to AMOC activity and wind forcing, including a strengthened leakage at the end of the MIS 11 that could even have contributed to renewed ice sheet build-up and the demise of MIS 11 (Dickson et al., 2010) (Fig. 1. 6). A high-resolution faunal record of tropical species *G. menardii* abundance at ODP Site 1087 in the southern Benguela region was used to assess the inter-ocean water transport south of Africa and suggested that the Agulhas leakage strengthened during every glacial termination of the past 1.3 Myr (Caley et al., 2012) (Fig. 1. 6).

Using an Agulhas leakage efficiency index, the first attempt to develop a quantitative approach palaeo-Agulhas leakage by Caley et al. (2014) suggested that the persistent peaks in Agulhas leakage during glacial terminations over the past 640 kyr were on the order of ~10 Sv or more, increasing from glacial levels ranging between ~1 Sv and ~7 Sv.

Fewer studies have concentrated on the Agulhas Current itself. SST and salinity records at an upstream location along the southeast African margin (26 °S) display a prominent 41-kyr cyclicity which was used to suggest that long-term Agulhas Current variations were associated with high latitude (as opposed to regional tropical) climate forcing (Caley et al., 2011a) (Fig. 1. 6). SST records and ocean productivity indicators presented by Bard and Rickaby (2009) suggest that during some full-glacial stages the STF moved northward by up to 7° in latitude thus potentially severely reducing Agulhas Current transports into the gateway and limiting leakage to the South Atlantic. A recent study from corals off Madagascar spanning the past 334 years indicates distinct surface water cooling associated with the Little Ice Age (early 14th century till ~1850) and warming during the late 18th, 19th and 20th centuries, suggesting a teleconnection between the Agulhas Current with the southern Indian and Atlantic Oceans (Zinke et al., 2014) (Fig. 1. 6).

1.3. Research scopes and outline

Throughout the introduction Agulhas leakage has been presented as an important component of present, past and potentially future ocean circulation. Leakage provides a

crucial connection between the Pacific/Indian and the Atlantic Oceans. The Agulhas Current system mainly consists of three components: Agulhas Current, Agulhas leakage and the Agulhas Return Current. For obvious reasons the focus of most palaeoclimatological reconstructions has been the variations of Agulhas leakage observed in the IAOG during the late Pleistocene.

On the search for a potential explanation for what controlled leakage various hypotheses related to the Southern Hemisphere wind fields have been put forward. Bard and Rickaby (2009) reconstructed SSTs of the Agulhas Current and noted that, in comparison to interglacial periods, the current was several degrees cooler during glacial times. They associated this fluctuation in temperatures to displacements of the STF south of Africa. Zahn (2009) suggested that such displacements would be caused by the adjustment of the large-scale circulation to altered Southern Hemisphere wind patterns. From these inferences, and in combination with results of Peeters et al. (2004), the common assumption is that shifts of the Southern Hemisphere westerly wind belt, (in particular the position of the zero wind stress curl) would have led to the widening/narrowing of the gap between Africa and the STF, thereby controlling the amount of warm salty Indian Ocean waters leaking into the South Atlantic. However, this assumption has recently been questioned (De Boer et al., 2013; Durgadoo et al., 2013). These studies showed that the position of the STF is not related to the position/shifts in the wind belt i.e., position of the zero wind stress curl and that Agulhas leakage increases with northward shifted westerlies a scenario originally proposed for a narrower IAOG. It is therefore unclear whether shifts of the wind fields did in fact act to alter past rates of Agulhas leakage, which might imply that other factors, despite the movement of the STF, were equally important in determining leakage.

This thesis shifts the focus away from Agulhas leakage and aims to better develop our understanding of the Agulhas Current's role within the broader Agulhas Current System during the late Pleistocene. For that reason two marine sediment cores from the Natal Valley, southwest Indian Ocean, CD154 17-17K and CD154 10-06P at a water depth of 3333 and 3076 m, respectively (see Fig. 2.1) were studied. The cores are situated in an ideal setting presently underneath the main trajectory of the Agulhas Current in the surface and associated with the return path of NADW in the deep to address three specific objectives in this work:

Did upstream Agulhas Current variability reflect inferred changes in Agulhas leakage and what drove these variations?

Agulhas leakage can be regarded as a by-product of variability within the Agulhas Current, which suggests a probable strong dynamic link between the two. Results from numerical modelling experiments show that changes to the Indian Ocean trade winds significantly induce changes in Agulhas Current transport and energetics (Loveday et al., in press). Despite large changes in the Agulhas Current dynamics, Agulhas leakage remains unaffected which led to the conclusion that Agulhas leakage is decoupled from the Agulhas Current. Considering that beyond the instrumental record dynamical reconstructions are difficult to achieve, the approach in **Chapter 3** is based on the reconstruction of upper ocean water mass properties of the Agulhas Current of the past 100 kyr. Reconstructions of SST of core CD154 17-17K are examined as well as the local oxygen isotope composition of seawater, which provides an indication of salinity, and foraminiferal assemblage variations from within the main flow of the Agulhas Current. These proxies, when considered in combination can directly be compared to records from the IAOG previously interpreted to reflect changes in Agulhas leakage. Furthermore, numerical modelling studies using a regional eddy-permitting an 'ocean only' model are included to better understand what might have driven the observed variability in the current itself.

What determined hydrographic variability of deep waters off southeast Africa and were they linked with contemporaneous Agulhas Current oscillations? Can co-evolving changes in the surface and deep waters unravel whether Agulhas leakage had an active or passive role during glacial terminations?

As part of the global overturning circulation, some NADW exits the Atlantic basin to the south of Africa into the southwest Indian Ocean as part of the Agulhas Undercurrent (Arhan et al., 2003). van Sebille et al. (2012) concluded on the basis of modelling results that the steering of the NADW by Agulhas rings implies that in this region the upper and lower branch of the global meridional overturning circulation are directly connected. A change in Agulhas leakage might, through a change in the eddy thickness flux, directly affect the strength of the flow of NADW exiting the Atlantic basin south of Africa. These finding are related to the modern system. On longer timescales records from the Agulhas Bank (Martínez-Méndez et al., 2008) and the Agulhas Plateau (Molyneux et al., 2007)

indicate that the NADW transport along its pathway around South Africa was reduced during late glacial stages and Northern Hemisphere Cold Stadials (NHCS) being substituted with waters from a southern origin. If true this might have had wider implications for the ventilation of the Indian Ocean as the AUC constitutes the connecting deep water link between ocean basins. In **Chapter 4,** the hydrographic variability of the NADW component of the AUC will be studied using benthic stable isotope records from core CD154 10-06P with the aim to document the timing and amplitude of variations in the deep water ventilation of the southwest Indian Ocean. Changes of the relative proportion between Northern Component Waters (NCW) and Southern Component Waters (SCW) might have been linked to AMOC mode shifts. Moreover, the results of **Chapter 3** will be used in conjunction to establish a potential linkage between Agulhas Current and deep water variations over time. The aim is to evaluate the possibility that the Agulhas salt-leakage events that are documented downstream in the IAOG do not simply reflect a passive response to the interhemispheric (bipolar seesaw) reorganisation but potentially actively could have triggered the AMOC resumption during terminations.

How did southernmost East African climate vary on different timescales, did Agulhas Current upper ocean temperature variability play a leading role in these oscillations and are these hydrological shifts part of a bigger global monsoon system?

Today, Agulhas warm water transports along the southeast African continental margin stimulates air-sea exchanges and drive interannual variability connected with the Indian Ocean Dipole mode with implications for southern Africa regional climate and weather systems (Reason, 2001). A connection between Agulhas Current upper ocean temperature variability and inferred precipitation changes have been assumed but never been directly tested on millennial nor orbital timescales.

In **Chapter 5** this connection will be tested using a suite of inorganic and organic geochemical proxies which provide direct and indirect evidence of terrestrial input from land at the site CD154 10-06P, retrieved close to the continental shelf. This approach builds on a previous study based on marine sediments of core CD154 17-17K from the same region which showed that precipitation over the southeast African continent responded positively to the abrupt cooling events that occurred repeatedly in the North Atlantic during the last glacial period (Ziegler et al., 2013b). Multi-proxy based SST estimates are derived in order to investigate if a warming in the Agulhas Current region is

associated with increased rainfall over neighbouring South Africa. Model experiments are involved to better understand the land-ocean climate dynamics in southeast Africa.

A recent research question is whether displacements of the ITCZ were substantially synchronous during climate changes of the late Pleistocene; in other words whether it is appropriate to consider a mechanism of Global-Palaeo-Monsoon (GPM), (Kutzbach et al., 2008; Wang, 2009; Caley et al., 2011b; Cheng et al., 2012). A connection has already been suggested between the palaeo-monsoons of Brazil in the Southern Hemisphere and the East Asian ones in the Northern Hemispheres (Wang et al., 2004) but has never been shown for South Africa on longer timescales. This question will be addressed in **Chapter 6** of this thesis, where the new record of CD154 10-06P records southeast African climate variability over the past 270 kyr and is correlated to the time series of East Asian summer monsoon (EASM).

In a final synthesising **Chapter 7** the findings of the individual chapters that emerged are linked to generate an overall picture of changes of the Agulhas Current System during the late Pleistocene. Moreover, this summary is an ideal platform to present ideas for future research in the area.

2. Material and Methodology

The marine sediment cores used in this study were recovered during the *RRS Charles Darwin* cruise number 154 in December 2003/ January 2004 (Hall and Zahn, 2004). Cruise CD154 was dedicated to retrieving sample material in support of the NERC-funded research project: “Agulhas leakage and abrupt climate change: the past 50,000 years”. The overarching scientific goal of the cruise was to collect a suite of sediment cores along the flow path of the Agulhas Current that would enable the reconstruction of the history of the current during the last glacial period to the present. Of particular interest are episodes of rapid climate change that punctuate glacial climates but are known to also exist during the current Holocene warm period.

The aim of this chapter is to describe the regional and sedimentary setting of the marine sediment cores. Moreover it will give a general overview and background of the palaeoceanographic proxies used in this study as well as their analytical details according to the focus of the individual chapters to reconstruct past land and ocean changes.

2.1. Site settings and regional oceanography

Marine sediment Kasten core CD154 17-17K (33°19.2’S; 29°28.2’E; 3333 m water depth) and piston core CD154 10-06P (31°10.36'S; 32°08.91'E; 3076m water depth) were retrieved from the Natal Valley (Fig. 2. 1) which is a north-south trending, sediment-filled ocean basin between the coast of SE Africa and the Mozambique Ridge underlying the central part of the Southwest Indian Ocean. The origin of the northern Natal Valley is controversial. Gravity studies indicate that the northernmost Natal Valley is floored by a thinned continental crust whereas the southern Natal Valley and Transkei Basin are underlain by typical oceanic crust (Reznikov et al., 2005). The Natal Valley is situated in a depocenter formed in the lee of the bottom water flow, where it emerges from the relatively constricted abyssal Agulhas Passage between the Agulhas Fracture Zone and the Agulhas Plateau. The abyssal topography and the underlying sedimentary sequences in the southern Natal Valley and Transkei Basin are conspicuously moulded by the strong, geostrophic bottom current flow emerging from the Agulhas Passage.

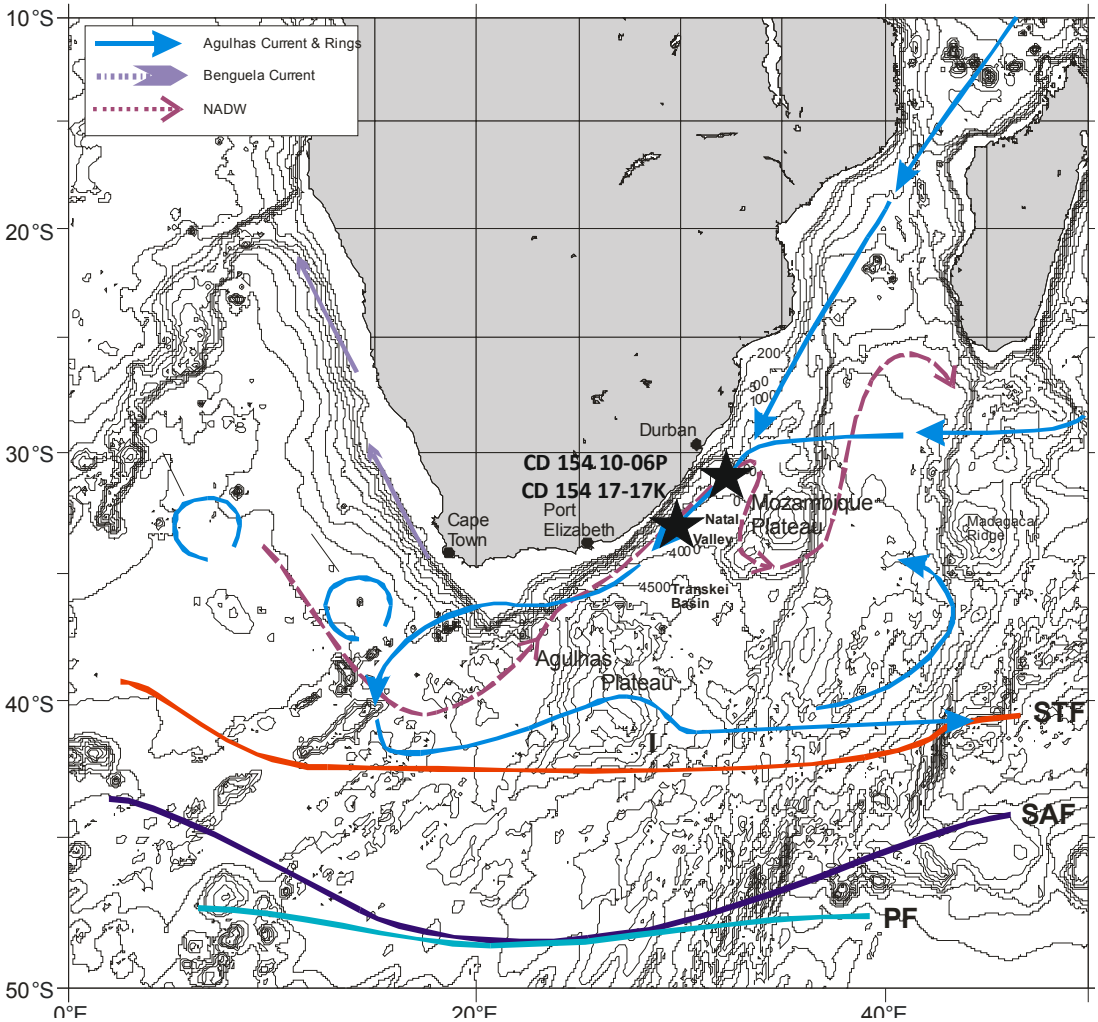

Fig. 2. 1 The Agulhas Current System with approximate flow paths of the major water masses, mainly after Dingle et al. (1997). For clarity the path of Antarctic Bottom Water (AABW) is not shown. NADW, North Atlantic Deep Water, STF, Subtropical front; SAF, Subantarctic front; PF, Polar front.

Comparatively large volumes of clastic sediment are delivered to a narrow continental shelf by numerous streams and rivers, including the larger Tugela River and, farther north, the Limpopo River (Fig. 2. 1). The inner and outer continental shelf is powerfully swept by the southwest flowing surface Agulhas Current, which entrains most of the incoming sediment and delivers it to the heads of well-developed submarine-canyon systems (Goodlad, 1986). It is then transported across the steep continental slope, mainly by turbidity currents, and is ultimately deposited above the thick continental-rise fans and abyssal plain sequences that are particularly characteristic of the Natal Valley (Flemming, 1981).

2.1.1. Modern regional surface water oceanography at the core locations

Surface waters at the core sites are within the main trajectory of the upstream 'northern' Agulhas Current where it follows a near rectilinear path along the narrow shelf and steep continental slope (Lutjeharms, 2006). The start of the northern Agulhas Current is approximately formed by the border between Mozambique and South Africa and stretches along the eastern seaboard of South Africa, down to Port Elizabeth (Fig. 2. 1). The trajectory of the northern Agulhas Current has been shown to be quite remarkable as a western boundary current for its invariant path. The current can be seen to follow the shelf edge very closely compared to other western boundary currents, such as the Gulf Stream or Kuroshio Current, which exhibit substantial lateral meanders (Gründlingh, 1983). The continental slope off southeast Africa is extremely steep and this is believed to account for the stability of the northern Agulhas Current constraining the growth of lateral meanders in the current (de Ruijter et al., 1999b). The Natal Bight, which is a wider part of the shelf located to the north of Durban, has been shown to be a region in which the northern Agulhas Current is unstable (Fig. 2. 1), (Lutjeharms, 2006). In general, the Northern Agulhas Current is at least 2000 m deep and carries a mass transport of about 69.7± 4.3 Sv, (1 Sv = 1 x 10^6 m^3/s) that increases downstream (Gründlingh, 1980; Gordon et al., 1987), (Beal and Bryden, 1997, 1999; Bryden and Beal, 2001). Furthermore it displays very steady flow characteristics with mean maximum velocities of 1.5 m/s and little variability in the path of the current on seasonal timescales (Gründlingh, 1983).

Downstream of Port Elizabeth the continental shelf widens considerably to form the broad expanse of the Agulhas Bank south of Africa (Fig. 2. 1). There the shelf morphology allows the Agulhas Current to meander in the manner of most western boundary currents, as eddies and plumes. Once past the most southern tip of the Agulhas Bank, the southern Agulhas Current proceeds into the South Atlantic as a free inertial jet, but still generates plumes of warm water at its northern border (Lutjeharms and de Ruijter, 1996). These so called 'Agulhas filaments' have been observed to be only about 50 m deep, but they carry anomalous warm, salty water into the Atlantic Ocean. Because of their limited vertical extent the heat in these filaments is soon lost to the atmosphere, resulting in the region having a large ocean to atmosphere heat flux (Walker and Mey, 1988; Rouault and Lutjeharms, 2000).

The Agulhas Current system is fed by various water sources. Most of its waters derive from the Mozambique Channel, from the southward flow to the east of Madagascar, from the Red Sea and from inertial recirculation in the southwest Indian Ocean (Beal et al., 2006). Recent studies have shown that the sources of the Agulhas Current are not dominated by the Mozambique Current (Saetre and Da Silva, 1984) or by the East Madagascar Current (Lutjeharms, 1988) but mostly by the recirculation in the Southwest Indian Ocean sub-gyre (SWIOSG), (Stramma and Lutjeharms, 1997). About 35 Sv is derived from the recirculation of waters within this gyre. These water masses comprise recirculated Indian Ocean waters, which peel off the Agulhas Return Current (ARC) west of 70 °E (Lutjeharms, 2006), and Antarctic Intermediate Waters (AAIW) injected northward into the SWIOSG at about 60 °E (Fine, 1993). These Agulhas return waters not only contribute substantially to the volume transport of the Agulhas Current, but they also provide an important control on the surface water properties and dynamics of the current itself (Gründlingh, 1978; Gordon et al., 1987; Stramma and Lutjeharms, 1997; Lutjeharms and Ansorge, 2001; Boebel et al., 2003; Lutjeharms, 2006; Hermes et al., 2007)

The Agulhas Current is only partly fed by waters from the East Madagascar Current in form of meso-scale rings and filaments. Stramma and Lutjeharms (1997) proposed that around 20 Sv of water comes from east of Madagascar but not necessarily directly from the current itself. On the other hand, contributions via the Mozambique Channel are estimated between 5 Sv (Stramma and Lutjeharms, 1997) and 21 Sv (di Marco et al., 1998).

The Agulhas Current Surface layer transports Indian Tropical Surface Water with potential temperature above 20 °C and salinity values between 34.7 and 35.3, along with South Indian Ocean Subtropical Surface Water with temperature above 17 °C and salinity values about 35.6. The excess of precipitation over evaporation in the tropical latitudes of the Indian Ocean can explain the lower salinities of Indian Tropical Surface Water. These water masses contribute to the flow via the Mozambique Channel and can be traced as a recognisable lower salinity strip on the inshore side of the Agulhas Current (Gordon et al., 1987). The South Indian Ocean Subtropical Surface Water is found in the Agulhas Current as a subsurface salinity maximum. Red Sea Intermediate Water (RSIW) is also part of the intermediate layer constituting the Agulhas Current and has been shown to move down the current as distinct lenses (Roman and Lutjeharms, 2009). In general, RSIW, which is formed in the northern Red Sea, passes the Gulf of Aden and enters the Indian Ocean via

the Socotra Passage or the Socotra Island (according to summer or winter monsoon). Afterwards it flows along the African slope via the Mozambique Channel or via the East Madagascar Current route. A further component of the Agulhas Current is the southwest Indian Ocean Central Water with roughly 13% volume amount, temperature range between 8 ° - 15 °C and salinities between 34.6 and 35.5.

Table 2. 1: Water masses of the Agulhas Current (Beal et al., 2006).

Abbreviation	**Water mass**	**Salinity**	**Temperature**
TSW	Tropical surface water	< 35.3	>20 °C
STSW	Subtropical surface water	>35.6	>17 °C
SICW	South Indian central water	34.6-35.5	8 ° - 15 °C
AAIW and RSIW	Antarctic Intermediate Water and Red Sea Intermediate water	<34.7 >35.4	9 ° - 12 °C

2.1.2. Modern regional deep-water oceanography at the core locations

In the deep-sea environment of the Cape Basin, the flow of both water masses Antarctic Bottom Water (AABW) and North Atlantic Deep Water (NADW) is reflected in a major zone of erosion of the sea floor, mantled by abundant ferromanganese nodules. This zone at the foot of the continental rise is fed by margin-perpendicular slumps, debris flows and canyon-fed turbidity currents. The northward flow of AABW is restricted by the topographic configuration of oceanic ridges and fracture zones (Fig. 2. 1). This eastern branch of AABW is predominantly produced in the Weddell Sea and enters the Agulhas Basin through the mid-Indian ridge between 20–25°E and possibly 35°E (Kolla et al., 1976). Furthermore, it flows from the Agulhas Basin through the 50 km wide Agulhas Passage into the Transkei Basin where it is forced eastwards by the northeast-shallowing contours of the Natal Valley (Fig. 2. 1). Further evidence of deep sea circulation-zones of erosion are thinned sediment, manganese nodules, sediment waves and drifts indicate that the AABW flows across the seafloor of the Cape, Agulhas, Transkei, Natal Valley, and Mozambique basins (Dingle and Camden-Smith, 1979; Rogers, 1987). One prominent example for the strength of the deep water currents in this area is the E-W-orientated Agulhas Drift, a

contourite drift, deposited as AABW swings eastwards on exiting the Agulhas Passage Plateau and into in the Transkei Basin. At this point the AABW parts company with the overlying NADW which continues to flow north eastwards into the Natal Valley depositing margin-parallel contourite drifts at the foot of the continental slope as far north as Durban, where the Central Terrace and then the Mozambique Ridge steer the NADW first east and then south back to the mouth of the Natal Valley (Fig. 2. 1). Afterwards it leaves the Valley and enters directly into the open Indian Ocean (Niemi et al., 2000).

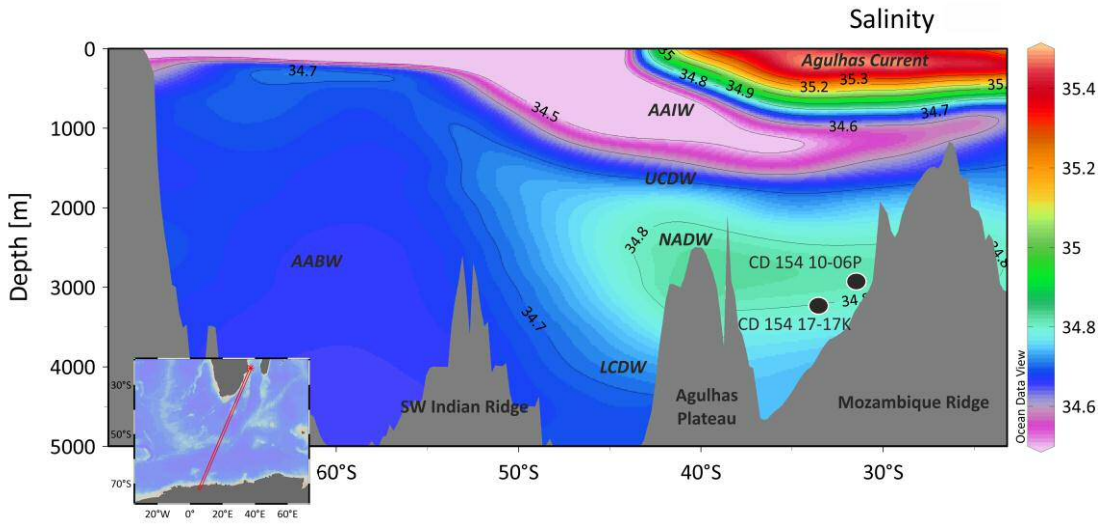

Fig. 2. 2 Present-day transect of salinity from the coast of South East Africa to Antarctica across the Southern Ocean (modified from Schlitzer (2012) showing the positions of the existing water masses. Agulhas Current sourced by Indian Ocean Waters; AAIW, Antarctic Intermediate Water; NADW, North Atlantic Deep Water; UCDW, Upper Circumpolar Deep Water; LCDW, Lower Circumpolar Deep Water, AABW, Antarctic Bottom Water.

The core sites are located on a contourite sediment drift that has been plastered to the lower continental slope under the influence of NADW. The sites today are predominantly bathed in NADW (Fig. 2. 2) within the Agulhas Undercurrent (AUC) flow. The AUC appears to be a permanent northward flow in the vicinity of the continental slope beneath the Agulhas Current (Donohue et al., 2000) with mean transport of 4.2 ± 2.9 Sv, (Bryden et al., 2005a). Transport of NADW below 2000m within the current is 2.3 ± 3.0 Sv. A study by Casal et al., (2009) confirmed the presence of the AUC from Port Elizabeth (~36°S) to Port Shepstone (~32°S) along the South African coast (Fig. 2. 1).

The Natal Valley is filled with NADW rather than Circumpolar Deep Water (CPW), which dominates only farther to the east (Fig. 2. 2), (Wyrtki, 1971). NADW can also be found as far north as the Mozambique Channel (van Aken et al., 2004). However, the Natal Valley is closed to the north below 2250 m (Beal, 2009). Hence, while some upper NADW appears

to reach the Mozambique Channel via the AUC, most of the undercurrent's lower NADW must recirculate to the south (Beal et al., 2006). Arhan et al. (2003) estimate that from 11 Sv of NADW exiting the South Atlantic around South Africa, only 2 Sv flow northward into the Natal Valley and the rest flows eastward underneath the ARC.

In summary, the AUC is a robust feature, carrying intermediate water and NADW north-eastward below the south-westward flowing Agulhas Current. This is of particular interest because of the implications for the ventilation of the deep Indian Ocean via a direct influx of NADW around South Africa and northward via the AUC.

2.2. Background –Palaeoceanographic proxies used in this study

2.2.1. Stable isotopes in planktonic and benthic foraminifera

Foraminifera are marine organisms belonging to the phylum of amoebid protists (d'Orbigny, 1826) that live either on/or within the sediment surface (benthos) or are passively floating within the upper water column (plankton). They form a $CaCO_3$ shell whose isotope composition records both, the isotopic composition of ambient water and the temperature of the water they live in. The temperature dependency of oxygen isotope fractionation has been quantified already in the early 1950s (Urey, 1947; Epstein et al., 1953).

Emiliani used this discovery in 1955 first as a palaeothermometer tool on planktonic foraminiferal shells. However, later Shackleton (1967) showed that changes in $\delta^{18}O$ of seawater can also be caused by preferential trapping of light ^{16}O in continental ice sheets (ice-volume effect) and changes in the evaporation-precipitation balance (salinity effect) These additional influences complicate their use as pure temperature signal. For a detailed review on oxygen isotopes in foraminifera see Pearson (2012).

The $\delta^{13}C$ values recorded in benthic and planktonic foraminifera mainly reflects the carbonate isotope composition of the Dissolved Inorganic Carbon (DIC) of the ambient seawater in which these organisms calcified (Turner, 1982). $\delta^{13}C_{DIC}$ is affected by changes in the global carbon cycle and more local changes such as the relative mixture of water masses, air-sea gas exchange and the balance between photosynthesis and respiration in the water column (Kroopnick, 1985). Especially the $\delta^{13}C$ of benthic foraminifera is among the most frequently measured ratios and widely used as palaeocirculation proxy, as

changes in the deep-ocean $\delta^{13}C_{DIC}$ are partly depend on circulation changes (e.g., Curry and Oppo, 2005).

When interpreting $\delta^{13}C$ records of benthic foraminifera in terms of deep-water circulation changes several additional competing factors need to be considered. The rate of air–sea gas exchange has a temperature, alkalinity and salinity controlled component related to carbon isotope fractionation. The $\delta^{13}C$ in the atmosphere is on average 9 ‰ lower than that in the surface ocean and the extent of fractionation is a function of temperature, with higher $\delta^{13}C$ and gas exchange occurring at lower temperatures due to increased CO_2 solubility (Broecker and Maier-Reimer, 1992). In equatorial regions where there is a net transfer of isotopically light CO_2 from the ocean to the atmosphere surface waters become enriched in $\delta^{13}C$. Conversely, in regions where isotopically light CO_2 is entering the ocean such as the North Atlantic surface waters become depleted in $\delta^{13}C$ (Lynch-Stieglitz et al., 1995). Surface waters having experienced varying degrees of isotopic equilibration with the atmosphere are subsequently incorporated in deep and intermediate water, and thus different thermodynamic influences are mixed throughout the ocean (Charles et al., 1993).

Changes in the global terrestrial carbon reservoirs, storage of carbon enriched in ^{12}C in trees and soils on the continent, which on glacial to interglacial timescales is known to have a substantial effect on the global mean ocean $\delta^{13}C$ (Keigwin and Boyle, 1985; Matsumoto et al., 2001). The transfer of ^{12}C-rich carbon from the continents to the ocean by the reduction of terrestrial biomass due to expanding glacial ice masses and changes in the water balance is thought to reduce the global mean deep-ocean $\delta^{13}C$ values during the Last Glacial Maximum (LGM) by between 0.32 ‰ (Duplessy et al., 1988) and 0.46‰ (Curry et al., 1988).

Changes in productivity will impact on the benthic $\delta^{13}C$ values. Upwelled nutrient-rich deep waters encourage increased biological activity in the surface waters which results in an increased organic carbon flux low in $\delta^{13}C$ to the seafloor, which alters the local $\delta^{13}C$ signal of the deep-waters. In areas of strong seasonal productivity particulate organic matter, with $\delta^{13}C$ values 3-4‰ lower than the surface sediment organic carbon (Mackensen and Bickert, 1999) is rapidly deposited in a phytodetritus layer on the sea floor. This food supply is thought to trigger the chamber building and reproduction of the epibenthic species with the $\delta^{13}C$ values of their shells, formed during remineralization of this phytodetritus layer, recording $\delta^{13}C$ values that are up to 0.6‰ lower than the ambient

bottom water (Mackensen and Bickert, 1999; Zarriess and Mackensen, 2011). The flux of organic matter to the seafloor is also known to affect benthic foraminifera in different microhabitats. Endobenthically or infaunally living species such as *Uvigerina* spp. record the $\delta^{13}C$ of the pore waters rather than ambient bottom water $\delta^{13}C$ and have therefore $\delta^{13}C$ values that are depleted to ambient bottom water $\delta^{13}C$ (Zahn et al., 1986; Mackensen et al., 1993). Pore water $\delta^{13}C_{\Sigma CO2}$ is consistently lower than bottom water $\delta^{13}C_{\Sigma CO2}$ as organic matter decomposition in the sediments releases ^{12}C- enriched CO_2 to the pore waters (McCorkle et al., 1985).

2.2.2. Mg/Ca in planktonic Foraminifera: Palaeotemperature proxy

The substitution of Mg^{2+} for Ca during the formation of biogenic calcium carbonate in foraminifera shells is sensitive to temperature changes of the surrounding seawater during their growth. Foraminiferal Mg/Ca ratios increase with increasing temperature a discovery made already in the early 1950's by Chave (1954) and Blackmon and and Todd (1959). Studies predict an exponential temperature dependence on Mg/Ca uptake into calcite of approximately 3% increase in Mg/Ca per °C (Lea et al., 1999), which is consistent with inorganic calcite precipitation experiments (Katz, 1973; Mucci, 1987; Oomori et al., 1987.). Biologically mediated calcite precipitation in foraminifera also supports the exponential temperature dependency of Mg/Ca uptake however the Mg/Ca ratios of natural foraminiferal calcite are generally 1–2 orders of magnitude lower than those predicted for inorganic precipitates (Lea et al., 1999). This fact highlights that vital effects play an important role during biogenic calcification and stresses the need for species-specific Mg/Ca thermometry calibrations.

Three different types of calibration approaches have been used in the study of the temperature dependence of Mg uptake into planktonic foraminiferal tests: (i) Culture-based (e.g., Nürnberg et al., 1996; Lea et al., 1999) (ii) Sediment traps (e.g., Anand et al., 2003) (iii) Core tops (e.g., Elderfield and and Ganssen, 2000). Results obtained using different approaches are remarkably consistent and present an exponential dependence of temperature on the Mg/Ca in foraminiferal calcite in the form of:

$$Mg/Ca = B \exp(AT) \qquad \text{Equation (1)}$$

Where T is the calcification temperature and A and B are first order coefficients, in planktonic foraminifera a value of ~0.1 is used for the B coefficient and A varies with the species (Elderfield and and Ganssen, 2000).

Paired δ^{18}Oc and Mg/Ca ratios in foraminiferal calcite provide a way to adjust for the temperature-dependency of $\delta^{18}O_c$ and isolate the δ^{18}O of ambient seawater ($\delta^{18}O_{sw}$). The composition of seawater varies both as a function of global ice volume and local salinity differences. It has been shown that there is a linear relationship between the isotopic compositions of surface seawater and sea surface salinity (SSS), which, at low latitudes, is inversely related to precipitation amount (LeGrande and Schmidt, 2006). In palaeoceanography reconstructions of past SSS based on $\delta^{18}O_{sw}$ have widely been applied and use the modern–day relationship between salinity and $\delta^{18}O_{sw}$ to infer past changes in the hydrological cycle (Schmidt, 1999; Leduc et al., 2009).

2.2.3. Planktonic foraminiferal assemblage counts

Planktonic foraminifera assemblages in marine sediments reveal distinct biogeographic pattern (Bé and and Tolderlund, 1971). The maximum relative abundances of planktonic foraminiferal correlate with ecologic optima (Kucera, 2007) displaying the species preference for certain environmental conditions. For this reason, planktonic foraminifera assemblage studies have long been recognised as surface-water property tracers (Murray, 1897). Based on modern studies of the foraminifera assemblage and distribution in the Indian and Atlantic Ocean (Bé and and Tolderlund, 1971) the proportion of tropical and subtropical planktonic foraminifera species can be used as indicators of past temperatures and particularly water mass distributions.

2.2.4. Elemental analysis

X-ray Fluorescence (XRF) is an analytical technique used to evaluate the composition of rocks and sediments (Ramsey et al., 1995; Jenkins, 1999). This technique allows nondestructive extraction of near-continuous records of element intensities from sediments cores with a minimum of analytical effort. It is essential however, for quantitative applications involving mass-balance and flux calculations, to convert the element intensities measured by XRF core scanners to element concentrations. This approach remains problematic and therefore, results obtained by XRF core scanning are

usually presented in the form of count rates (expressed as counts per unit time per unit area), or as ratios of counts, which only permit estimation of their relative abundances (Richter et al.; Rothwell, 2006). XRF analysis is based on excitation of electrons by incident X-radiation. Ejection of electrons from inner atomic shells creates vacancies, which are filled by electrons falling back from the outer shells, whereby surplus energy is emitted as a pulse of secondary X-radiation. Emitted fluorescence energy and wavelength spectra are characteristic for atoms of specific elements, which permit estimation of their relative abundance (Weltje and Tjallingii, 2008). XRF scanning derived intensities of terrestrial elements in marine sediment cores have been applied in many studies to trace the supply of terrestrial material to the ocean. In particular, Fe-XRF counts have been used in palaeoceanographic studies as a proxy for varying river discharge in tropical regions (e.g., Adegbie et al., 2003; Arz et al., 1998; Schefuß et al., 2011).

2.2.5. Organic geochemical proxies

Molecular organic geochemical proxies are increasingly being utilized to reconstruct past environmental conditions as organic matter preserved in geologic materials provides a direct indicator of environmental conditions at the time of deposition and thus is important to palaeoenvironmental studies. Individual compounds, or compound classes (biomarkers), preserved in geological materials can be traced to a particular source organism, group of organisms, or to a particular process (e.g., photosynthesis). Biomarkers allow for the examination of certain groups of algae and microorganisms that lack hard silica or carbonate shells and typically are absent from the fossil record.

2.2.6. UK'_{37} index: Palaeotemperature proxy

Alkenones are highly resistant organic compounds (ketones) produced by phytoplankton of the class *Prymnesiophyceae*. Marine coccolithophorid *Emiliania huxleyi,* for example, produces these long-chain (C_{37}, C_{38}, C_{39}), primarily di- and tri-unsaturated methyl and ethyl ketones (Brassell et al., 1986). Laboratory cultures experiments with algae showed that the degree of unsaturation in the ketone series biosynthesized depends on growth temperature (Brassell et al., 1986). Coccolithophoroids respond to changes in water temperature by altering the production of long-chain unsaturated alkenones in the structure of their cell. At higher temperatures, more of the di-unsaturated molecules are produced than tri-unsaturated (Prahl and Wakeham, 1987). The modified Unsaturation

Index of di versus tri unsaturated C_{37} alkenone is calculated according to the following relationship from Prahl and Wakeham (1987):

$$UK'_{37} = C_{37:2}/(C_{37:2} + C_{37:3}) \qquad \text{Equation (2)}$$

The unsaturation index can then be used to estimate the water temperature.

2.2.7. Stable hydrogen isotopic (δD) composition of long chain alkenones- proxy for palaeosalinity

Studies have shown that the δD of C_{37} alkenones of *E. huxleyi* and other common oceanic haptophyte algae, largely depend on salinity, the δD of water, which is correlated to salinity as well and to some degree to growth rate (Schouten et al., 2006). Salinity changes, therefore, form a key aspect of changes in the δD of C_{37} alkenones, suggesting it could be useful as a palaeosalinity proxy. A variety of studies have applied the hydrogen isotopic compositions of long-chain alkenones to record freshwater flooding in marine environments (van der Meer et al., 2007; van der Meer et al., 2008; Leduc et al., 2009).

2.2.8. Marine crenarchaeotal membrane lipids: a tool for reconstructing ancient sea water temperatures

Glycerol dialkyl glycerol tetraether (GDGT) lipids are membrane lipids, which were thought for decades to be exclusively synthesized by extremophilic archaea (Schouten et al., 2013 and references therein). Archaea, the second domain of the prokaryotes in addition to Bacteria, are exceptional since they synthesize membrane lipids in which isoprenoid (a common organic compound) rather than straight chain carbon skeletons are ether bound to glycerol. The membranes are made up of fatty acids esterified to glycerol containing a polar head group such as phosphocholine, phosphoethanolamine and sulfoquinovose. Culture experiments with hyperthermophilic archaea established early on that growth temperature had an effect on the distribution of GDGTs, i.e., an increasing number of cyclopentane (an alicyclic hydrocarbon) moieties (a part or functional group of a molecule) with increasing temperature (Lai et al., 2008; Boyd et al., 2011).

Schouten et al. (2002b) introduced the TEX_{86} (tetraether index of tetraethers consisting of 86 carbons) as a sea surface temperature proxy based on the membrane lipids of mesophilic marine Thaumarchaeota (phylum of the Archaea). It is based on the idea that

temperature is one of the main factors influencing the relative number of cyclopentane moieties, as well as the distribution of cyclopentane moieties in GDGTs in marine surface sediments varies of the upper mixed layer of the ocean and showed that for SST between 5 and 30 °C between different latitudes. Kim et al. (2008) further developed the initial linear core top calibration of TEX_{86} of Schouten et al. (2002) to a more extensive, global core top dataset. This calibration study supported the initial finding that TEX_{86} relates well to annual mean temperature.

2.2.9. Branched isoprenoid tetraether index -a tracer for soil organic matter

The branched isoprenoid tetraether (BIT) index is a proxy for the relative abundance of terrestrial organic matter (OM), (Hopmans et al., 2004). Branched GDGT seems to occur predominantly in the terrestrial environment (i.e., soils, peats, lakes and rivers), while crenarchaeol is thought to be the dominant GDGT in the marine environment. Consequently, index ratios are close to 1 in soils and peats, whereas values close to 0 are found in open marine sediments (Hopmans et al., 2004). Later studies showed that the index was not as much a measure of total terrestrial OM but rather a measure of only soil OM, since branched GDGTs were ubiquitously present in soil (Weijers et al., 2006) and the index did not correlate well with other terrestrial proxies ($\delta^{13}C_{org}$) in sediments (Huguet et al., 2007). The BIT index has therefore been frequently used to trace the input of soil OM via fluvial transport into marine environments (Kim et al., 2006; Herfort et al., 2007; Kim et al., 2012).

2.3. Core Chronology

The core chronologies produced for the sediment cores presented here are based on radiocarbon dating in the upper parts of the records. Radiocarbon dating is a radiometric dating technique that uses the decay of carbon-14 (^{14}C). It has a half-life of 5730 years making it a valuable tool in the construction of chronologies in deep sea sediments for the last 40 kyr (Stuiver, 1998).

Radiocarbon is a cosmogenic isotope that is formed in the atmosphere by cosmic radiation interacting in a neutron reaction with atmospheric nitrogen (^{15}N). The radiocarbon formed in the upper atmosphere is mostly in form of CO_2 molecules that then enter the global carbon cycle, including the ocean in the form of DIC.

The ^{14}C age determined by AMS radiocarbon dating assumes that the concentration of radiocarbon in the atmosphere has remained constant in the past (Pilcher, 1991). Studies showed that the atmospheric levels of ^{14}C have fluctuated markedly, both in production and concentration over the past 50 kyr. Therefore dates have to be calibrated for the potential variability of ^{14}C production in the atmosphere as a result of magnetic field intensity and solar variability (Stuiver and Braziunas, 1993) and/or changes in the partition of ^{14}C between the different reservoirs, particularly the ocean (e.g., Siegenthaler and Sarmiento, 1993).

The mixing time between the surface and the deep ocean is very slow and therefore ^{14}C in the deep ocean can decay without any replenishment (Lowe and and Walker, 1997). The average difference between a radiocarbon date of a terrestrial sample such as a tree, and a shell from the marine environment is about 400 radiocarbon years (Stuiver and Braziunas, 1993). This apparent age of oceanic water is caused both by the delay in exchange rates between atmospheric CO_2 and ocean bicarbonate, and the dilution effect caused by the mixing of surface waters with upwelled deep waters which are very old (Mangerud, 1972). This phenomenon is known as the marine reservoir effect.

It was generally assumed that the reservoir effect was about 400 years in all the oceans, but it is now known that the size of the effect varies geographically and through time. Surface water ^{14}C of the North Atlantic is approximately 400 years (Bard, 1988; Bard, 1991) older than the atmosphere ^{14}C, deep waters in the Pacific Ocean for example are apparent 2000 years older. This is because certain deep waters have been separated from the atmosphere for longer and are thus of an older radiocarbon age (Stuiver and Braziunas, 1993).

Other possible biases on radiocarbon dating can result from bioturbation (Keigwin and Guilderson, 2009), fragmentation and differential dissolution effects (Barker et al., 2007; Mekik, 2014).

2.4. Methodology

2.4.1. Sediment processing and analytical approach

Marine sediment core CD154 17-17K recovered 363 cm and CD154 10-06P 969 cm of sediment mainly composed of foraminiferal ooze. The cores was sliced and sampled at 1cm intervals, the wet sediment was weighed, disaggregated on a rotating wheel for approximately 24 hours, washed over a 63 μm sieve using fine water spray and dried in the oven at 40 ° C. The fine (<63 μm) and coarse (>63 μm) fractions were then weighed for the calculation of the weight % of the coarse and fine fractions. Between 4-5 g of the dried fine fraction were weighed into jars and processed for sortable silt grain size measurements. The coarse fraction was dry sieved into narrow size ranges and different planktonic and benthic foraminifera species were then picked and processed for stable isotope and Mg/Ca analysis. The samples were first sieved to separate the fine and coarse fraction, with the fine fraction being used for grain-size analysis (not discussed) and the coarse fraction for isotope and trace element analysis.

A turbidite was detected during sampling in core CD154 10-06P in the interval 490-440 cm through visual inspection (Fig. 2. 3a). A turbidite is the geologic deposit of a turbidity current, which is a type of sediment gravity flow responsible for distributing clastic sediment into the deep ocean. Samples in that interval were noticeably sandy. Moreover, the colour contrast between the undisturbed and disturbed sediment interval is obvious in the image of the core section (Fig. 2. 3a). The turbidite is also evident in the coarse fraction weight %, showing a rapid increase. A sharp drop in the L* record is also evident (Fig. 2. 3b-d). As such, the identified turbidite interval (~50 cm) was not used for the palaeoceanographic records. The age model construction was performed on the new adjusted composite depth of core CD154 10-06P thereafter.

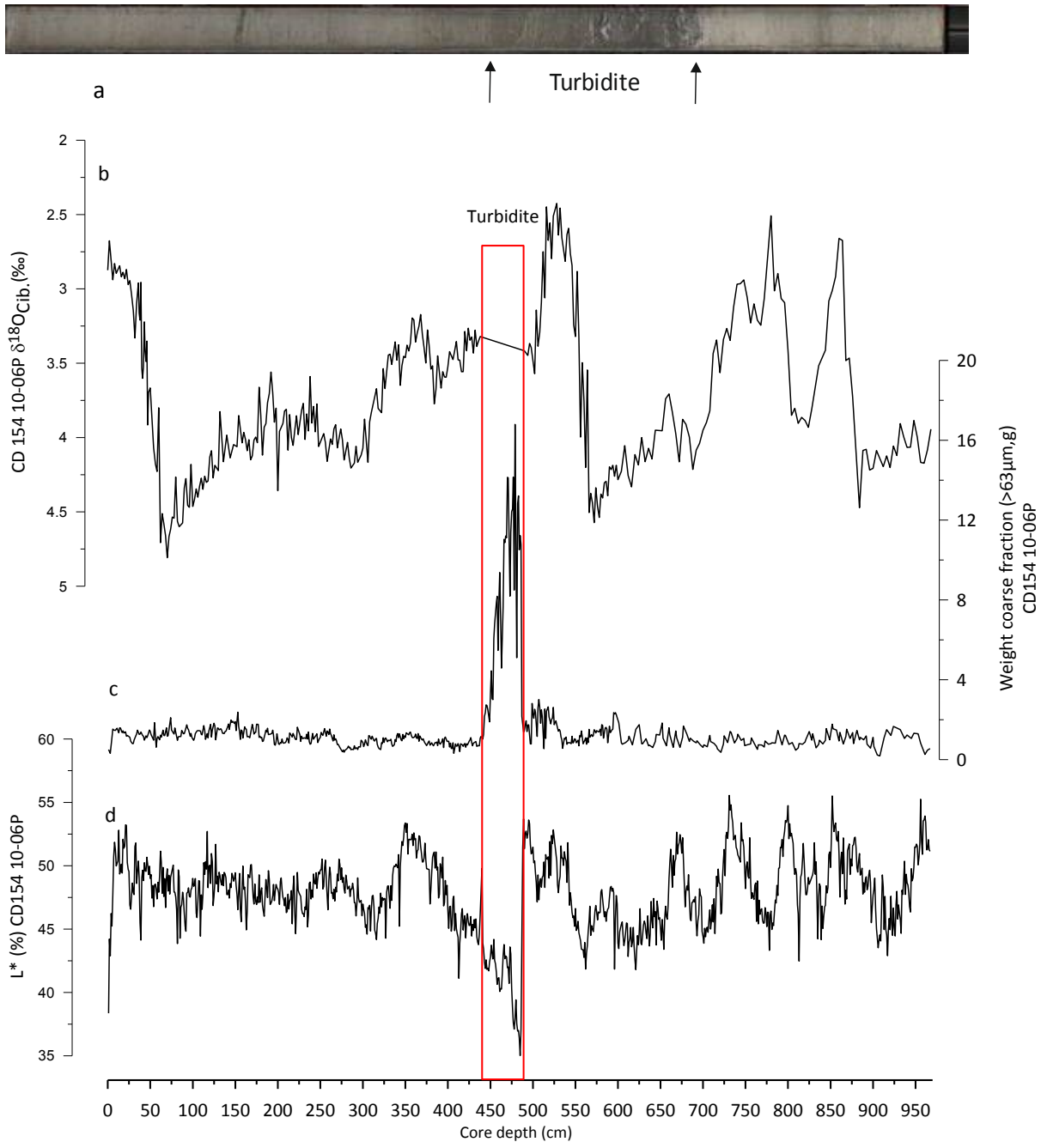

Fig. 2. 3 (a) Core section from 527-377 cm containing turbidite of core CD154 10-06P. Onset and ending of the turbidite is labelled. Core length of marine sediment core CD154 10-06P with intervals highlighted (red box) which is affected by turbidite (b) Benthic isotope record of CD154 10-06P (c) Weight coarse fraction in gram (d) L* (light reflectance) record.

2.4.2. Stable Isotope Analysis (Planktonic and Benthic foraminifera)

Combined stable oxygen isotope ($\delta^{18}O$) and Mg/Ca measurements in the planktonic foraminifera species *Globigerinoides ruber* (sensu stricto; this morphotype is characterised by spherical chambers in the last whorl located symmetrically over previous sutures with a wide, high arched aperture) (Wang, 2000) are here used to reconstruct changes in the

surface hydrography of the Agulhas Current (Chapter 3-5). Around 30-60 individuals were picked from the 250-315 μm size fraction every 2 cm along core CD154 17-17K (363 cm total length) providing a temporal resolution of ~0.5 ka over the last 100 kyr. Along core CD154 10-06P samples were picked every 1 cm in upper part of the core (0-76cm) providing a temporal resolution of 0.2 ka over the last 21 kyr and every 4 cm between 76-152cm and every 8 cm thereafter (see age models section 2.8.2).

G. ruber is a typical warm water species, which is highly abundant in the tropical-subtropical waters of the Indian Ocean and makes up to 40-60 % of the planktonic foraminiferal assemblage of the Agulhas Current today. *G. ruber* is a spinose, symbiont-bearing species which inhabits surface (0–50 m) waters (Fairbanks et al., 1980; Erez and Honjo, 1981; Hemleben et al., 1989; Ravelo and Fairbanks, 1992; Peeters and Brummer, 2002; Peeters et al., 2002). A study of calcification depths of planktonic foraminifera in the tropical Indian Ocean showed that *G. ruber* calcifies within the mixed-layer, between 20-50 m (Mohtadi et al., 2009; Birch et al., 2013).

Epibenthic foraminifera *Cibicidoides mundulus* (Brady, Parker & Jones, 1888) and/or *Cibicides wuellerstorfi* (Schwager, 1866) were chosen for benthic stable isotope analyses because they live on the sediment surface (Lutze and Thiel, 1989) and therefore they are expected to directly record ambient near surface bottom water chemical and isotope composition (Duplessy et al., 1984). In this study, three to ten tests of epibenthic foraminiferal species *Cibicidoides* spp. were picked in core CD154 10-06P from the 250-315 μm size fraction or < 250 μm in sections of low abundance of *Cibicidoides* spp. A study by Ruiz et al. (2013) showed that shell size does not influence the isotopic composition of *Cibicidoides* spp. Measurements were performed, if enough material was available, at 2cm intervals until 550 cm core depth and thereafter every 4 cm (Chapter 4).

Stable isotopes were measured using either a ThermoFinnigan MAT 252 mass spectrometer linked online to a Carbo Kiel II carbonate preparation device (long-term external precision is 0.06‰ for $\delta^{18}O$ and 0.02‰ $\delta^{13}C$) or a Thermo Scientific Delta V Advantage mass spectrometer coupled with a Gas Bench III automated preparation device (long-term external precision is 0.08‰ for $\delta^{18}O$ and 0.06‰ $\delta^{13}C$) depending on the sample size. The stable isotope measurements were expressed relative to the Vienna Peedee Belemnite scale (VPDB) through calibration with the NBS 19 carbonate standard.

2.4.3. Mg/Ca measurements in planktonic foraminifera

Samples for Mg/Ca analysis were prepared and cleaned following the protocol outlined by Barker et al. (2003). The cleaning comprised several steps which is intended to remove potential contaminants: (i) the clay removal step involved repeated UHQ water and methanol rinses aided by intervals of ultrasonication (ii) the oxidation step aimed to remove the organic matter by oxidation, this was achieved using alkali (NaOH 0.01M) buffered 1% H_2O_2 (iii) the dilute acid leach step (0.002M HNO_3) is done with the purpose of removing authigenic Mn-Fe coatings on the foraminifera shells and was only done once. Between step (ii) and (iii) the samples were taken out of the centrifuge tubes into a slide with a cavity and were screened under a light microscope for any remaining coarse-grained silicate particles and discoloured foraminiferal calcite that had not been removed by the cleaning steps. These were taken out using a single-lash brush and were introduced back into centrifuge tubes. When the three cleaning steps were completed the samples were dissolved in 120 µl of 0.065M HNO_3 and centrifuged to remove any remaining small silicate particles. Samples were transferred to clean vials before stages involving acid and two water rinses were carried out in between each step

The samples were analysed using a Thermo Element XR High Resolution Inductive Coupled Plasma Mass Spectrometer with a long-term precision of element ratios, determined by replicate analyses of standard solutions containing Mg/Ca = 1.15 mmol mol^{-1} and Mg/Ca = 6.9 mmol mol^{-1}, of ±1.25 % and ±0.52 % respectively.

The Mg/Ca of *G. ruber* were converted to calcification temperature using the calibration by Anand et al. (2003):

$$T=(1/0.09)*\ln((Mg/Ca)/0.449) \qquad \text{Equation (3)}$$

Where T is the calcification temperature. The standard error associated with this calibration is ±1.1 °C on the temperature estimates. The Anand et al. (2003) Mg/Ca calibration equation was used because (i) the calibration used foraminifera tests from a very similar size fraction (250-350 µm) as this study (250-315 µm) and (ii) inter-laboratory comparisons have shown that Mg/Ca results are dependent on the procedure used to clean foraminifera shells (Rosenthal et al., 2004) and, similar to this study, Anand et al. (2003) used the cleaning procedure from Barker et al. (2003).

2.4.4. Quality control for Mg/Ca measurements for core CD154 17-17K/CD154 10-06P

To monitor sample cleaning, Fe, Mn and Al concentrations (Boyle, 1983; Barker et al., 2003; Pena et al., 2005) were measured in each sample and in protocol blanks that were routinely run between samples. Co-variability of the Mg/Ca record with metals such as Fe and Al was used to assess whether trace metal contamination might have altered the primary Mg/Ca signal (Barker et al., 2003; Boyle, 1983; Pena et al., 2005). Based on this quality control 7 samples were rejected out of the total of 180 included within the data set in core CD154 17-17K (Fig. 2. 4a,b). Moreover, one more sample, with particularly low Mg/Ca ratios, was rejected as its value falls out of the 2σ standard deviation range of the entire dataset (Fig. 2. 4).

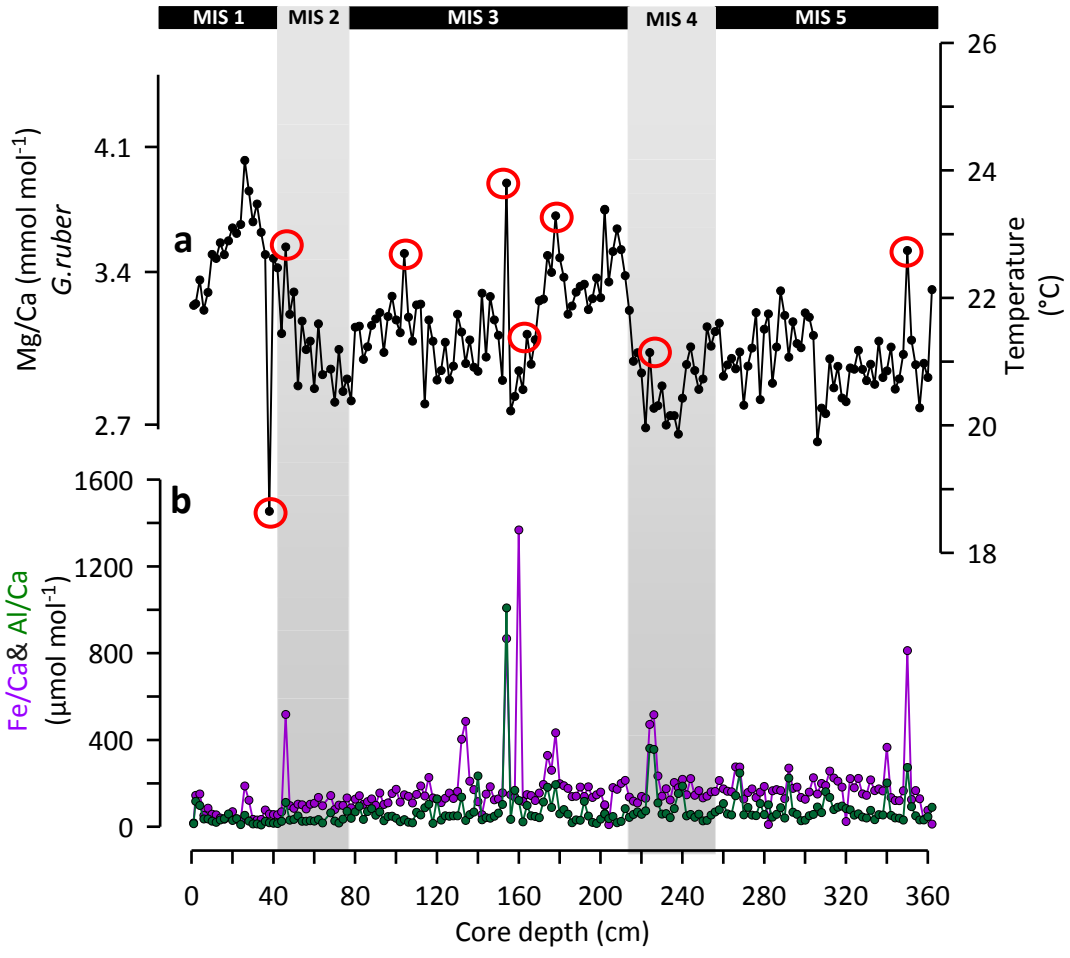

Fig. 2. 4 Quality control for Mg/Ca measurements and Sea surface temperature (SST) estimates along the core depth (cm) for core CD154 17-17K (a) Mg/Ca (µmol mol^{-1}) (black) with SST estimates from Mg/Ca (black), (b) Fe/Ca (purple) and Al/Ca (green). Circles represent data points that were rejected due to possible contamination.

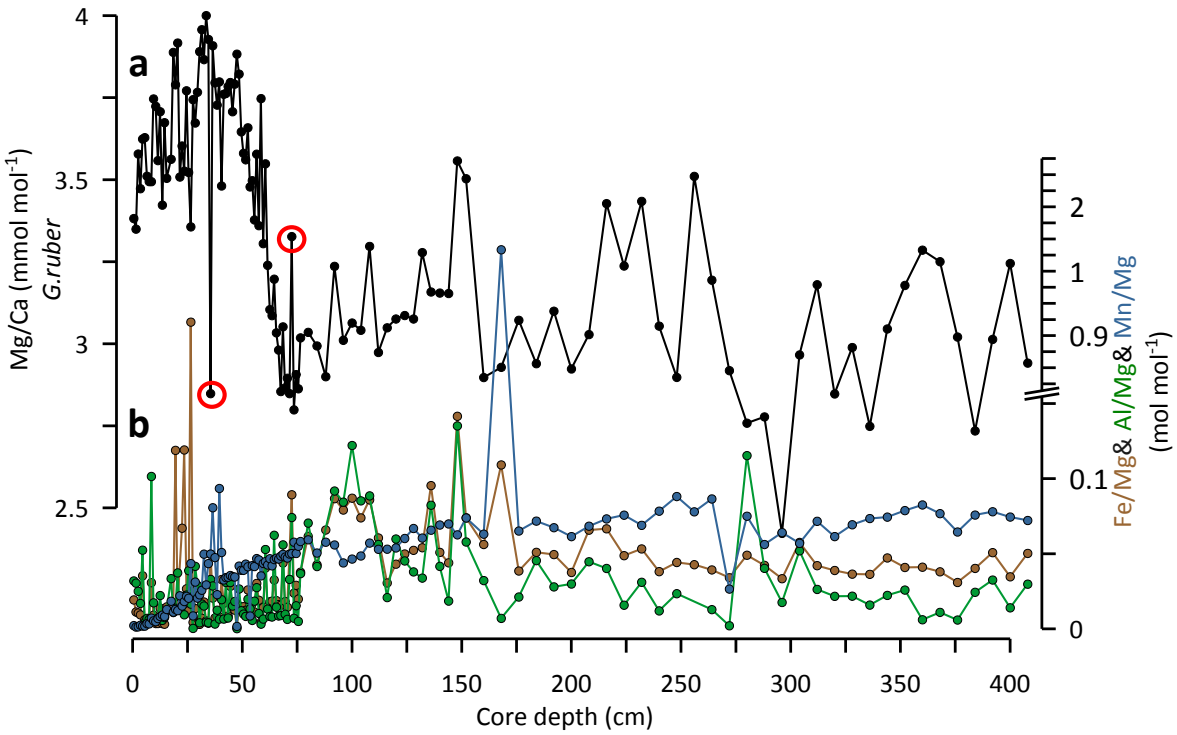

Fig. 2. 5 Quality control for Mg/Ca measurements in core CD154 10-06P (a) *G. ruber* Mg/Ca ratios (mmol mol^{-1}) (black circle) (b) Fe/Mg (mol mol^{-1}) (black), Al/Mg (mol mol^{-1}) (green) and Mn/Mg (mol mol^{-1}) (blue) ratios, red circled samples have been removed from the data set.

Fe/Mg and Al/ Mg can be used to monitor the potential influence of silicate contamination in foraminiferal Mg/Ca whereas Mn/Mg can determine potential contaminiation through Mn-Fe oxide coatings (Barker et al., 2003). Values above 0.1 for those elemental ratios suggest contamination may be significant. Elevated Fe/Mg ratios (> 0.1) are occurring in the core interval 20-27 cm of core CD154 10-06P but do not seem to co-vary with higher Mg/Ca ratios. For that reason no samples in this core interval have been rejected. However, high XRF-scanning Mn counts and pyrite (during sample examination) have also been detected in parts of that interval (Fig. 2. 10) which suggest that foraminferal shells have oxide coatings due to redox processes which occurred in the deep-sea. One sample (35.5cm) with particularly low Mg/Ca ratios, was rejected as its value falls out of the two sigma standard deviation range of the entire dataset. Co-variability of the higher Mg/Ca values with elevated Al/Mg and Mn/Mg in the deeper part of the core section let to the rejection of one more sample (Fig. 2. 5).

2.4.5. Estimation of carbonate dissolution in CD154 17-17K

The accuracy of Mg/Ca-based SST (and $\delta^{18}O$) reconstruction can be affected by dissolution (e.g., Barker et al., 2005). Previous studies showed evidence from core top samples that planktonic foraminiferal Mg/Ca is susceptible to post depositional alteration on the seafloor through under-saturated bottom or pore waters (Rosenthal and Boyle, 1993; Russell et al., 1994; Brown and Elderfield, 1996; Rosenthal et al., 2000). The preferential dissolution of high Mg/Ca regions of the test causes a reduction in those sections of the foraminiferal shell formed in warmer waters (Brown and Elderfield, 1996; Rosenthal et al., 2000). This will bias the mean test Mg/Ca values towards colder temperatures. Although dissolution and fragmentation can affect planktonic faunal assemblages and corresponding SST estimates based on foraminifera assemblage counts (Le and Thunell, 1996; Kimoto et al., 2003) this is unlikely to dominate the signal in the faunal records. For example, the 'warm' interval of Heinrich Stadial (HS) 6 (~63-60 ka) displays moderate dissolution (fragmentation of up to 50 %, Fig. 2. 6e) but at the same time a high percentage of ALF, (see Chapter 3, Fig. 3.2f) which mainly consists of warm, tropical species. Warmer species tend to have more fragile shells and might be expected to fragment earlier through dissolution (Berger, 1970). Hence a decrease in these species during HS 6 might be expected if dissolution were a dominating control. However, ALF abundances reach up to 30-45 % during HS 6 in the record.

Core site CD154 17-17K at 3333 m water depth is above the modern calcite saturation horizon in the eastern equatorial Indian Ocean (Peterson and Prell, 1985). A study from the eastern Indian Ocean (Martinez et al., 1998) showed that for the region south of 15 °S, the foraminiferal calcite saturation horizon presumably is deeper than the maximum sampling depth in this study, i.e., 3600 m. However, the depth of the calcite saturation horizon is known to vary through time and thus dissolution can occur above it leading to a carbonate loss of 20-30 % before reaching the depth of the actual horizon (Peterson and Prell, 1985). Regenberg et al. (2006) used core tops from the Caribbean to show that the onset of selective Mg^{2+} removal starts to take place considerably above (between 2000–3000 m water depth) the present-day calcite saturation horizon (~4600 m). Moreover, the depth of the foraminiferal calcite saturation horizon has varied considerably during past glacial-interglacial cycles leading to variable foraminiferal preservation within the sediment (de Villiers, 2005). In order to gain a first order impression of the potential

impact of dissolution on the core site the carbonate ion saturation, Δ[CO3=], a measure of calcite saturation of the deep-water overlying the core site for the modern state (Regenberg et al., 2006), was calculated. This was achieved using the CO2SYS program (Pelletier et al., 2005) and employing the Global Ocean Data Analysis Project (GLODAP; (Key et al., 2004) and World Ocean Atlas data 2009 (Locarnini et al., 2010) according to the method described by (Yu and Elderfield, 2007). At our core site the calculated modern Δ[CO3=] value is 0 µmol/kg and is equivalent to the value which is defined as calcite saturation horizon. As already described above, dissolution can affect foraminiferal preservation above the calcite saturation horizon as shown by Regenberg et al. (2006), starting at critical level of Δ[CO3=] ~20 µmol/kg. In comparison, a study by Johnstone et al. (2011) revealed that cores (~4000 m deep) from the western Indian Ocean, north of Madagascar, used previously to study tropical Indian Ocean surface hydrography (Kiefer et al., 2006), were significantly affected by dissolution displaying Δ[CO3=] of ~ -12 µmol/kg.

There are several additional ways to reconstruct the history of carbonate dissolution in marine sediments. A problem inherent in each of the dissolution parameters is that none of them are exclusively related to dissolution alone, instead they also respond to changes in ecological and sedimentological factors (Barker, 2006). As such a combination of four measured dissolution indices has been used to evaluate potential influences of carbonate dissolution on the Mg/Ca ratios (Fig. 2. 6a). Briefly, they are: (i) fragmentation index, (ii) % coarse fraction, (iii) Ca-X-ray Flouresence counts of the bulk sediment, and (iv) shell weights of *G. ruber* (Fig. 2. 6b-e).

Shell weights of *G. ruber* were determined. A total of 30-60 individuals were picked from the size fraction 250–315 µm for combined stable isotope and trace element analysis. These samples were weighed prior to analysis using Sartorius microbalance (precision ±1 µg), (Fig. 2. 6b). The total weight was divided by the number of individuals to obtain a weight estimate for individual shells within a narrow size fraction. Previous studies have shown that the initial shell weight of foraminifera might vary due to other controls than dissolution, e.g., optimal growth rate (de Villiers, 2004), or Δ[CO3=] state (Barker et al., 2005; Marshall et al., 2013).

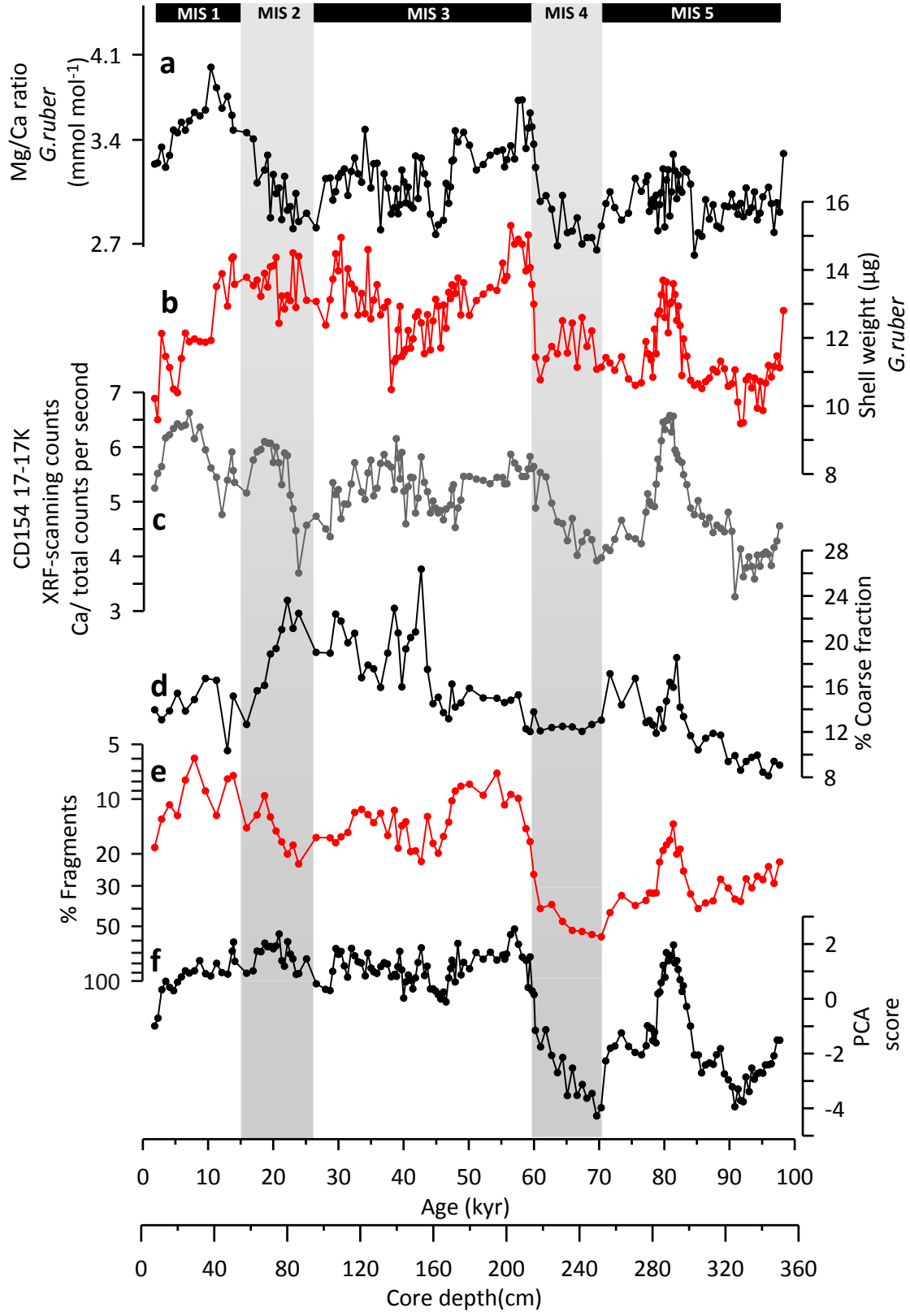

Fig. 2. 6 Estimate of carbonate dissolution in core CD154 17-17K (a) Mg/Ca (mmol mol^{-1}) *G. ruber* (black), (b) *G. ruber* shell weight (µg), (red) (c) XRF-scanning counts Ca/ total counts, (grey) (d) Coarse fraction %, (>63 µm), (black) (e) % foraminiferal fragments, (red) (f) Principal component analysis scores, (PCA), (black).

The weight % of coarse fraction (>63 μm) is sensitive to dissolution at the seafloor but also to primary changes in the dominating organisms that are deposited at the core site (e.g., the relative contributions from diatoms, coccolithophores and foraminifera). A lower weight % of coarse fraction in the sediment might result from greater dissolution or, for example, a lower relative contribution of organisms with large shells such as foraminifera, versus smaller particles (Fig. 2. 6d).

Foraminiferal Fragmentation Index, (FI) was calculated after Le and Thunell (1996). It contains a devisor relating the number of fragments to the number of tests, so that the percentage fragmentation is more likely to respond linearly to dissolution (Fig. 2. 6e).

Variations in Ca (Calcium)-XRF counts (see section 2.2.4. and 2.4.9. for further method description) are used as proxies for calcium carbonate content in the sediment record (Fig. 2. 6c). Scanning Ca-XRF records have been successfully applied in a large number of palaeoceanographic studies as a proxy for varying calcium carbonate content, biogenic carbonate flux and preservation in marine sediments (Peterson et al., 2000; Bozzano et al., 2002).

An R-mode Principal Component Analysis (PCA) was performed on all the four measured dissolution indices in the down core record to derive a Composite dissolution index (CDI) according to the approach used by (Peterson and Prell, 1985), (Fig. 2. 6f). The PCA was then used to partition the common variance attributable to dissolution in the data set and can serve as an indication of relative dissolution intensity in the down core record. The first principal component, by definition, is linearly independent eigenvector positioned through the direction of maximum variance within the original data. The CDI is simply the first component from the analysis of the four dissolution indicators. The CDI in this record explains 62.3 % of the variance in the raw data. This extremely high concentration of information in the first component suggests that dissolution is likely to be the dominant process modifying the character of carbonate sediment out our core site.

2.4.5.1. Adjustment for dissolution in core CD154 17-17K

The unexpectedly low values of foraminiferal Mg/Ca during the Holocene, MIS 4 and MIS 5a and MIS 5c (Fig. 2. 6a) are coeval with intervals of increased fragmentation, lower shell weights, lowered coarse fraction percentage, as well as lower Ca-XRF counts (Fig. 2. 6b-e).

This is likely to be a result of partial dissolution following deposition (Barker et al., 2005). As ideally it is preferable to adjust the record of Mg/Ca for the effects of dissolution rather than simply discard the intervals affected by potential dissolution. Various approaches have been described in order to adjust Mg/Ca records for the effects of dissolution (Lea et al., 1999; Dekens et al., 2002; Rosenthal and Lohmann, 2002; Barker et al., 2005; Mekik et al., 2007; Barker et al., 2009).

After assessing different possibilities to adjust the Mg/Ca record of CD154 17-17K the approach of Rosenthal and Lohmann (2002) has been followed here. This involves incorporating test weight variability into temperature reconstructions. This approach seems to be the most appropriate method for these data as an adjustment based on the CDI leads to an overcorrection of Mg/Ca values during MIS 4, which results in unrealistically warm temperatures during this cold period as compared with the faunal estimates and previous studies from the region (Kirst et al., 1999).

De Villers (2005) demonstrated that variations in the shell weight of planktonic foraminiferal species *G. ruber* in core tops from Indian Ocean are largely controlled by dissolution of sedimentary calcite overlain by corrosive bottom waters. However, a recent study (Marshall et al., 2013) showed that changes in surface [CO3=] is responsible for 89 and 86 % of the variability of calcification efficiency for both *G. ruber* (pink) and *G. sacculifer*, respectively. If changes in surface [CO3=], caused by varying atmospheric CO_2 levels, were the main control on the *G. ruber* shell weight record then it would be expected that low values occur during interglacial MIS 5 and high values during the LGM, (given that all of the other indicators of dissolution suggest that the level of carbonate preservation was approximately the same for these two intervals). However, shell weights of *G. ruber* between 75-85 ka, (Fig. 2. 6b) are as high as during the LGM, suggesting that changes in the carbonate ion concentration in surface waters are unlikely to be the main control on shell weights in CD154 17-17K. It is also noted that all dissolution indices suggest increased dissolution over the course of the Holocene. This is in keeping with previous studies from the global ocean (Broecker and Clark, 2003). Therefore, acknowledging this potential caveat, a shell-weight based adjustment seems to be the most appropriate because this approach is based on the same species and material that the Mg/Ca measurements were performed on. Moreover, this adjustment term is not static and can instead change temporally. That's important as the factor controlling the

dissolution can change over time. The final shell weight is the product of any dissolution that may have impacted the shell.

Dissolution adjusted temperatures were derived using a calibration for Mg/Ca-palaeothermometry in which the pre-exponent constant is a function of shell weight for *G. ruber* (Rosenthal and Lohmann, 2002):

$$Mg/Ca_{G.ruber} = (0.025\ wt + 0.11)\ e^{0.095T}) \qquad \text{Equation (4)}$$

In this study the A component (0.095) was adjusted to 0.090, which is the same used for *G.ruber* by Anand et al. (2003).

2.4.5.2. Estimation of carbonate dissolution in CD154 10-06P

At a water depth of 3076 m marine sediment core CD154 10-06P could be influenced by post-depositional calcium carbonate dissolution as it has been shown and assessed in detail above for core CD154 17-17K located at a similar water depth (3333 m) and ~ 400 km to the south. However, CD154 10-06P is shallower compared to CD154 17-17K and might be less impacted by dissolution processes as Mg/Ca ratios continuously decreasing with increasing water depth (Regenberg et al., 2014).

Mg/Ca ratios in this study display a minor decreasing trend towards lower values from ~50 cm towards the core top (Fig. 2. 7a). This pattern co-varies with decreasing Ca-XRF counts in the same interval but counts decrease later (Fig. 2. 7b). Shell weights are variable in this section but no clear decline in the shell weights would suggest a large impact of dissolution on the foraminiferal shell weights despite from potentially 160-220 cm (Fig. 2. 7c). These findings suggest that over the course of the Holocene carbonate dissolution as well as SST cooling of the Agulhas Current itself (Hutson, 1980) might have influenced the reconstructions in this study contemporary. Therefore the same approach as in core CD154 17-17K is followed and the dissolution adjustment of Rosenthal and Lohmann (2002) in which the pre-exponential constant of the paleothermometry equation is a function of the shell weight of *G. ruber* with a modified exponential constant A is applied here: ($Mg/Ca_{G.\ ruber}$ = (0.025*shell weight + 0.11) $e^{0.090T}$ (Fig. 2. 7a). Measured shell weights are a composite signal of dissolution related weight loss (Lohmann, 1995; Broecker and Clark, 2001) superimposed upon initial shell weight variability (Barker and Elderfield, 2002).

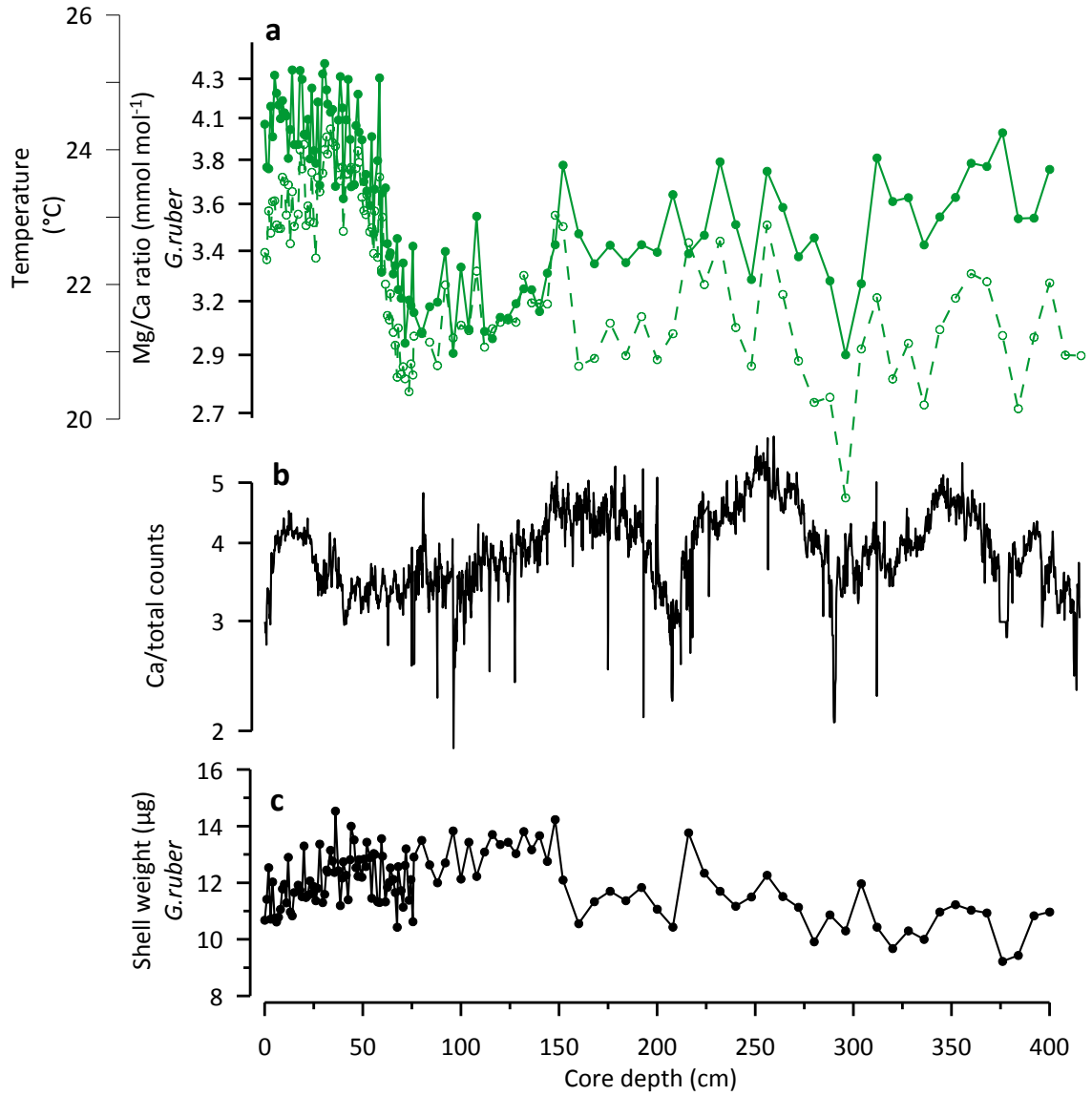

Fig. 2. 7 Evaluation of post-depositional calcium carbonate dissolution impact on Mg/Ca measurements (a) *G. ruber* Mg/Ca ratios (mmol mol^{-1}). (open green circle), dissolution adjusted SST (green circle) (b) XRF-scanning counts Ca/total counts per second (3 point running mean, black) (c) *G. ruber* shell weight (µg), (black circle).

2.4.5.3. Reproducibility of the planktic foraminiferal Mg/Ca data and error analysis

The error on the reproducibility of the cleaning protocol was calculated by picking a large sample of approximately 1000 individuals from the Holocene section of core CD154 17-17k, each of them was crushed and homogenised and in turn split into 7 aliquots. The 7 samples were cleaned and run separately. All the Mg/Ca values yielded values within 4.6 %RSD (1σ). The deviation for Mg/Ca is better considered with respect to calcification temperature. Using the Mg-calibration equation of Anand et al. (2003) the calculated

average temperature for these separate samples was 21.54 ±0.5°C (1σ). This variability is within the error generally quoted for Mg/Ca thermometry (±0.5–1°C).

The Mg/Ca data from core CD154 17-17K were tested for reproducibility by replicating analyses of ~20% of the record. Samples (*N*=34) were re-picked in core interval 210-270 cm, crushed, cleaned, and analysed for Mg/Ca ratios (Fig. 2. 8). Average standard deviation between the original and the replicated samples was 0.2 mmol/mol (7.2% RSD) that results in an average temperature deviation of ± 0.8C (3.8%) when calibrated with Anand et al. (2003). These values include artefacts associated with picking, cleaning, and natural variability of the *G. ruber* populations. Hence, a standard error propagation calculation is followed in order to propagate these uncertainties along with those associated with the conversion of Mg/Ca to calcification temperatures (±1.13 °C) and the analytical procedures involved in the Mg/Ca measurements (0.88% RSD = ±0.1 °C). The resulting mean error for palaeotemperature is ± 1.3 °C for both cores.

The effect of changing carbonate ion concentration of the surface ocean and salinity on the *G. ruber* Mg/Ca data was not considered as additional source of uncertainty here, given that the changes in these components during the geological past are not well constrained. However, a recent study suggests a Mg/Ca-sensitivity to salinity of 3.3%± 1.7% per salinity unit for the foraminiferal species *G. ruber* (Hönisch et al., 2013). Glacial salinity was ~3% (~1psu) higher compared to the modern ocean, hence the expected salinity effect on Mg/Ca in glacial foraminifera would result into an approximate temperature bias of +0.3-0.5°C (Hönisch et al., 2013).

In order to account for the uncertainties related to the here applied dissolution adjustment in core CD154 17-17K thirty four *G.ruber* duplicates were picked and weighed and were used to test the natural variability of the shell weights (Fig. 2. 8). Results revealed an average relative standard deviation (1σ) of 1.1 µg (10% RSD), which is probably a result of the large error associated with the rather large size range used as opposed to individual shell size measurements. As the dissolution adjustment is based on shell weights the original and replicated records of Mg/Ca ratios and shell weights were compared and the difference used to evaluate the uncertainties associated with that method. The average standard deviation between the two datasets when converted to temperature was ± 0.9°C (4.3 %RSD). This value includes the reproducibility of the shell weights which add an extra ±0.15°C on the variability when compared to unadjusted

temperature estimates. The average temperature difference between the unadjusted and adjusted temperature estimates is ± 0.95 °C. Concerning these additional uncertainty factors the error estimates for the dissolution adjusted palaeotemperature in core CD154 17-17K is ±1.4 °C.

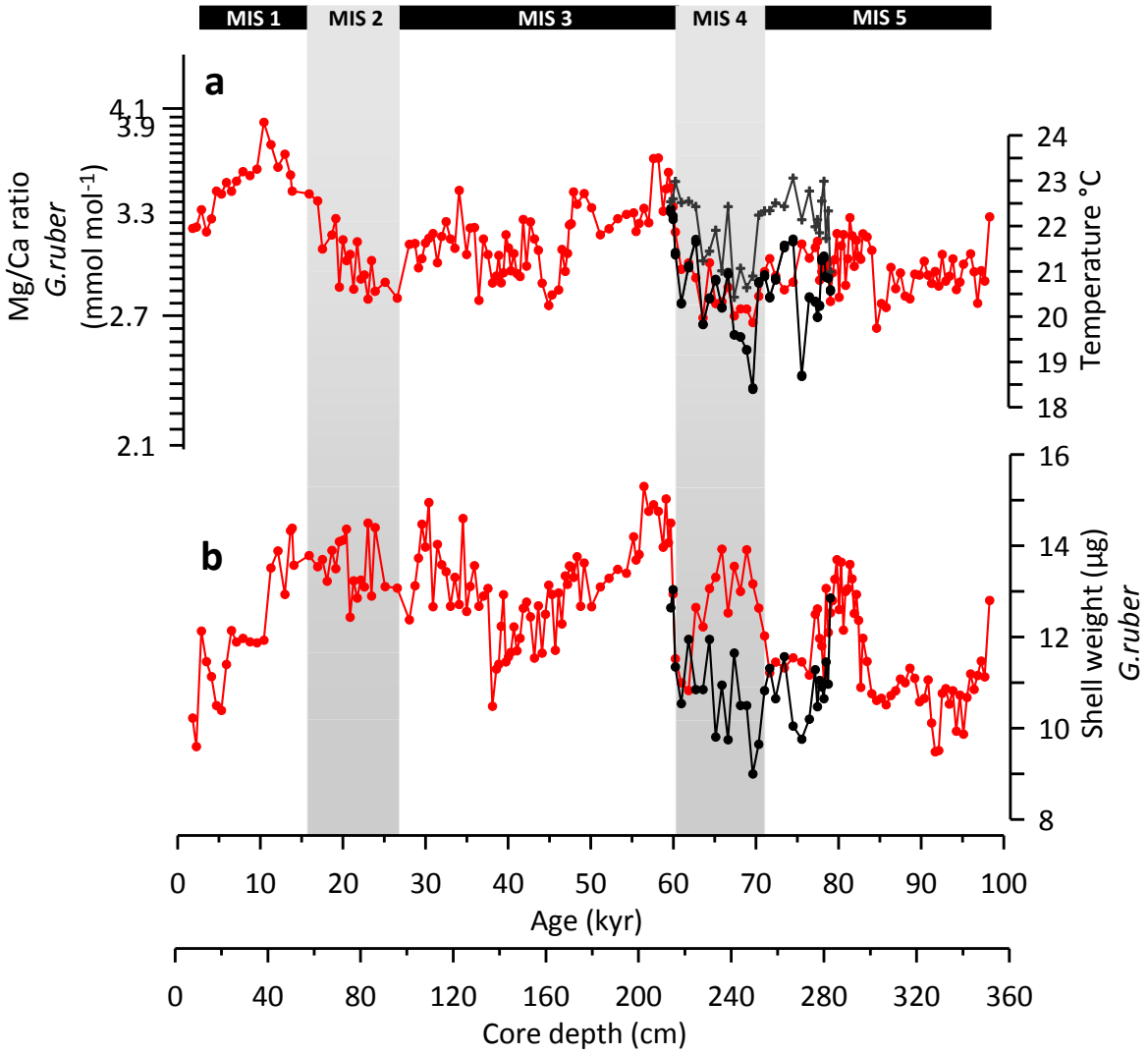

Fig. 2. 8 Reproducibility of the planktic foraminiferal Mg/Ca and shell weights in core CD154 17-17K during MIS 4/late MIS 5 (a) Mg/Ca (mmol mol-1) *G. ruber* (red original measurement, black replicates, dark grey crosses dissolution adjusted temperature estimates resulting from an average of original measurement and replicates) (b) *G. ruber* shell weight (µg), (red original measurement, black replicates)

2.4.6. Seawater Oxygen Isotope Reconstruction ($\delta^{18}O_{sw}$)

(Chapter 3,4,5)

The Mg/Ca derived *G. ruber* calcification temperatures were used to determine the oxygen isotopic composition of seawater ($\delta^{18}O_{sw}$) by extracting the temperature component from the $\delta^{18}O$ of the calcite using the palaeotemperature equation of Kim and O´Neil (1997), (5), with a VPDB to Standard Mean Ocean Water (SMOW) $\delta^{18}O$ correction of 0.27 ‰ (Hut, 1987), (6).

$$T=16.1-4.64\ (\delta^{18}O_c - \delta^{18}O_{sw}) + (0.09\ (\delta^{18}O_c - \delta^{18}O_{sw}))^2 \quad \text{Equation (5)}$$

$$\delta^{18}O_{sw}=\delta^{18}O_c-0.27‰ \quad \text{Equation (6)}$$

Applying this approach in this study (Chapter 3) using late Holocene (0-5 ka) values in core CD154 17-17K yields a $\delta^{18}O_{sw}$ of 0.62 ‰ (±0.3 ‰, propagated error) which is consistent with the 0.60 ‰ (±0.1 ‰, 1σ standard deviation) derived from modern seawater observations in the subtropical Indian Ocean between 24 °S to 43 °S (Tiwari et al., 2013).

The $\delta^{18}O_{sw}$ was corrected for changes in global ice-volume to produce ice-volume corrected local $\delta^{18}O_{sw}$ estimates ($\delta^{18}O_{ivc\text{-}sw}$) following Grant et al. (2012) assuming a glacial $\delta^{18}O$-enrichment in seawater of 0.008‰ per meter sea level lowering (Schrag et al., 2002). The global $\delta^{18}O_{sw}$ records were synchronized with the planktonic $\delta^{18}O$ record by optimizing their graphical fit. This was done to minimize stratigraphic misfits between the global $\delta^{18}O_{sw}$ and the local record that would potentially generate artefacts in the computed local $\delta^{18}O_{ivc\text{-}sw}$ record.

Full error propagation (uncertainty associated with temperature estimation from Mg/Ca, with the $\delta^{18}O_{calcite}$ analysis of *G. ruber*, with the $\delta^{18}O_c$ palaeotemperature equation, with the sea level estimates, with the conversion of sea level values to mean ocean $\delta^{18}O$ analytical) yields 1σ uncertainties for the $\delta^{18}O_{ivc\text{-}sw}$ data of ±0.4‰.

The conversion from $\delta^{18}O_{sw}$ to salinity is generally accompanied with large uncertainties (Rohling, 2000). Therefore all data is shown here in $\delta^{18}O_{sw}$ values and is indirectly inferred to salinity changes. However, to provide an estimate for relative shifts in the $\delta^{18}O_{sw,}$ the

regional southern tropical Indian Ocean (24°S-44°S) $\delta^{18}O_{sw}$ -salinity relationship (Tiwari et al., 2013):

$$\delta^{18}O_{sw} = (0.44 \pm 0.03)SSS-(14.93\pm1.14) \text{ Equation (7)}$$

Using this equation (Chapter 3, Fig. 3.3) a $\delta^{18}O_{sw}$ change of 0.1‰ would translate into a 0.4 psu shift.

2.4.7. Planktonic Foraminiferal Census Counts, Agulhas leakage fauna

*(**Chapter 3**, census counts performed by Kristina Arthur, University of Amsterdam)*

The size fraction >150 μm was split to yield a minimum of 350 individuals, and the abundance of the most dominant species relative to the total planktonic foraminiferal assemblage were calculated every 4 cm.

Sea Surface Temperature estimates were generated from the assemblages using the modern analog technique with similarity index (SIMMAX) transfer function following the approach described in Pflaumann et al. (1996), (Fig. 2. 9). The SIMMAX technique uses a modern calibration dataset to correlate foraminiferal assemblages with known SST estimates, then compares downcore assemblages with the calibration dataset using a similarity equation from (Pflaumann et al., 1996). Here an additional step was employed using a logarithmic transformation of the downcore and calibration datasets, which yields an improvement in the resulting SST estimation. Using this approach the standard deviation of residuals is 0.99 ˚C for the global database, and the estimation of the annual mean temperature is 1.0 ˚C and 0.9 ˚C for the South Atlantic Ocean and Indian Ocean, respectively), (Fig. 2. 9). The original percentage and log-transformed databases were tested by calculating the SST for both the global database and for individual ocean sectors (e.g., South Atlantic Ocean; Indian Ocean), using each sector as a discrete dataset. Here, SST estimates were calculated by assessing the similarity of modern day core top assemblages with the down core assemblages of CD154 17-17K, thereby choosing the mean of the ten closest modern analogues. The MARGO dataset (Kucera et al., 2005; Waelbroeck et al., 2009) was used as the reference database, and used present day annual mean and seasonal SST values from the World Ocean Atlas 1998 (NOAA) measurements. The dataset includes further core top samples to increase coverage of modern day

analogues in the Agulhas region. Annual average, summer/warm season and winter/cold season sea surface temperatures were estimated. The annual average SST estimates resemble the Mg/Ca derived SST data of *G. ruber* in terms of both temperature range and variability.

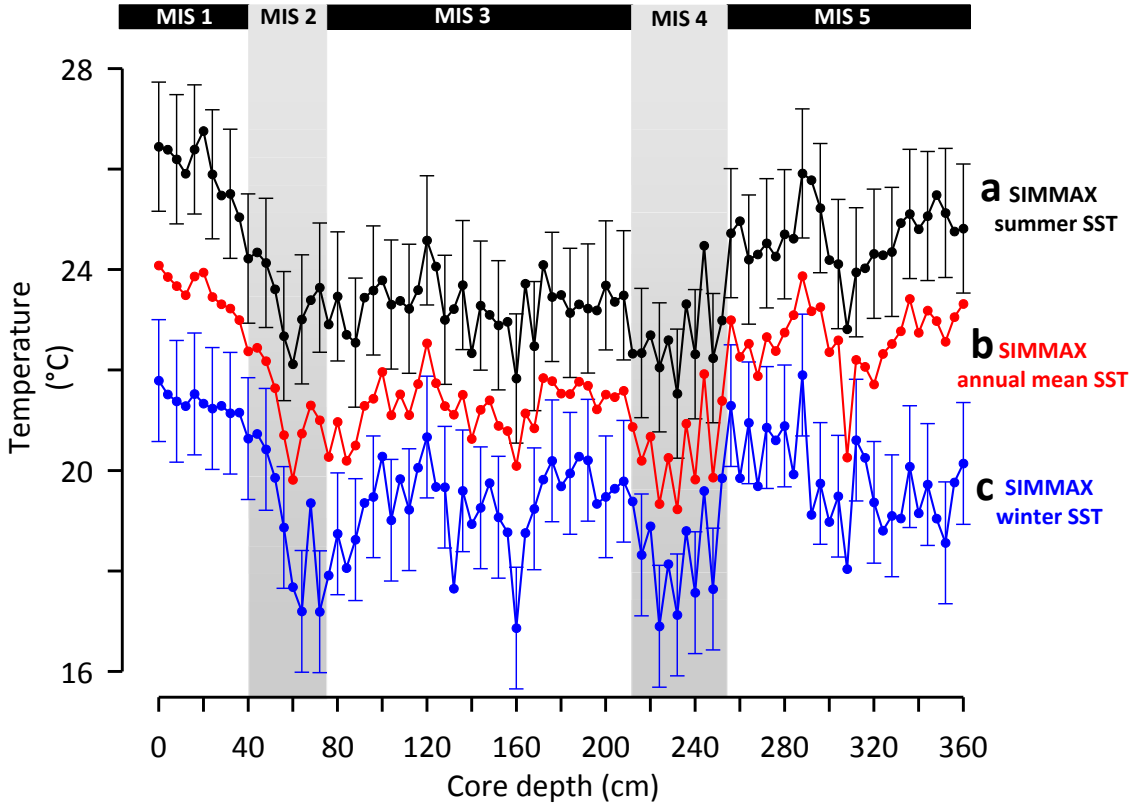

Fig. 2. 9 SST estimates from SIMMAX transfer functions of core CD154 17-17K for (a) summer, (b) annual mean, and (c) winter. Error bars on the SIMMAX estimates are the standard deviation of the estimates.

The Agulhas leakage fauna proxy (ALF) is considered to reflect the intensity of past Indian-Atlantic water exchange via Agulhas leakage in the South Atlantic (Peeters et al., 2004). The quantification of the ALF assemblage in the upstream Agulhas Current is important in evaluating the connection between the upstream variability and the downstream response within the Agulhas leakage corridor. To calculate the ALF index in CD154 17-17K, the sum of the relative abundance of the species *Pulleniatina obliquiloculata, Globigerinita glutinata, Hastigerina pelagica, Globorotalia menardii, Globigerinoides sacculifer, Globigerinella siphonifera, Globigerinoides ruber (sensu stricto), Orbulina universa, Globorotaloides hexagona* and *Globorotalia scitula* was taken.

Species which are presently found at higher latitudes, i.e., associated with colder water masses near the dynamic STF, (Graham et al., 2012), or further south in polar waters, have

been defined here as the transitional to polar group (TPG) which includes the species *Neogloboquadrina pachyderma* (sin.+ dex.), *Globorotalia inflata, Globigerina bulloides and Globorotalia truncatulinodes* (sin.+ dex.) (Peeters et al., 2004).

2.4.8. Ice-Rafted Detritus

*(**Chapter 3**, counts performed by Martin Ziegler)*

Lithic fragments (>150 μm fraction) embedded in pelagic sediment are assumed to be IRD and therefore a proxy for iceberg flux to the core site. In order to identify northward shifts of the Southern Ocean frontal system the occurrence of IRD was recorded at the southern Agulhas Plateau located seven degrees further to the south of Agulhas Current core locations (Fig. 2. 1). Lithic fragments were counted in marine sediment core MD02-2588, (41°19.9'S; 25°49.4'E; 2907 m water depth) every 2 cm between MIS 1-5. The results are expressed as grains per gram of dry sediment (grains/g sed). The data are shown on their independent age model for core MD02-2588 (Ziegler et al., 2013a).

2.4.9. Elemental records

(Chapter 5 and 6)

Core scanning was performed using the ITRAX™ XRF Core scanner at the British Ocean Core Research Facility (BOSCORF, Southampton). Measurements were made at 0.1 cm resolution with a count time of 30 s, at 30 kV and 50mA for the XRF scan. Additionally, for validation of the XRF scans, major and trace elements were analysed in a discreet subset of bulk sediment samples. Analysis of the bulk sediment samples was performed using a Thermo X Series II inductively coupled plasma mass spectrometer (ICP-MS). Approximately 0.1 g of freeze-dried and ground sediment was ignited in a furnace at 900 °C (58) loss on ignition values. Whole-sediment major element concentrations were obtained following Li metaborate fusion. The internationally recognized standard JB-1A was run alongside the sample batch. Long-term relative standard deviations (1σ) show precision of 1–2% for major trace elements for JB-1A. XRF scanning-derived element counts as well as absolute bulk sedimentary elemental concentrations have been log transferred and are displayed on logarithmic scale (Weltje and Tjallingii, 2008).

Here the variations in Fe/K ratios are used as an indicator for changes between humid and dry conditions in the southeast African hinterland. The spatial distributions of Fe/K in

marine core-top sediments reflect the relative input of intensively weathered material from humid regions versus less weathered particles from drier areas (Govin et al., 2012).

In tropical and subtropical humid regions, intense chemical weathering of bedrocks takes place due to high precipitation and temperatures (Middelburg et al., 1988; Driessen et al., 2001). This leads to the presence of highly weathered soils with a geochemical signature that is rich in Fe (Driessen et al., 2001) and which is transferred to marine sediments by fluvial input. Potassium in marine sediments is mostly associated with potassium feldspar ($K[AlSi_3O_8]$), (Zabel et al., 2001) or illite ($((K,H_3O)Al_2[(OH)_2Si_3AlO_{10}])$, (Yarincik et al., 2000), which are both characteristic of drier regions with low chemical weathering rates and in which physical weathering is dominant (Zabel et al., 2001). Palaeoclimate reconstructions suggests that Fe/K values increasing downcore in marine sediments indicate the presence of more humid climatic conditions within the catchment area (Mulitza et al., 2008). Therefore the Fe/K ratio of surface sediments should be appropriate for reconstructing African climatic zones (Govin et al., 2012) but does not allow any quantitative estimate of terrigenous material supplied to the ocean via the river system. However, in comparison to the use of Fe/Ca ratios this method is independent of possible variations in biogenic carbonate input or post-depositional calcium carbonate dissolution. Elemental ratios including Ca do not simply reflect the flux of terrigenous material, but they rather reflect the amount of terrigenous input relative to the biogenic carbonate flux/preservation.

Diagenetic Fe remobilization can, however, occur during redox processes in the sediment (e.g., Middelburg et al., 1988; Zwolsman and van Eck, 1999) which will be in form of Fe-Mn oxyhydroxides dispersed as micronodules in the sediments and as coatings on sedimentary particles (Libes, 2009). Fe-Mn oxides are precipitated directly from seawater, from interstitial water during diagenesis and from oxygenated hydrothermal fluids, and concentrate trace elements greatly (Libes, 2009).

Evidence for diagenetic processes in the deep-sea can be gained by assessing downcore Fe concentrations and their co-variation with Mn as this is also produced during redox processes (Middelburg et al., 1988). Within the studied section of core CD154 10-06P two intervals between 25-30cm and 37-40 cm show elevated XRF Mn counts (Fig. 2. 10a). While, neither interval occurs coevally with elevated Fe concentrations suggesting limited diagenetic overprint, the latter Mn peak occurs directly after a maximum in Fe concentrations centred at ~42 cm core depth. While a diagentic influence on this Fe peak

cannot be ruled out it appears of secondary importance to change in supply of the terrigenous components. Considering the entire core length no obvious co-variation between downcore Fe and Mn counts is obvious excluding redox processes in the sediment as possible source here.

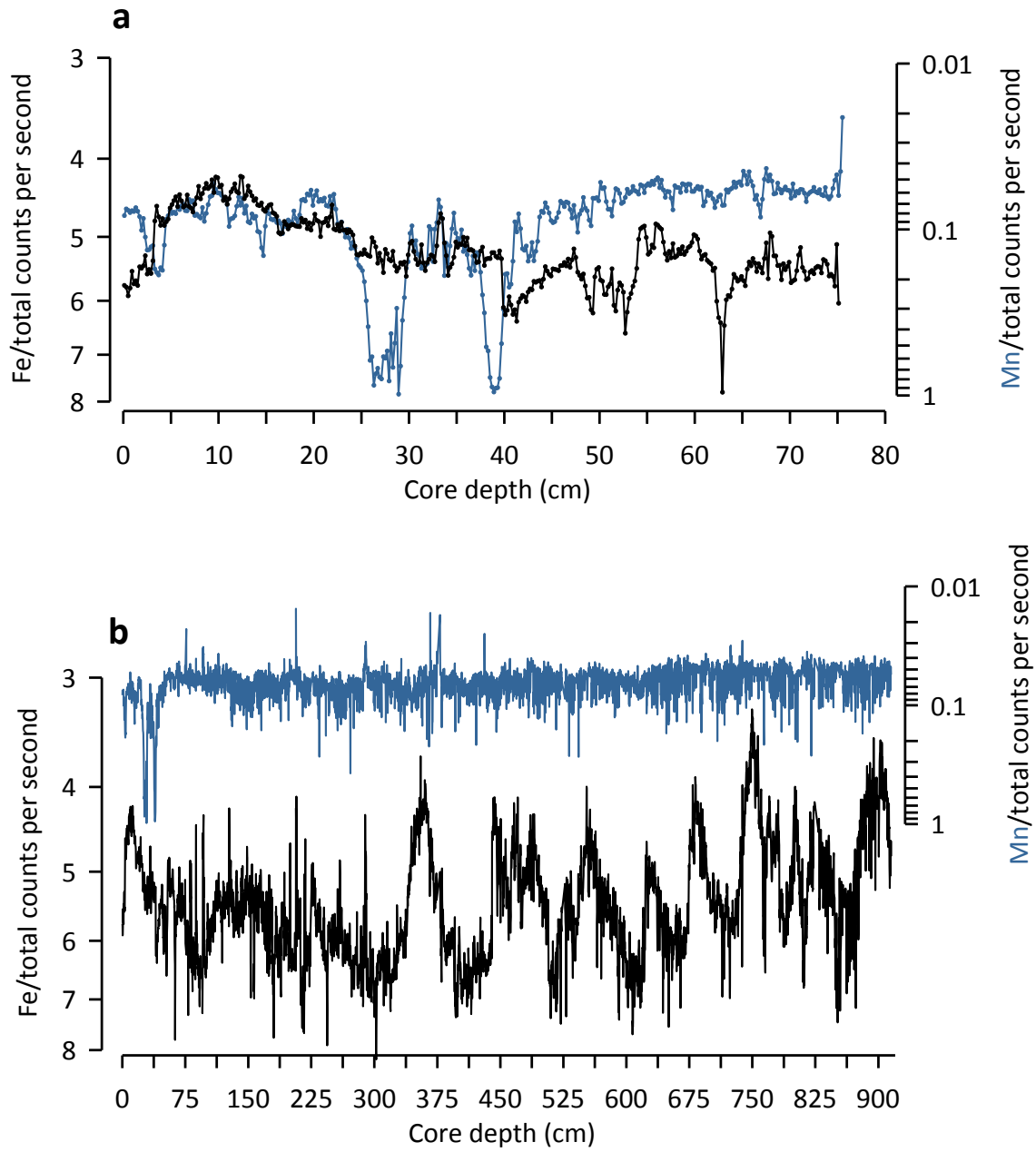

Fig. 2. 10 Additional XRF scanning profile from marine sediment core CD154 10-06P for (a) Core interval 0-76 cm equivalent to the past ~21 kyr and (b) the entire core length. Fe normalised (Fe/ total counts per second; black) and Mn normalised (Mn/ total counts per second; blue).

2.5. Organic proxies

(Chapter 5)

2.5.1. Sample preparation

Forty sediment samples were freeze-dried and homogenized with a mortar and pestle. The homogenized material was then extracted using an accelerated solvent extractor with dichloromethane (DCM):methanol 9:1 (*v/v*) and a pressure of 1000 psi in 3 extraction cycles. The total lipid extract was separated over an Al_2O_3 column into a polar, ketone and polar fraction using hexane:DCM 9:1, hexane:DCM 1:1 and DCM:methanol 1:1, respectively. The ketone fractions were analysed for the alkenone unsaturation index ($U^{K'}_{37}$) using a gas chromatograph (GC). The polar fractions were redissolved in hexane/isopropanol (99:1) to a concentration of 2 mg/ml and filtered over a 0.45 PTFE filter and analyzed for the Glycerol dialkyl glycerol tetraether (GDGT) lipid based TEX_{86} and BIT index using high performance liquid chromatography mass spectrometry (HPLC/MS).

2.5.2. $U^{K'}_{37}$ analysis

Ketone fractions were analysed by GC using an Agilent 6890 gas chromatograph with a FID and an Agilent CP Sil-5 fused silica capillary column (50m×0.32mm, film thickness = 0.12µm) with helium as the carrier gas. The GC-oven was programmed to subsequently increase the temperature from 70 to 130 °C with 20° C min^{-1} steps, and then with 4°C min^{-1} steps to 320°C, at which it was held isothermal for 10 min. The analytical error associated with this method is ±0.2°C (standard error), $U^{K'}_{37}$ values were calculated according to Prahl and Wakeham (1987). Subsequently, SST was calculated using the core top calibration established by Müller et al. (1998). The error associated with this calibration is ±1.5 °C on the SST estimates.

2.5.3. δD of alkenone analysis

Alkenone hydrogen isotope analyses were carried out on a Thermo-Finnigan DELTA^{Plus} XL GC/TC/irMS. The temperature conditions of the GC increased from 70 to 145 °C with 20 °C min−1 steps, then to 320 °C with 4 °C min^{-1} steps, at which it was held isothermal for 13 min using an Agilent CP Sil-5 column (25m×0.32mm) with a film thickness of 0.4 µm and 1 ml min^{-1} helium at constant flow. The thermal conversion temperature was set to 1425°C.

Isotopic values for alkenones were standardized against pulses of H_2 reference gas, which was injected three times at the beginning and two times at the end of each run. Alkenone δD values were measured as the combined peak of the C37:2 and C37:3 alkenones (van der Meer et al., 2013) and three fractions were analysed as duplicate if a sufficient amount of sample material was available. Standard deviations of replicate analyses varied from ±0.1‰ to ±5.9‰.

2.5.4. GDGT analysis

Analyses for GDGTs were performed as described by Schouten et al. (2007). In summary, an Agilent 1100 series HPLC/MS equipped with an auto-injector and Agilent Chemstation chromatography manager software was used. Separation was achieved on an Alltech Prevail Cyano column (2.1mm×150mm, 3 µm), maintained at 30 °C. GDGTs were eluted with 99 % hexane and 1 % propanol for 5 min, followed by a linear gradient to 1.8 % propanol in 45 min. Flow rate was 0.2 mL min^{-1} by back-flushing hexane/propanol (90:10, *v/v*) at 0.2 mL min^{-1} for 10 min. Detection was achieved using atmospheric pressure positive ion chemical ionization mass spectrometry (APCI-MS) of the eluent. Conditions for the Agilent 1100 APCI-MS 5 were as follows: nebulizer pressure of 60 psi, vaporizer temperature of 400 °C, drying gas (N2) flow of 6 $Lmin^{-1}$ and temperature 200 °C, capillary voltage of −3kV and a corona of 5 µA (~3.2 kV). GDGTs were detected by Single Ion Monitoring (SIM) of their $[M+H]^+$ ions (dwell time = 234ms), (Schouten et al., 2007) and quantified by integration of the peak areas. TEX_{86} and BIT index were calculated as described by Schouten et al. Schouten et al. (2002b) and Hopmans et al. (2004), respectively. The TEX^H_{86} SST calibration model by Kim et al. (2010) was used to transfer TEX_{86} values to absolute SST. This calibration model is recommended for temperature reconstruction above 15 °C (Kim et al., 2010) and therefore appears to be the most suitable model for reconstructing subtropical temperatures, as found in the Agulhas Current area. The analytical error associated with this method is ±0.3°C (standard error), (Schouten et al., 2006). The error associated with the calibration is ±2.5 °C on the SST estimates (Kim et al., 2010). The analytical error for BIT index is ± 0.01. Concentrations of GDGTs were calculated by reference to a C_{46} GDGT internal standard (Huguet et al., 2006).

As highlighted by Schouten et al. (2013), a change in the accumulation rates of crenarchaeol, as a result of shifting marine productivity for example, might cause

variations in the BIT index even though the concentration of branched GDGTs, and thus soil input, stays constant (e.g., Castaneda et al., 2010; Smith et al., 2012). Therefore records of branched GDGTs and crenarchaeol accumulation rates are shown below to better understand the controls on the BIT index variability (Fig. 2. 11).

High BIT index values in the core interval 65-60 cm as well as around 52 cm are mainly driven by high accumulation rates of branched GDGT's rather than by variable accumulation rates of crenarchaeol which confirms that elevated terrestrial input from the continent to the core side occurred as displayed by high BIT index values.

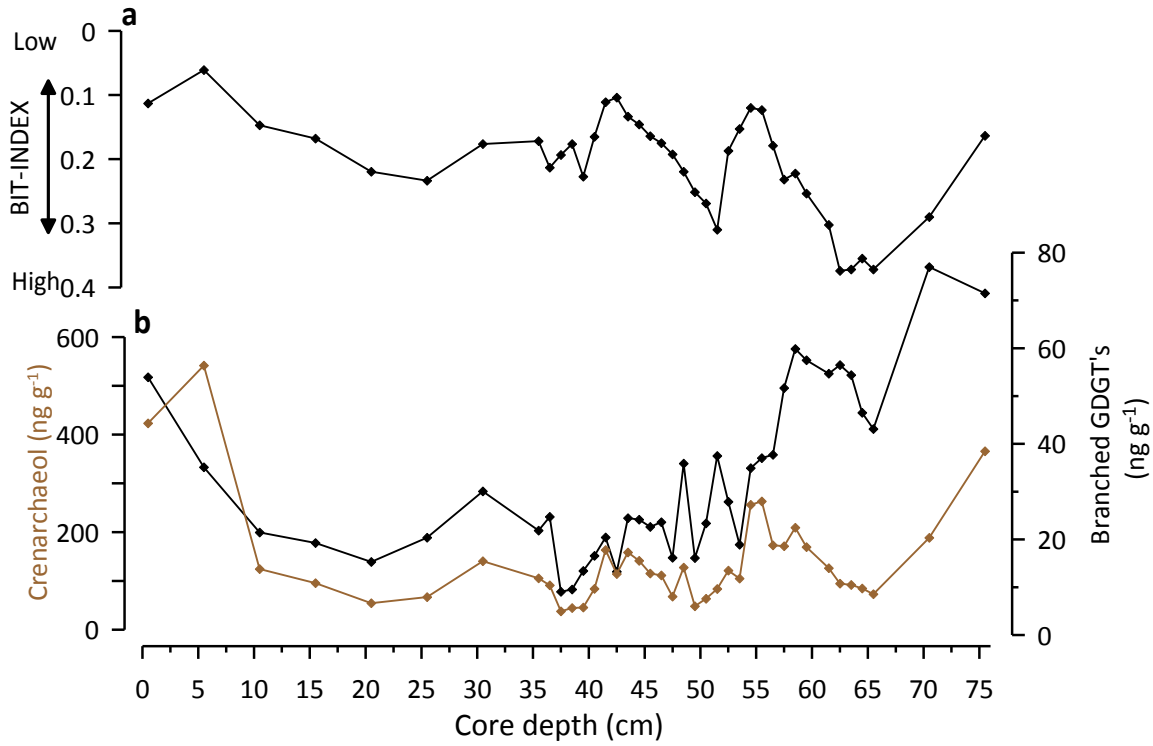

Fig. 2. 11 (a) BIT index of CD154 10-06P, reflecting changes in relative soil organic matter contributions. (b) Absolute bulk concentration of branched Glycerol dialkyl glycerol tetraether (GDGT, black) in the sediment (nanogram GDGT/gram dry bulk sediment) and absolute bulk concentration of crenarchaeol (brown), (nanogram crenarchaeol /gram dry bulk sediment).

2.6. Statistical analysis

Time-series analysis aims to investigate the temporal behaviour of one of several variables (*x*)t. The evaluation of the temporal pattern of a sequence can be done via spectral analysis to detect cyclicities in a single time series (auto-spectral analysis) or to determine the relationship between two timeseries as a function of frequency (cross-spectral analysis) (Weedon, 2003).

The Pearson coefficient is a widely applied statistical tool that quantifies the linear correlation between two variables. However, the inherent element of persistence in climate time-series makes the confidence intervals difficult to calculate. In this study, time-series correlation was performed using the PearsonT programme (Mudelsee, 2003). In PearsonT, the Pearson's correlation coefficient is estimated employing a nonparametric stationary bootstrap confidence interval with an average block length proportional to the maximum estimated persistence time of the data (Mudelsee, 2003).

Auto-spectral analysis purpose to describe the distribution of variance contained in a single signal x(t) as a function of frequency or wavelength. One widely employed method to compute power spectra is the Blackman-Tukey algorithm which is based on a standard Fourier transform of a truncated and tapered (to suppress spectral leakage) autocovariance function (Weedon, 2003). The major disadvantage of the Blackman-Tukey method is its inability to process unevenly spaced data. An alternative, employed here, is the Lomb-Scargle Fourier Transform for unevenly spaced data (Schulz and Stattegger, 1997). Hence, unevenly spaced time series can be directly analysed by SPECTRUM without preceding interpolation. Interpolation can lead to an underestimation of high-frequency components, independent of the interpolation technique (Schulz and Stattegger, 1997).

Power spectra were calculated with the REDFIT software (Schulz and Mudelsee, 2002) employing a Welch-Overlapped-Segment-Averaging procedure, a Hanning window and four overlapping (50%) segments; red-noise boundaries were estimated as upper 80, 90 and 95% chi-square limits of a fitted first order autoregressive process AR(1). According to Mann and Lees (1996) a large proportion of the spectra of climatic-proxy data have backgrounds which correspond to a first order autoregressive process AR(1).

Cross-spectral analysis correlates two times series in the frequency domain in order to determine if statistically significant peaks at the same frequency occur and if these periodicities are related with each other and if so, what the phase relationship is between them. The cross-spectrum is used as part of a frequency domain analysis of the cross correlation or cross covariance between two time series. The correlations between the two spectra can be calculated by means of coherence, where 0 indicates no correlation and 1 indicates maximum correlation between the two time series in the frequency domain. A significant degree of coherence is an important precondition for computing phase shifts between two signals (Weedon, 2003). Cross-spectral analysis to compute phase estimates

and coherences were calculated with the SPECTRUM software (Schulz and Stattegger, 1997). Gaussian filtering was performed using the software Analyseries (Paillard et al., 1996).

Wavelet is a type of evolutionary spectra and it is often used in the study of non-stationary processes in which the frequencies and power change with time. It is common to produce a time/frequency with power distribution contour map that aims to improve the visualisation of the time evolution of the statistically significant frequencies. In this study, wavelet analysis was performed using *Wavelet* from Torrence and Compo (1998) and was used in order to study the presence and timing of the periodicities obtained in the single spectral analysis.

2.7. Numerical model simulations

2.7.1. Regional Ocean Modelling System AGIO

*(**Chapter 3;** performed by Benjamin Loveday, University of Cape Town)*

In order to better understand the forcing driving Agulhas Current variability a sub-domain of a regional eddy-permitting model of the greater Agulhas Current system, AGIO, was analysed. This configuration has been demonstrated to realistically simulate the complicated circulation around South Africa (Loveday et al., in press). AGIO is a 1/4 ^{o}, eddy-permitting representation of the Indian Ocean basin, produced using v. 2.1 of the Regional Ocean Modelling System (ROMS) (Shchepetkin and McWilliams, 2005) and constructed with ROMSTOOLS (Penven et al., 2008). The model simulates the large-scale features of the Indian Ocean and regional transport in the Agulhas source regions. Using the methodology described in Bryden et al., (2005a), AGIO records an Agulhas Current volume transport of 76.9 ± 19.9 Sv, consistent with the 78.6 ± 19.9 Sv observed over the same section (Bryden et al., 2005a; Biastoch et al., 2009a). Here, as the CD154 17-17K Agulhas core lies at 33 ^{o}S, Agulhas transport estimates are calculated from the barotropic stream function along a transect that spans the core site on a line perpendicular from the shore to the first recirculation (AC33, Fig. 3.4a).

The low numerical viscosity of ROMS allows for a well-captured eddy field at this resolution. Eddy kinetic energy (EKE) patterns in the source regions and at the retroflection are well represented. Low viscosity also reduces viscous choking at the

retroflection, allowing inertia to govern the local dynamic (Dijkstra and de Ruijter, 2001). AGIO estimates an Agulhas leakage of 27.6 ± 2.8 Sv through quantifying the Eulerian flux of an Indian Ocean passive tracer across the Cape Basin.

AGIO was bulk forced by the CORE v. 2b normal year surface fluxes (Large and Yeager, 2009). Modification of the wind field in the sensitivity experiments was achieved through the addition of anomalies that modify the zonal component of the westerly wind stress (see Loveday et al. (in press) and Durgadoo et al. (2013), for full methodology), (Fig. 3.4b). Anomalies were based on the reference zonal wind-stress between 20 ^{o}E and 115 ^{o}E, but were applied across the model domain. Two sensitivity experiments were performed, one in which the westerly wind-stress was increased by 40 % (Wp40), and the other where the westerly winds were shifted equatorward by 4 degrees (Nth4).

Reference boundary conditions were supplied by a 1/2 ^{o} ORCA05 reference run (Biastoch et al., 2008a), also forced with CORE v. 2b normal year fluxes. Boundary conditions for the Wp40 and Nth4 sensitivity experiment were derived from ORCA05 runs forced with the appropriate wind stress changes applied throughout the Southern Hemisphere(Durgadoo et al., 2013) .

2.7.2. Comprehensive fully-coupled Earth System model COSMOS

*(**Chapter 5**; performed by Conor Purcell, Cardiff University)*

In order to better evaluate precipitation changes and associated land-ocean climate dynamics in southeast Africa the COSMOS comprehensive fully-coupled Earth System model (Jungclaus et al., 2006) was used to perform a North Atlantic freshwater perturbation experiment, analogous to the iceberg/meltwater discharge thought to be associated with a Heinrich Event (Heinrich, 1988). The COSMOS platform utilised the MPIOM ocean component which has an effective resolution of ~3° over 40 vertical layers (Marsland et al., 2003). The ECHAM5 atmospheric component (Roeckner et al., 2006), utilises a ~3.75° resolution. The model has previously been used to simulate pre-industrial (Wei et al., 2012) as well as other climate scenarios (Zhang et al., 2013). In order to simulate the LGM, (~23–19 ka), (Clark and Mix, 2002) climate state, simulation was integrated for ~4000 years in order to reach a state where the entire ocean was equilibrated (Zhang et al., 2013). LGM boundary conditions were adopted from the PMIP3 (Palaeo Modelling Intercomparison Project 3) protocol (available at

http://pmip3.lsce.ipsl.fr/). A freshwater perturbation of magnitude 0.2Sv was applied across the North Atlantic ice rafted debris belt around 40°N-55°N, 45°W-20°W (Hemming, 2004). The forcing was applied over a period of 150 years until a new quasi-equilibrium (the deep ocean was not in equilibrium; Zhang et al. 2013) AMOC state was obtained. Thereafter the system was allowed to recover via the removal of the freshwater forcing; a process taking ~200 years.

2.8. Age Models

2.8.1. CD154 17-17K

The age model for sediment core CD154 17-17K is presented in Ziegler et al. (2013b). In summary, the age model is based on a combination of eight mono-specific planktonic foraminiferal (*G. ruber*) radiocarbon dates within the upper part of the record (< 40 kyr) and additional graphical correlation of the *G. ruber* stable oxygen isotope ($\delta^{18}O$) record to the Deuterium (temperature) record of Antarctic ice core EPICA Dome C (EPICA, 2004) on the Speleo-age model of Barker et al. (2011). The radiocarbon ages were converted into calendar years using the Marine09 data set with a global mean reservoir correction of (R) 400 years (Reimer et al., 2009) . In order to provide a detailed millennial-scale resolution age model, Ziegler et al. (2013b) further fine-tuned the CD154 17-17K age model by visually matching common transitions within the Fe/K ratio of the core and the $\delta^{18}O$ speleothem records from Chinese Caves, Hulu (Wang et al., 2001) and Sanbao (Wang et al., 2008). The average age difference between the two independent age models (low resolution planktonic $\delta^{18}O$-based tuning and high resolution Fe/K-based tuning) is minor and demonstrates that the Fe/K tuning approach provides a robust millennial-scale resolution stratigraphic framework. According to this age model sediment core CD154 17-17K spans approximately the last 100 kyr (MIS 1-5c), with an average linear sedimentation rate of 4 cm/ka, ranging between 2 to 5 cm/ka.

2.8.2. CD154 10-06P

The age model for the core was developed using ten ^{14}C accelerator mass spectrometer (AMS) dates measured from samples containing approximately 1000 tests of *G. ruber* (>250-315 μm). Radiocarbon measurements were made at the Natural Environment Research Council (NERC) Radiocarbon Laboratory (Table 2. 1). The radiocarbon ages were

converted into calendar years using the Marine09 data set with a global mean reservoir correction of (R) 400 years (Reimer et al., 2009). The core chronology was constructed using the statistical package BChron (Parnell et al., 2011) using a Bayesian approach to calculate the 95% uncertainty on the calibrated ages (Table 2. 1) and the 95% probability envelope for the time period studied (Fig. 2. 12). In the range of the ^{14}C dates relatively constant sedimentation rate of ~ 4.0 cm ka^{-1}, ranging from 4.8-1.9 cm ka^{-1} and a sample integration of ~300 years for every 1 cm sample is achieved.

Table 2. 2 ^{14}C dates for CD154-10-06P

Depth (cm) CD154 10-06P	Species	^{14}C age BP (yr)	Error +/- 1σ (radiocarbon yrs BP)	95% confidence age interval Lower limit (ka BP)	95% confidence age interval Mid-point (ka BP)	95% confidence age interval Upper limit (ka BP)	Code
0-1 cm	*G.ruber*	2359	35	1.88	1.98	2.09	SUERC-45072
14-15 cm	*G.ruber*	4774	35	4.89	5.03	5.20	SUERC-45075
26-27 cm	*G.ruber*	7681	40	8.02	8.14	8.26	SUERC-45076
40-41 cm	*G.ruber*	10409	49	11.26	11.48	11.71	SUERC-45077
51-52 cm	*G.ruber*	12403	63	13.70	13.85	14.01	SUERC-45078
64-65 cm	*G.ruber*	15082	89	17.50	17.85	18.40	SUERC-45079
78-79 cm	*G.ruber*	17863	132	20.37	20.79	21.29	SUERC-45080
83-84 cm	*G.ruber*	18786	148	21.51	21.91	22.31	SUERC-45081
92-93cm	*G.ruber*	20682	191	23.69	24.19	24.76	SUERC-45082
99-100 cm	*G.ruber*	23498	273	26.97	27.90	28.48	SUERC-45085

Beyond the limits of radiocarbon method graphic tuning of the benthic $\delta^{18}O$ record to the global benthic stack LR04 (Lisiecki and Raymo, 2005), (Table 2. 3, Fig. 2. 13) was used to establish the age model. Ages between each age control point were estimates by linear interpolation. Only nine tuning points were used to achieve a good match with the LR04 record (Fig. 2. 13a,c). However, it was not possible to establish a continuous age model on the turbidite adapted depth scale of the core as the event caused sediment erosion in that interval. In order to adapt for the time gap (~7 ka) two additional tuning points (out of the total nine) were used. It should be noted that beyond the last radiocarbon date at 99.5 cm no additional tuning point was used until 305.5 cm core depth in order to establish a high degree of synchronicity between this record and the LR04 which result in a nearly untuned MIS 3 and MIS 4 (Fig. 2. 13).

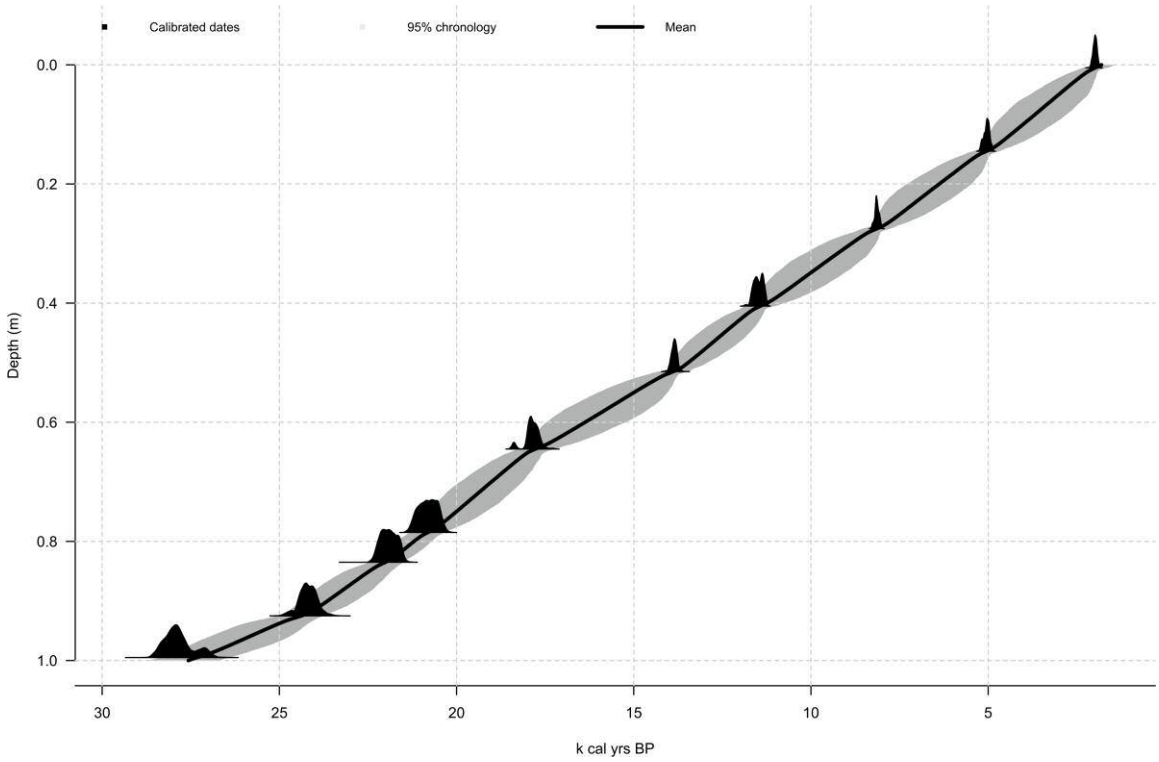

Fig. 2. 12 The Bayesian age-model obtained by Bchron (black) for the top 100cm of CD154 10-06P incorporating a local reservoir uncertainty of 400 years (ΔR=0). Each date is represented by the probability distribution of the intersection between the radiocarbon ages at those depths and the Marine09 calibration curve. The grey shaded area indicates the 95% probability based on the calibrated dates using the Bayesian statistical package, Bchron.

Table 2. 3 Tuning points for the age model of sediment record CD154-10-06P

Tuning points of benthic $\delta^{18}O$ of core CD154-10-06P to LR04	
Depth (cm)	Age (ka)
305.5	69
405.5	92
440	100
441	107
460.5	116
504.5	131
658.5	191
748.5	219
822.5	244

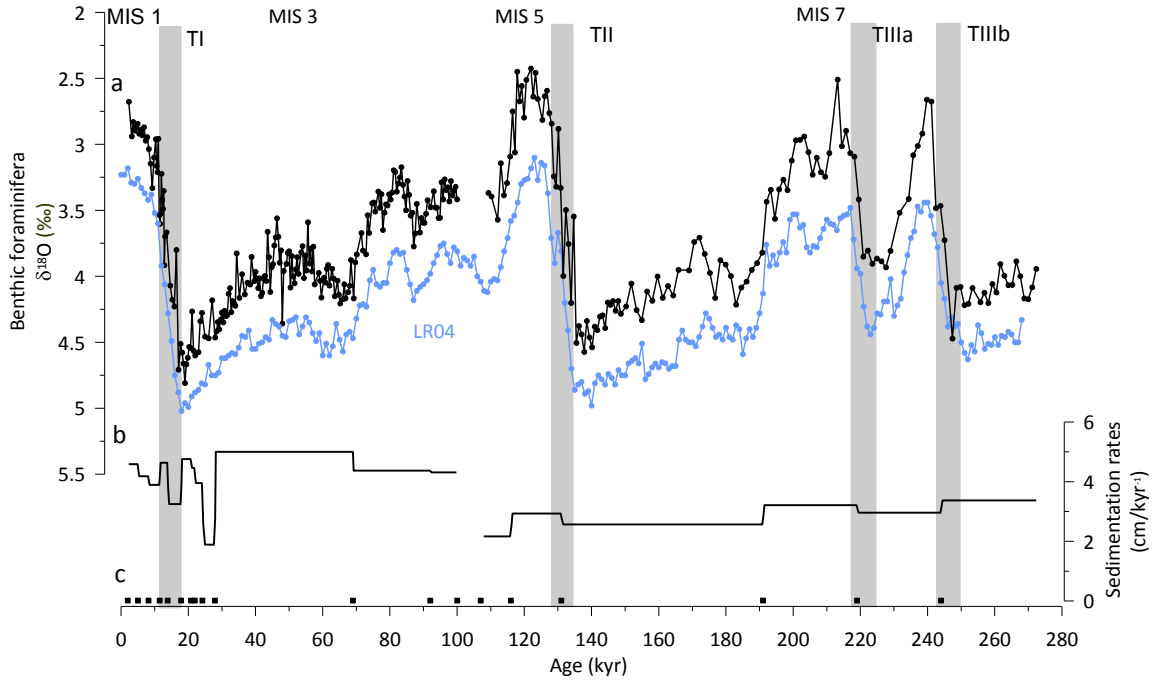

Fig. 2. 13 Chronology of core CD154 10-06P - Grey bars indicate glacial terminations and Marine Isotope Stages (MIS) are highlighted on top (a) Benthic $\delta^{18}O$ record and global benthic $\delta^{18}O$ stack (LR04, light blue) is shown for comparison (Lisiecki, and Raymo, 2005) (b) Sedimentation rates (c) ^{14}C age dates in the upper part und tuning points in the lower part of the core.

3. Millennial-scale Agulhas Current variability and its implications for salt-leakage through the Indian-Atlantic Ocean Gateway

3.1. Introduction

Palaeoceanographic studies suggest that increased input of relatively warm, saline Agulhas Current waters in the South Atlantic are associated with late Pleistocene deglaciations (e.g., Peeters et al., 2004; Martínez-Méndez et al., 2010; Caley et al., 2012; Marino et al., 2013; Scussolini and Peeters, 2013). This implies that the transfer of water masses may effectively regulate the buoyancy of the (South) Atlantic Ocean thermocline, and consequently impact the strength of the Atlantic Meridional Overturning Circulation (AMOC), (Weijer et al., 2002; Knorr and Lohmann, 2003).

Most palaeo-proxy reconstructions to date have focussed on: 1) the Agulhas leakage area in the South Atlantic (Peeters et al., 2004; Martínez-Méndez et al., 2010; Caley et al., 2012; Marino et al., 2013; Kasper et al., 2014); 2) the Agulhas rings pathway in the South Atlantic subtropical gyre (Rackebrandt et al., 2011; Scussolini and Peeters, 2013; Scussolini et al., 2013); 3) outside of the Agulhas Current trajectory (Bard and Rickaby, 2009); or 4) the "precursor" region of the Agulhas Current (Caley et al., 2011a) and/or concentrate mostly on orbital timescales. Furthermore, studies from the Agulhas leakage corridor that show variability in temperature, salinity and Agulhas Leakage Fauna (ALF) over time have mainly been interpreted in terms of qualitative changes in the leakage (Peeters et al., 2004; Martínez-Méndez et al., 2010; Caley et al., 2012; Marino et al., 2013). However, importantly it should be recognised that changes in the water mass properties in the Agulhas leakage corridor can be potentially altered either by changes in the amount of water (volume transport) which is transferred between the Indian and South Atlantic Ocean or by hydrographic changes in the upstream Agulhas Current that are subsequently transferred downstream to the Agulhas leakage corridor without altering the actual amount of leakage itself. To date, palaeoceanographic oriented studies from the Agulhas leakage corridor have not considered changes in the upstream Agulhas Current to account

for the variability seen in the leakage records. To fill this gap, the first high–resolution multi-proxy record was produced from within the main flow of the Agulhas Current (sediment core CD154 17-17K) in the southwest Indian Ocean (Fig. 3. 1).

Reconstructions of Sea Surface Temperature (SST), the local oxygen isotope composition of seawater ($\delta^{18}O_{sw}$), which provides an indication of salinity, and foraminiferal assemblage variations, were examined from within the main flow of the Agulhas Current. These proxies, when considered in combination, allow hydrographic changes within the current itself to be compared with previously published records from the Agulhas leakage corridor. The records studied here highlight the importance of considering upstream Agulhas Current variability when explaining Agulhas leakage variability over time.

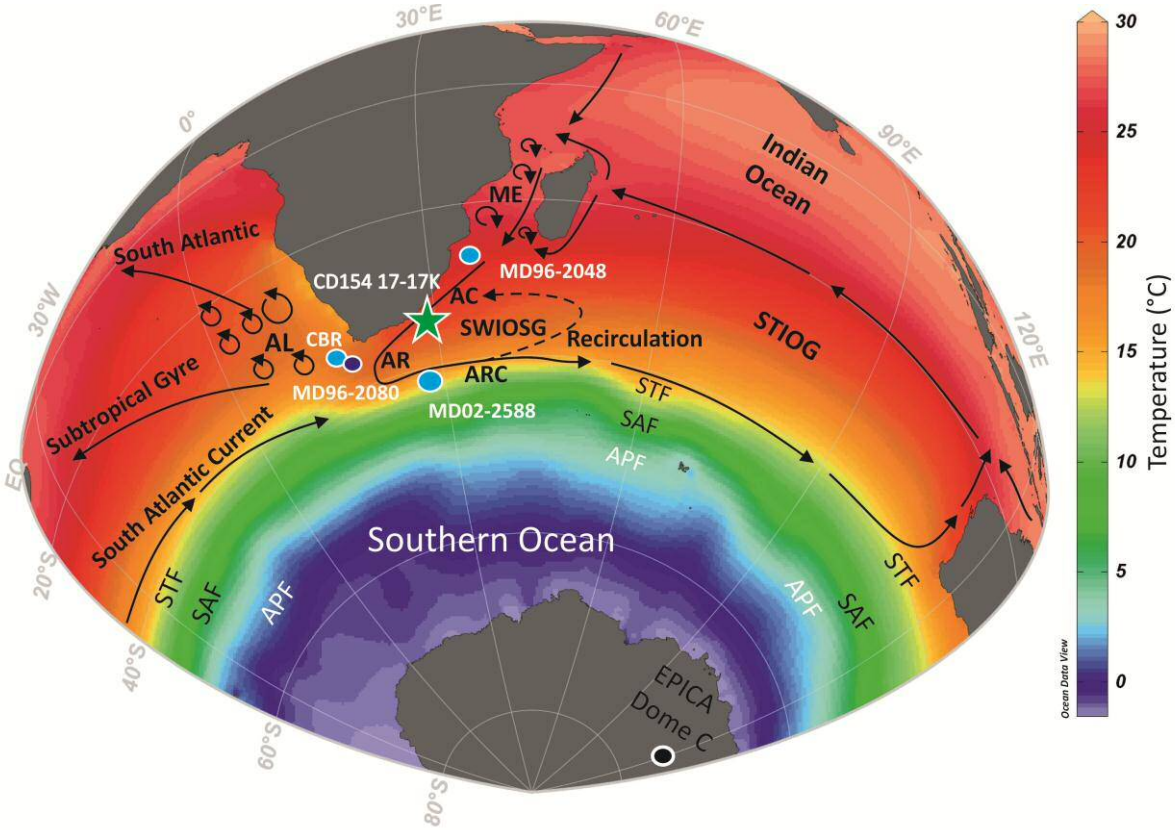

Fig. 3. 1 Location of the Agulhas Current system and palaeoclimate archives used as a reference. Base map illustrates Southern Hemisphere annual mean surface temperatures compiled using the Ocean Data View program (Schlitzer, 2012) and World Ocean Atlas Data 09 (Locarnini et al., 2010). Location of this study is indicated by the star, reference locations are indicated as circles: Agulhas Current (CD154 17-17K, green star, this study), Cape Basin record (CBR, light blue circle, GeoB3603, MD96-2081, Peeters et al., 2004), Agulhas Bank (MD96-2080, dark blue circle, Marino et al., 2013), Agulhas Plateau (MD02-2588, blue circle, Ziegler et al., 2013a), 'precursor' region Agulhas Current (MD96-2048, light blue circle, Caley et al., 2011), Antarctic Ice core (EPICA Dome C, black circle). Black arrows indicate the main

surface ocean circulation patterns with emphasis on the key components of the inter-ocean transport across the Agulhas Current system, Agulhas Current (AC), AL (Agulhas leakage in the Agulhas leakage corridor), AR (Agulhas retroflection), ARC (Agulhas Return Current), ME (Mozambique Eddies), STF (Subtropical Front), SAF (Subantarctic front), APF (Antarctic Polar Front), STIOG (Subtropical Indian Ocean gyre), SWIOSG (Southwest Indian Ocean sub-gyre).

Model simulations have also tested the sensitivity of the Agulhas Current system to different climatological forcings, such as shifted or intensified Southern Hemisphere westerlies, as well as the impact of the Agulhas Current strength itself on Agulhas leakage (Biastoch et al., 2009b; Rojas et al., 2009; van Sebille et al., 2009; Durgadoo et al., 2013). Additionally, satellite altimetry observations were used by Backeberg et al. (2012) and suggest that intensified Indian Ocean winds caused enhanced mesoscale variability of the Agulhas Current system, potentially resulting in an increase in Agulhas leakage. These studies emphasise the importance of changes in the Indian Ocean winds fields on Agulhas Current variability and its associated leakage.

Currently, evidence for changes in the strength and position of Southern Hemisphere westerlies during the last glacial cycle, based on both terrestrial and marine palaeo-evidence remains equivocal. Reconstructions from the southwest Pacific argue for a maximum in the Southern Hemisphere westerlies during the Last Glacial Maximum (LGM) and studies from southern South America hint towards a northward movement of the westerly storm tracks during the LGM (Lamy et al., 1998, 1999). In a recent synthesis by Kohlfeld et al. (2013), however, it was concluded that the position and strength of Southern Hemisphere westerlies during the LGM remains inconclusive based on data reconstructions alone. Model simulations also remain unclear regarding the position and strength of the Southern Hemisphere westerlies during the LGM. General circulation model (GCM) simulations by Wyrwoll et al. (2000) found evidence for a poleward displacement of the westerlies under glacial conditions while Rojas et al. (2009) conclude that the Southern Hemisphere westerlies were weaker and less zonally symmetric during the LGM. Recently, Sime et al. (2013) suggest that an equatorward shift of the Southern Hemisphere westerlies of more than three degrees during the LGM was unlikely based on their atmospheric modelling study.

Nevertheless, increased emphasis has been placed on the impact of the Southern Hemisphere westerlies on Agulhas leakage and its consequences for AMOC stability (e.g.,

Beal et al., 2011 and references therein). Reduced Agulhas leakage during the LGM compared to today has been inferred from a decrease in the proportion of ALF (Peeters et al., 2004) and linked to equatorward shifts in the position of the Subtropical Front (STF) and the Southern Hemisphere westerlies (Bard and Rickaby, 2009). However, reductions in Agulhas leakage may also be associated with strengthened Southern Hemisphere westerlies (Beal et al., 2011, Nof et al., 2011). This underscores the fact that the present understanding of the impacts on the Agulhas Current system of changes in the strength and position of the Southern Hemisphere westerlies is incomplete. Therefore a suite of experiments using an 'ocean only' model of the Agulhas Current system subjected to an equatorward shift (Nth4) and strengthening of the Southern Hemisphere westerlies (Wp40) have been performed, both scenarios are representative of plausible LGM conditions. This approach provides an idealised framework under which potential palaeo-scenarios may be interpreted and allows, at least, a first order approximation for comparison with the here employed proxy reconstructions.

3.2. Results

The $\delta^{18}O_{G.ruber}$ profile of the Agulhas Current core CD154 17-17K displays clear orbital modulations, with glacial-interglacial amplitudes of 1 ‰ to 1.8 ‰ during MIS 5a/4 transition and Termination I (TI), respectively (Fig. 3. 2a). Superimposed on the orbital oscillations is higher frequency variability that alludes to millennial-scale variability in the surface water hydrography of the Agulhas Current, even if less pronounced.

The SST variations inferred from the $Mg/Ca_{G.ruber}$ record (Fig. 3. 2b) and transfer function derived annual, summer and winter temperatures (Fig. 3. 2c-e) also show a distinct glacial-interglacial pattern. An obvious feature within the record is the cooling into MIS 4 and 2 when winter SSTs decrease to 17 °C and Mg/Ca based SST reconstructions suggest SSTs of 20 °C. Warm conditions (23-26 °C) during the interglacial MIS 5 and the Holocene co-vary with highest percentages of tropical-subtropical foraminiferal species (ALF) varying between 40-65 % (Fig. 3. 2b-f).

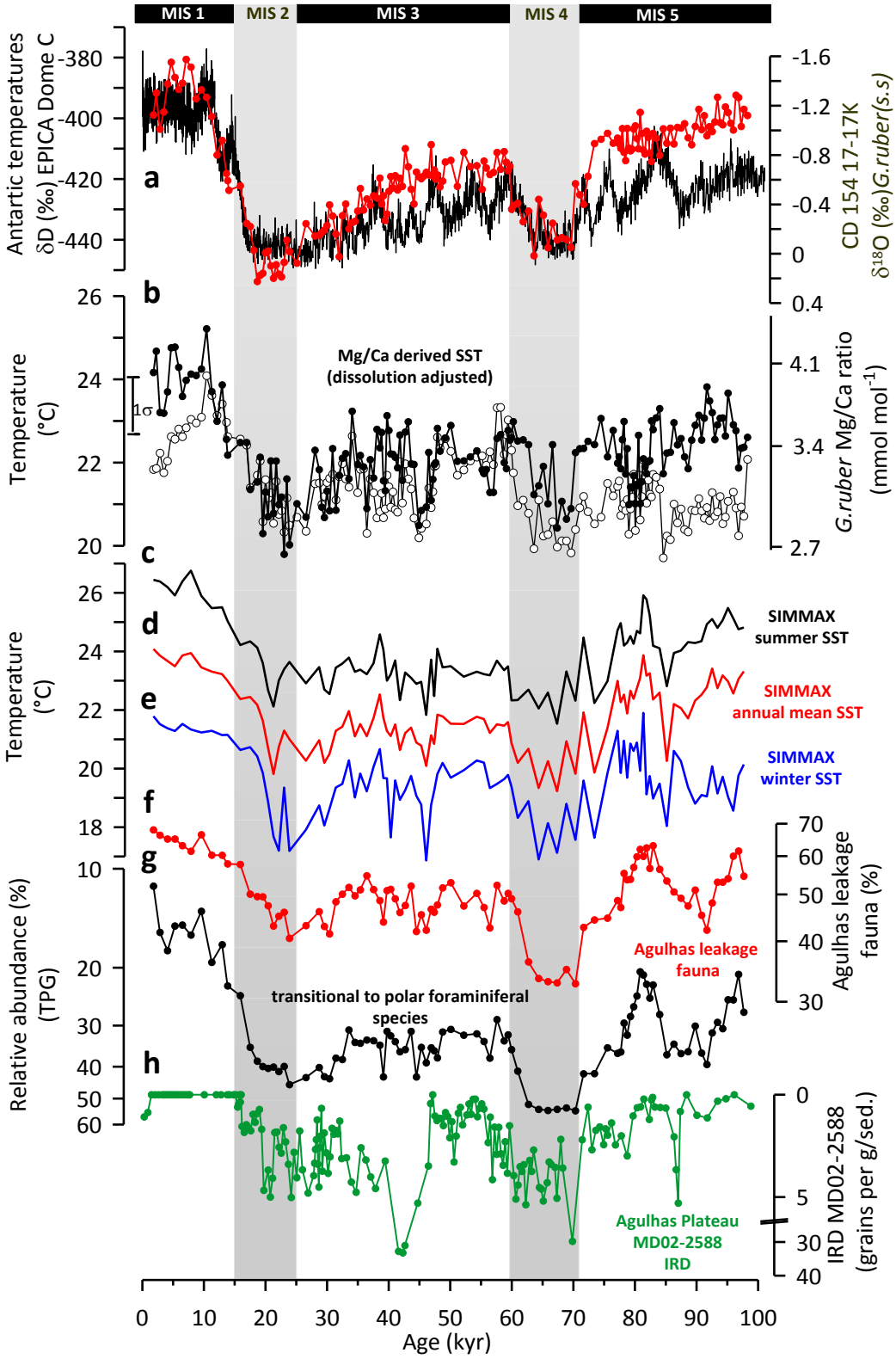

Fig. 3. 2 Comparison of past hydrographic changes in the upstream Agulhas Current (CD154 17-17K) with hydrographic changes in the Southern Ocean and temperatures over Antarctica. Data is shown in comparison with other regional and global climate record. (a) Antarctic temperatures δD (black), (EPICA DOME C) (a) Planktonic foraminiferal (*G. ruber*) $\delta^{18}O$ record from CD15417-17K, (red) (b) *G. ruber* Mg/Ca ratios and derived SSTs (white) and dissolution adjusted SSTs, (black) (c) SIMMAX method

derived summer/warm season SSTs, (black) (d) SIMMAX method derived annual mean SSTs, (red) (e) SIMMAX method derived winter/cold season SSTs, (blue) (f) Tropical-subtropical planktonic foraminifera marker species (Agulhas leakage fauna, ALF), (logarithmic scale, red) (g) Relative abundance of transitional to polar foraminifera species group (TPG), *G. inflata, N. pachyderma* (dex), *G. bulloides and G. truncatulinoides* (dex+sin) as an indicator of southern sourced/transitional water mass influence on the core site and strength of recirculation, (logarithmic scale, black) (g) IRD record of Agulhas Plateau, (green), (MD02-2588). Error bar represents the 1σ propagated error for the Mg/Ca-derived temperature reconstructions.

Throughout the entire record intervals of high abundances of transitional to polar foraminifera species (TPG) from transitional/frontal water masses (Fig. 3. 2g) co-vary with pronounced cooling events and high Ice-rafted detritus (IRD) accumulation rates at the Agulhas Plateau (Fig. 3. 2h). Ice-rafted debris deposition rates in core MD02-2588 are quite variable over the past 100 kyr and generally resemble the temperature pattern of the Agulhas Current, with less IRD deposited at the Agulhas Plateau during times of warmer SSTs recorded at CD154 17-17K and vice versa (Fig. 3. 2b-e,h). Notably, within MIS 4 (~70 ka), the SST cooling of up to 4 °C coincides with peak IRD deposition rates of 30 grains/g sed (Fig. 3. 2b,h).

The SST and $\delta^{18}O_{ivc\text{-}sw}$ profiles from the Agulhas Current display clear millennial-scale variability with abrupt increases up to 2 °C and ~0.8 ‰ (~2 psu) respectively, aligning with Northern Hemisphere cold events (NGRIP, 2004), (Fig. 3. 3a-c). Synchronously, ALF abundances rise by about 15 % at the same time mostly resembling features recorded in the Antarctic temperature record (Fig. 3. 3d,e). Notably, the Northern Hemisphere Cold Stadial (NHCS) cooling that precedes Dansgaard-Oeschger oscillation (D/O) events 21 - 19 (Dansgaard et al., 1993), as well as Heinrich Stadial (HS) 6 (Heinrich, 1988) are key examples of intervals of more warm, saline conditions on millennial timescales (Fig. 3. 3a,b,c).

3.3. Modelling results

In order to better understand the mechanism driving the large orbital to millennial-scale surface waters changes in the Agulhas Current observed in the proxy reconstructions idealised model experiments results are utilised here. The sensitivity of regional Agulhas transport to basin-scale intensification or an equatorward shift of the westerly wind changes is clearly highlighted in Figure 3. 4c-d, which shows the respective anomalies in the barotropic transport function as compared to the reference state (Fig. 3. 4a).

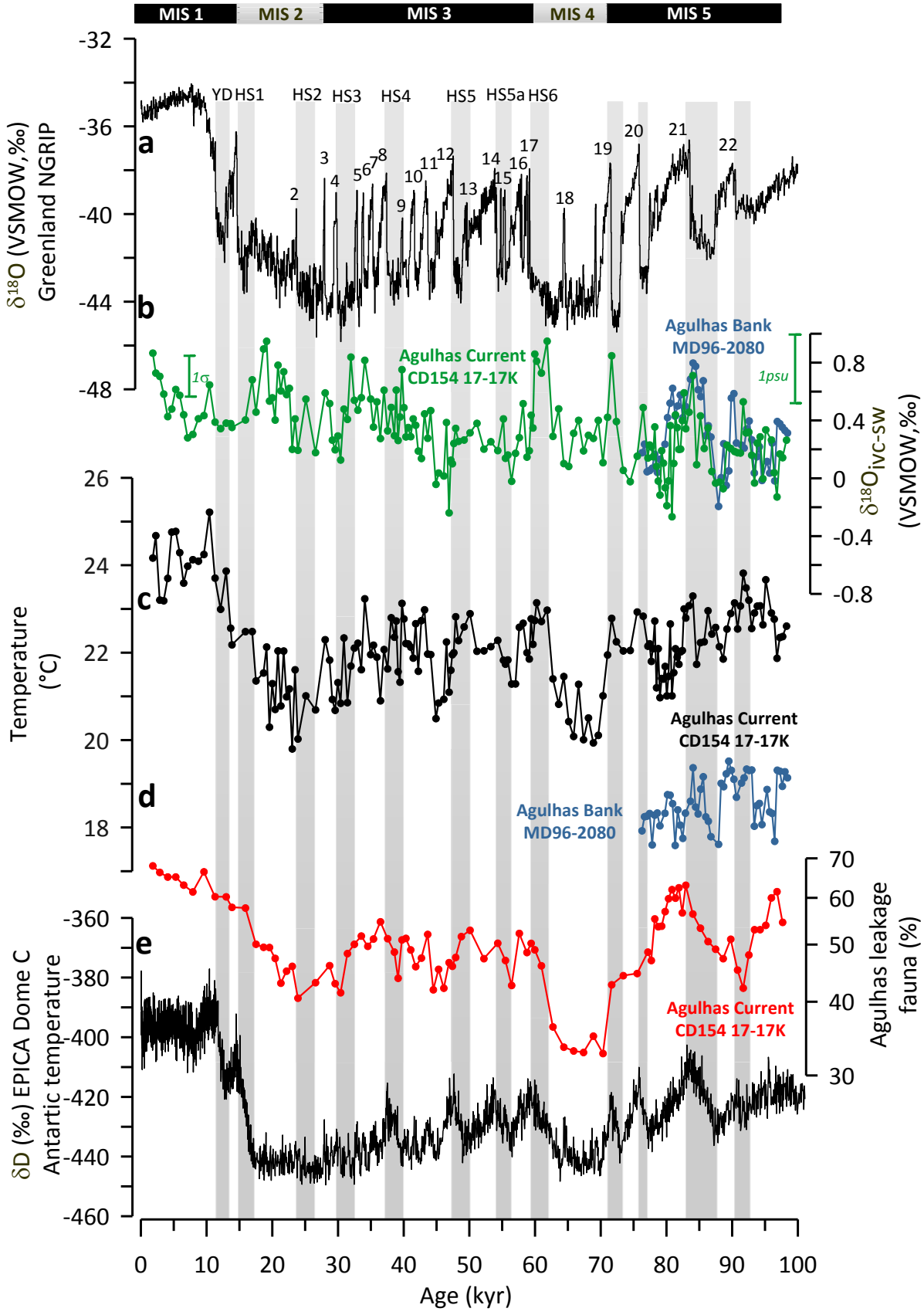

Fig. 3. 3 Comparison of millennial-scale climate change in Greenland with surface water changes in the southwest Indian Ocean since 100 kyr. (a) $\delta^{18}O$ record from Greenland ice core NGRIP, (black), (NGRIP,

2004) displaying abrupt temperature variability in the North Atlantic (Northern Hemisphere Stadials and Heinrich Stadials are marked as grey bars), numbers indicate warm D/O interstadials (b) Ice-volume corrected $\delta^{18}O_{SW}$ reconstruction ($\delta^{18}O_{ivc\text{-}sw}$) based on *G. ruber* Mg/Ca-derived SSTs, (green); $\delta^{18}O_{ivc\text{-}sw}$ reconstructions of Agulhas Bank record (MD96-2080, blue, Marino et al., 2013) is shown in comparison (c) Dissolution adjusted SSTs based on *G. ruber* Mg/Ca ratios, (black); SSTs of Agulhas Bank record (MD96-2080, blue, Marino et al., 2013) is shown in comparison (d) Relative abundance of tropical-subtropical planktonic foraminifera marker species, (logarithmic scale, red), (Agulhas leakage fauna, ALF) (e) Antarctic temperatures δD, (black), (EPICA, 2004)(Error bar represents the 1σ propagated error for the $\delta^{18}O_{ivc\text{-}sw}$ reconstructions and estimated equivalent changes translated into salinity units following Tiwari et al. (2013).

Anti-cyclonic flow in the sub-gyre, shown in blue shading and highlighted with the black ellipse, is more intense when winds are strengthened (Fig. 3. 4c), although both sensitivity experiments show increases in the local recirculation (Fig. 3. 4d) with increased wind-stress at 40 °S (Fig. 3. 4b). This enhancement in wind stress (and wind stress curl) at 40 °S drives an increase in northward transport, forcing an intensification of the Southwest Indian Ocean sub-gyre (SWIOSG), and an enhancement of local circulation.

The SWIOSG intensification augments the recirculation component of the Agulhas Current, but only significantly impacts the flow south of 32 ^{o}S. At 33 ^{o}S, the CD154 17-17K Agulhas core location, barotropic transport anomalies for the Wp40 and Nth4 cases are 13 Sv and 6 Sv, respectively (Fig. 3. 4c,d). The contributions from the northern source regions (e.g., Mozambique Channel and EMC) remain largely unchanged. Panels e to h of Figure 3.4 shows the anomalies in mean (MKE) and eddy (EKE) kinetic energy for the two sensitivity experiments. In both cases, the Agulhas Current south of 33 ^{o}S, Agulhas retroflection and Agulhas Return Current shows large increases in MKE (Fig. 3. 4e,f), consistent with higher transports. In the Southern Agulhas, around the core site, there is a decrease in EKE, suggesting that the current becomes less variable here (Fig. 3. 4g,h). However, the EKE increases at the retroflection, and in the Agulhas Return Current (ARC). The response to the changes in wind-shift are much more pronounced in the case of the Wp40 experiment (Fig. 3. 4h), due to the larger change in wind stress applied in this experiment (Fig. 3. 4b).

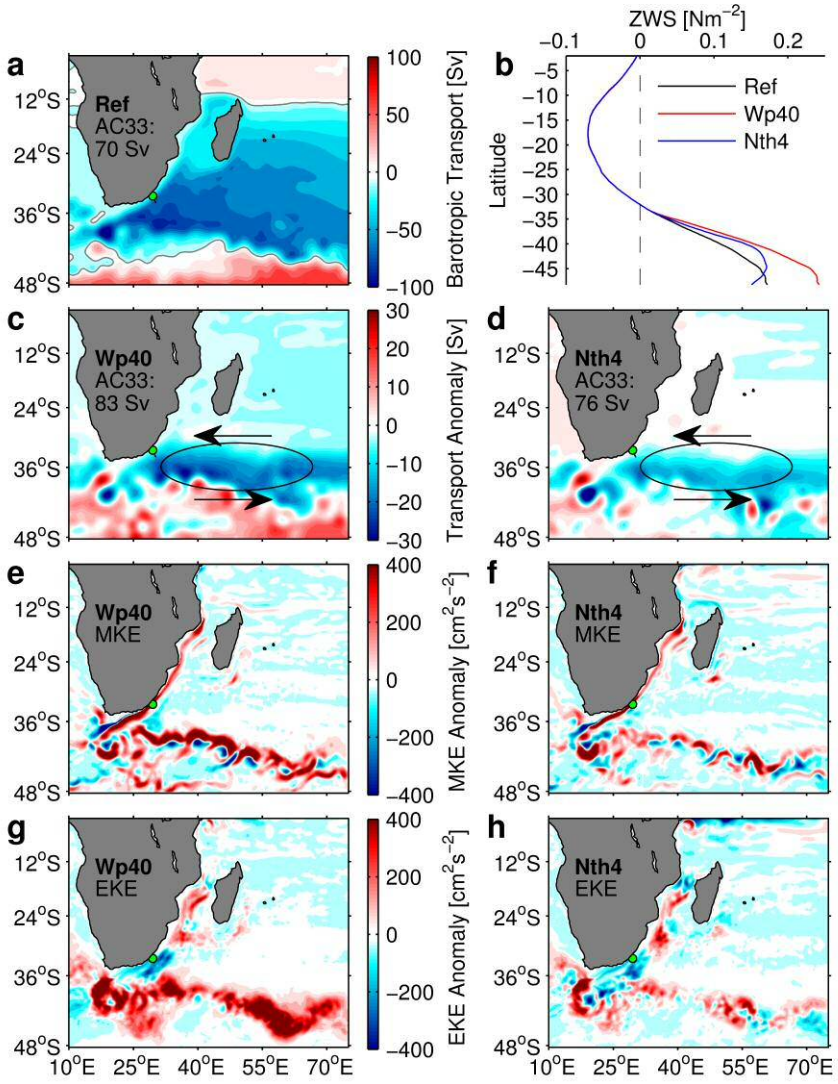

Fig. 3. 4 Changes in regional transport and mesoscale variability with Indian Ocean wind-stress. (a) the barotropic transport function for the southwest Indian Ocean, as extracted from the AGIO climatological reference experiment. The green dot shows the core site. The barotropic AC33 transport is measured across the Agulhas Current along a transect perpendicular to the shore, bisecting the core site. The grey line nominally separates cyclonic (red) from anticyclonic (blue) flow (b) the mean zonal wind-stress across the Indian Ocean between 20 oE and 115 oE, for the regional Wp40 and Nth4 sensitivity experiments (c, d) The anomaly in the barotropic transport (sensitivity - reference) associated with the Wp40 and Nth4 experiments, respectively. The black ellipse highlights the increase in anti-cyclonic circulation in the STIOG and SWIOSG (e, g) The respective anomalies in the 20-year mean (MKE) and eddy kinetic energy (EKE) fields for the Wp40 case. (f, h) as in (e, g), but for the Nth4 experiment.

3.4. Discussion

3.4.1 Long-term and millennial-scale variability of the Agulhas Current – linking changes in the Agulhas Current with Agulhas leakage variability.

The high-resolution multi-proxy record from the Agulhas Current provides insights into the nature and timing of the hydrography and climatic variability of the wider Agulhas Current system, with distinct variability on both orbital as well as millennial timescales over the past 100 kyr. In order to compare this variability with the reconstructions of the Agulhas leakage from the Agulhas corridor, Cape Basin Record (CBR; Peeters et al., 2004), the benthic $\delta^{18}O$ records were used to synchronise the CBR to the CD154 17-17K age scale (Fig. 3. 5a). Major SST decreases which are accompanied by decreasing abundances in the ALF can be recognised in both regions throughout the entire record (Fig. 3. 5b,c). Notably, during the last deglaciation, both regions show an SST increase of ~3 °C with ALF abundance increasing from ~40-65 % and 7-27 % at the CD154 17-17K and CBR sites respectively (Fig. 3. 5b-c). The similarities between these records strongly implies that changing environmental conditions impacted the wider Agulhas Current simultaneously and suggests a close connection between upstream Agulhas Current variability and its transmission further downstream within the Agulhas leakage corridor. To date a lack of proxy records from the Agulhas leakage corridor and the Agulhas Current resolving millennial-scale resolution has prevented a direct comparison between these two areas. However, a recently published high-resolution record from the Agulhas Bank, South Atlantic (Marino et al., 2013), (sediment core MD96-2080, 36°19.2'S, 19°28.2'E, 2488 m water depth, Fig. 3. 1) spanning MIS 5-8 offers the opportunity to compare both locations on millennial-scale basis, as both records overlap during the period between 76-98 ka. Importantly, Marino et al. (2013) also used the same planktonic foraminiferal species (*G. ruber*) to monitor changes in temperature and $\delta^{18}O_{ivc\text{-}sw}$ as used in this study, therefore avoiding the complications arising from comparing signals of differing foraminiferal species. The MD96-2080 record displays two distinct $\delta^{18}O_{ivc\text{-}sw}$ maxima during this time interval at 87-84 ka and at 94-90 ka, defined in their study as Agulhas Salt-leakage Maxima (ASM), ASM 21 and 22 with $\delta^{18}O_{sw}$ increases of ~1 ‰ and 0.6 ‰, respectively. Both $\delta^{18}O_{ivc\text{-}sw}$ anomalies are accompanied by temperature increases of up to ~2 °C.

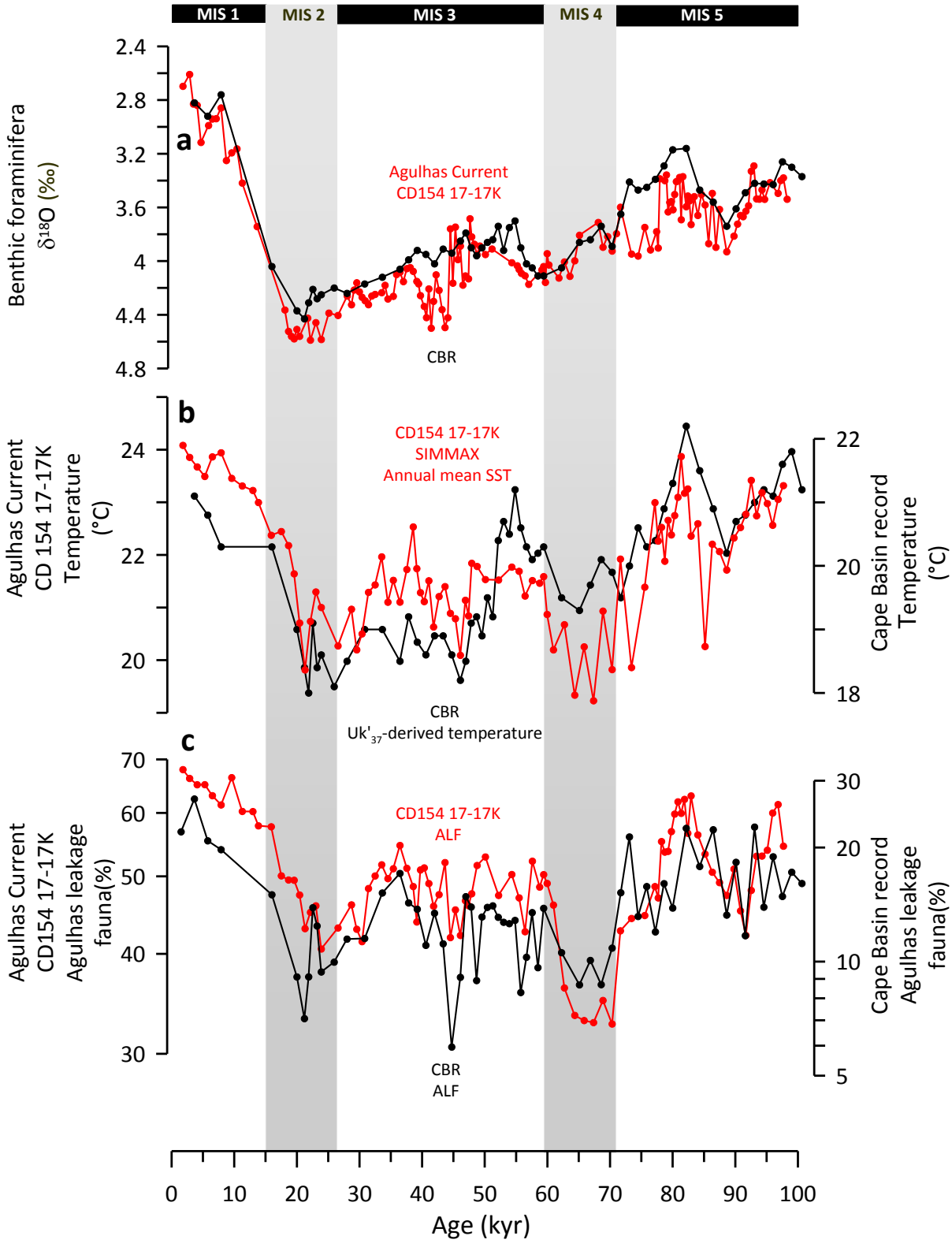

Fig. 3. 5 Comparison between the upstream Agulhas Current (CD154 17-17K) variability the past 100 kyr and Agulhas leakage (a) Benthic foraminifera $\delta^{18}O$ records in comparison to age model alignment (CD154 17-17K, red, CBR, black) (b) Annual mean transfer function derived SSTs in the Agulhas Current (CD154 17-17K, red) and Uk'_{37} derived SSTs in the Agulhas leakage corridor (CBR, black, Peeters et al., 2004) (c) Relative abundance of tropical-subtropical planktonic foraminiferal marker species (Agulhas

leakage fauna, ALF) in the upstream Agulhas Current (CD154 17-17K, logarithmic scale, red) and in the Agulhas leakage corridor (CBR, logarithmic scale, black).

Similar oscillations are recorded, within the combined age uncertainties, in the upstream Agulhas Current during these intervals with positive $\delta^{18}O_{ivc\text{-}sw}$ excursions of 0.7 ‰ at 87-84 ka and 0.5 ‰ at 94-90 ka (Fig. 3. 3b) and temperature increases of up to 1.5 °C (Fig. 3. 3c). However, even considering analytical uncertainties, the $\delta^{18}O_{ivc\text{-}sw}$ and SSTs excursions in the Agulhas Bank record appear slightly more pronounced compared to core site CD154 17-17K in the southwest Indian Ocean. The reason for these differences is unclear but could be related to changes in the oceanographic setting of the core sites, which may affect the sensitivity of the geochemical proxies. Nevertheless, the striking correspondence of the observed variability in SST, ALF abundances and $\delta^{18}O_{ivc\text{-}sw}$ in both areas suggests that the documented surface water signals recorded in the Agulhas leakage area are representative of changes in the wider Agulhas Current system as a whole or plausibly form in the upstream Agulhas Current and are transmitted to the downstream region by the current itself.

Millennial-scale SST, ALF and $\delta^{18}O_{ivc\text{-}sw}$ changes in the Agulhas Current align with NHCS (i.e., Heinrich Stadials; Fig. 3. 3). The increases in these features during maximum cooling in the North Atlantic, peak in step with the rapid shifts to interstadial conditions in Greenland (Fig. 3. 3a), and abruptly decreases shortly thereafter. Examples of this phasing in the Agulhas Current, among others, are seen at 87-84 ka, and at 63-59 ka, where the temperature, ALF and salinity build-up in the Agulhas Current parallels the cold stadial conditions in the north (Fig. 3. 3a-d). These intervals suggest an interhemispheric teleconnection between millennial-scale climate variability in the North Atlantic and observed changes in the Agulhas Current properties. These findings are consistent with the 'bipolar seesaw' pattern of Northern Hemisphere cooling and Southern Hemisphere warming during the last glacial period (Broecker, 1998; Stocker and Johnsen, 2003; Barker et al., 2009). Such a pattern has been explained by changes in the cross-equatorial heat flux connected to variability of the AMOC (Knutti et al., 2004).

Millennial-scale warming events, revealing an out-of-phase relationship with stadial conditions in the North Atlantic, have also been observed elsewhere within the Indian Ocean and suggest that the oscillations of the Agulhas Current are likely coherent with the wider regional bipolar response. Mg/Ca-derived SST records from the Indonesian

Throughflow region immediately south of Indonesia (Levi et al., 2007) indicate a temperature increase of about 2 °C during HS 2, HS 1 and the Younger Dryas (YD). Faunal assemblage based SST estimates from a core site in the Mozambique Channel (Levi et al., 2007) display warming during HS1 and YD of about 1.5 °C. The Indonesian Throughflow and the Mozambique Channel are considered important source water areas supplying the Agulhas Current (Beal et al., 2011). A more recent study by De Deckker et al. (2012) show millennial-scale warm phases south of Australia during HS 1- 3 and YD with temperature increases between 1.5-3 °C during these intervals. Millennial-scale warm phases south of Australia are linked in their study to the position of the dynamic STF which is determined by latitudinal shifts of the Southern Hemisphere westerlies. A study from the Antarctica zone in the Pacific Ocean (Anderson et al., 2009), based on opal deposition events, further infers latitudinal shifts of the Southern Hemisphere westerlies during millennial-scale NHCS.

Numerical modelling simulations suggest that in response to a NHCS the Hadley Cell in the southern tropics weakens which ultimately strengthens and/or shifts the Southern Hemisphere westerlies towards Antarctica (Toggweiler and Lea, 2010; Lee et al., 2011). However, a new study by Sime et al. (2013) challenges the link between the strength of the Hadley Cell and the associated impact on the westerlies. Nevertheless, these findings suggest that the reorganisation of the atmospheric circulation, position and strength of the Southern Hemisphere westerlies, during NHCS might have played an important role in determining the bipolar warming response of the Southern Ocean. Therefore the response and sensitivity of the Agulhas Current system to shifted Southern Hemisphere westerlies is further explored.

3.4.2 Southwest Indian Ocean sub-gyre dynamics and its impact on Agulhas Return Current variability.

The coldest upper ocean conditions in the Agulhas Current prevailed during MIS 4 and 2/3 boundary (Fig. 3. 2). These intervals are marked by a reduced abundance of the ALF (and warm water species) and a higher proportion of TPG associated with polar to transitional water masses. Ice-rafted debris events at the Agulhas Plateau have been interpreted as indicating episodes of intensified northward advection of polar waters associated with the northward shift of regional oceanic fronts supporting iceberg survivability as far north as

the Agulhas Plateau, 41 °S (Fig. 3. 1). Increased IRD is closely related to the local cooling events observed in the upstream Agulhas Current (Fig. 3. 2b,h) implying a tight coupling between both regions. Therefore it can be assumed that the synchronous cooling events of both areas are related to changes in the dynamics of SWIOSG and associated ARC that allowed a stronger influence of colder southern component surface waters to modify the hydrography of the upstream Agulhas Current. Cold, transitional water masses occurring along the dynamic STF are entrained into the ARC due to the recurrent eddy generation and shifts in its trajectory that closely follows the front (Lutjeharms and Ansorge, 2001), (Fig. 3. 1).

Evidence from the numerical model simulations strongly suggests a strengthening and zonal expansion of the SWIOSG under intensified or equatorward-shifted Southern Hemisphere westerlies (Fig. 3. 4c,d). Additionally, the increase in wind stress curl south of 35 ^{o}S in both cases results in an enhancement of the transport in the ARC. This stronger transport is reflected in both the MKE and EKE immediately north of the STF (Fig. 3. 4e-h). Increasing EKE reflects an enhanced prevalence or propagation speed of mesoscale features, such as eddies and meanders. The increase in turbulence associated with these features may facilitate increased cross frontal mixing by weakening the thermal gradients associated with the STF, resulting in increased export of Indian Ocean waters to the south, and entrainment of Southern Ocean derived water masses into the ARC. Such a scenario could enable a redistribution of these waters into the Agulhas Current itself via enhanced recirculation leading to the SST cooling and increase in abundance of the TPG observed in the CD154 17-17K record. Equally, theses cold(er) Southern Ocean derived waters would also influence the surface waters near the Agulhas Plateau, potentially enabling increased iceberg survivability in the region. Conversely, warm periods during which Sea surface salinity (SSS) are increased and warm tropical Indian Ocean foraminifera dominate the waters of the Agulhas Current, the influence of the ARC recirculation on the CD154 17-17K site is likely to have been reduced. A suggested southward displacement (or weakening) of the Southern Hemisphere westerlies during NHCS and interglacials, which is in agreement with previous studies (Lamy et al., 2004; Lamy et al., 2007), would create a less vigorous SWIOSG diminishing the influence of cold, transitional water masses on the Agulhas Current. The lowest IRD accumulation rates at the Agulhas Plateau, indicative of a southward contraction of the Subantarctic zone and associated frontal system, strengthen

the interpretation that both areas were less affected by southern sourced waters at these times.

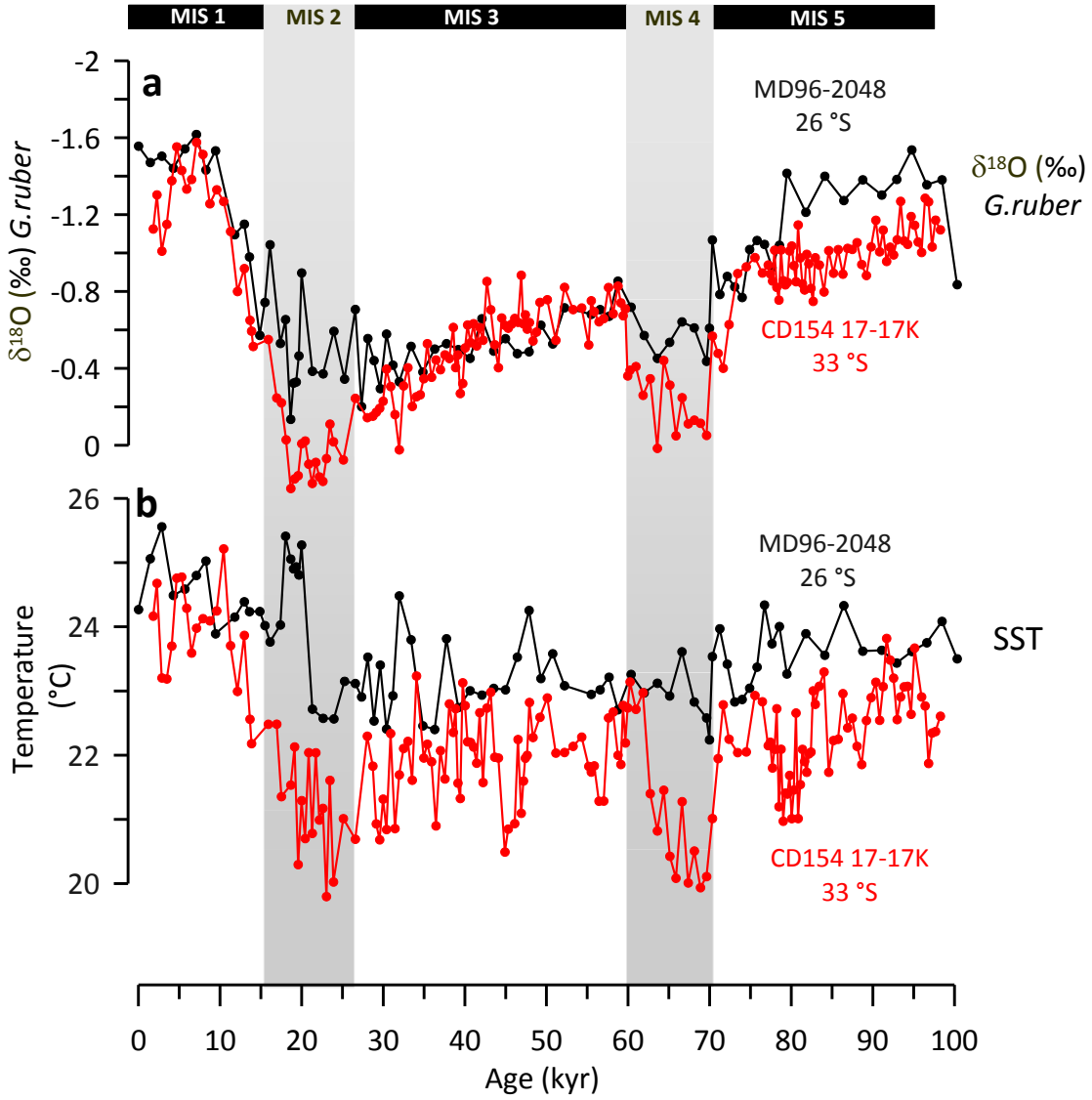

Fig. 3. 6 Comparison between the upstream "precursor" region of the Agulhas Current (MD96-2048, 26 °S, Caley et al., (2011)) and Agulhas Current variability (CD154 17-17K, 33 °S, this study) (a) Planktonic foraminiferal (*G. ruber*) $\delta^{18}O$ records in comparison for age model alignment (CD154 17-17K, red, MD96-2048, black) (b) *G. ruber* Mg/Ca-derived SSTs (CD154 17-17K, red, MD96-2048, black).

A comparison of the here studied record with data by Caley et al. (2011a), from the 'precursor' region of the Agulhas Current (sediment core MD96-2048, 26 °S, 660 m water depth, Fig. 3. 1), provides further evidence of the Agulhas Current sensitivity to changes in the intensity and influence of the SWIOSG. The lower temporal resolution of the Caley et al. (2011a) record, which spans the past 800 kyr, only allows comparison at orbital (glacial-interglacial) timescales, following the synchronisation of the $\delta^{18}O_{G.ruber}$ record of MD96-2048 to the CD154 17-17K age scale (Fig. 3. 6a). The $\delta^{18}O_{G.ruber}$ records (Fig. 3. 6a) from

both sites exhibit prominent glacial-interglacial modulation, for example during the warm conditions of MIS 5a, 3 and the Holocene, where the $\delta^{18}O_{G.ruber}$ records show similar absolute isotopic values. The decoupling of $\delta^{18}O$ values of both records during the cold periods of MIS 4 and 2 indicate generally cooler conditions in the Agulhas Current, highlighted by heavier $\delta^{18}O$ values in the CD154 17-17K core, and further supported by the comparison of the Mg/Ca (*G. ruber*) derived SSTs of both records (Fig. 3. 6a,b). The varying temperature contrasts between these two areas are most likely a result of changes in the intensity and impact of the SWIOSG on the Agulhas Current. Such that during periods when the SWIOSG was more vigorous, the Agulhas Current at 33 °S experienced a stronger influence of cold, transitional waters masses while the 'precursor' regions located further to the north, upstream of the main Agulhas system, remained outside the direct influence of the ARC recirculation. Such a scenario would augment the temperature difference between both core locations. Conversely, a less intense SWIOSG would explain the observed similarities and reduced temperature contrast between both sites observed during warm interglacial conditions. The results demonstrate that the surface water properties of the Agulhas Current are particularly sensitive to SWIOSG-variability, and the signature of this variability is subsequently transferred into the South Atlantic via Agulhas leakage.

The interplay between waters feeding the Agulhas, either originating from the Southern Ocean frontal system or the tropical Indian Ocean, demonstrates the potential sensitivity of the Agulhas Current hydrography towards varying source influences. This also highlights the different response patterns of the Agulhas Current, one being connected with Southern Hemisphere warming in response to the bipolar seesaw during NHCS, and the other being connected with a shifted ocean circulation pattern in the SWIOSG in response to a modified atmospheric circulation.

3.5. Conclusions

Upper ocean temperature, salinity and planktonic foraminiferal assemblage records from the Agulhas Current exhibit a high variability on orbital to millennial timescales. Agulhas leakage records (Peeters et al., 2004; Marino et al., 2013), show a high degree of similarity in this variability and phasing of temperature, salinity and planktonic foraminiferal-based Agulhas leakage. The observed orbital and millennial-scale SST, ALF and salinity oscillations of the Agulhas Current can largely be explained by the bipolar seesaw response of the

Indian Ocean itself and the varying influence of the SWIOSG on the Agulhas Current system. A present lack of records of equivalent temporal resolution and stratigraphic reach from within the source areas of the Agulhas Current as well as in the wider Subtropical Indian Ocean gyre prevent an up to date, clear separation between the two dominant forcing mechanisms (westerlies vs. low-latitude tropical Indian Ocean/Pacific) which ultimately determine Agulhas Current properties variability and its inferred leakage.

The findings suggest that the temperature and salinity changes in the Agulhas leakage area, i.e., in the southeast Atlantic Ocean, is at least partly a result of upstream variability in these properties within the source region of the Agulhas leakage. Thus observed changes in the Agulhas leakage corridor need not be necessarily related to changes in the amount of water being transferred through the Indian-Atlantic Ocean Gateway via the Agulhas leakage but rather a consequence of changes in the composition of the Agulhas Current itself. This highlights the care that must be taken when interpreting Agulhas salt-leakage from the Agulhas corridor alone.

Additionally, similarities of the here established SST record of the past 100 kyr in the Agulhas Current, southwest Indian Ocean and the Agulhas Plateau suggest a strong connection between the two regions on both orbital and millennial timescales. As the most plausible mechanism a transfer of Southern Ocean temperature anomalies via the Agulhas Return Current can be suggested. The modelling exercise demonstrates that increased ARC dynamics and recirculation can be explained by changes in the strength of the SWIOSG forced by either a northward displacement or strengthening of the Southern Hemisphere westerlies. Coldest upper ocean temperatures occurred during MIS 4 and MIS 2/3 boundary in the Agulhas Current and are accompanied by an increased abundance of southern ocean TPG foraminiferal species. During these periods the SWIOSG was likely intensified, causing an enhanced ARC transport and recirculation south of Madagascar. This enhanced ARC allows cold, transitional water masses originating from the frontal zones further to the south to become entrained, and upon reaching the Agulhas Current potentially influence its hydrographic properties. This implies that the large-scale wind fields (Southern Hemisphere westerlies) over the subtropical Indian Ocean are one of the main controls on the Agulhas Current variability with consequences for Atlantic surface waters buoyancy as well as AMOC stability.

4. Deep water variability off southeast Africa during the past 270 kyr

4.1. Introduction

The region around South Africa constitutes a critical oceanic gateway, the Indian-Atlantic Ocean Gateway (IAOG), within the global ocean overturning circulation where Indian-Pacific Ocean and South Atlantic water masses meet and mix (Gordon, 1985; Gordon, 1986). Offshore South Africa is the key area where the surface Agulhas Current and the deep water currents are fully concentrated and flowing strongly in opposing directions.

Currently, about 15 to 20 Sv (1 Sv = 1 x 10^6 m^3/s) of North Atlantic Deep Water (NADW) is exported through the South Atlantic and contributes directly to the deep water flow entering the Indian Ocean through the IAOG (Bailey and Rogers, 1997). The Indian Ocean is an important part of the global ocean overturning circulation, receiving deep waters sourced from the North Atlantic and Southern Ocean and being a location of upwelling to the surface return flow that balances the southward flux of NADW. The modern circulation of deep waters in the southwestern Indian Ocean comprises the saline NADW, its derivative in the Antarctic Circumpolar Current (ACC), Lower Circumpolar Deep water (LCDW), and the aged variety of deep water, North Indian Deep water (NIDW), (van Aken et al., 2004). Circumpolar Deep water is a mixture of NADW, AABW, and Antarctic Intermediate Waters (AAIW) recirculating within the ACC (Orsi et al., 1995). In the deeper water column of the Southern Ocean the high salinity, oxygen-rich and nutrient depleted NADW is injected into the CDW at a water depth between 2.5 and 4 km (Reid, 1989) and splits the CDW into an upper- (Upper Circumpolar Deep water (UCDW)) and lower component (LCDW).

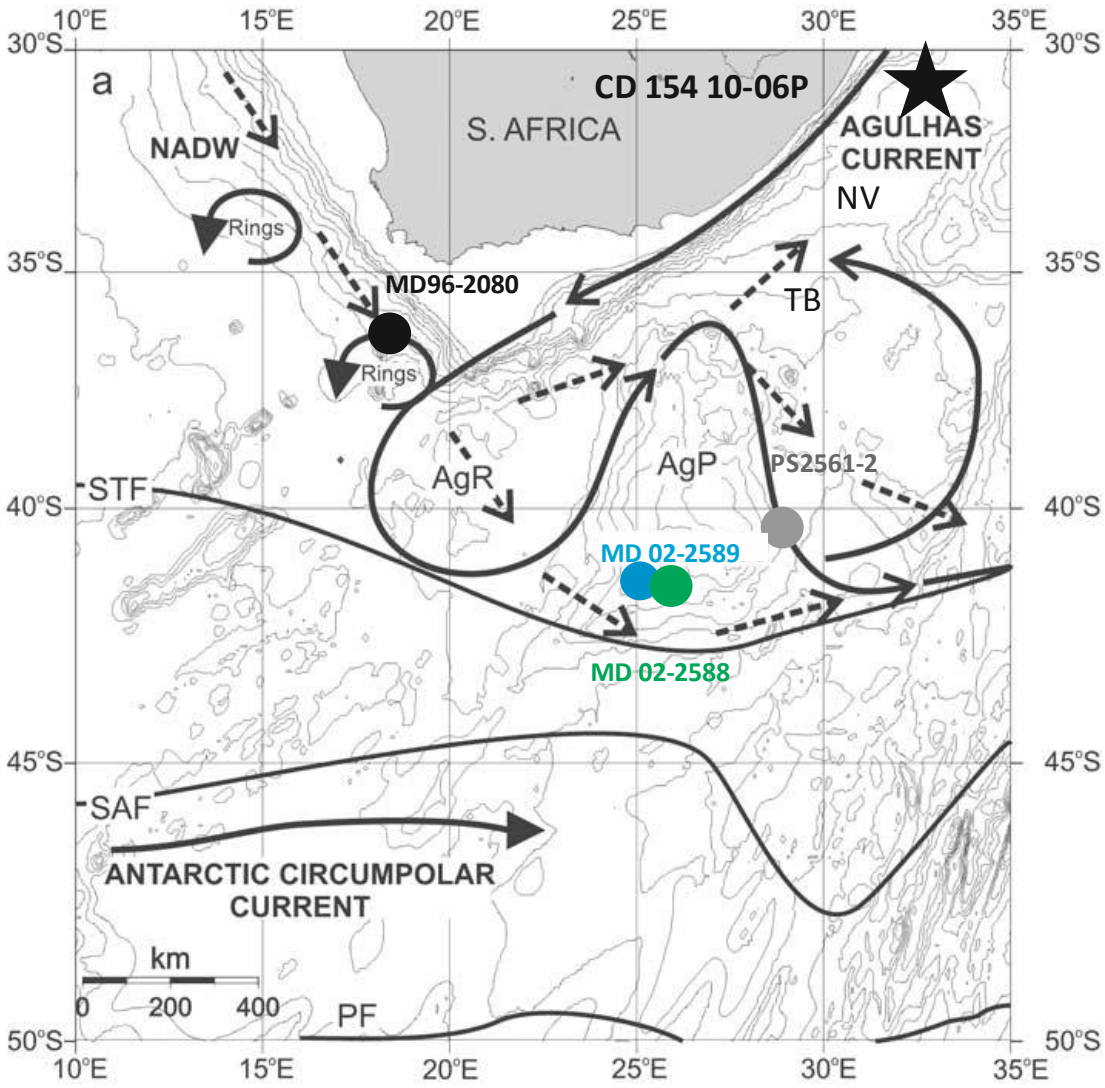

Fig. 4. 1 (a) Study area and position of cores used in this study together with present-day position of the oceanic fronts (Beal and Bryden, 1997) and generalised ocean circulation after Richardson et al. (2003). CD154 10-06P, this study, 31°S,32°E, 3076 m; Agulhas Plateau, MD 02-2589, Molyneux et al. (2007), 41°S,25°E, 2660 m; Agulhas Plateau, MD 02-2588, Ziegler et al., (2013a), 41°S, 25°E, 2907 m, Agulhas Plateau, PS2561-2, 4465, Krueger et al., (2012), 41°S,28°E, Agulhas Bank, MD96-2080 , Martínez-Méndez et al. (2008), 36°S, 19°E , 2488 m. Position of the fronts after Belkin and Gordon (1996) and Orsi et al. (1995). Solid arrows are surface water currents, and dashed arrows are bottom water currents. NADW, North Atlantic Deep water; AgP, Agulhas Plateau; AgR, Agulhas Retroflection; TB, Trankei Basin; NV, Natal Valley; STF, Subtropical Front; SAF, Subantarctic Front; PF, Polar Front (Map modified from Molyneux et al. (2007)).

The first direct observations of the full-depth velocity structure of the Agulhas Current were made in March 1995. During this experiment Acoustic Doppler Current Profiler transects identified the presence of a deep counter-current beneath the Agulhas Current, a feature not previously observed and now known as the Agulhas Undercurrent (AUC), (Fig. 4. 2) (Beal and Bryden, 1997). At 32 °S in the southwest Indian Ocean the AUC

transports in the region of 10 Sv of NADW and AAIW rapidly northward (McDonagh et al., 2008). This transport represents about 20% of the total overturning in the Indian Ocean (Bryden and Beal, 2001) and highlights the importance of this current for the ventilation of the deep Indian Ocean and thus global ocean circulation.

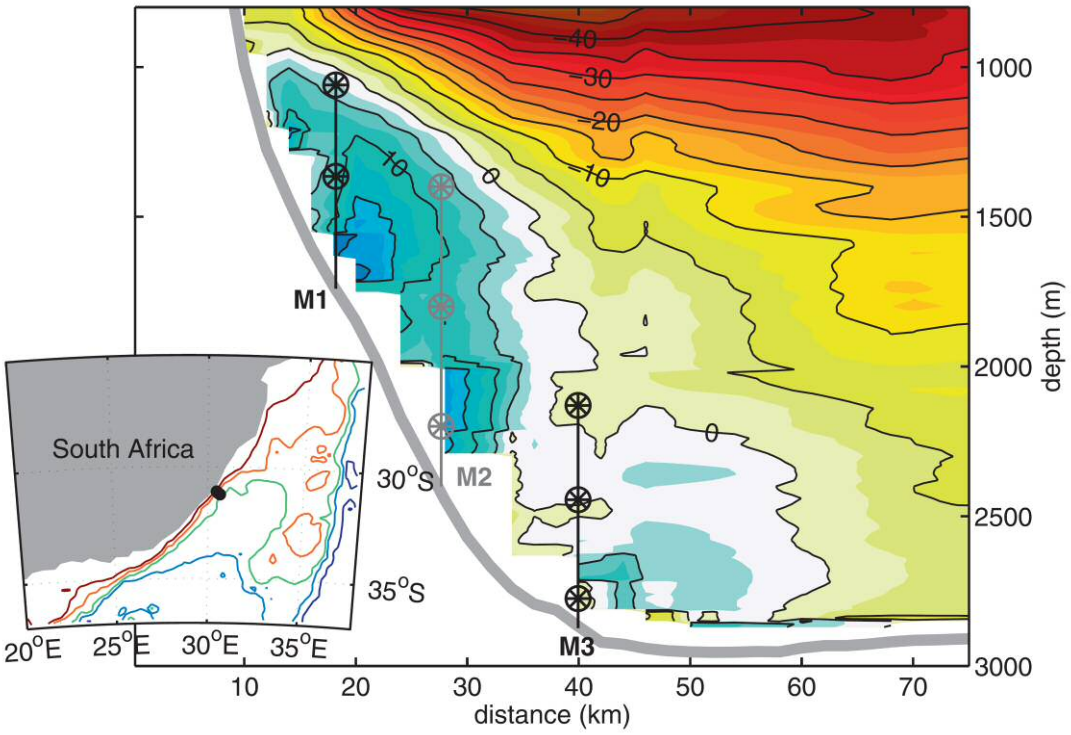

Fig. 4. 2 The average velocity structure of the Agulhas Undercurrent from Beal et al., (2009) with positions of the instruments on all Agulhas Undercurrent Experiment (AUCE) moorings (M2 in gray was not recovered). Velocities to the southwest are shown in shades of yellow through red. Velocities in the undercurrent are shown in shades of white through blue. Black contours every 5 cm s^{-1}. Bathymetry is depicted by the thick gray line. The inset map shows the geographical position of the AUCE moorings (black dots), on the eastern continental slope of South Africa. The bathymetries of the Natal Valley and Mozambique Plateau are shown in color contours: red through blue, 1000 to 5000 m, in intervals of 1000 m.

NADW occupied shallower depths during glacials (e.g., Marchitto and Broecker, 2006). Therefore its place within the water column (~2500 and 4000m) was substituted by a mid-depth water mass of southern origin (e.g., Oppo and and Curry, 2012) enriched in $\delta^{13}C$ relative to the deeper layers in the South Atlantic and southwest Indian Ocean (Molyneux et al., 2007; Martínez-Méndez et al., 2008). Palaeoceanographic studies from the equatorial Indian Ocean based on Neodymium (Nd) isotope records show that there was reduced NADW present during glacials (Marine Isotope Stage (MIS) 2, 4, and 6) in

comparison to the modern and evidence points towards Dansgaard-Oeschger oscillations (D/O) type millennial-scale variability during MIS 3. Deep water palaeocenographic records

from the South Atlantic have traditionally been used to infer the interplay between NADW and Southern Hemisphere water masses i.e., Southern Component Waters (SCW) as a function of mode shifts in the AMOC. Reduced southward spread of NADW during glacial periods has been suggested by studies using Nd isotope ratios (e.g., Rutberg et al., 2000; Piotrowski et al., 2004, 2005), benthic $\delta^{13}C$ records (Streeter and Shackleton, 1979; Sigman and Boyle, 2000; Martínez-Méndez et al., 2008) and clay-mineral tracers (Krueger et al., 2008). At the same time export of AABW from the Southern Ocean intensified (Robinson et al., 2005; Negre et al., 2010; Hall et al., 2011). Although, the view that NADW shoaled during the Last Glacial Maximum (LGM), forming the so called Glacial North Atlantic Intermediate Water, (GNAIW), (Lynch-Stieglitz et al., 2007; Gebbie, 2014) and was replaced below about 2000 m water depth by nutrient-rich waters from the Southern Ocean (Boyle and Keigwin, 1987; Curry and Oppo, 2005; Marchitto and Broecker, 2006) is now well established, there is no clear consensus reached yet, whether these changes were related to a more, less, or similarly vigorous AMOC at that time (Kitoh et al., 2001; Lynch-Stieglitz et al., 2007; Hesse et al., 2011; Lippold et al., 2012).

Nutrient proxies ($\delta^{13}C$ and Cd/Ca) suggest that the South Atlantic (Martínez-Méndez et al., 2008) and the western most Indian Ocean (Molyneux et al., 2007; Krueger et al., 2012) deep water mass distribution has varied on glacial–interglacial and shorter timescales. However, currently no study exists from the southwest Indian Ocean that has monitored NADW oscillations north of the Agulhas Plateau. Here, a new benthic stable isotope record of a marine sediment core located in the Natal Valley in the deep southwest Indian Ocean at modern NADW depths is presented (Fig. 4. 1, see also Fig. 2. 2). The core location can be seen as an ideal strategic location to monitor the timing, amplitude and propagation of changes in the advection of NADW, from the southeastern Atlantic into the central Indian Ocean via the AUC, which might have been related to AMOC mode changes. The record is compared with previously published deep water records in the region to investigate the relationship between deep water hydrographic variability in the southwest Indian Ocean and South Atlantic. These additional records include: 1) core MD96-2080 (41°S, 28°E; 2488m water depth) located at the Agulhas Bank in the southeastern Atlantic, and influenced today by the southern extension of NADW as it spreads in the South

Atlantic between 2000 and 3500 m (Martínez-Méndez et al., 2008). 2 and 3) cores MD02-2589 (41°S, 25°E, 2660 m water depth), (Molyneux et al., 2007) and MD02-2588, (41°S, 25°E, 2907 m water depth), (Ziegler et al., 2013a) which are both situated on the southwestern flank of the Agulhas Plateau and predominantly bathed in the southern extent of NADW with a substantial CDW component as those cores are positioned near the mixing zone between NADW and LCDW (Molyneux et al., 2007). 4) core PS2561-2 (41°S,28°E, 4465m), (Krueger et al., 2012) which lies on the southeastern flank of the Agulhas Plateau, but at a much deeper water depth it sits within the mixing between LCDW and AABW. Combined with the Agulhas surface water records presented in Chapter 3 (and new surface records of core CD154 10-06P) potential linkages between surface- and deep water changes can be evaluated and their climatic implications are discussed. Special emphasis is placed on the last deglaciation in order to evaluate if changes in the Agulhas Current led changes in the deep-circulation or vice versa. That approach might unravel whether Agulhas leakage had an active or passive role during glacial terminations.

4.1.1. Study Approach

In order to define changes in water mass structure and circulation in the southwest Indian Ocean over the past 270 kyr, stable isotope records based on measurements of benthic foraminifera of the genus *Cibicidoides* have been conducted over the entire core length. Temperature, salinity and global ice-volume changes generally are mirrored by variations in benthic $\delta^{18}O$ whereas the nutrient content largely follows water mass structure and circulation in the modern ocean and is incorporated in the $\delta^{13}C$ signature of the benthic foraminiferal shell. Interpretation of deep water inventory changes will be based in this study on the benthic $\delta^{18}O$ and $\delta^{13}C$ data of core CD154 10-06P whereas low-resolution Mg/Ca-derived temperatures of planktonic foraminifera *Globigerinoides ruber* are used to infer Agulhas Current variability from the same core material. Moreover, paired $\delta^{18}O$ and Mg/Ca ratios of foraminifera *G.ruber* in high-resolution over Termination I (TI) display relative salinity changes in the current. In conjunction with the previously discussed data in Chapter 3 and published deep water records based on sedimentary $^{231}Pa/^{230}Th$ ratios (Negre et al., 2010) and Nd isotope (Piotrowski et al., 2005; Piotrowski et al., 2012) from the southeast Atlantic the timing of changes in the Agulhas Current and inferred leakage can be monitored in respect to the NADW influence around South Africa.

4.2. Results and Discussion

4.2.1. Orbital-scale deep water variability off southeast Africa during the past 270 kyr

The high-resolution benthic $\delta^{18}O$ profile displays orbital modulation caused by changing ice volume as the dominant control (Fig. 4. 3a). Benthic $\delta^{18}O$ shifts for terminations are 1.8‰ (TI), 2‰ (TII) and 1.79‰ (TIII), which are well in excess of the mean-ocean change of 0.8-1.1‰ (Schrag et al., 2002; Waelbroeck et al., 2002). The residual $\delta^{18}O$ isotopic change documents changes in deep water temperature and/or $\delta^{18}O$ water (salinity) at the core site (Fig. 4. 3a).

The benthic $\delta^{13}C$ record shows large glacial-interglacial (G-I) amplitudes of ~1.1 -1.4‰ during the last three terminations with lower values during glacial stages MIS 8, 6, 4 and LGM (Fig. 4. 3b). Temporal changes in the benthic $\delta^{13}C$ at any location reflect a combination of changes in the marine carbon reservoir, ocean circulation, air-sea gas exchange and marine biological productivity. Negative carbon anomalies during glacials of up to 0.4‰ have been suggested for the Southern Ocean due to the influence of fluctuating primary productivity (the so called Mackensen effect, see Chapter 2) (Mackensen et al., 1993). Mean ocean $\delta^{13}C$ shifts during glacial-interglacial changes were shown to be around 0.32‰ (Duplessy et al., 1988) to 0.4‰ (Curry et al., 1988). In order to account for these mean ocean benthic $\delta^{13}C$ changes a stacked record, originally employed by Zahn and Stüber (2002) and further described by Martinez-Mendez et al. (2008), from 11 sediment cores from the Atlantic-Pacific and Indian Ocean has been used here to correct core CD154 10-06P for longer-term ocean carbon pool variations (Fig. 4. 3b-c). A detailed description about the stacked benthic $\delta^{13}C$ record can be found in Martínez-Méndez et al. (2008). Additionally, benthic $\delta^{13}C$ in core CD154 10-06P also display a secular increase in values ~0.4‰ between ~270 ka and the LGM (Fig. 4. 3b). A similar trend exists in other records (e.g., ODP 1123, Hall et al., 2001; MD01-2378, Holbourn et al., 2005, MD96-2080, Martínez-Méndez et al., 2008) and has been associated with the long-term evolution of the marine carbon pool (e.g., Mix et al., 1995, Hoogakker et al., 2006, Rickaby et al., 2007) probably related to the 400 kyr eccentricity cycle.

It can be seen that, despite the mean ocean $\delta^{13}C$ correction, large residual $\delta^{13}C$ amplitude shifts occur during terminations of ~0.8‰ with generally more depleted values during glacials indicative of low ventilation at these times (Fig. 4. 3c). Generally, shifts in the $\delta^{13}C$

of core CD154 10-06P towards higher values during glacial terminations are more gradual and occur earlier compared to the $\delta^{18}O$ changes in the same record. NADW originates with $\delta^{13}C$ values above 1‰ in the North Atlantic (Kroopnick, 1985) and as it extends southward it mixes with Southern Ocean source water resulting in lower $\delta^{13}C$ values. According to the GEOSECS stations established in the 1980's (Kroopnick, 1985) and recently confirmed by the new GEOTRACERS program present-day ambient seawater $\delta^{13}C$ at ~3000 m water depth in the western Indian Ocean has values of ~0.5‰ which are typical values for the core of CDW (see http://www.egeotraces.org/sections/GI04_DIC_13_D_DELTA.html).

The average late Holocene (0-5 ka) values of core CD154 10-06P are ~0.72‰ and thus slightly higher than the modern seawater values in the western Indian Ocean (Fig. 4. 3c). This could be related to the position of the GEOSECS/GEOTRACER transects which lie further to the east compared to our core location and thus might represent ambient seawater $\delta^{13}C$ values representative of CPW, which are generally lower compared to NADW (Kroopnick, 1985). Modern physical oceanographic studies suggest that the Natal Valley is strongly influenced by NADW rather than CPW, which only dominates further to the east (Wyrtki, 1971). Present day NADW $\delta^{13}C$ in the South Atlantic typically has values of 0.8‰ (Bickert and Wefer, 1996). This might suggest that core CD154 10-06P is currently positioned near the mixing zone between NADW and CDW with a higher proportion of NADW.

Evidence for changes in water-mass provenance and circulation is suggested by the G-I changes in the residual benthic $\delta^{13}C$ record of CD154 10-06P (Fig. 4. 3c), which is likely to reflect variability in NADW ventilation over time. A variety of records across the wider South Atlantic, independent of sedimentary environments, primary productivity regimes, or chosen benthic foraminifera species, have previously shown that high $\delta^{13}C$ signatures during interglacials signify young, nutrient-depleted, well-ventilated NADW, whereas lower increasingly negative $\delta^{13}C$ values during glacials are assigned to older, nutrient-enriched Antarctic water masses which have reduced ventilation due to long isolation from the atmosphere (e.g., Michel et al., 1995; Mackensen, 2001; Ninnemann and Charles, 2002; Hodell et al., 2003; Marchitto and Broecker, 2006).

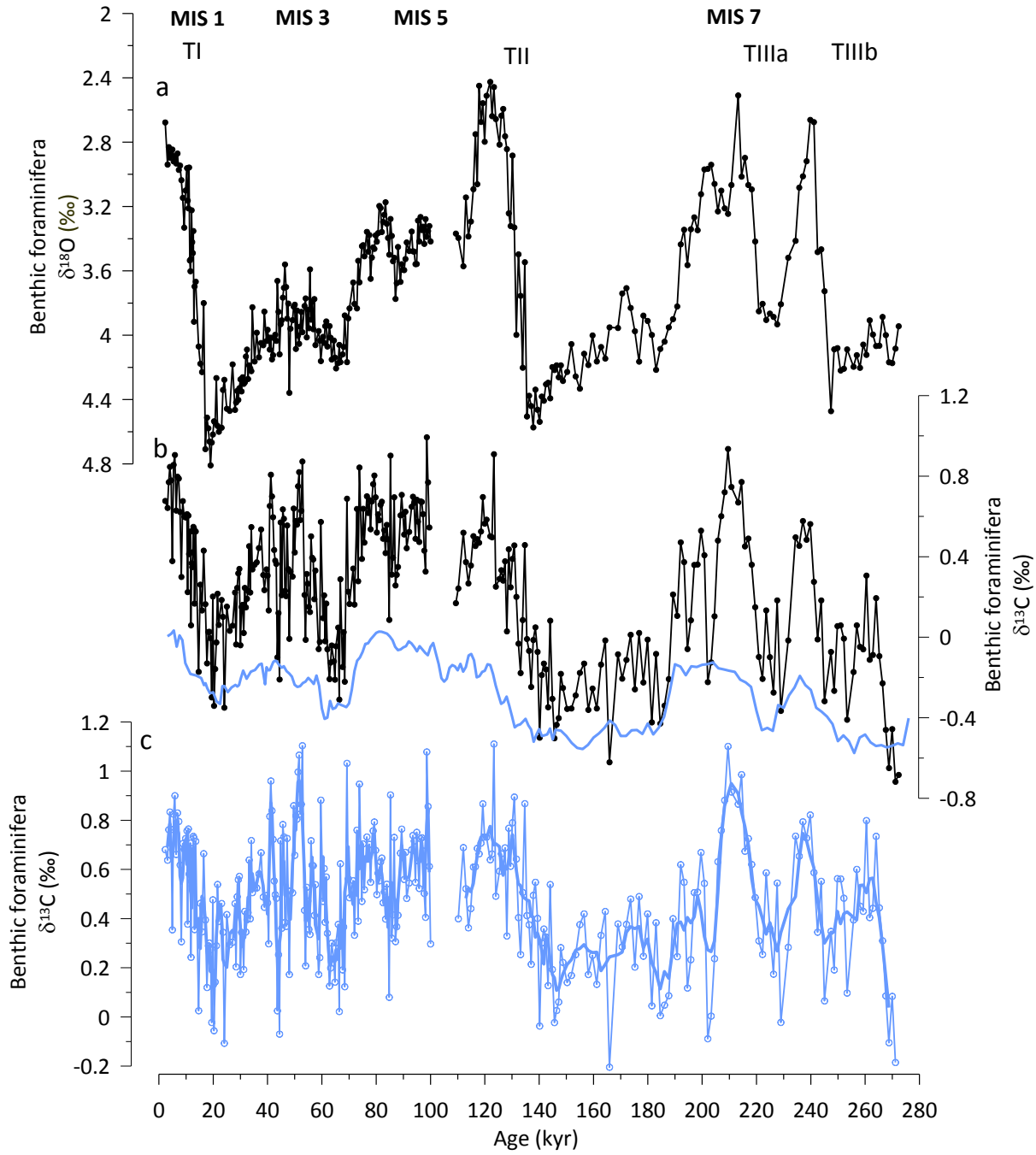

Fig. 4. 3 (a) Benthic $\delta^{18}O$ record of CD154 10-06P (b) Benthic $\delta^{13}C$ record of CD154 10-06P (black) and original benthic stack employed to correct for mean-ocean $\delta^{13}C$ (blue) from Zahn and Stüber (2002) (c) Benthic $\delta^{13}C$ record of CD154 10-06P after correction for changes in mean-ocean $\delta^{13}C$.

The more positive benthic $\delta^{13}C$ isotope values observed in core CD154 10-06P during interglacial intervals are consistent with these findings and suggest an increased influence of well-ventilated NADW in the southwest Indian Ocean during these times. In comparison the lower $\delta^{13}C$ isotopic values evident during glacial intervals suggest a reduced influence of NADW and increased dominance of poorly-ventilated SCW in the southwest Indian Ocean.

4.2.2. Regional comparison

To assess in more detail the benthic foraminiferal stable isotope patterns in CD154-10-06P in the regional framework, the $\delta^{18}O$ and $\delta^{13}C$ records are compared with equivalent records from the Agulhas Plateau, southwest Indian Ocean and the southeast Atlantic (Fig. 4. 1). As all $\delta^{13}C$ records were equally affected by the mean ocean $\delta^{13}C$ shift during the past no correction has been applied here and records are shown on their original $\delta^{13}C$ values.

In order to secure accurate comparison between all of these cores their age models in the upper part of the records are based on the published ^{14}C dates for each core and beyond the radiocarbon dating limits age models were adapted to the LR04 chronology (Lisiecki and Raymo, 2005) which also constitutes the basis of the CD154 10-06P age model.

All benthic stable isotope records were measured on *Cibicidoides* spp. and are presented on a VPDB scale (Fig. 4. 4). Changes in the $\delta^{18}O$ pattern between all cores are similar regarding the $\delta^{18}O$ G-I amplitude shifts as well as the general value range plausibly reflecting analogous temperature and salinity variability during the past 270 kyr in the southeast Atlantic and southwest Indian Ocean. However, core MD02-2589 shows on average higher benthic $\delta^{18}O$ values compared to all other cores not only limited to glacial intervals (Fig. 4. 4a). This feature was already noticed by Molyneux et al. (2007) while comparing the MD02-2559 benthic $\delta^{18}O$ to core sites in the North and South Atlantic and Pacific. The difference was attributed to a divergence in salinity between these cores, with more saline waters (higher $\delta^{18}O_{seawater}$) influencing the Agulhas Plateau during glacials in agreement with studies from Adkins et al. (2002) showing that the Southern Ocean potentially had the saltiest LGM deep waters. However, salinity differences can't be the reason for the offset as core MD02-2588, which is also located at the Agulhas Plateau at similar depths, and influenced by the same water mass changes, does not show similar offsets. The reason for the deviation remains equivocal, however $\delta^{13}C$ values of core MD02-2589, are in better agreement with data derived from MD02-2588.

The $\delta^{13}C$ signature of cores MD02-2588 and CD154 10-06P show a very close correlation both in absolute values and their pattern (Fig. 4. 4b). This might be related to the similarity in the core depths at 2907 m and 3076 m respectively, and hence the influence of the similar source waters at both locations.

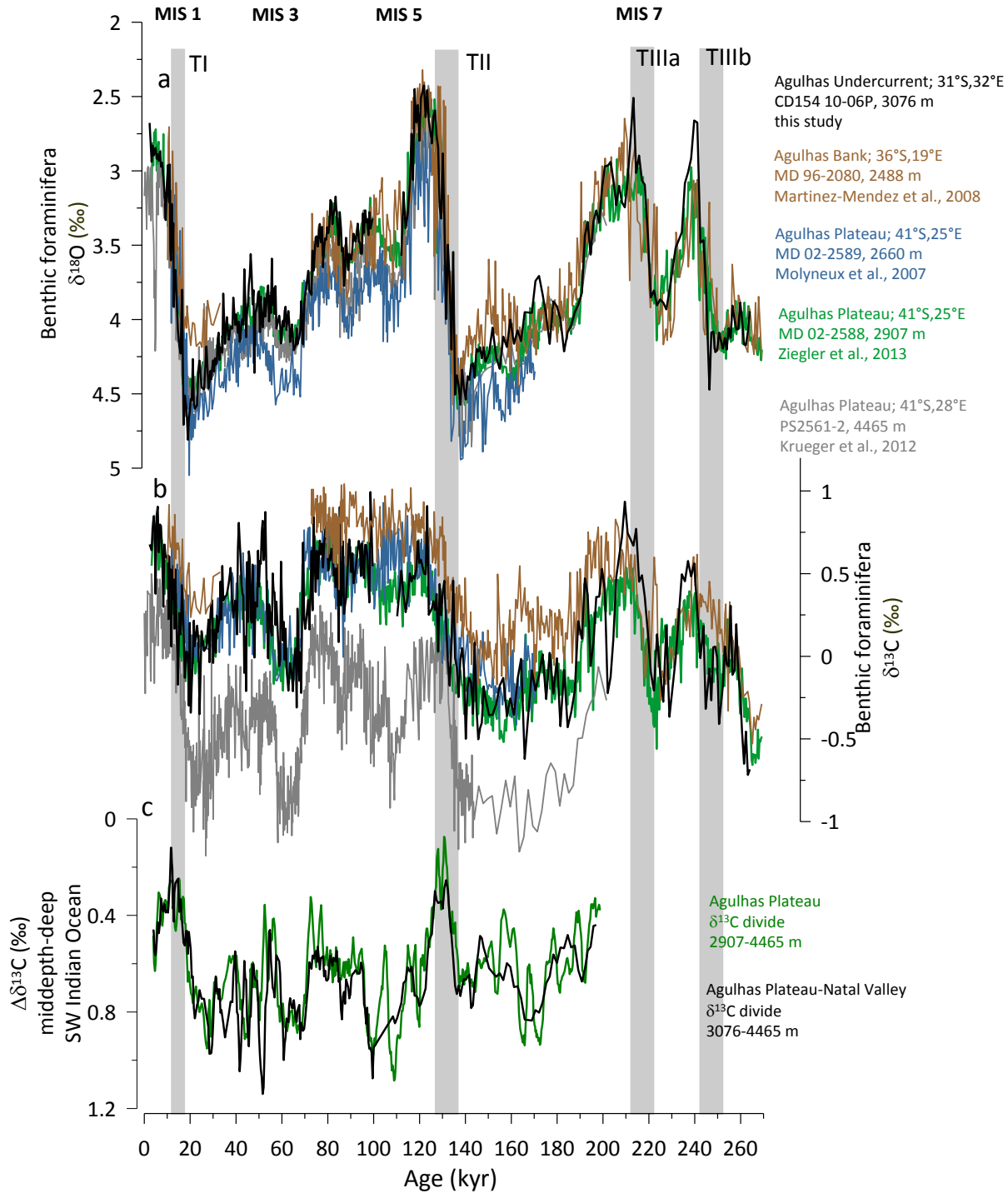

Fig. 4. 4 Regional deep water oceanography (a) Records of benthic $\delta^{18}O$ and (b) $\delta^{13}C$ of *Cibicidoides* spp. from southwest Indian Ocean, CD154 10-06P, this study, (black), 31°S,32°E, 3076 m; Agulhas Plateau, MD 02-2589, Molyneux et al. (2007), (blue), 41°S,25°E, 2660 m; Agulhas Plateau, MD 02-2588, Ziegler et al., (2013a), (green) 41°S, 25°E, 2907 m, Agulhas Plateau, PS2561-2, 4465m, Krueger et al., (2012), (grey), 41°S,28°E, Agulhas Bank, MD96-2080, Martínez-Méndez et al. (2008), (brown), 36°S, 19°E, 2488 m. Grey bars indicate glacial terminations and Marine Isotope Stages (MIS) are highlighted on the top. (c) Vertical $\delta^{13}C$ gradient in the southwest Indian Ocean (in black) between CD154 10-06P, 3076m, this study and Agulhas Plateau deep record of PS2561-2, 4465m, Krueger et al., (2012) and between Agulhas Plateau core MD 02-2588, Ziegler et al., (2013a), 2907 m and deep record of PS2561-2 in green.

It further implies that although modern physical oceanographic studies suggest that the Natal Valley is strongly influenced by NADW rather than CDW, core CD154 10-06P appears to be bathed in a similar water mass to the Agulhas Plateau core site (MD02 2588 and 2589) and therefore includes a substantial component of CDW (Molyneux et al., 2007; Ziegler et al., 2013a).

Offsets towards higher $\delta^{13}C$ values are apparent between the Agulhas Bank record (ABR) of core MD96-2080 and cores in the southwest Indian Ocean (Agulhas Plateau and the Natal Valley) during both G-I stages (Fig. 4. 4b). Core MD96-2080 located in the southeast Atlantic and at shallower depth (2488 m water depth) might be influenced by a higher proportion of nutrient-depleted NADW during interglacials, which shifts the $\delta^{13}C$ values towards more positive values. The combined Cd/Ca and benthic $\delta^{13}C$ pattern recorded in the ABR suggested that during late glacials the core site was prominently influenced by nutrient-laden SCW maintaining a positive $\delta^{13}C$ signature, presumably through air-sea gas exchange. Martínez-Méndez et al. (2008) concluded that the signature of ABR was most likely a result of mixing between Upper Southern Component Water (USCW) and Lower Southern Component Water (LSCW). It therefore appears feasible that CDW would invade further north into the South Atlantic and South Indian Ocean during glacial periods when the rate of formation or southward advection/depth of NADW was reduced. The ~0.2 ‰ $\delta^{13}C$ difference between values in ABR and the here studied record suggest that both sites were influenced by a different mixing ratio of USCW and LSCW during glacials. A higher proportion of more positive USCW potentially influenced the shallower ABR compared to core CD154 10-06P in southwest Indian Ocean which results higher $\delta^{13}C$ values in the ABR. Regardless both records are consistent with previous data suggesting that under glacial conditions nutrient-poor NADW ventilated a much smaller fraction of the deep Atlantic, which was dominated by SCW from the Southern Ocean (Curry and Oppo, 2005; Marchitto and Broecker, 2006; Lynch-Stieglitz et al., 2007).

The difference in the modern source water provinces in the wider region is also evident when comparing the CD154 10-06P record with core PS2561 from the eastern-flank of the Agulhas Plateau at 4465 m water depth. Values are on average ~0.8‰ more negative than observed in the shallower cores, which is related to the greater influence of nutrient-rich (light $\delta^{13}C$) AABW on core PS2561. The $\delta^{13}C$ signature and pattern of core PS2561 is in agreement with other deep abyssal cores in the Cape Basin RC11-83 and TNO57-21

confirming the influence of AABW on those sites (Krueger et al., 2012). Moreover these studies suggested that these core sites strongly remained under the persistent influence of SCW (i.e, AABW) during both glacial and interglacial periods (Charles et al., 1996; Ninnemann and Charles, 2002; Krueger et al., 2012).

4.2.3. Benthic Carbon Isotope Gradients in the South Atlantic and southwest Indian Ocean

Benthic $\delta^{13}C$ signatures in the shallower cores remained consistently more positive during glacial intervals than the deeper AABW-influenced cores. With a reduction of Northern Component Waters (NCW) during glacials all core sites should display a similar shift towards lower $\delta^{13}C$ values similar to those recorded in the deep core site PS2561 if during this time the entire region was bathed in SCWs. Nonetheless, all shallower core sites between ~2500 and 3000m water display higher values during glacials compared to the core site PS2561 positioned at the abyssal Agulhas Plateau which suggests the development of a strong $\delta^{13}C$ chemocline at mid-depths (defined here between ~2500-3700m) in the glacial South Atlantic and southwest Indian Ocean (Fig. 4. 4c). The computed $\delta^{13}C$ gradient between the mid-depth and deep overturning circuit in southwest Indian Ocean during the past 200 kyr using CD154 10-06P from the Natal Valley (3076 m water depth), MD02-2588 (2907 m water depth) from the Agulhas Plateau and core PS2561 from 4465 m water depth on the Agulhas Plateau (Fig. 4. 5c) confirms $\delta^{13}C$ divide between the different water depths. The results show that the largest difference coincides with full glacial conditions indicating a stronger chemical gradient between mid-depth/ upper deep waters, when $pCO2_{atm}$ was lowest (Fig. 4. 4c), (Hodell et al., 2003). An intriguing feature is that the chemical divide rapidly vanished during glacial Termination II and I. Monitoring the development of the $\delta^{13}C$ pattern of these cores before and during the G-I transitions displays that $\delta^{13}C$ values in the mid-depth cores are rising more gradually whereas shifts in the deep core PS2561 on the Agulhas Plateau are rather abrupt (Fig. 4. 4c). This indicate that upon terminations the deep water circuit experienced sudden better ventilation which result into the rapid shift towards more positive $\delta^{13}C$ values and hence the breakdown of the chemical divide which is evident in the decline of the calculated $\delta^{13}C$ gradient between cores.

This chemical divide is a well-known feature in the glacial South Atlantic with better-ventilated deep and mid-depth water masses and a poorly ventilated, nutrient-rich water mass that filled the South Atlantic basin (Ninnemann and Charles, 2002; Hodell et al., 2003; Molyneux et al., 2007; Martínez-Méndez et al., 2008; Krueger et al., 2012; Ziegler et al., 2013a). Hodell et al. (2003) proposed that the chemocline also existed in previous glacial times back to 1.1 Ma. Ninnemann and Charles (2002) suggested that the chemocline in the Atlantic Sector of the Southern Ocean was predominantly driven by deep water variability. It has been suggested that poorly ventilated and dense bottom waters formed in the glacial Weddell Sea and that these waters were bounded vertically and laterally by a better ventilated mid-depth water mass, with more positive $\delta^{13}C$ values, therefore creating a $\delta^{13}C$ divide. This is in accordance with results of numerical models of Toggweiler (1999) that suggest that the isolation of the glacial deep waters results in an increase in regenerated nutrients in the deep and preformed nutrients in the intermediate waters which would lead to the development of a chemocline at mid-depths. Other studies in the Indian (Kallel et al., 1988; Naqvi et al., 1994; McCorkle et al., 1998) and the Pacific (Mix et al., 1991; Herguera et al., 1992; Keigwin, 1998) suggest that similar, but less pronounced, chemoclines developed as well between intermediate and deep waters in these basins.

Results and discussion from Molyneux et al. (2007) and Martínez-Méndez et al. (2008) in combination with results from earlier studies of Oppo and Horowitz (2000) and Curry and Oppo (2005) hint at the suggestion that during glacial periods a second shallower deep water mass i.e., USCW formed around the Subantartic Front (SAF), an area of increased air-sea gas exchange during glacials (Sigman and Boyle, 2000). The increased air-sea gas exchange would create a relatively high $\delta^{13}C$ water mass, which would have penetrated to mid-depths above the low $\delta^{13}C$ deep waters, i.e., LSCW, forming under the extended winter sea-ice region south of the Polar Front (Rosenthal et al., 1997; Mackensen, 2001; Bickert and Mackensen, 2003). Molyneux et al. (2007) and Martínez-Méndez et al. (2008) found that during glacials negative $\delta^{13}C$ excursions in the southeast Atlantic and the Agulhas Plateau records correlate with periods of high-near bottom flow speeds inferred from grain-size analysis of the so-called sortable silt mean grain-size paleocurrent indicator. These findings led to the conclusion that a relatively high $\delta^{13}C$ water mass might have formed during cold glacial stages when the ACC had expanded bringing it closer to the core sites. Conventional deep water formation sites in the Weddell Sea were blocked

due to grounding ice sheets and the region of intense air-sea gas exchange migrated into the subantartic zone due to shifts in the zonal wind patterns and sea-ice expansion around Antarctica during glacials. This mechanism could explain the presence of a better ventilated mid-depth water mass in the South Atlantic and southwest Indian Ocean.

In order to further investigate the glacial Southern Ocean high $\delta^{13}C$ water mass a suite of cores were used here to assess the glacial water column structure of the southeastern Atlantic sector of the Southern Ocean additionally with adding the above discussed cores in the southwestern Indian Ocean sector following Martínez-Méndez et al. (2009) (Table 4. 1). The cores form both a latitudinal transect from 25.5-51.5 °S over the present day and glacial positions of the Polar Front (PF), SAF and STF and a depth transects from 1330-4980m water depth. The comparison was focussed on the Holocene-LGM interval (23-19 ka) as indication also for previous glacial periods. The largest amplitude change in benthic $\delta^{13}C$ from the LGM to Holocene (up to 1.3‰) occurs in the deep cores that are currently located well below the direct influence of NADW (Fig. 4. 5b), whilst cores that are currently positioned in modern day NADW display much smaller change in $\delta^{13}C$ (Rutberg and Peacock, 2006). Figure 4. 5a shows the $\delta^{13}C$ divide as proposed by Hodell et al. (2003) and Figure 4. 5b displays the same sites despite additional sites and discriminating the spatial distribution of the core sites between those located north (25.5- 42.5 °S) and south (42.5 - 51.5 °S) of the assumed SAF at the LGM (Fig. 4. 5, Table 4. 1). This regional separation is based on evidence that suggests that the SAF during the LGM was ~3-5 °N of its present position at 45 °S (Kohfeld et al., 2013).

Sites north of the SAF exhibit a LGM-Holocene benthic $\delta^{13}C$ ($\delta^{13}C_{LGM-Hol}$) depletion of 0.2‰ at shallower sites and up to 0.6-0.8 ‰ at mid-depth water sites, only slightly greater (at least at shallower mid-depth sites) than the 0.32-0.46 ‰ global carbon shift, while the $\delta^{13}C_{LGM-Hol}$ depletion of 1.1-1.5 ‰ are recorded at deep water sites (Fig. 4. 5b). Sites to the south of the SAF display consistently higher $\delta^{13}C_{LGM-Hol}$ depletion at around 1.2 ‰ from mid-depth to deep waters, with the offset in glacial benthic $\delta^{13}C$ between the mid-depth sites (2500-3700m) north and south of the SAF being striking (Fig. 4. 5b). The presence of high $\delta^{13}C$ waters at glacial mid-depth north of SAF supports the previous findings based on the CD154 10-06P benthic $\delta^{13}C$ record. These findings suggest that the chemocline also exhibits a strong meridional gradient as well as being a vertical feature. Increased export productivity, extensive sea-ice and northward migration of the westerly winds reducing

the ventilation of deep waters and $\delta^{13}C$ values south of the SAF, whereas a faster flowing ACC and formation of a shallower deep water mass, with high $\delta^{13}C$ values due to increased air-sea gas exchange and upwelling around (north of) the position of the SAF could potentially explain the chemical divide as a latitudinal feature.

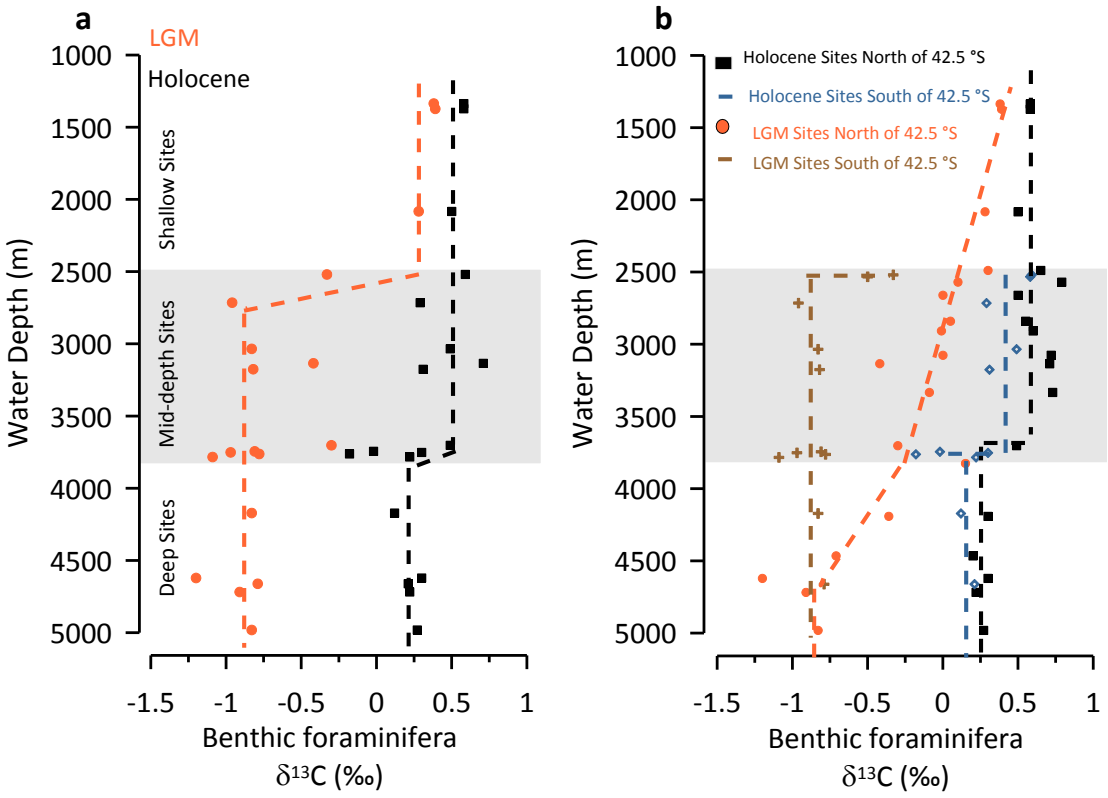

Fig. 4. 5 Reconstruction of vertical $\delta^{13}C$ in the South Atlantic over the Holocene and LGM (a) Vertical carbon gradients in the South Atlantic for Holocene and LGM taken from Hodell et al. (2003) (b) Vertical carbon gradients in the South Atlantic for the Holocene and LGM with sites divided into those north of 42.5 °S and those south of 42.5 °S.

Moreover, Martínez-Méndez et al. (2008) showed based on Cd_{sw} data in the South Atlantic that the mid to deeper water column was homogenous in terms of nutrient content compared to the divide inferred from $\delta^{13}C$ data which led to the conclusion that the chemocline was a 'carbocline' rather than a strict nutricline. The differential vertical distribution between $\delta^{13}C$ and Cd/Ca suggest that the source of well-ventilated upper waters in the glacial South Atlantic was USCW with a similar nutrient content to LSCW but with a positive $\delta^{13}C$ signature due to enhanced air-sea-gas exchange.

Table 4. 1 Cores used to investigate the interglacial to glacial water column structure with position north and south of the assumed glacial SAF (42.5°S) and $\delta^{13}C$ values of both the Holocene and LGM: N= North, S=South, $\delta^{13}C_{Hol.}$ = Average $\delta^{13}C$ Holocene values, $\delta^{13}C_{LGM}$= Average $\delta^{13}C$ LGM values.

Core	Depth	Lat.	Long.	N/S	$\delta^{13}C$(‰) Hol.	$\delta^{13}C$(‰) LGM	Reference
TN057-20	1335	-42.1	0.6	N	0.58	0.38	Hodell et al. (2003)
ODP 1087	1372	-31.27	15.18	N	0.58	0.39	Hodell et al. (2003)
ODP 1088	2082	-41.8	13.33	N	0.50	0.28	Hodell et al. (2003)
MD96-2080	2488	-36.27	19.47	N	0.65	0.30	Martínez-Méndez et al. (2008)
GeoB2004	2569	-30.87	14.54	N	0.79	0.10	Bickert and Mackensen (2003)
MD02-2589	2660	41.26	25.15	N	0.50	0.00	Molyneux et al. (2007)
GeoB3603-2	2840	-35.13	17.54	N	0.55	0.05	Bickert and Mackensen (2003)
MD 02-2588	2907	-41	25	N	0.60	0.00	Ziegler et al. (2013a)
CD15410-06P	3076	-31	32	N	0.72	0.00	this study
PS2495-3	3134	-41.28	-14.49	N	0.71	-0.42	Hodell et al. (2003)
CD15417-17K	3333	-33	29	N	0.73	-0.09	this study
ODP 1090	3702	-42.5	8.53	N	0.49	-0.30	Hodell et al. (2003)
GeoB2019-1	3825	-36.06	-8.78	N	n.d.	0.15	Bickert and Mackensen (2003)
RC13-229	4191	-25.49	11.3	N	0.30	-0.36	Curry and Oppo (2005)
PS2561-2	4465	-41	28	N	0.20	-0.71	Krueger et al., (2012)
ODP 1089	4621	-40.56	9.53	N	0.30	-1.20	Hodell et al. (2003)
RC11-83	4718	-41.36	9.48	N	0.22	-0.91	Hodell et al. (2003)
TN057-21	4981	-41.08	7.49	N	0.27	-0.83	Hodell et al. (2003)
PS1754-1	2519	-46.77	7.61	S	0.59	-0.33	Hodell et al. (2003)
ODP 704	2532	-46.88	7.42	S	0.58	-0.50	Bickert and Mackensen (2003)
RC15-93	2714	-46.06	-13.13	S	0.29	-0.96	Hodell et al. (2003)
PS2464-3	3034	-46.14	35.9	S	0.49	-0.83	Hodell et al. (2003)
PS2499-5	3175	-46.51	-15.33	S	0.31	-0.82	Hodell et al. (2003)
TN057-15	3744	-51.54	4.31	S	-0.02	-0.81	Hodell et al. (2003)
TN057-06	3751	-42.54	8.58	S	0.30	-0.97	Hodell et al. (2003)
RC15-94	3762	-42.59	-20.51	S	-0.18	-0.78	Hodell et al. (2003)
PS2498-1	3783	-44.15	-14.49	S	0.22	-1.09	Hodell et al. (2003)
V22-108	4171	-43.11	-3.15	S	0.12	-0.83	Hodell et al. (2003)
PS2082-1	4661	-43.13	11.45	S	0.21	-0.79	Hodell et al. (2003)

4.2.4. Linking Agulhas Current variability with deep water ventilation changes off southeast Africa during the past 100 kyr

The previously discussed deep water provenance changes around South Africa and the surface Agulhas Current reconstructions from core CD154 17-17K (Chapter 3) with new additional data from core CD154 10-06P can now be combined and discussed in terms of linkages between surface and deep water variability with the attempt to identify common forcing mechanism (Fig. 4. 6). As temperature and $\delta^{13}C$ data are all derived from the same material of core CD154 10-06P (Fig. 4. 6b,c) there is no ambiguity about the relative timing of the events. The abundance of Agulhas Leakage Fauna (ALF) from core CD154 17-17K in the Agulhas Current (Chapter 3) is shown in combination with SST estimates of core CD154 10-06P.

Severe surface and deep water changes occurred during glacials (MIS 2, 4) when the Agulhas Current cooled, and potentially a higher intrusion of Southern Ocean derived waters impacted on the Currents variability (Fig. 4. 6). The time of the greatest surface cooling was also the interval when older, poorer-ventilated, nutrient-enriched waters were carried northward beneath the Agulhas Current most likely from a Southern Ocean source. Coevolving changes on longer timescales in the surface and deep water properties seem to be a response of the Agulhas Current system to similar forcing mechanism. During glacial stages orbital induced changes in the distribution of solar radiation in combination with feedback mechanism causes the growth of the Antarctic ice sheets and winter (summer) sea-ice to extend (Carter et al., 2009). In consequence to the expansion of the Antarctic cryosphere the Southern Ocean frontal system experienced equatorward shifts and pronounced ocean surface cooling (Carter et al., 2009). These frontal migrations are often thought to imply a shift in the ACC as well (Kohfeld et al., 2013). Circulation in the Southern Ocean is directly related to the mean position and intensity of the westerlies, as these winds drive both the zonal flow of the ACC and the meridional overturning of deep water associated with Ekman divergence and upwelling. Today, the eastward flow of the SAF, found between 48 °S and 58 °S in the Indian and Pacific Ocean and between 42 °S and 48 °S in the Atlantic Ocean, defines the ACC's northern boundary. It has been argued for an intensification of the fast flowing ACC as aerosol and dust concentration data from Antarctic ice cores suggest a glacial increase in the strength of westerlies (Gaiero et al., 2003; Lambert et al., 2008; Hodgson and Sime, 2010).

Northward shifts of the main axis of the ACC during glacials have also been inferred from evidence from increased bottom flow speed at sites close to areas under the influence of the ACC (Pudsey and Howe, 1998; Hall et al., 2001; Molyneux et al., 2007; Martínez-Méndez et al., 2008). Notwithstanding, the glacial position and strength of the westerlies wind belt (Kohfeld et al., 2013; Sime et al., 2013) and the ACC remain part of ongoing discussions (McCave et al., 2014).

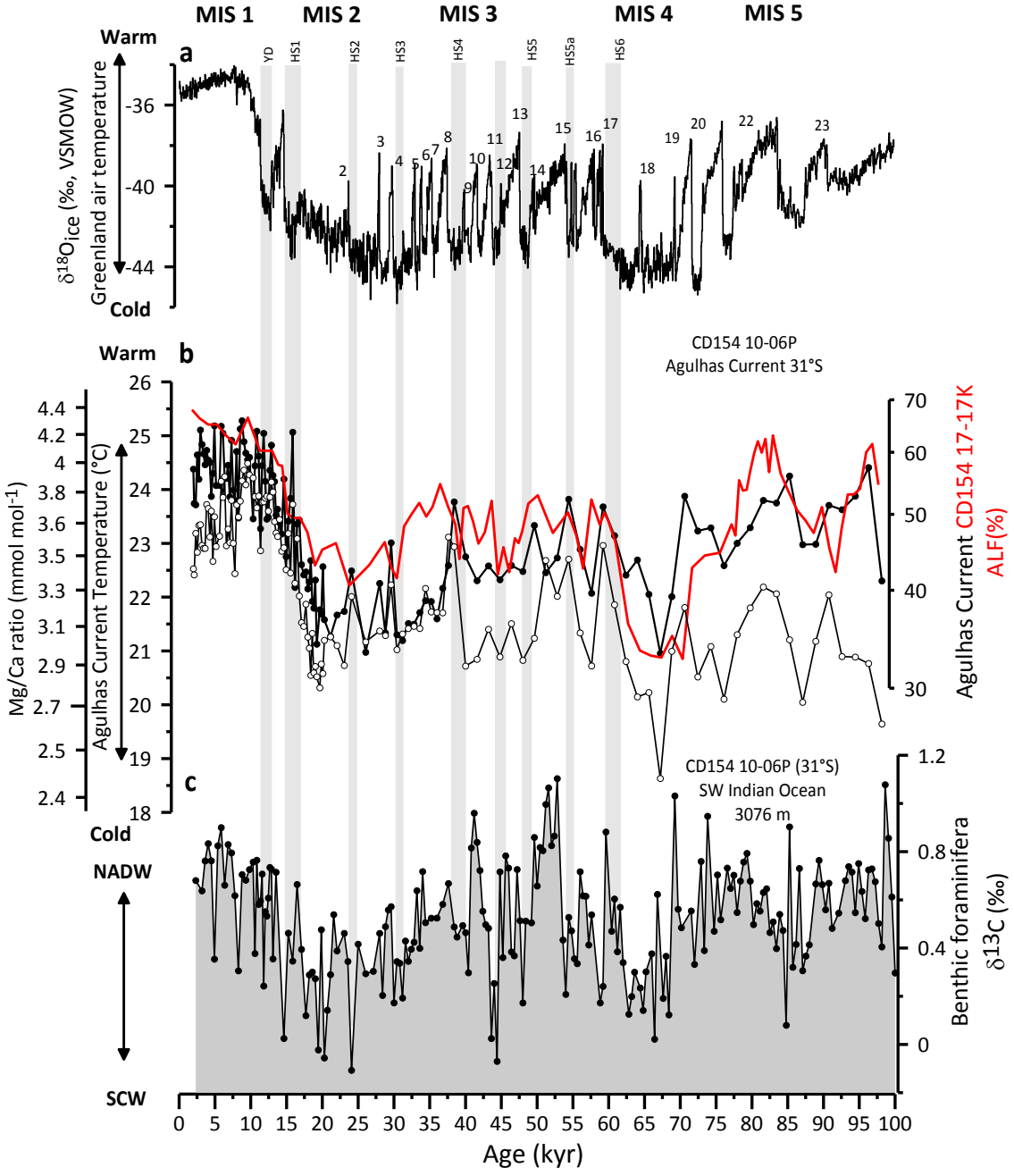

Fig. 4. 6 Agulhas Current and deep water mass variability during the past 100 kyr (a) $\delta^{18}O$ record from Greenland ice core NGRIP (NGRIP, 2004), (black, speleo-age model presented in Barker et al., (2011)) displaying abrupt temperature variability in the North Atlantic. Marine isotope stages (MIS) are labelled and underlying grey bars indicate Northern Hemisphere Cold Stadials (b) Agulhas Current Mg/Ca-derived

temperature estimates of core CD154 10-06P (black) and relative abundance of tropical-subtropical planktonic foraminiferal marker species (Agulhas leakage fauna, ALF) in core CD154 17-17K, (red, logarithmic scale) (c) Benthic $\delta^{13}C$ record of CD154 10-06P displaying changing influence between Northern and Southern Component Waters (SCW) on the core site.

The consequences of the growth and decay of the Antarctic cryosphere, however, might have had wider implications for the Agulhas Current as well as for the deep water ventilation around South Africa at the same time. Conventional deep water formation sites in the Weddell Sea were blocked due to grounding ice sheets (Rosenthal et al., 1997) and the region of intense air-sea gas exchange migrated into the subantartic zone due to shifts in the zonal wind patterns and sea-ice expansion around Antarctica during glacials (Sigman and Boyle, 2000). USCW, the water mass which has been shown to increasingly influence core site CD154 10-06P during glacials, formed around the SAF during these times. At the same time cores at the Agulhas Plateau and southeast Atlantic were equally bathed in a higher proportion of the same water mass and evidence from bottom flow speed records from the Agulhas Plateau and southeast Atlantic suggested that these cores came within the reach of the ACC (Molyneux et al., 2007; Martínez-Méndez et al., 2008). Simultaneously, a northward displaced Southern Ocean frontal system associated with shifted westerlies did impact on the Agulhas surface waters in that the spin up the Southwest Indian Ocean sub-gyre (SWIOSG) enhanced the recirculation of cold Southern Ocean waters into the system thereby cooling its waters and potentially enhancing the import of transitional to polar foraminiferal species (Chapter 3). The consequence of these environmental changes was an Agulhas Current signature that was colder with less ALF compared to the Holocene propagated downstream at the same time when less NADW invasion occurred around the southern tip of Africa.

A northward expanded and faster flowing ACC (Dezileau et al., 2000; Noble et al., 2012) plausibly could have acted to impede the southward penetration of NCW in the Southern Ocean by forming an efficient physical barrier to latitudinal mixing between SCW and NCW. Moreover, several studies suggested that sea-ice extent in the Southern Ocean may actually drive AMOC (Kim et al., 1998; Keeling and Stephens, 2001; Shin et al., 2003), with changing outflow of SCW, linked to sea-ice extent and wind forcing changing the relative abundance of NCW at any particular site, rather than being controlled by NCW strength itself (Kim et al., 1998; Toggweiler, 1999; Bayon et al., 2003; Raymo et al., 2004).

4.2.5. Millennial-scale deep water variability off southeast Africa

Beyond the orbital-scale variability several abrupt millennial-scale excursion are evident in the CD154 10-06P $\delta^{13}C$ record during the last glacial (Fig. 4. 7). Negative $\delta^{13}C$ shifts coincide, within age model uncertainties, with intervals of Northern Hemisphere Cold Stadials (NHCS) (Fig. 4. 7a,b). It is also worth noting that in the CD154 10-06P chronology most of the MIS 3 and MIS 4 interval is untuned, as the last ^{14}C datum is at 27.9 ka and the first tie-point to the LR04 $\delta^{18}O$ stack is placed at 69 ka, which demonstrates the high level of interhemispheric synchrony (Fig. 4. 7c). The amplitude of stadial/interstadial $\delta^{13}C$ shifts are equal to G-I changes. Moreover the observation that benthic $\delta^{13}C$ values during the MIS 3 interstadials are similar to the interglacial levels suggests that the southwest Indian Ocean was as well ventilated with NADW during D/O interstadials as during interglacials. Indeed, some of these interstadial values during MIS 3 are even more positive than the values recorded at the CD154 10-06P during the Holocene.

The benthic $\delta^{13}C$ variability during MIS 3 strongly suggests that on these D/O timescales a changing proportion of NCW reached the southwest Indian Ocean and during stadial condition was substituted by the increased influence of SCW. Sediments in cores from the Iberian Margin indicate shifts to much colder SSTs simultaneously with the deep water hydrographic changes in the Natal Valley in phase with NHCSs (Fig. 4. 7b). Cold episodes after relatively warm and largely ice-free periods occurred at the Iberian Margin when the predominance of deep water influence changed from northern to southern sources. That demonstrates the connection between rapid climate changes at Mediterranean latitudes and millennial-scale variability in northern and southern Polar Regions (Martrat et al., 2007).

The glacial North Atlantic ice-rafted detritus events are thought to be accompanied by significant changes in the deep ocean circulation (e.g., Oppo and and Curry, 2012). Studies suggest that the contribution of NADW to the deep Atlantic decreased during these events (e.g., Boyle & Keigiwn 1987, Thornalley et al. 2011, Lynch-Stieglitz et al. 2007). The current prevailing view of the climate variability during NHCS/Heinrich Stadials is that instabilities in the Northern Hemisphere ice sheets resulted in catastrophic iceberg discharges accompanied with freshwater discharge into the North Atlantic Ocean (Bond et al., 1992; Bond et al., 1997).

The input of fresh water into the North Atlantic is postulated to have disrupted deep and bottom water formation, leading to a weaker and/or shallower AMOC and hence shallower NADW cell and reduced equatorward penetration (McManus et al., 2004; Gherardi et al., 2005; Hall and Becker, 2007; Lippold et al., 2012; Lynch-Stieglitz et al., 2014). Consistent with that idea are freshwater hosing experiments from conceptual and simplified numerical models, which suggest that the AMOC may have two stable states, transitioning from a strong AMOC to a weak or collapsed AMOC following a freshwater perturbation to the North Atlantic (Stocker and Wright, 1991; Rahmstorf, 1995; Rahmstorf, 1996).

Fully coupled Atmosphere-Ocean Global Circulation Models (AOGCM) also indicate a slowing of the AMOC when freshwater is added to the North Atlantic (Stouffer et al., 2006). When the freshwater forcing is stopped, the AMOC recovers fully over 120–260 years in all but one of the AOGCMs (Otto-Bliesner et al., 2006).

Recently Oppo and Curry (2012) used a compilation of benthic $\delta^{13}C$ data from the western Atlantic to show that the deep water mass geometry during HS 1 was quantitatively different from either the modern or LGM configuration, with the core of nutrient-poor, high $\delta^{13}C$, NCW above ~1000 m water depth and restricted to the sub-polar North Atlantic during HS 1. Furthermore decreasing $\delta^{13}C$ values suggest a progressive increase in the proportion of nutrient-rich SCW below 1000 m water depth. Radiocarbon evidence support the idea that during HS 1 and the YD the deep Atlantic was invaded by a southern-sourced carbon-rich, low $\delta^{13}C$, radiocarbon depleted water mass, which was isolated from the atmosphere during the glacial period. In comparison, today, the deep Atlantic's carbon pool is invaded from the north by NADW export. These findings alluded to a "bipolar seesaw" in the deep Atlantic ventilation during the last deglaciation with a dominant source from the South during millennial-scale cold intervals (Skinner et al., 2014).

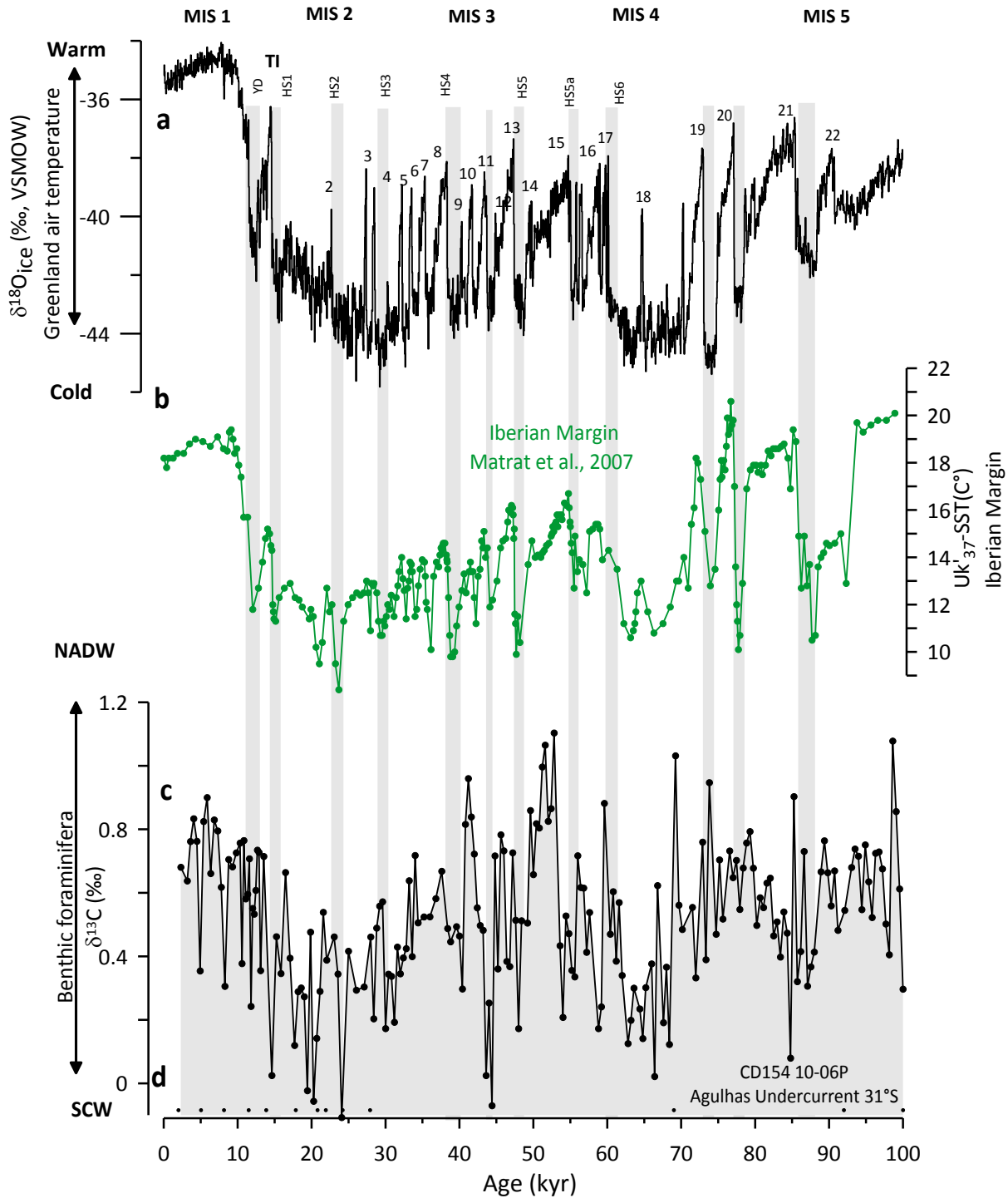

Fig. 4. 7 Millennial-sale hydrographical variability in the southwest Indian Ocean (a) $\delta^{18}O$ record from Greenland ice core NGRIP (NGRIP, 2004), (black), displaying abrupt temperature variability in the North Atlantic. Marine isotope stages (MIS) are labelled and underlying grey bars indicate Northern Hemisphere stadials (c) Uk'_{37}-SST in a composite of cores MD01-2444 and MD01-2443 from the Iberian Margin (Martrat et al., 2007) (c) Benthic $\delta^{13}C$ record of CD154 10-06P displaying changing mixing ratios between Northern and Southern component waters (SCW) (d) Radiocarbon dates and tuning points.

However, it raises the question of the origin of the water mass present during NHCS in the southwest Indian Ocean as $\delta^{13}C$ levels are similar to glacial values. Pahnke and Zahn (2005) suggested a bipolar seesaw system for NHCSs, whereby cold intervals in the North Atlantic and the reduction in NCW production are compensated by warming in the Southern Ocean and increased AAIW production. If this seesaw system was operating then it would be expected that during NHCSs in the north, a high $\delta^{13}C$ mid-depth water would be forming in the South and extending to mid-depths influencing core CD154 10-06P. At the present day no such SCW mass exists at the water depth of core CD154 10-06P and the core of high $\delta^{13}C$ AAIW lies ~1500 m above the core site which initially would exclude AAIW to be that water mass. The high $\delta^{13}C$ SCW mass suggested for a glacial scenario probably requires increased air-sea gas exchange linked to sea-ice expansion, which would not occur during millennial-scale warming in the Southern Hemisphere. Nonetheless, Pahnke and Zahn (2005) suggested intensified AAIW formation during NHCS with increased depth of penetration (Bostock et al., 2004). This may suggest that a different mechanism is operating during glacial periods and NHCS, perhaps with AAIW being the source during NHCS and an alternative SCW mass being the source for glacial periods. However the role of AAIW during millennial-sale climate change remains discussed as well (Came et al., 2008; Pahnke et al., 2008; Xie et al., 2012; Pena et al., 2013; Huang et al., 2014).

A high degree of common surface and deep water variability also occurred on millennial timescales in response to an apparent Northern Hemisphere control on the climate system. Especially during MIS 3, NHCS were times when the Agulhas Current warmed and salinified (Fig. 4. 6b, Fig. 4. 8b, Fig. 3.3), while the deep waters off southeast Africa experienced profound source water changes, as displayed by recurrent negative shifts in the benthic $\delta^{13}C$ record, with less NADW being present in the southwest Indian Ocean. Heinrich Stadial 6-2 constitute good examples for the synchronous surface and deep water coupling in the Agulhas Current system (Fig. 4. 6). Owing to the thermal bipolar seesaw behaviour the Southern Ocean warms during NHCS (Broecker, 1998; Stocker and Johnsen, 2003). A warmer Southern Ocean is accompanied by a salinification of the surface waters (Lohmann, 2003). The heat and salinity build up in the south is caused by a shut-off of the AMOC, which triggers a rapid cooling in the north, because heat is no longer exported northwards. Small reduction in SSS altering the rate of NADW formation due to large inputs of fresh water from melting ice sheets to the North Atlantic are thought to be the

initial trigger for reductions in the AMOC (Broecker et al., 1990; Clark et al., 1999; Stouffer et al., 2006). This in turn leads to less NADW production and propagation to the Southern Hemisphere where the lack of NCW will be substituted by deep waters of southern origin (Oppo and and Curry, 2012).

4.2.6. Surface and deep water linkages off southeast Africa during Termination I

Termination I is discussed in detail as the combined surface and deep water records might reveal if Agulhas leakage played an active or passive role during glacial terminations.

If deep water changes around South Africa were purely controlled by AMOC mode shifts, i.e., less NADW in the region would suggest a weaker AMOC and vice versa, and variations in the Agulhas Current imply contemporaneous changes in leakage than the evolution of changes recorded in core CD154 10-06P over TI could potentially reveal if Agulhas leakage had an active or passive role during glacial terminations. The approach is the following: If warming and salinification in the Agulhas Current occurred contemporaneously downstream in the IAOG and before changes in the NADW advection around South Africa than this might imply that the salinity buildup in the Agulhas System during the deglaciation, may have had important implications for the buoyancy budget of the Atlantic Ocean and, in turn, for the AMOC. Conversely, if NADW advection around South Africa occurred coincidently with or before the upstream-downstream salinification/warming than its role might be rather passive.

In the last deglacial period two abrupt climatic shifts are known when the North Atlantic was abruptly changing to cold conditions: the HS 1 and the YD. Glacial terminations in the late Pleistocene were in general characterised by oscillations of the bipolar seesaw and it has been proposed that they are an important and necessary component to shift the climate from an glacial to an interglacial state (Barker et al., 2011). With the onset of HS 1, salinity and SST increased in the Agulhas Current (Fig. 4. 8). Unfortunately no equivalent record exists from the IAOG to compare this pattern in detail over TI. However, the comparison with Marino et al.'s (2013) data set during MIS 5 in Chapter 3 and the similarities of the two step bipolar seesaw salinification during TII recognised in their record with the features here during TI further strengthens the conclusions of Chapter 3, that Agulhas Current variability imply contemporaneous changes in leakage.

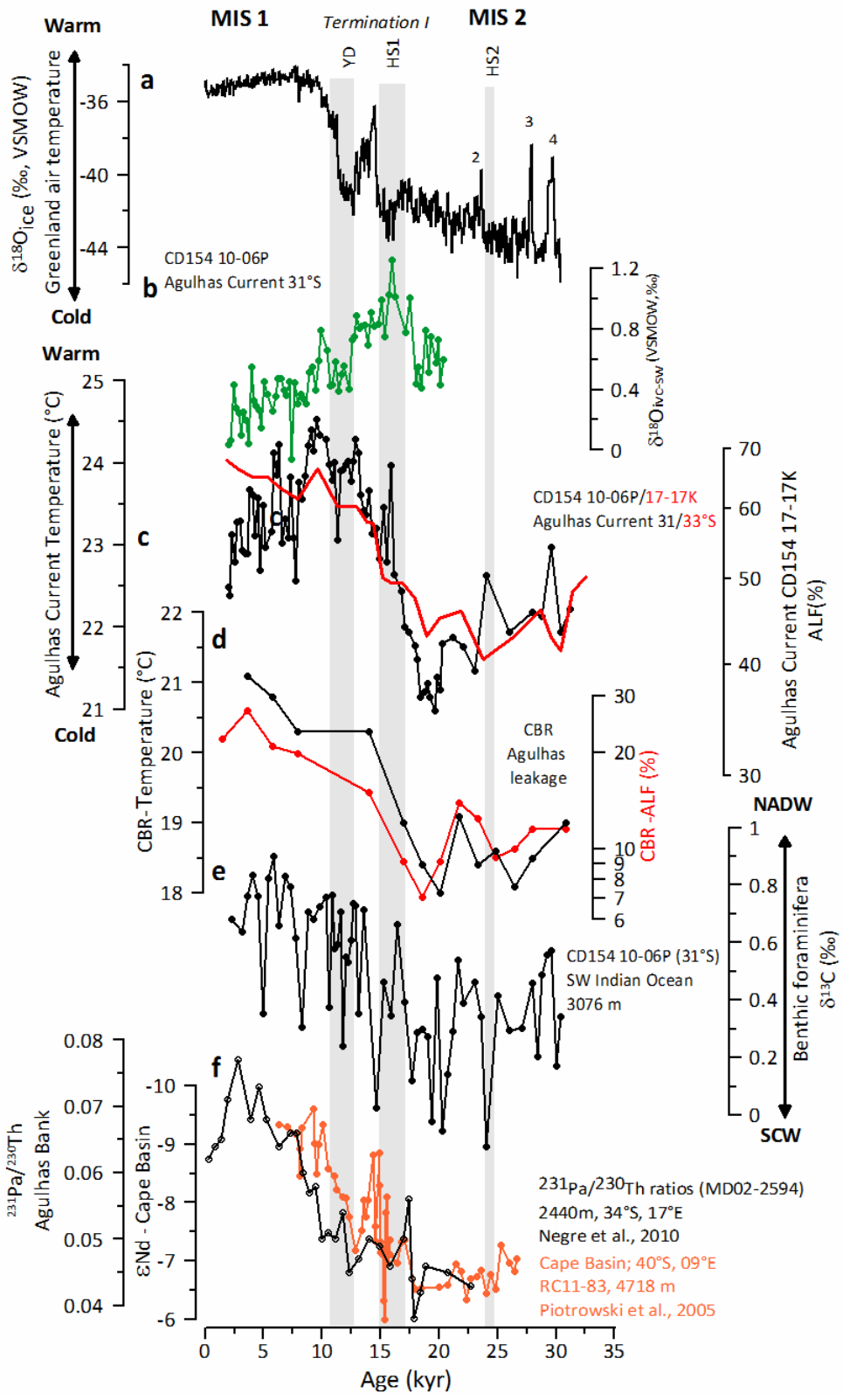

Fig. 4. 8 Agulhas Current and deep water mass variability in the southwest Indian Ocean over Termination I (a) $\delta^{18}O$ record from Greenland ice core NGRIP (NGRIP, 2004), (black, speleo-age model presented in Barker et al., (2011)) displaying abrupt temperature variability in the North Atlantic. Marine isotope stages (MIS) are labelled and underlying grey bars indicate Northern Hemisphere Cold Stadials (b) $\delta^{18}O_{ivc-sw}$ of core CD154 10-06P inferred indication of salinity changes (green) (c) Agulhas Current Mg/Ca- derived temperature estimates of core CD154 10-06P (black) and relative abundance of tropical-

subtropical planktonic foraminiferal marker species (Agulhas leakage fauna, ALF) in core CD15417-17K, (red, logarithmic scale) (d) Uk'_{37} derived SSTs in the Agulhas leakage corridor (Cape Basin Record (CBR), black, Peeters et al., 2004) and relative abundance of tropical-subtropical planktonic foraminiferal marker species (Agulhas leakage fauna, ALF) in the Agulhas leakage corridor (CBR, logarithmic scale, red) (e) Benthic $\delta^{13}C$ record of CD154 10-06P displaying changing influence between Northern and Southern component waters (SCW) (f) Bottom, sedimentary $^{231}Pa/^{230}Th$ ratios from Agulhas Bank (MD02-2594; 2440 m, black; Negre et al. (2010) and Nd isotope ratios (εNd) in the Southeast Atlantic (RC11-83, 4718 m; orange; Piotrowski et al. (2005)).

The concurrent SSTs and ALF increase during the course of the termination in the Cape Basin Record (CBR) as well as in the upstream cores CD154 17-17K and 10-06P further underlines this assumption (Fig. 4. 8c,d).

The onset of the shift from negative to more positive benthic $\delta^{13}C$ values in core CD154 10-06P, generally implying a change from SCWs to higher proportion of NCW, occurred at around ~20 ka (Fig. 4. 8e). During the deglaciation the $\delta^{13}C$ change was rather gradual with the onset being synchronous with the SST and salinity rise (Fig. 4. 8b,c,e). Viewed in a simplistic way that would indicate that the recovery of NADW around South Africa occurred at the same time as increases in salt-leakage which would mean leakage can't have actively triggered the AMOC resumptions. However, processes are more complex.

It has been stated that the AMOC might have been as vigorous as today during the LGM (Yu et al., 1996; McManus et al., 2004; Gherardi et al., 2005; Lippold et al., 2012). However, GNAIW was shallower and might not have reached the deeper region of the South Atlantic and southwest Indian Ocean, which was in turn invaded by southern waters instead (Lynch-Stieglitz et al., 2007).

As the $\delta^{13}C$ record of CD154 10-06P can only reveal information about the presence or absence of NADW in the southwest Indian Ocean, the core position is not ideal to examine the timing of the res-invasion of the NADW into the Southern Hemisphere because the extension and retreat of SCW in that region might have happened independently from a weak or a strong AMOC state in the North Atlantic (Negre et al., 2010). Moreover, an enhanced SCW northward extension during glacials might have even blocked the NCW intrusion into the South Atlantic (Kim et al., 1998; Toggweiler, 1999; Bayon et al., 2003; Raymo et al., 2004). In other words: a change in the benthic $\delta^{13}C$ in CD154 10-06P between the LGM and the Holocene indicate the relative proportion of SCW versus NADW in the southwest Indian Ocean it however does not reveal if that was driven by AMOC changes in the North or deep water changes in the South.

For that reason two additional deep water records from the Agulhas leakage corridor are discussed in combination (Fig. 4. 8f). The deep Cape Basin Nd isotope record on bulk sediment leachates from core RC11-83 (40 °S, 9 °E, 4,718 m; (Fig. 4. 8f; black) was interpreted as a record of the relative balance of NADW and AABW in the southeastern South Atlantic. It further supported the hypothesis that deep ocean circulation changes were linked to G-I cycles and millennial timescales (Piotrowski et al., 2005). Neodymium isotopes are useful proxy to reconstruct deep water sources and structure because they vary between deep ocean water masses. The advantage of Nd isotopes over nutrient-based proxies such as benthic foraminiferal $\delta^{13}C$ and Cd/Ca, is that they are not controlled by changes in pre-formed nutrient content of a water mass and export productivity, and carbon isotopic fractionation during air–sea CO_2 exchange which can bias the interpretation of these proxies as pure deep water circulation tracers (Goldstein and and Hemming, 2003). The observation of a deglacial Nd isotope change in core RC11-83 suggests that during the LGM, less NADW reached the Southern Ocean, but that increases in the amount of NADW present in the Cape Basin occurred during the glacial termination, the B/A, and after the YD, following Greenland ice core temperature records (Piotrowski et al., 2005). Moreover the bottom, sedimentary $^{231}Pa/^{230}Th$ ratios from Cape Basin core MD02- 2594 (Fig. 4. 8f, orange); (Negre et al., 2010) are shown here. Information on the abyssal flow rate of Meridional Overturning Circulation can be deduced from the radiogenic isotope pair ^{231}Pa and ^{230}Th in sea-floor sediments (Marchal et al., 2000). At a water depth of 2,440 m, the site is positioned in the present-day flow path of NADW, and its southerly position makes it particularly appropriate to reconstruct the strength of NADW relative to SCW. Results display a pronounced increase from low glacial values to higher Holocene values which reflects a change from SCW to NADW over the termination (Negre et al., 2010). The benthic $\delta^{13}C$ results of core CD154 10-06P substantiate the deglacial trend observed in both independent deep water records, based on $^{231}Pa/^{230Th}$ and Nd isotopes (Piotrowski et al., 2005; Negre et al., 2010) confirming that the LGM to Holocene shift towards greater NADW and less southern-sourced water is a robust finding in the area (Fig. 4. 8e-f).

Constructing a $^{231}Pa/^{230}Th$ gradient between $^{231}Pa/^{230}Th$ profiles from North Atlantic sites (McManus et al., 2004; Gherardi et al., 2005) and the Cape Basin one (Negre et al., 2010) the authors suggested that the AMOC was restructured with enhanced deep water convection in the Southern Ocean during the LGM promoting flow of these waters from

the Southern to the Northern Hemisphere. This northward dominated SCW flow was apparently maintained until ~9.7 ka before a modern flow pattern with vigorous basin-scale southward transport of NADW was re-established (Negre et al., 2010). It was argued that the absence of any larger-scale deglacial $^{231}Pa/^{230}Th$ shifts in the MD02- 2594 record suggests that the transient episodes of changing convective activity at the sources of the northern water mass were not strong enough to allow the NADW flow to overcome SCW in the South Atlantic (Negre et al., 2010).

During the LGM evidence suggest a dominance of SCW around South Africa (Ninnemann and Charles, 2002; Piotrowski et al., 2004, 2005; Molyneux et al., 2007; Martínez-Méndez et al., 2008; Negre et al., 2010). According to the bipolar seesaw theory the following HS 1 period should also be a time of a resumption of SCW in the area which would imply that only with the onset of the B/A, NADW should be expected to invade the South Atlantic and southwest Indian Ocean again. This would be in agreement with studies from the North Atlantic which determine the resumption of the AMOC at the HS 1/B/A transition around ~14.7 ka (McManus et al., 2004; Gherardi et al., 2005) and benthic $\delta^{18}O$ data from the South Atlantic (Waelbroeck et al., 2011). Waelbroeck et al. (2011) argued that the South Atlantic remained isolated from better-ventilated NCWs until after the resumption of NADW formation at the onset of the Bølling-Allerod, which led to the propagation of NADW into the South Atlantic. As the last glacial termination was composed of two abrupt bipolar events a resumption of SCW is indicated by nutrient proxy records in the subtropical North Atlantic during the subsequent YD cold stadial (Oppo and and Curry, 2012). These results considered in combination might indicate that the initial shift in the benthic $\delta^{13}C$ record of core CD154 10-06P towards more positive values between the LGM and the B/A might be related to an increase in southern-sourced deep water $\delta^{13}C$ in response to either, increased surface waters $\delta^{13}C$ due to sea-ice retreat, increased deep water formation around Antarctica, a change in the location of deep water formation as suggested by (Mackensen, 2001) or a combination of these three factors rather than indicating NADW recovery at the core site.

It can therefore be concluded that Agulhas salt-leakage might have acted as a source of negative buoyancy for the perturbed AMOC, possibly aiding its return to full strength as SST and salinity build-up in the Agulhas system occurred during the HS 1 well before the reestablishment of a vigorous AMOC at the onset of B/A. Thornalley et al. (2011) stated

that based on their reconstructions the strengthening of the AMoOC at the onset of B/A and Holocene may have been promoted by the subsurface warming of subpolar/polar water, brine formation that drew warm saline Atlantic water northwards, and the high background salinity of the Atlantic Inflow. Enhanced advection of saltier Agulhas derived waters during the HS 1 and YD might have been one component contributing to the "high background salinity of the Atlantic Inflow". However, only fully coupled climate models run with glacial boundary conditions can potentially resolve the role of Agulhas salt-leakage during terminations as palaeoclimate records around South Africa alone are not appropriate for that task.

4.3. Conclusion

The results presented here show that the chemical structure of the glacial ocean around South of Africa was different from the modern one. The comparison of this record with other studies in the region revealed that all cores between 2500-3000m were equally bathed in a mixture of USCW and LSCWs during glacials. During millennial-scale NHCSs the southwest Indian Ocean experienced deep water source changes where NCW were equally substituted by a high $\delta^{13}C$ SCW mass possibly a denser, therefore deeper version of AAIW. Due to prevailing warm conditions in the Southern Hemisphere during NHCS different processes need to be operating during formation, perhaps with AAIW being the source of deep waters during e.g., NHCSs and an alternative SCW mass being the source for glacial periods.

A strong $\delta^{13}C$ divide in the glacial southwest Indian Ocean between 3000 and 4500m was recognised, deeper than previously reported from the southeastern Atlantic (Hodell et al., 2003). However, since it is only a feature observed in benthic $\delta^{13}C$ but not in Cd/Ca, the pattern excludes a nutricline (Martínez-Méndez et al., 2008). Moreover, concerns were raised if the vertical extent is only a latitudinal one as only cores south of the glacial SAF display much depleted $\delta^{13}C$ values from 2500m down to the water column. This observation reinforces, however, older hypotheses that the Southern Ocean became isolated during extreme glacial times with implications for the trapping of atmospheric CO_2 with rapid upwelling of previously sequestered "marine" CO_2 to the atmosphere which might have caused the rapid deglacial CO_2 rise (Toggweiler, 1999; Anderson et al., 2009).

The results of the comparison between surface and deep Agulhas waters showed a strong coupling between the two hinting at the fact that variability has a common forcing mechanism. The positions of the major fronts encircling Antarctica, potentially associated with the westerly wind belt and ACC, were shifted northward under glacial conditions by several degrees of latitude. That forced enhanced SCW intrusion into the southwest Indian Ocean in the mid-depths at the same time it enabled the penetration of cold Southern Ocean surface waters into the Agulhas Current via enhanced recirculation processes. The result of these forcings was an Agulhas Current transporting less warm tropical/subtropical waters towards the retroflection area during glacials with potential implications for the leakage signature.

Modelling studies suggest that the northward propagation of heat and salt from the South Atlantic to the convection regions of NADW in the North Atlantic takes 1-1.5 ka to intensify convection (Knorr and Lohmann, 2003; Knorr and and Lohmann, 2004). The here observed salinity build-up starting at around ~17 ka is thus well in time to potentially act on the convection regions of NADW which would put Agulhas salt-leakage into an active role during terminations.

5. Millennial-scale land-ocean climate dynamics in southernmost East Africa: A multiproxy data and model integration

5.1. Introduction

The modern day precipitation pattern over Africa is determined by seasonal oscillation of the rain belt between ~20 °N and ~20 °S characterising the diverse range of climates across the continent (Fig. 5. 1). On longer timescale the distribution of rainfall in tropical and subtropical Africa has fluctuated along with Northern Hemisphere high-latitude climate change (Schefuß et al., 2005; Gasse et al., 2008; Tierney et al., 2008; Tjallingii et al., 2008), ocean circulation (Mulitza et al., 2008) and low-latitude insolation (deMenocal et al., 2000). Large-scale meridional shifts in the position of the Intertropical Convergence Zone (ITCZ) are often invoked to explain the tight link between the African monsoon and northern high latitude climate change. Southward latitudinal migrations of the position of the ITCZ in response to Northern Hemisphere cooling forced either by large ice sheets (during glacials) (Braconnot et al., 2007), or during AMOC slowdowns (such as Heinrich Stadials), (Stouffer et al., 2006), are believed to result in an opposing rainfall pattern in both hemispheres.

Palaeoclimatological reconstructions in southeast Africa are consistent with this picture. Several archives located north (Johnson et al., 2002), or in the vicinity (Tierney et al., 2008), of the modern position of the ITCZ hint towards arid conditions during Northern Hemisphere Cold Stadials (NHCS), such as Heinrich Stadial (HS) 1 and Younger Dryas (YD). In contrast, records from south of the present day East African rain belt document more humid conditions associated with NHCS (Thomas and Shaw, 2002; Burrough et al., 2009; Schefuß et al., 2011; Ziegler et al., 2013b).

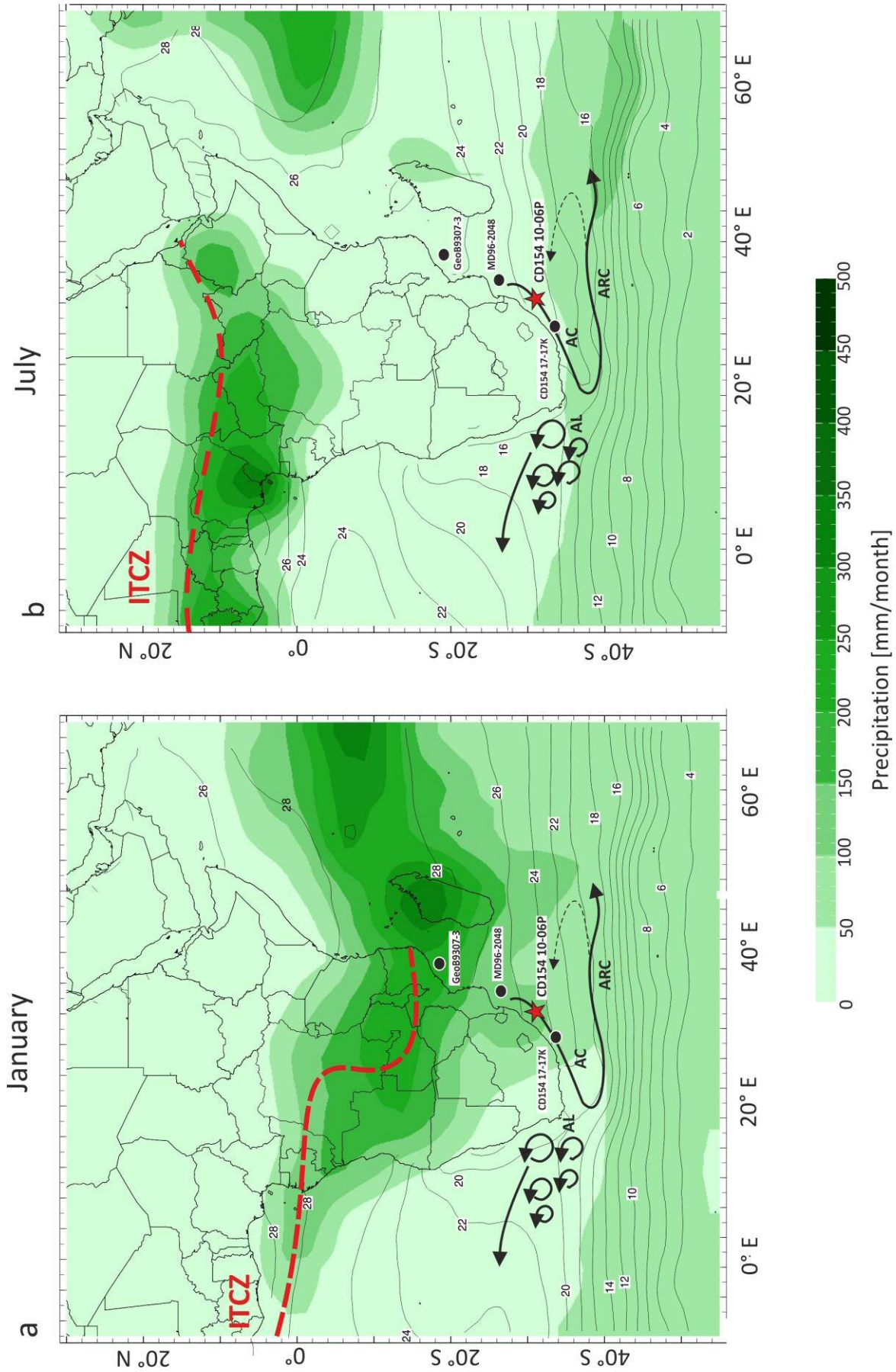
a
January
b
July
ITCZ
GeoB9307-3
MD96-2048
CD154 10-06P
CD154 17-17K
AC
ARC
AL
20° N
0°
20° S
40° S
0° E
20° E
40° E
60° E
Precipitation [mm/month]
0
50
100
150
200
250
300
350
400
450
500

Fig. 5. 1 Modern rainfall variability over Africa (a) January (b) July. Colours indicate modern rainfall changes recorded in mm per month. The climate over large parts of Africa is characterised by a strong seasonality with summer monsoonal rainfall and the approximate position of the ITCZ (red band), (Nicholson, 2000) and its associated rainbelt migrating between the North and South continent over the course of the year (a) January (b) July monthly mean sea surface temperature (SST) field (1971-2000) in the area in °C [http://iridl.ldeo.columbia.edu]. Ocean circulation features around South Africa and marine sediment core locations discussed in the text are indicated: Geo B9307-3; black circle, Schefuß et al. (2011); CD154 17-17K, black circle, Ziegler et al. (2013b); CD154 10-06P, red star, this study. Main feature of the Agulhas Current System around South Africa are shown: Agulhas Current- AC, Agulhas leakage-AL, Agulhas Return Current (ARC) and associated recirculation at 40 °E.

However, two alternate forcing mechanisms to explain the rainfall variability in these southerly areas have been put forward: one related to the southward shift of the main position of the ITCZ during NHCS, leading to higher precipitation over southeast Africa; whereas other studies infer a predominant influence of Indian Ocean sea surface temperatures (SST) on regional rainfall changes (Tierney et al., 2008; Stager et al., 2011). These latter interpretations rely on modern meteorological observations (e.g., Jury et al., 1993) as well as numerical model simulations (Reason and Mulenga, 1999), which link rainfall in eastern and southern Africa to increased SST in the western and southwestern Indian Ocean, respectively. Notably, the warm waters transported along the southeast coast of Africa by the Agulhas Current, are thought to have a particularly strong impact on the regional atmospheric circulation (Reason, 2001). Large amounts of heat are lost from the surface of the Agulhas Current to the atmosphere due to strong winds over the warm core of the Agulhas Current which results in weather disturbances, such as extra tropical cyclones and intense rainfall over large parts of the adjacent Southern African continent (Reason, 2001).

5.1.1. Study approach

Previous findings from Mozambique (Schefuß et al., 2011) and the Eastern Cape province (Ziegler et al., 2013b) suggest that, on millennial timescales, humid conditions in southeast and southernmost East Africa are preliminary forced by Northern Hemisphere climate variability. This assumption remains tentative as results were, at least in the southernmost East Africa part, the first in the area and purely based on XRF-scanning derived relative elemental intensities. In order to further test the interhemispheric teleconnection and inferred sensitivities of the southeast African hydrological cycle during millennial-scale climate change a data-model integration approach was adopted here. First, a new marine sediment core, CD154 10-06P (031°10.36' S, 032° 08.91' E, 3076 m

water depth), recovered from offshore KwaZulu-Natal (KZN) Province (Fig. 5. 1), situated in the vicinity but further upstream in the Agulhas Current, compared to the location investigated by Ziegler et al., (2013b) was studied. The Ziegler et al. (2013b) XRF-based approach was further augmented by measuring, in addition to the sedimentary terrestrial ratios/concentrations of Iron (Fe) to Potassium (K), other organic (based on branched glycerol dialkyl glycerol tetraether (GDGT) lipids; Hopmans et al., 2004) and inorganic geochemical proxies, which provide direct and indirect evidence of terrestrial input from land at the CD154 10-06P site. Organic ($U^{K'}_{37;}$ TEX_{86}) and inorganic proxy based SST estimates from the same core material were also derived in order to investigate if a warming in the Agulhas Current region is associated with increased rainfall over neighbouring South Africa. Relative salinity changes in the Agulhas Current were reconstructed using the combined hydrogen isotope (δD) composition of the di- and tri-unsaturated C_{37} alkenones, produced by haptophyte algae, as well as paired $\delta^{18}O$ and Mg/Ca ratios of foraminifera *Globigerinoides ruber* (white).

Finally, a numerical model simulation using the fully coupled Community Earth System Model (COSMOS) was performed. The model simulates quantitative estimates of precipitation changes over southeast Africa and provides indications about the areas of maximum net freshwater flux by local rivers along the southeastern African continental margin. Moreover, changes of surface level pressure (SLP) systems over South Africa and the South Atlantic and Indian Ocean are provided in conjunction with Agulhas Current SST and sea surface salinity (SSS) changes simulated by the model under glacial boundary and reduced AMOC conditions (via freshwater hosing). This approach enables to evaluate how changes in the hydrological balance of southeast Africa are propagated to and documented in the marine sediment record and how well the documented environmental response agrees with the simulated model results.

5.2. Background

5.2.1. Climatology and vegetation of southeast Africa

KwaZulu-Natal forms the northernmost province on the eastern Indian Ocean coastline of South Africa. The modern day rainfall regimes over South Africa are generally complex and controlled by quite diverse dynamic causes (see below). Rainfall is greatest in the east and gradually decreases westward, with some semi-desert areas along the western edge of

South Africa. For most of the country, rain falls mainly in the austral summer months (November through March). The exception is the Western Cape where the climate is Mediterranean and it rains more in the wintertime (June to August).

The regional climate in the KZN is dominated by austral summer rainfall (Gasse et al., 2008), which is primarily dictated by the seasonal interplay between subtropical high-pressure cells and the migration of easterly winds which are associated with the ITCZ that brings rain to the tropics (Gasse et al., 2008). The resulting moisture transfer from the Indian Ocean brings rain to the area (Gasse et al., 2008), (Fig. 5. 1a). During austral winter months the region receives less rainfall (Fig. 5. 1b) as the land surface cools relative to the warm southwest Indian Ocean and broad anticyclonic atmospheric circulation prevails over the region (Gasse et al., 2008). Specifically, three weather phenomena dominate the modern climatology of KZN province, as well in the wider southeast African coastal region: ridging anticyclones, cut off lows and tropical-extra tropical cloud bands (Singleton and Reason, 2007; Hart et al., 2010; Weldon and Reason, 2014). Anticyclonic ridging events produce onshore flow which, when strong and moist enough, can lead to orographic rainfall as the southeast African coastline is mountainous (Weldon and Reason, 2014). Cut-off low pressure systems are cold lows (depression) in mid-latitudes which are often linked with deep moist convection, which can lead to significant amounts of rainfall over short periods of time and therefore flash-flooding (Singleton and Reason, 2007). They can have a substantial influence on the regional weather patterns, as seen in 1987 during which time severe flooding affected the coastal areas of the KZN province when a cut off low led to rainfalls in excess of 90 cm over 3 days (Singleton and Reason, 2007). Moreover, cold fronts which during the summer half of the year link up with a tropical disturbance over the low latitude in southern Africa to tropical–extratropical cloud bands, can be formed, resulting in substantial rainfall over the South Coast (Weldon and Reason, 2014). The intensity of these weather systems broadly depends on the mean positions of the South Indian Ocean (SIO) and South Atlantic Ocean (SAO) anticyclones, which are centred respectively off the southern coast of South Africa and south of Madagascar. Both systems are subtropical high pressure cells and semi-permanent manifestations of the subtropical part of the global atmospheric circulation (Asani, 2005).

The modern natural vegetation ranges from closed forest to dry scrubland and from alpine open grassland to semi-evergreen lowland forest (White, 1983). Along the rivers, wet

forest alternates with floodplain savannah and herb communities (White, 1983). As a consequence of the high austral summer rainfall, C4 grass is the primary vegetation in the region, which is in contrast to the Western Cape where C3 grasses dominate as a result of higher winter rainfall (Vogel et al., 1978).

5.2.2. Geology and geochemical characteristics of the southeast African river catchments

Several rivers traverse the KZN province before flowing into the adjacent southwest Indian Ocean. These include, among others, the Umfolozi, Mgeni, Umzimkulu, Umzimvubu Rivers, with the largest being situated north of Durban, the Tugela River, which is some 502 km long, has a catchment of ~ 29,000 km^2 (Begg, 1978) and annual mean freshwater discharge of 3865x10^6m^3 (Whitfield and Harrison, 2003). Marine sediment core CD154-10-06P was retrieved from the southwest Indian Ocean ~160 km off the KZN province coast (Fig. 5. 1). The core is situated on the lower southern flanks of the Tugela Cone sediment fan, which is supplied by terrigenous sedimentary material discharged by the Tugela River (6.79x10^6m^3/yr), (Bosman et al., 2007). While this is the closest source for terrigenous material, other smaller rivers of the KZN province might also contribute material to the core site.

Fig. 5. 2 Satellite image of the Great Kei river mouth, Eastern Cape province, southeast Africa, with its typical brownish-red river water derived from a high, iron-rich, sediment load (Ziegler et al., 2013b).

Southeast African rivers are all typical brown-water rivers characterised by high sediment loads, which are notably rich in iron oxides (Fig. 5. 2) derived from mudstones and

sandstones of the Karoo Supergroup and associated intruded dolerites ('Ironstone') within the catchment areas (Johnson et al., 1996; de Oliveira and Cawthorn, 1999). Soils formed from the Karoo sedimentary rock contain abundant quartz, K-feldspar and illitic as well as smectitic clay minerals (Compton and Maake, 2007). Consequently, the terrestrial versus marine elemental ratio recorded in marine sediments can be used as a first-order indication of relative changes in the amount of fine (Fe-rich) terrigenous components supplied to the core site from regional river discharge (Ziegler et al., 2013b).

5.3. Results and discussion

5.3.1. Land-ocean climate dynamics

The most prominent intervals during the last deglaciation (~19-11 ka), are HS 1 (~18–14.7 ka) and the YD (~12.9–11.7 ka), (Alley and Clark, 1999) when the Northern Hemisphere experienced abrupt cold stadials, as documented in Greenland Ice core records (NGRIP, 2004); Fig. 5. 3). These events were associated with a combination of ocean and atmospheric circulation changes including changes in the AMOC strength and its associated heat distribution between hemispheres (Broecker, 1998; Stocker and Johnsen, 2003). The East Asian Indian Monsoon system is thought to have weakened in intensity in response to abrupt NHCS as a result of a southward shift in the annual average position of the ITCZ (Wang et al., 2008). The East Asian summer monsoon (EASM) $\delta^{18}O$ record from Chinese speleothems (Hulu and Sanbao Cave, Wang et al., 2008; Wang et al., 2001) is suggested to represent changes in the proportion of low $\delta^{18}O$ (summer monsoon) rainfall within annual totals and can be considered a measure of the amount of summer monsoon rainfall or monsoon intensity (Cheng et al., 2012). However, variations in the $\delta^{18}O$ records in the EASM region are still widely debated as to what they ultimately represent, because, among other reasons, a significant component of EASM precipitation is derived from the Indian Summer Monsoon domain (e.g., Clemens et al., 2010; Pausata et al., 2011). Pausata et al. (2011) proposed, based on modelling results, that changes in the $\delta^{18}O$ of cave carbonates associated with Heinrich events reflect changes in the intensity of the Indian rather than East Asian monsoon precipitation.

In the offshore KZN province the sedimentary record of core CD154 10-06P shows recurrent increases in the terrestrially-influenced Fe/K ratios during the course of the last deglaciation (Fig. 5. 3). The measured range of absolute bulk sedimentary concentrations

in Fe/K ratios in the CD154 10-06P record (ln(Fe/K) = Ø 1.6) reproduce ratios from the suspended sediment load of rivers in South Africa (ln(Fe/K = Ø 1.16, Compton and Maake, 2007) and from samples along the African margin between 17 °N and 8 °S, i.e., in areas receiving strong fluvial input from the Senegal, Niger and Congo Rivers (ln(Fe/K) = 1.34±0.32, Govin et al., 2012), thereby confirming the local origin of the terrestrial material delivered to the CD154 10-06P core site. Owing to the prevailing easterly winds, aeolian transport of terrigenous material from subtropical southern Africa towards the southwest Indian Ocean is negligible (Nicholson, 2000).

Enhanced chemical weathering and iron oxide mobilisation, as well as soil erosion, on land requires frequent rainfall over the continent and so are indicative of more humid conditions in the hinterland climate. Elevated chemical weathering rates, due to increased precipitation, result in highly-weathered soils typical for tropic and subtropical environments. As clay minerals are intensely weathered, the structure of silicates clays change as they lose silica and the remaining soil is enriched in iron oxides, such as Goethite (FeO(OH)) or Hematite (Fe_2O_3), (Schaetzl and and Anderson, 2005) which is ultimately recorded as high Fe/K values in the sediment. Conversely, drier conditions in the hinterland favour reduced chemical weathering, resulting in low Fe/K ratios in marine sediments (Govin et al., 2012).

Branched GDGTs are abundant lipids derived from bacteria that thrive in soils and peats (Weijers et al., 2006; Weijers et al., 2007b) as well as in rivers (Zell et al., 2013). Branched GDGT concentrations depend on changes in aridity/humidity (e.g., Dirghangi et al., 2013). Wet soils and peats contain higher concentration of branched GDGTs than soils from arid environments, which is related to the preferred ecological niche of the GDGT forming bacteria (Dirghangi et al., 2013). Branched GDGTs are introduced from soils to marine environments via erosion and will be transported as river-suspended matter, with both iron oxides and membrane lipids largely associated with the clay fraction (<2 μm), (Libes, 2009; Ingalls et al., 2012). This material is subsequently transported to the deep sea either by direct settling from the surface ocean (primarily via aggregate formation associated with biological production), or by down-slope gravity-driven flows in turbidity currents and debris flows. This material is then potentially re-suspended and further transported by deep ocean currents to sites of deposition (McCave and Hall, 2006). Consequently, higher Fe/K ratios and BIT values in CD154 10-06P are interpreted as an indication of higher soil

erosion and enhanced chemical weathering processes on land due to changes to more humid climate conditions in the KZN province.

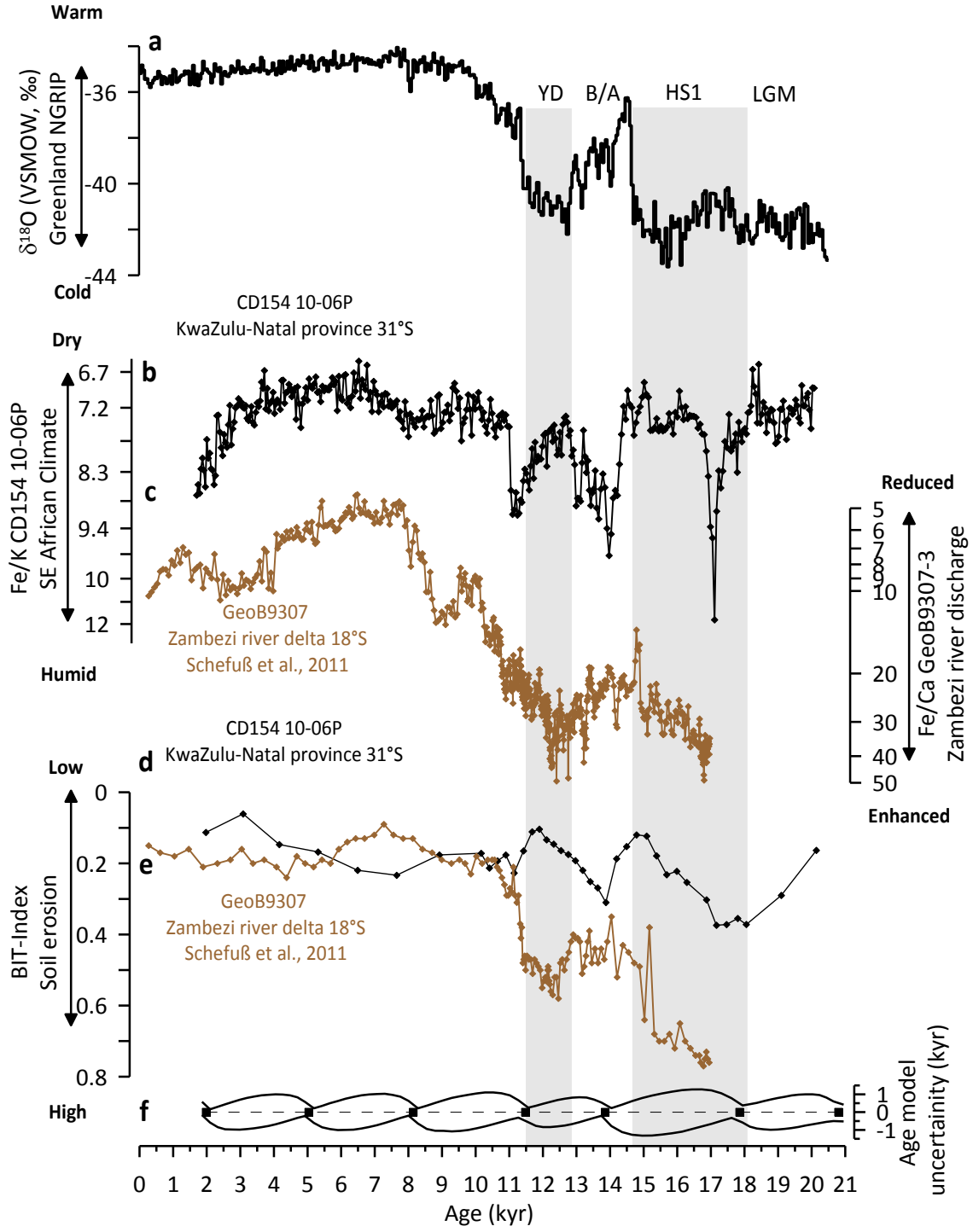

Fig. 5. 3 Records of environmental variability in southeast Africa over the past 21 kyr (a) $\delta^{18}O$ record from Greenland ice core NGRIP (NGRIP, 2004), (black, speleo-age model presented in Barker et al., (2011)) displaying abrupt temperature variability in the North Atlantic. Underlying grey bars indicate Last Glacial Maximum (LGM), Heinrich Stadial 1 (HS 1), Bølling-Allerød interstadial (B/A) and Younger Dryas. (b) Fe/K of CD 154 10-06P (black, this study) indicating climate variability in the KZN province, (c) Fe/Ca ratios, indicating terrestrial versus marine elemental contributions to sediments of GeoB9307-3 (Schefuß et al., 2011) (d) BIT index of CD154 10-06P, reflecting changes in relative soil organic matter

contributions to the core site (e) BIT index of GeoB9307-3 (Schefuß et al., 2011), reflecting changes in relative soil organic matter contributions to the core site (f) Radiocarbon dates and age model uncertainty.

Intriguingly, high values in Fe/K (4.2) and BIT (0.4) values occurred contemporaneously at the onset of HS 1 (~18-17.5 ka), with an abrupt shift back to low Fe/K values shortly after (Fig. 5. 3a, b, d). Conversely, BIT values display a more gradual pattern pointing towards drier conditions developed over the course of HS 1. A second maximum in both proxies is evident within the Bølling-Allerød interstadial (B/A), (~14.7-12.9 ka), (Alley and Clark, 1999). However, contrary signals are seen during the course of the YD with the Fe/K indicating the development of more humid conditions whereas the BIT index indicates a trend towards increased aridity. Although both iron oxides and membrane lipids are thought to derive from a similar source (soils) and are associated with the same size fraction and hence transport and sedimentation processes should be similar, discrepancies cannot be ruled out. For examples, differences in the pattern between organic and inorganic proxies in the CD154 10-06P records might potentially be associated with different transport times, degradation processes of organic matter or differential intermediate storage on shelf areas.

The timing and pattern inferred from the CD154 10-06P proxies during the last deglaciation is rather unexpected because previous studies from southeast Africa point towards continuous humid conditions during HS 1 and the YD in that area (e.g., Schefuß et al., 2011), (Fig. 5. 3). The direct comparison with the environmental record of core GeoB9307 (18° 33.99’ S, 37° 22.89’E, 542m water depth) from the Zambezi river delta (Fig. 5. 1) clearly highlights these differences. However, it needs to be recognised that both core locations differ significantly in respect to their environmental setup. Marine sediment core GeoB9307 is located closer to the river mouth. In addition the Zambezi River delivers more terrestrial material to the southwest Indian Ocean compared to smaller local rivers in the KZN province (Flemming, 1981; Schefuß et al., 2011). Regardless of the different core locations, changes in the BIT index in both cores during the course of HS 1 are in agreement and confirm that HS 1 was an interval of more humid conditions in southeast Africa (Fig. 5. 3). The excursion towards more humid climate as recorded in CD154 10-06P during the B/A is not evident in the Zambezi River record. Moreover, the magnitude of changes during the YD is much more pronounced in the GeoB9307 record.

Increases in precipitation over the wider region of southeast Africa during NHCS should equally impact the catchment areas of the Zambezi and other smaller southeast African rivers such as the Tugela. Assuming, that the environmental response to the climate change during NHCS was coincident in both areas, the differences between proxy records might suggest that different land–ocean dynamics occurred and ultimately influenced how the climate signal was recorded in the marine record. During the last deglaciation pronounced sea level fluctuations (Fairbanks, 1989; Grant et al., 2012) as well as the changes in the Agulhas Current circulation (e.g., Chapter 3, Franzese et al., 2006; Franzese et al., 2009) might have impacted the sedimentation processes from land. In comparison to core GeoB9307 the core site of CD154 10-06P is in the direct influence of the Agulhas Current and adjacent continental shelf area is narrower (Fig. 5. 1), (Bosman et al., 2007). Early studies along the southeast African continental margin have previously alluded to the complex interaction between fluvial and oceanographic processes (Flemming, 1981; Bosman et al., 2007). Changes in the Agulhas Current path or flow velocity might have impacted or delayed sediment delivery to the CD154 10-06P core site which could potentially explain the low Fe/K values during HS 1 and the delayed onset of the signal detected during the B/A.

In order to evaluate if the pattern evident in core CD154 10-06P is unique or representative of the wider regional signal it is directly compared with the data available from core CD154 17-17K located ~400 km further downstream within the Agulhas Current (Fig. 5. 1), (Ziegler et al., 2013b). Excursions in Fe/K in core CD154 17-17K over the past 100 kyrs were directly correlated to the EASM record assuming an interhemispheric asymmetry and in time relationship between records.

As the Fe/K records of both cores share similar variance with clear similarities in the millennial structure a composite record representative of the wider KZN and Eastern Cape province was produced in order to evaluate the timing of the changes in the southeast African climate between local regions (Fig. 5. 4) and towards their Northern Hemisphere counterparts the EASM records (Fig. 5. 5). The KZN-Eastern Cape province composite Fe/K record was developed by initially correlating the common Fe/K excursions in both records (Fig. 5. 4) within the depth domain. The validity of this approach is confirmed by the resulting independent chronological fit of the two *G. ruber* derived $\delta^{18}O$ records of the cores (Fig. 5. 4 b-c).

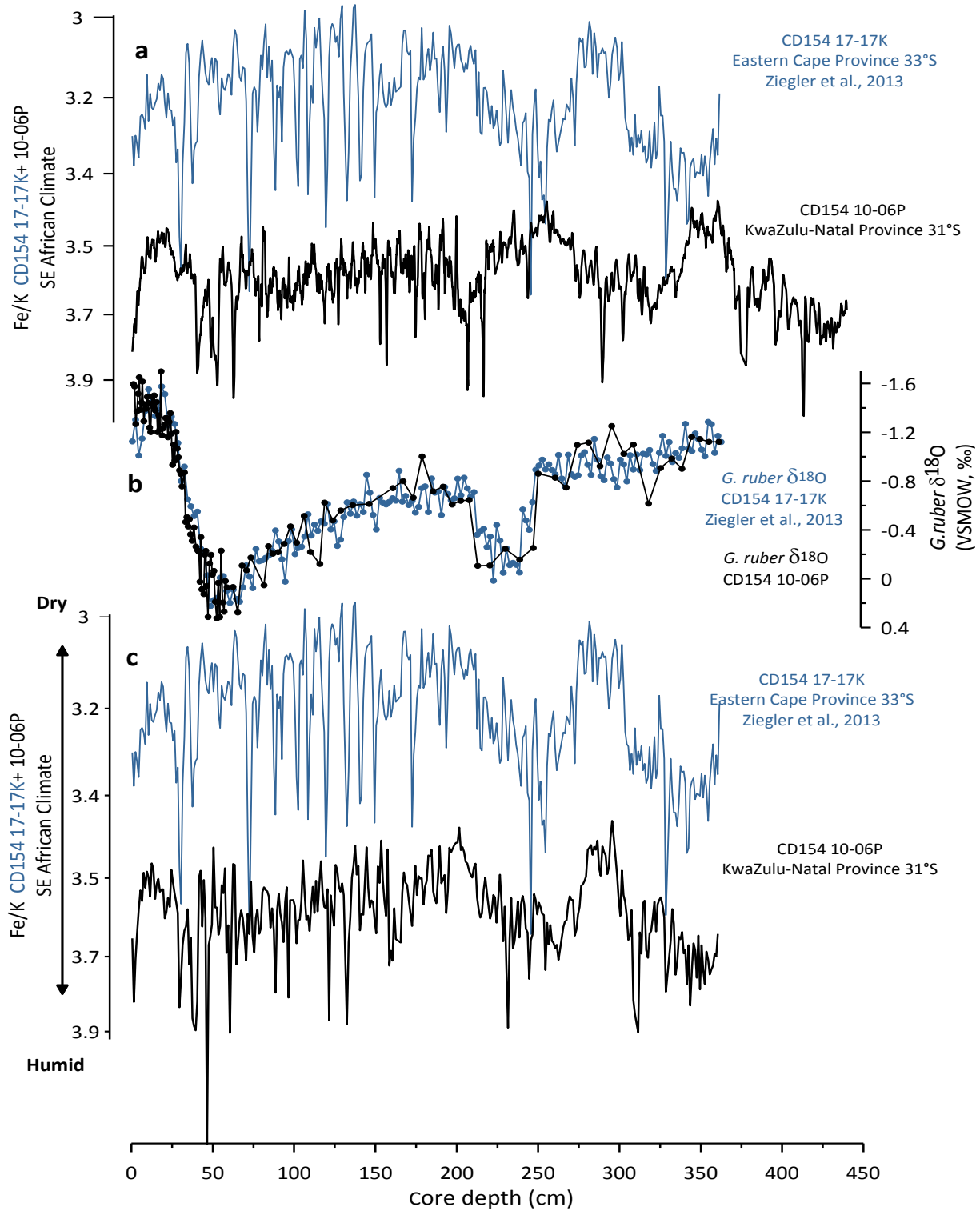

Fig. 5. 4 Composite record of CD154 17-17K/ CD154-10-06P (a) Fe/K of CD154 17-17K (blue, Ziegler et al., 2013b) and CD 154 10-06P (black, this study) on individual core depths (b) $\delta^{18}O$ record of CD154 17-17K (blue, Ziegler et al., 2013b) and CD 154 10-06P (black, this study) on composite core depth (c) Fe/K of CD154 17-17K (blue, Ziegler et al., 2013b) and CD 154 10-06P (black, this study) on composite core depth.

After developing a common depth scale for both cores a composite age model was constructed based on the combined twenty radiocarbon dates available from both cores which allows an evaluation of the correlation and timing of the wider regional pattern of southeast African climate variability and the EASM record independently within the limits of the radiocarbon dating method (Fig. 5. 5, Table 5. 1).

Table 5. 1 ^{14}C dates for composite record of CD154 17-17K/ CD154-10-06P. Calibration of radiocarbon dates was performed using the Bchron software package (Parnell et al., 2011) using Marine09 (Reimer et al., 2009) and a reservoir age correction of 400 years (Bard, 1988) and to calculate the 95% uncertainty on the calibrated ages.

Core	Composite Depth (cm)	Species	^{14}C age BP (yr)	Error +/- 1σ (radiocarbon yrs BP)	1σ confidence age interval Lower limit (yrs BP)	1σ confidence age interval Mid-point	1σ confidence age interval Upper limit (yrs BP)	Lab Code
CD154 17-17K	0.5	*G. ruber*	2200	25	1.71	1.8	1.87	KIA 47083
CD154 10-06P	1.2	*G. ruber*	2359	35	1.88	1.98	2.09	SUERC-45072
CD154 10-06P	11.1	*G. ruber*	4774	35	4.89	5.03	5.20	SUERC-45075
CD154 17-17K	18.5	*G. ruber*	6735	+40/-35	7.17	7.26	7.36	KIA 47084
CD154 10-06P	20.3	*G. ruber*	7681	40	8.02	8.14	8.26	SUERC-45076
CD154 10-06P	29.5	*G. ruber*	10409	49	11.26	11.48	11.71	SUERC-45077
CD154 10-06P	38.4	*G. ruber*	12403	63	13.70	13.85	14.01	SUERC-45078
CD154 17-17K	38.5	*G. ruber*	12500	60	13.79	13.94	14.12	KIA 47085
CD154 10-06P	47.9	*G. ruber*	15082	89	17.50	17.85	18.40	SUERC-45079
CD154 17-17K	48.5	*G. ruber*	16120	90	18.66	18.85	19.27	KIA 47086
CD154 10-06P	60.6	*G. ruber*	17863	132	20.37	20.79	21.29	SUERC-45080
CD154 10-06P	64.5	*G. ruber*	18786	148	21.51	21.91	22.31	SUERC-45081
CD154 10-06P	70.7	*G. ruber*	20682	191	23.69	24.19	24.76	SUERC-45082
CD154 10-06P	75.4	*G. ruber*	23498	273	26.97	27.90	28.48	SUERC-45085
CD154 17-17K	78.5	*G. ruber*	24050	+200/-190	27.96	28.39	29.073	KIA 47087
CD154 17-17K	126.5	*G. ruber*	35340	+820/-720	37.86	39.95	41.447	KIA 47088
CD154 17-17K	156.5	*G. ruber*	45470	+3080/-2220	43.17	47.35	49.846	KIA 47089

On the basis of the established composite depth scale and age model a nearly identical pattern in the Fe/K is evident in both core locations offshore Eastern Cape and KZN province which confirms that the KZN region was sensitive to changes in the adjacent terrestrial regime confirming the initial results of Ziegler et al (2013b). Within the uncertainty of the ^{14}C based composite age model (Table 5. 1) it is possible to link

individual events in the Fe/K record to a corresponding NHCS. The Fe/K excursions during MIS 3, specifically HS 5-2 are good examples of an "in phase" relationship with the Chinese speleothem record (Fig. 5. 5).

In comparison to the direct tuning approach to the EASM record applied by Ziegler et al. (2013b) this match is simply based on independent ^{14}C age control. While, the scarcity of dates within MIS 3 makes it difficult to evaluate the timing in detail, it is evident that the pattern in both cores during the deglaciation deviates from the good fit observed during MIS 3. As highlighted earlier excursions in the Fe/K ratios in both cores, as well the BIT values in core CD154 10-06P, deviate from the assumed "in phase" relationship with the Chinese speleothem records during HS 1 and B/A interval, if the age control is purely based on ^{14}C age. Peak Fe/k ratios in both cores and high BIT values in core CD154 10-06P occurred within the B/A rather than during HS 1 which is rather unexpected if an anti-phased pattern with the Chinese speleothem records would be assumed. The time deviation during HS 1 in comparison to the EASM record is a feature which is evident in both cores, CD154 17-17K and 10-06P, which implies that environmental processes impacting on the sedimentation processes potentially influenced the wider region, not just one core location. The reason for the offset is likely to be multifaceted. As noted above there are complex interaction between fluvial and oceanographic processes along the southeast African continental margin (Flemming, 1981; Bosman et al., 2007). Changes of the Agulhas Current itself, such as flow speed, onshore–offshore position along the continental margin, eddies and meanders impacting on the continental sedimentation processes might have affected both core positions which might explain their common offset during this period.

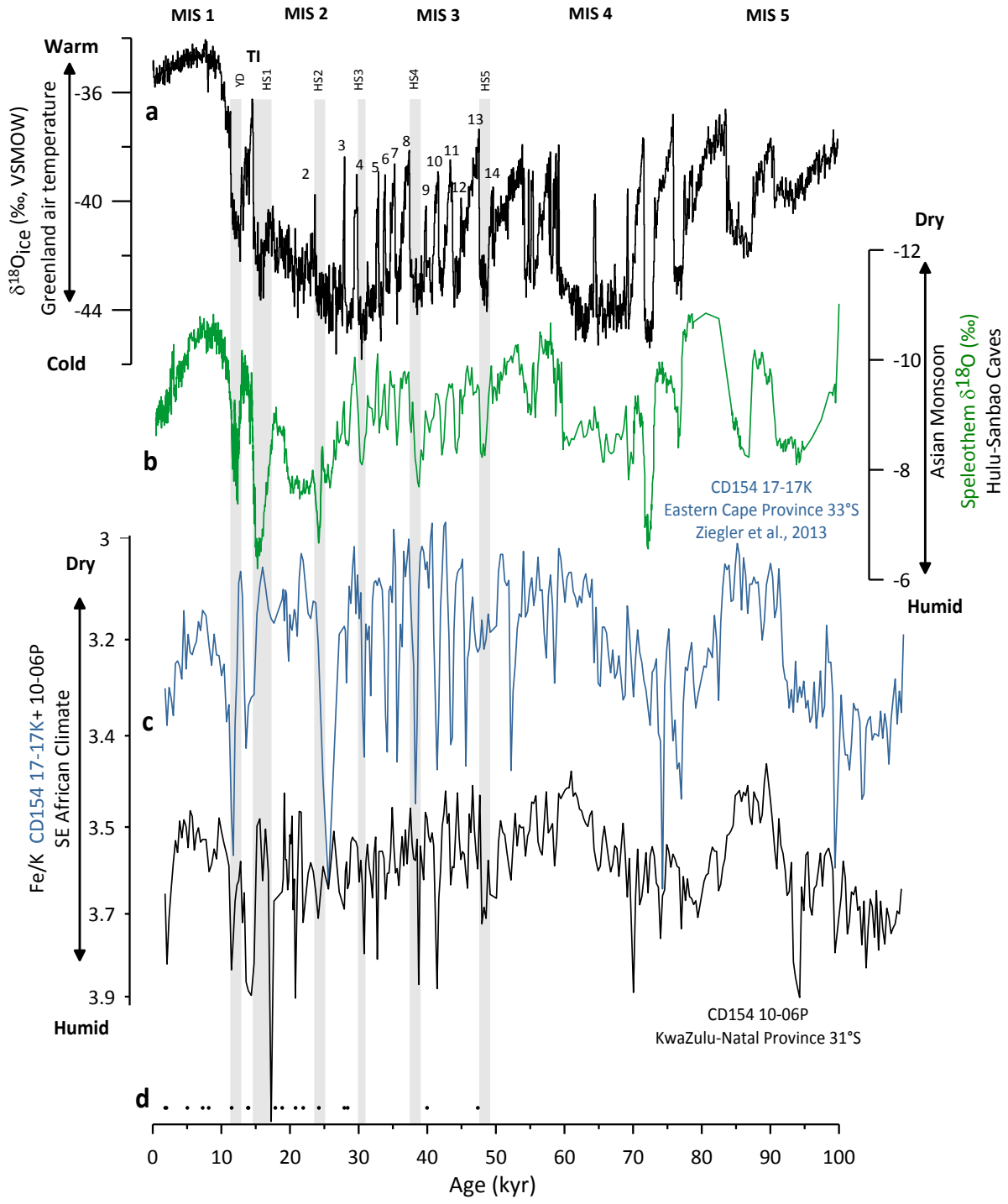

Fig. 5. 5 (a) $\delta^{18}O$ record from Greenland ice core NGRIP (NGRIP, 2004), (black, Speleo-age model presented in Barker et al., (2011)) displaying abrupt temperature variability in the North Atlantic. Underlying grey bars indicate Heinrich Stadial 5-2 and Younger Dryas (b) $\delta^{18}O$ splice from Chinese speleothems (green, Hulu and Sanbao Cave, (Wang et al., 2008; Wang et al., 2001) showing synchrononous variability of the East Asian monsoon with climate variability during Northern Hemisphere stadials (c) Fe/K of CD 154 17-17K (blue, Ziegler et al., 2013b) and CD 154 10-06P (black, this study) (d) Radiocarbon dates

One could also consider that the assumptions associated with the radiocarbon dating are incorrect (e.g as discussed in Chapter 2, section 2.3.). For example, Skinner et al. (2010) demonstrated that there might have been a large increase in surface reservoir ages

occurring during HS 1 in the South Atlantic (MD07- 3076 CQ (44° 4.46'S, 14°12.47'W, 3770 m), which led the authors to apply variable reservoir correction during the last deglaciation for that core. In the generation of the KZN-Eastern Cape province composite, radiocarbon ages were uniformly corrected for a global average reservoir age of 400 years (Bard, 1988). However, if the regional reservoir age was greater, then the phase offset towards the ESAM records would increase suggesting that this potential bias seems unlikely.

The high degree of synchronicity between the EASM events and the Fe/K pattern identified originally by Ziegler et al. (2013b) could be further strengthened with the KZN-Eastern Cape province composite record. Moreover, the mismatch between the Fe/K record in both cores and the speleothem $\delta^{18}O$ record is only restricted to HS 1 which leads to the conclusion that most likely southeast African climate variability was coupled with, but anti-phased to the EASM intensity in the Northern Hemisphere on suborbital timescales.

In summary, these results confirm the initial tuning approach of Ziegler et al., (2013b) however, sedimentation processes are more multifaceted than previously thought and independent age control is necessary to check for potential "phase shifts" within glacial terminations.

5.3.2. Agulhas Current sea surface temperature variability and its implications for southeast African humid phases

In order to assess the relationship between changes in the SST of the Agulhas Current and variability of the regional hydrology, the temperature pattern derived from organic (TEX_{86} and) as well as inorganic (Mg/Ca ratios) proxies from core CD154 10-06P is evaluated (Fig. 5. 6). Over the deglaciation SST estimates derived from each of these proxies display warming trends of 3 °C, with coldest SST occurring at the LGM (~20 ka) and warmest conditions during the regional Holocene Thermal Maximum (HTM; 11-5 ka, Renssen et al. (2012)). However, substantial differences are observed in the absolute SSTs estimated by the different proxies. The and TEX_{86}-derived SSTs are typically between 3-4°C warmer in comparison with the *G. ruber* based Mg/Ca SSTs during the past 21 kyr (Fig. 5. 6b).

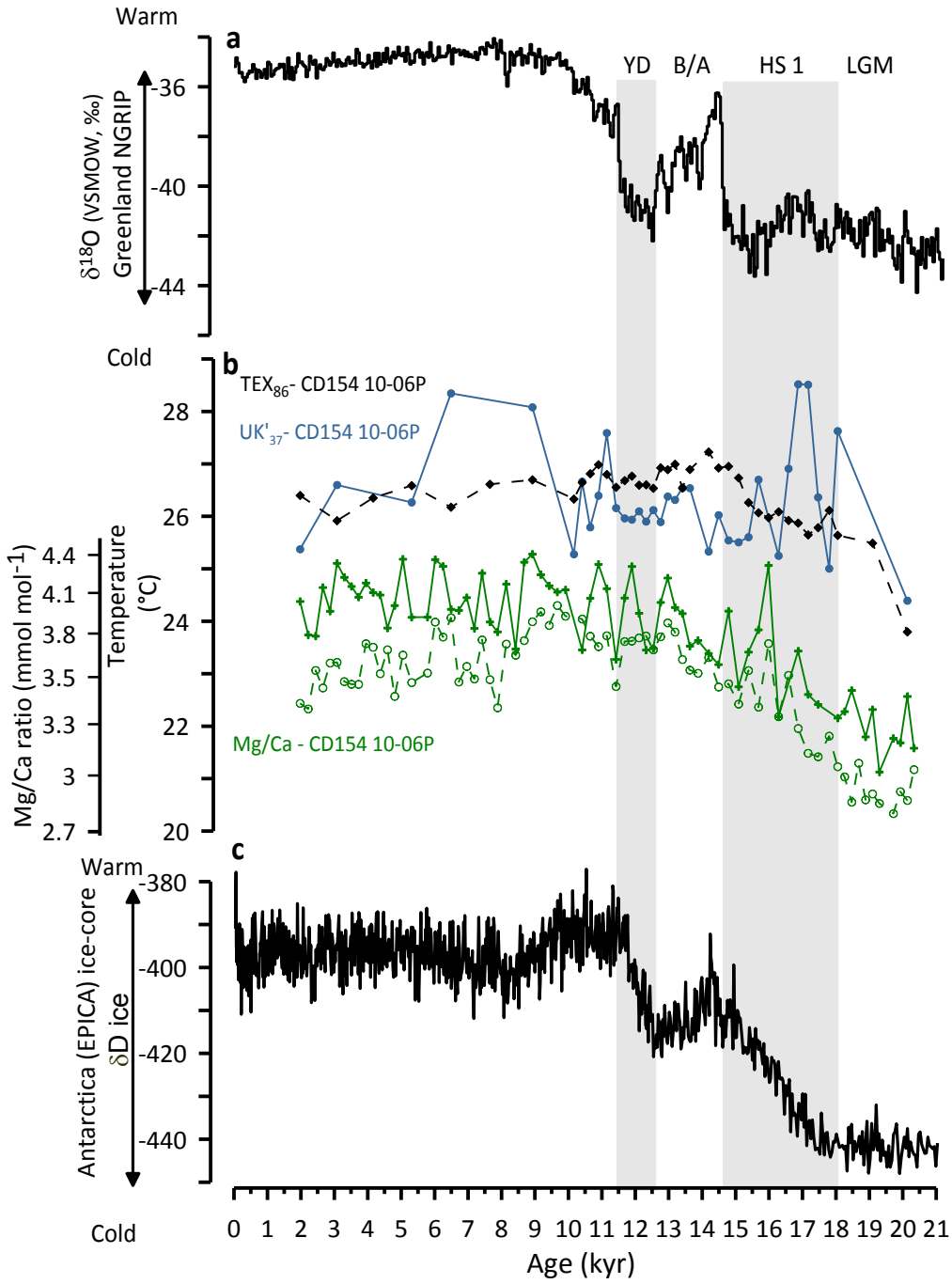

Fig. 5. 6 (a) $\delta^{18}O$ record from Greenland ice core NGRIP (NGRIP, 2004), (black, Speleo-age model presented in Barker et al., (2011)) displaying abrupt temperature variability in the North Atlantic. Underlying grey bars indicate Last Glacial Maximum (LGM), Heinrich Stadial 1 (HS1), Bølling-Allerød interstadial (B/A) and Younger Dryas (b) Tex_{86} derived SST record CD 154 10-06P (black diamonds) reflecting ocean temperature changes in the Agulhas Current, UK'_{37} derived SST record (blue circles) from CD 154 10-06P, *G. ruber* Mg/Ca ratios (mmol mol^{-1}) and derived SST record (open green circles), and dissolution adjusted SST (green crosses) (c) Antarctica (EPICA) temperature variability as inferred from δD ice record.

Several studies from the tropical Western Indian Ocean have similarly observed apparent differences among these SST proxies (Bard et al., 1997; Levi et al., 2007; Kim et al., 2010; Caley et al., 2011a). These observations suggest that warmer and TEX_{86} SSTs and

cooler Mg/Ca SSTs are a robust feature in the Western tropical Indian Ocean. There are several potential explanations for these proxy-based differences in absolute temperatures which may be explained by a variety of reasons such as growth seasons and/or depth habitats between the alkenone producers, the Thaumarchaeota (GDGT producers) and the planktonic foraminifera (Müller et al., 1998; Bard, 2001; Karner et al., 2001; Wuchter et al., 2006; Lee et al., 2008; Saher et al., 2009; Lopes dos Santos et al., 2010; Fallet et al., 2011; Huguet et al., 2011). Moreover, organic proxies can be strongly affected by current advection and subsequent lateral transport over long distances (Benthien and Müller, 2000; Sicre et al., 2005; Kim et al., 2009). In contrast, foraminifera are less affected by ocean current transport due to their relatively fast sinking speeds (Takahashi, 1984; Gyldenfeldt et al., 2000).

Comparison with modern SST data derived from NODC world ocean atlas database nearby the CD154 10-06P core location (Locarnini et al., 2010), (Fig. 5. 1) indicate austral summer SSTs of ~25 °C in the area. These values closely resemble the temperature range recorded in the and TEX_{86} core tops (Fig. 5. 6). Indeed, the growth of alkenone-producing coccolithophorids peaks during the austral summer season (December–February) in the southwest Indian Ocean (Raj et al., 2010). Conversely, core top *G. ruber* Mg/Ca temperature estimates (~22°C) at the CD154 10-06P site more closely resemble the modern observed austral winter (July) temperature in the area (~21°C), (Fig. 5. 1b). However, considering that *G. ruber* calcifies within the mixed-layer, between 20-50 m (Mohtadi et al., 2009), and highest fluxes of this species are found during austral summer in the Mozambique Channel (Steinhardt, 2012), it is possible that the observed temperatures could reflect its habitat within the deeper water layer of 30-50 m (annual mean temperature at 50 m water depth is 22°C). These results strongly suggest that seasonal differences in production or habitat of the different species can indeed explain the observed SST offsets recorded between the organic and inorganic based palaeotemperature proxies.

The SST records derived from $TEX_{86,}$ and Mg/Ca ratios show warming of ~1.5°C in the Agulhas Current during HS 1 (Fig. 5. 6) whereas estimates based on are considerably more variable. This could be related to low unsaturated $C_{37:3}$ alkenone abundances in combination with high values of the measured material which can lead to noise in the temperature record (S. Schouten personal communication, 2014).

However, the warming trend during the course of HS 1, as displayed by all three proxies, is within the uncertainty of each of the methods and can potentially be attributed to the general warming trend over the last deglaciation in the Southern Hemisphere (Fig. 5. 6c). Moreover, the temperature increase continued throughout the B/A interstadial and reached values similar to the early Holocene range with the onset of the YD, which demonstrates that the warming trend was not exclusively related to the timing of the NHCS (Fig. 5. 6a-c). SSTs remained rather constant during the YD showing no significant excursions in either of the proxies.

Regardless, the timing and magnitude of SST changes observed in core CD154 10-06P do not correspond to the co-registered hydrological changes that are recorded in the core or the wider southeast African region during the last termination (Schefuß et al., 2011), (Fig. 5. 6). This strongly suggest that while the generally warm surface waters of the Agulhas Current may have been important as a source of moisture, hydrological changes in the KZN and Eastern Cape province over the deglaciation were not primarily driven by the regional Agulhas Current SST dynamics. This is consistent with the recent evidence from the Zambezi River mouth that also suggest that southwest Indian Ocean SSTs changes did not drive hydrological changes over the Zambezi catchment during HS 1 and YD (Schefuß et al., 2011). However, the data shown and discussed in Chapter 3 and 4 indicate that the Agulhas Current surface temperatures were increased during older HSs 2-6, in both of the here studied cores (CD154 17-17K, Chapter 3 and 10-06P, Chapter 4) consistent with a bipolar thermal seesaw response to reduced AMOC during NHCSs. This might suggest that the bipolar-warming was potentially less pronounced during TI but was generally a persistent feature in the Agulhas Current during the past 100 kyr.

5.3.3. Millennial-scale salinity changes in the Agulhas Current

River run-off is an important measure of the intensity of the continental hydrological cycle. Past variability in riverine freshwater input can influence/lower surface salinity in the adjacent ocean by the development of freshwater plumes, which can be potentially captured by salinity reconstructions based on proxies such as $\delta D_{alkenone}$ applied in marine sediments (Weldeab et al., 2007; Bahr et al., 2013; Leduc et al., 2013).

The $\delta D_{alkenone}$ values in core CD154 10-06P show negative excursions of about ~10-15 ‰ during the course of HS 1 and YD (Fig. 5. 7b). Several factors can cause shifts in the

$\delta D_{alkenone}$ values including: (1) regional salinity change; (2) decreasing δD of sea water (δD_{sw}) as an effect of decreasing global ice volume during the terminations (Rohling, 2000) (Rohling, 2000); (3) algal growth rate, and (4) haptophyte species composition (Schouten et al., 2006). A recent study from the Indian-Atlantic Ocean Gateway (IAOG) in the South Atlantic (Kasper et al., 2014) used $\delta D_{alkenone}$ to infer relative changes in SSS and demonstrated that regional changes in algal growth rate and haptophyte species composition did not affect the reliability of the $\delta D_{alkenone}$ SSS estimates during TI. Similar to Kasper et al. (2014) the effect of changes in global ice volume on the $\delta D_{alkenone}$ were estimated by using the global mean ocean $\delta^{18}O_{sw}$ record from Grant et al., (2012) assuming a glacial $\delta^{18}O-$ enrichment in sea-water of 0.008 ‰ per meter sea level lowering (Schrag et al., 2002). The equivalent changes in $\delta^{18}O_{sw}$ were calculated by applying a local Indian Ocean meteoric waterline (Srivastava et al., 2010):

$$\delta Dsw = 7.32 * \delta^{18}O_{sw} + 0.29 \quad \text{Equation (7)}$$

These estimates were subtracted from the $\delta D_{alkenone}$ record. Since the residual $\delta D_{alkenone}$ shifts cannot be explained by either ice volume, growth rate or species composition changes, it is suggested that the residual $\delta D_{alkenone}$ reflects the relative changes in the regional SSS at the CD154 10-06P site. Comparison between the CD154 10-06P data set and Kasper et al., (2014) shows that the ice volume corrected residual $\delta D_{alkenone}$ record similar relative changes in salinity within the IAOG and the Agulhas Current (CD154 10-06P site) over TI (Fig. 5. 7b). However, salinities in the IAOG are typically slightly higher compared to the estimates made for the CD154 10-06P site, but this is difficult to evaluate in detail due to the lower resolution of the Kasper et al. (2014) record.

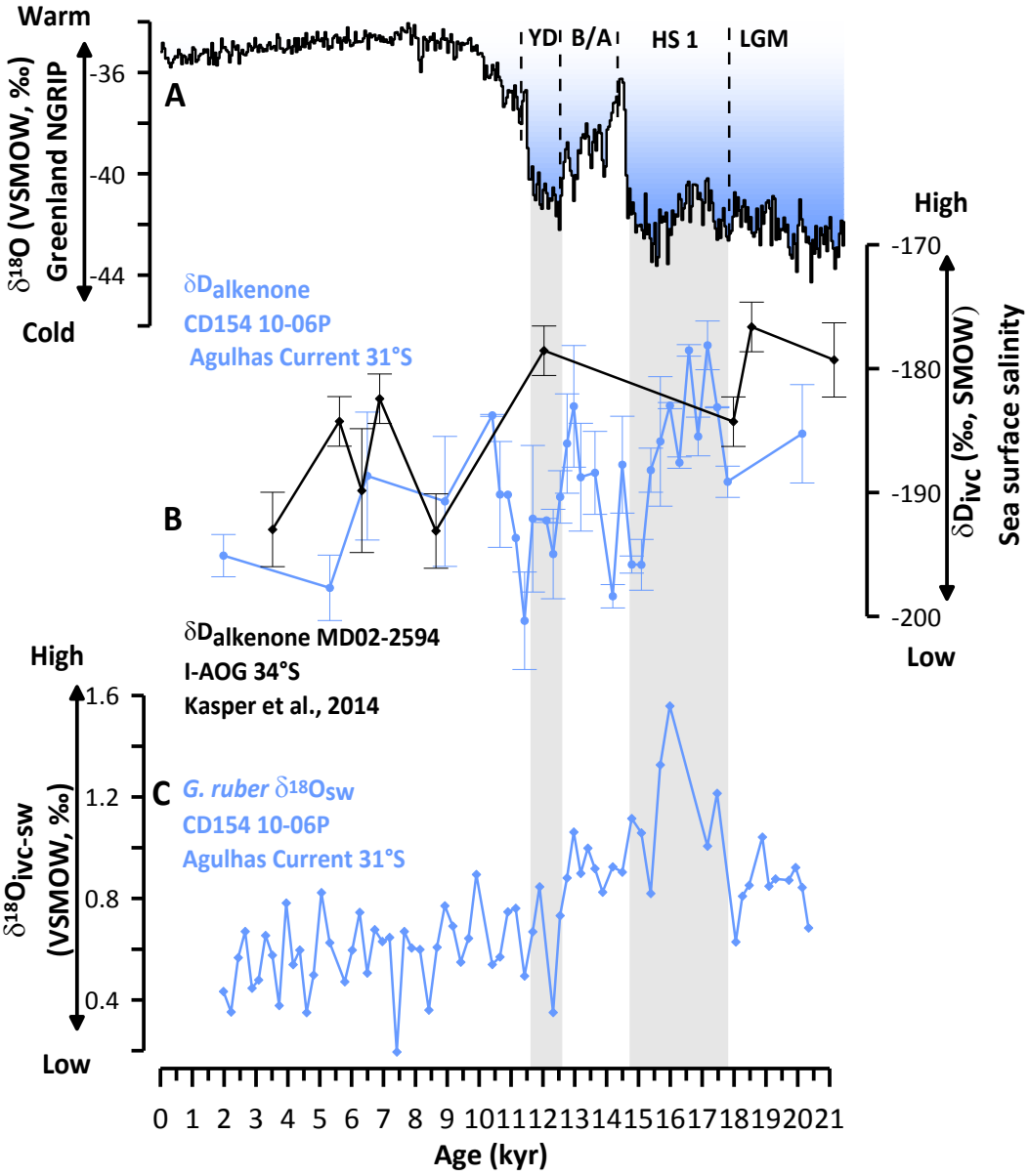

Fig. 5. 7 (a) $\delta^{18}O$ record from Greenland ice core NGRIP (NGRIP, 2004), (black, Speleo-age model presented in Barker et al., (2011)) displaying abrupt temperature variability in the North Atlantic. Underlying grey bars indicate Last Glacial Maximum (LGM), Heinrich Stadial 1 (HS1), Bølling-Allerød interstadial (B/A) and Younger Dryas (b) Hydrogen isotope composition of C37:2−3 alkenones (blue,) for core CD154 10-06P reflecting Sea Surface Salinity changes in the Agulhas Current and core MD02-2594 (black), Kasper et al., 2014. Error bars indicate standard deviations based on replicate analyses of each sample (c) Ice-volume corrected $\delta^{18}O_{SW}$ reconstruction ($\delta^{18}O_{ivc\text{-}sw}$) for core CD154 10-06P.

During almost the entire interval of HS 1 $\delta D_{alkenone}$ values ranging from ~-180 and -185‰ suggesting high saline conditions prevailed at the CD154 10-06P site (Fig. 5. 7a-b). $\delta D_{alkenone}$ values exhibit a negative shift reaching values of ~-195 ‰, indicating a freshening of surface waters, with the minimum in relative salinity occurring within the later stage of HS 1. Generally more positive $\delta D_{alkenone}$ values (higher salinity) are observed during the B/A. A substantial freshening trend is observed with the onset of the YD with $\delta D_{alkenone}$ values

shifting to more negative values that reach similarly low values as observed during the end of HS 1 (~-195 ‰).

The transition into the Holocene was associated with increasing salinities at the CD154 10-06P site. Variability in the $\delta^{18}O_{sw}$ record, derived from the same core material, is in good agreement with the $\delta D_{alkenone}$ record (Fig. 5. 7b-c). With the onset of HS 1 the $\delta^{18}O_{sw}$ values display an abrupt shift toward higher values, indicative of enhanced salinities, which remained high until the onset of the YD. Thereafter values decrease which also marks the overall shift from glacial (~0.8 ‰) to interglacial values (~0.2 ‰) in that record. Both proxies indicate elevated salinity in the Agulhas Current during HS 1.

Following the observations that Agulhas Current SSS are generally increasing during NHCS one might expect the same pattern to occur during the YD. However, the YD seems to mark the point when higher salinities during glacials and the termination are dropping to lower interglacial values. Analogous to the thermal bipolar seesaw (Stocker and Johnsen, 2003), Lohmann (2003), based on modelling results, suggested the presence of an additional quasi-bipolar salt–seesaw that reflects changes in the salt advection throughout the Southern Hemisphere supergyre in response to the interhemispheric seesaw. It is possible that the Agulhas Current hydrography was influenced by such a salt–seesaw mechanism causing the salinification of the upper layers. This would further imply that although local southeast African rivers might have had higher freshwater discharge during NHCS, their impact on surface ocean salinities was not strong enough to alter the high salinities of the Agulhas Current itself. As such millennial-scale salinity changes in the Agulhas Current seem to be predominantly driven by interhemispheric seesaw processes rather than local forcing.

5.3.4. Simulated millennial-scale climate variability in southeast Africa

In order to test the general assumption that Northern Hemisphere climate variability forces hydrological changes in southeast Africa (Schefuß et al., 2011; Ziegler et al., 2013b) an idealised North Atlantic freshwater perturbation experiment, analogous to the iceberg/meltwater discharge thought to be associated with a Heinrich Event (Heinrich, 1988), was performed (in collaboration with C. Purcell) using the COSMOS Earth System Model (Fig. 5. 8). Moreover, this numerical model study offers the opportunity to better

evaluate the mechanism driving the observed features in the multiproxy record of core CD154 10-06P.

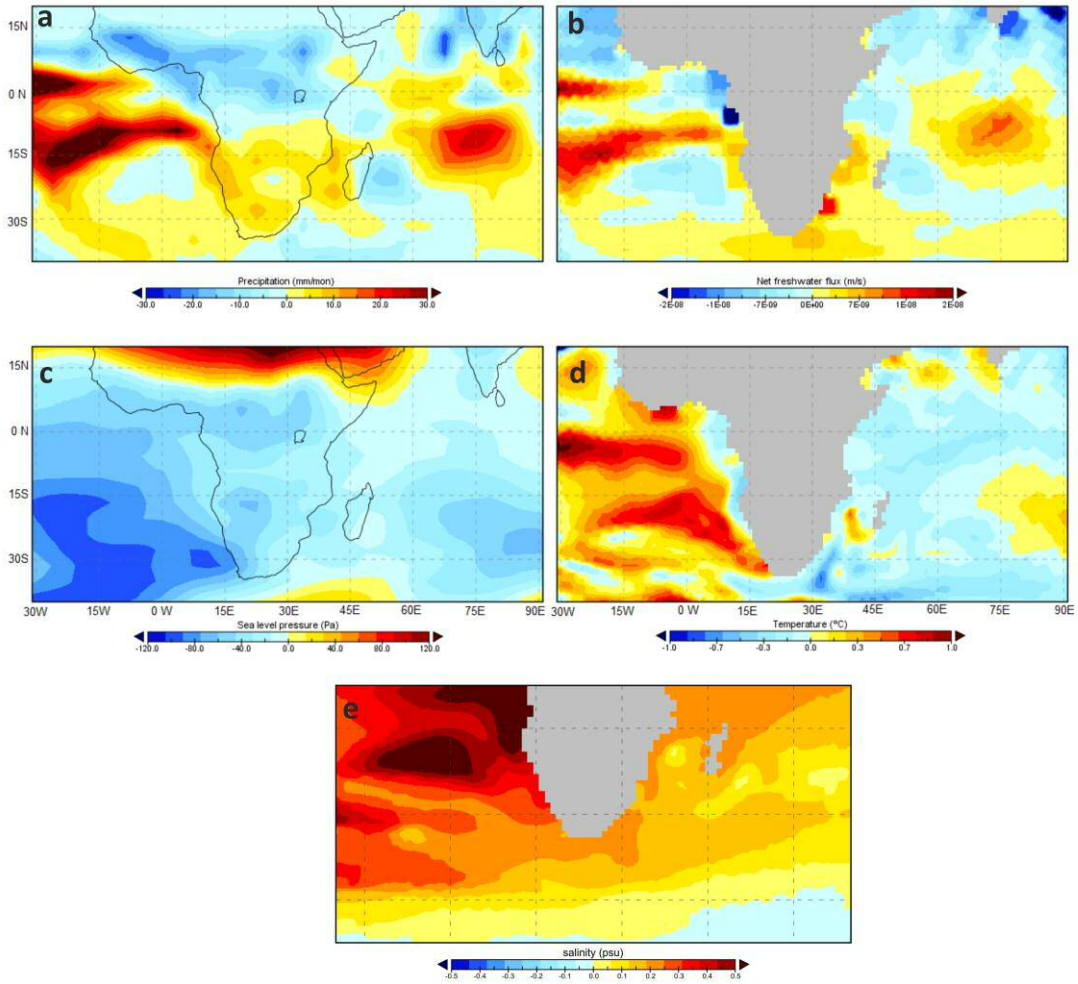

Fig. 5. 8 Modelled response to North Atlantic freshwater perturbation (a) Annual mean precipitation anomaly (in mm/mon) demonstrating the southward shift of the equatorial precipitation belts, including increases of precipitation in the range of 5-10 mm over the South-east African river catchment areas (b) Net freshwater flux at the ocean surface (in m/s), including the effects of precipitation, evaporation and river run-off. Evident are the anomalously fresh regions of increased river run-off along the south-east coast of Africa (c) Annual mean surface level pressure anomaly (in Pa) showing anomalously low surface level pressure over the entire southern part of the African continent, south-east Atlantic, and southwest Indian Ocean. Increased sea-level pressure is simulated over northern Africa. (d) Sea surface temperature anomaly (in °C) showing anomalously high temperatures occurring in the Atlantic sector of the Southern Hemisphere. A ~0.1 - 0.2°C temperature decrease is simulated in the region encompassing the Agulhas Current (e) Sea surface salinity anomaly (in psu). All anomalies are between the perturbed and background LGM climate states.

In response to a North Atlantic freshwater perturbation, the simulation shows a southward shift of the equatorial and near-equatorial precipitation belts associated with the ITCZ (Fig. 5. 8), in agreement with PMIP ensemble-model studies (Stouffer et al., 2006).

Precipitation in southeast Africa increases by ~10-15% compared to the LGM background state (Fig. 5. 8a). These finding are in agreement with previous modelling studies, which have suggested that South Africa experienced wetter conditions during NHCS due to remote atmospheric forcing (e.g., ITCZ shifts), (Thomas et al., 2009; Lewis et al., 2010).

As a result of the elevated rainfall over the continent higher river runoff into the southwest Indian Ocean is simulated and occurs along the southeast African continental margin with a maximum developing in the vicinity to the CD154 10-06P core site (Fig. 5. 8b). These results are in good agreement with the previously discussed proxy data in that the location of core CD154 10-06P is ideally situated to receive and trace terrestrial input by southeast African rivers.

Additionally, an anomalously low SLP system (Fig. 5. 8c) is simulated over the entire southern part of the African continent and Madagascar. Taken together these results suggest that a southern shift of the ITCZ occurs in association with a weakening of the Hadley cell in the southern tropics (Lee et al., 2011), implying that during NHCS remote forcing of the hydrological variability in southeast Africa primarily occurs through an atmospheric adjustment which leads to the development of humid conditions. These patterns are consistent with the interhemispheric teleconnections associated with the bipolar thermal seesaw (Broecker, 1998; Stocker and Johnsen, 2003). It is known that the ITCZ is sensitive to shifts in the cross-equatorial SST gradient (Moura and Shukla, 1981) and that changes in the position of this gradient can influence precipitation patterns in the low latitudes (Dong and Sutton, 2002). In the COSMOS model experiment shown here the equatorial and near-equatorial precipitation changes are mainly determined by a shift in the thermal equator, and the associated SLP changes.

In contrast to southeast Africa, dryer conditions associated with NHCS have been inferred from palaeoclimatological reconstructions in Lake Malawi (Johnson et al., 2002), Lake Tanganyika (Tierney et al., 2008) and the Sahel (Mulitza et al., 2008), reflecting the southward shift of the ITCZ during these periods. While large parts of sub-Saharan Africa faced severe dry conditions during NHCS (Stager et al., 2011), southeast Africa apparently experienced more humid conditions (Schefuß et al., 2011; Ziegler et al., 2013b). This contrast is also evident in the model results where large parts of North Africa show significant dryer conditions in comparison to the southern part of the continent (Fig. 5. 8a). Especially, the reduction in the Congo and Niger River runoff in Northwest Africa evident in

the model (Fig. 5. 8b) is a well-documented feature in palaeoclimatological studies from that area (Weijers et al., 2007a; Weldeab et al., 2007; Weldeab, 2012).

COSMOS modelling results also indicate cooling in the wider Agulhas Current region but increased precipitation at the same time (Fig. 5. 8d). This would imply that anomalously warm Agulhas Current temperatures were not required to cause increases in precipitation in southeast Africa on millennial-timescales. These findings are not consistent with the proxy based results of core CD154 10-06P as well as 17-17K as they generally indicate warming during NHCS. The slight (0.1 - 0.5 °C) SST cooling in the southwest Indian Ocean in the model during the freshwater experiments occurs in response to a weakening of the Subtropical Indian Ocean gyre (STIOG). The weakening of the STIOG results in a reduction of the volumetric transport in the Mozambique Channel and the Agulhas Current, thereby transferring less heat from the equatorial regions to the southwest Indian Ocean. This further strengthens that surface warming in the southwest Indian Ocean may have been important as a source of moisture, however hydrological changes in Mozambique (Schefuß et al., 2011), KZN and Eastern Cape province over the deglaciation were not primarily driven by the regional Agulhas Current SST dynamics.

Proxy based salinity reconstructions of core CD154 10-06P/CD154 17-17K and from the IAOG (Marino et al., 2013) are consistent with the SSS increases around South Africa as well as in the Agulhas Current core region simulated by the model during the hosing experiment (Fig. 5. 8). These idealised experiments suggest that the salt accumulation in the Agulhas system is most likely Atlantic sourced and occurs via salt advection throughout the Southern Hemisphere supergyre in response to the quasi-bipolar salt seesaw (Lohmann, 2003; Purcell et al., in review). This appears in response to the reduction of the AMOC (forced in the experiments by North Atlantic freshwater). The slowdown of the AMOC results in a reduced transport of salt across the equator in the Atlantic Ocean, and a recirculation throughout the South Atlantic Subtropical gyre (STG) system. This also results in a distribution of salt throughout the Southern Hemisphere supergyre and recirculation in the STIOG system, effectively acting to increase salinity in the greater Agulhas region.

Near the Limpopo River mouth the model simulates the highest river freshwater runoff into the southwest Indian Ocean (Fig. 5. 8b). Simultaneously this area is also the region were surface salinity increases less compared to other areas in the Agulhas Current during the hosing experiment (Fig. 5. 8e). This might imply that the increase in precipitation over

southeast Africa during NHCS might have impacted Agulhas Current salinities near big river mouths, such as the Limpopo, discharging high amounts of freshwater into the Agulhas waters during that time.

5.4. Summary and conclusions

Overall, this study suggests that:

1) There was an apparent Northern Hemisphere control on the subtropical southeast African climate during abrupt climate periods. This interhemispheric teleconnection involves the southward migration of the equatorial and near-equatorial precipitation belts associated with the ITCZ, a weakening of the Hadley cell in the southern tropics and changes in the SLP systems across the South African continent and Southern Ocean. These atmospheric circulation changes most likely influenced the local weather phenomena in that their constellation created favourable conditions for enhanced rainfall in southeast Africa.

2) Numerical modelling experiments are generally in good agreement with results derived from the marine sediment core CD154 10-06P offshore KZN province based on multiproxy reconstruction.

The results show that:

- core locations along the southeast African continental margin were sensitive to local river discharge and can be used to reconstruct past variations in the continental regime.

- land-ocean climate dynamics in southeast Africa underlay a variety of factors controlling sedimentation processes. The observed timing and features of the climatic changes recorded in this study are partly unexpected and highlight the complexity of the system and the strong impact of the Agulhas Current on outer shelf processes. Results confirm the initial assumption of Ziegler et al., (2013b) that changes in the southeast African climate occurred in phase with NHCS. However, sedimentation processes are more multifaceted than previously thought and independent age control is necessary to check for potential “phase shifts” within glacial terminations.

- in comparison to modern climate where on decadal timescales changes in the SST of the Agulhas Current exert a major impact on the rainfall in neighbouring South Africa this study suggest that temperature oscillations did not appear to have been the primary forcing of past millennial-scale hydrologic oscillations.

- local southeast African rivers might have had higher freshwater discharge during NHCS, as evident from the COSMOS model results, nonetheless their impact on surface ocean salinity was not strong enough to alter the high salinity of the Agulhas Current itself. Salinity changes in the Agulhas Current seem to have been dominantly determined by global circulation changes (e.g., bipolar seesaw phenomena) rather than local freshwater forcing.

6. A 270 kyr-long record of southeast African climate variability in the context of a global-palaeo-monsoon

6.1. Introduction

6.1.1. Global-Palaeo-Monsoon (GPM)

The term 'monsoon' arises from the Arabic word 'Mausim' which signifies season (Cheng et al., 2012). The monsoon system is known since ancient times as a seasonal reversal in the direction of near-surface wind and a seasonal alteration of dry versus humid climate driven by differential solar heating between sea and land (Wang, 2009). While the major regional monsoon systems in the tropics and subtropics on both sides of the Equator can be considered as local phenomena the connection among them led to the assumption that they are part of global-scale seasonal change in the atmospheric circulation- a Global Monsoon (GM), (e.g., Trenberth et al., 2000).

Persistent global-scale overturning of the atmosphere that varies according to the time of year constitutes the GM system. These changes are linked with seasonal reversal in surface winds and shifts in precipitation tied to the seasonal migration of the Intertropical Convergence Zone (ITCZ) and reversal in the northern and southern hemispheric heating and temperature gradients between continent and ocean in response to the annual solar cycle (e.g., Trenberth et al., 2000; Qian et al., 2002; Wang and Ding, 2006). As the ITCZ is a circum-global feature, the monsoon is therefore a global system which occurs in all continents except Antarctica. Based on modern precipitation patterns, a GM domain has been defined with 6 similar monsoon regions (three in each hemisphere): North American, South American, North African, South African, Asian and Australian-Indonesian (Fig. 6. 1), (Wang and and Ding 2008). The Asian Monsoon domain (ASMD) regime includes two interactive sub-components: the East Asian Summer Monsoon (EASM) and the Indian summer monsoon (ISM). The South American summer monsoon (SASM) is a large-scale atmospheric circulation system over most of the tropical and subtropical South American

continent and exhibits many similar features of its ASMD counterpart (Zhou and Lau, 1998). The North American Monsoon prevails mainly over the southwestern US and northwestern Mexico (Fig. 6. 1). The North African summer monsoon (NASM) and the South African monsoon system comprise the atmospheric circulation features over the entire African continent including the Eastern Mediterranean domain.

Since the monsoon arises from seasonal migrations of the ITCZ and this migration is predetermined by the earth's rotation around the sun and the tilt/orientation of its axis, the monsoon should be a perpetual feature existing throughout geological history (Wang, 2009). The Global-Palaeo-Monsoon (GPM) considers all regional high-resolution and absolute-dated palaeoclimate records from both sides of the Equator to enable past reconstructions of the global changes in atmospheric circulation in the tropics and subtropics (Fig. 6. 1), (Cheng et al., 2012). It has been argued that the GPM alters its intensity on different timescales i.e., tectonic- (10^6-10^8 years); orbital- (10^4-10^5 years) and millennial-scale (10^3-10^2 years) and that the extent is global with an anti-phased inter-hemispheric pattern (Cheng et al., 2012).

6.1.2. Long-term climate variability in (southeast) Africa

During the late Pleistocene, changes in the African climate were apparently paced by periodic variations in insolation resulting from the Earth´s orbital precession (23-19 ka) (Rossignol-Strick, 1983; Kutzbach and Street-Perrott, 1985; Ziegler et al., 2010). Stronger summer insolation over the South African continent intensifies atmospheric convection and leads to higher rainfall. Orbital precession changes lead to anti-phased summer insolation maxima between the hemispheres (Berger, 1978), resulting in opposing maxima in monsoonal intensities in North and South Africa, with the average position of the ITCZ migrating latitudinally (Gasse, 1977; Rossignol-Strick, 1983; deMenocal et al., 1993; Trauth et al., 2003). Most studies examining the evolution of the monsoon system over Africa during the late Pleistocene are based on NASM records from the Mediterranean (e.g., Rossignol-Strick, 1983). Ziegler et al. (2010) proposed that the NASM and EASM vary synchronously, in-line with the concept of a GM driven by the seasonal migration of the ITCZ (Fig. 6. 1), (Trenberth et al., 2000; Wang, 2009). By extrapolating this concept to the orbital-scale, Ziegler et al. (2010) suggested that the timing of sapropel deposition in the Eastern Mediterranean, an indicator of NASM intensity, coincided with the 3 kyr lag

observed in EASM speleothems. This implies a nonlinear response to insolation forcing together with weakening of the summer monsoon during Northern Hemisphere Cold Stadials (NHCS), (Cheng et al., 2009; Ziegler et al., 2010). The nature of orbital-scale climate change in southeast Africa is still not well constrained as currently only a few terrestrial and marine records extend back as far as ~350 kyr (Fig. 6. 1). The Pretoria Saltpan time series (now named the Tswaing Crater) from a 200 kyr-old Crater Lake in South Africa, shows that South African summer precipitation co-varied with changes in Southern Hemisphere summer insolation (Fig. 6. 1), (Partridge et al., 1997).

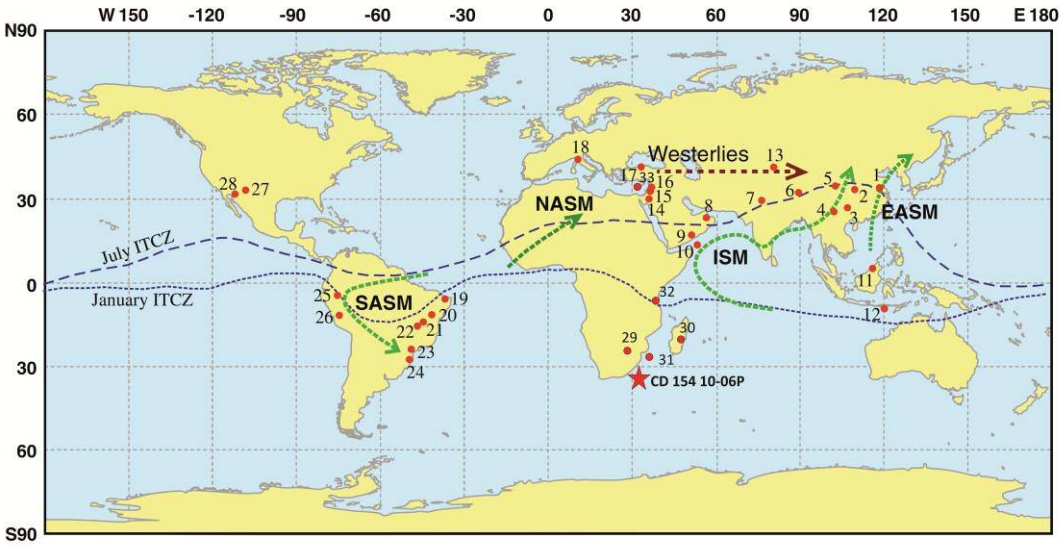

Fig. 6. 1 Map of cave locations modified after Cheng et al. (2012), (see references therein) and climate records of southeast Africa. Red dots (1-28) indicate cave sites, terrestrial (29;30;32) and marine (31;33; CD154 10-06P) records: 1-Hulu (32°30'N, 110°10'E), 2-Sanbao (31°40'N, 110°26'E), 3-Dongge (25°17'N, 108°50'E), 4-Xiaobailong (24°120'N, 103°21'E), 5-Wanxiang (33°19'N, 105°00'E), 6-Tianmen (30°55'N, 90°40'E), 7-Timta (29°50'N, 80°20'E), 8-Hoti (23°50'N, 57°21'E), 9-Qunf (17°10'N, 54°18'E), 10-Moomi (12°30'N, 54°E), 11-Borneo (4°N, 114°E), 12-Liang Luar (8°32'S, 120°26'E), 13-Kesang Cave (42°52'N, 81°45'E), 14-Caves in southern Israel, 15-Soreq Cave (31.45°N, 35.03°E), 16-Peqiin Cave (32.58°N, 35.19°E), 17-Sofular (41°25'N, 31°56'E,), 18-Corchia (44°2'N, 10°17'E), 19-Rio Grande do Norte (5°36'S, 37°44'W), 20-Paixa˜o (12°39'S, 41°30'W), 21-Padre (13°13'S, 44°30'W), 22-Lapa Grande (14°25'S, 44°22'W), 23-Santana (24°32'S, 48°44'W), 24-Botuvera´ (27°13'S, 49°9'W), 25-Cueva del Tigre Perdido (5°56'S, 77°18'W), 26-Pacupahuain Cave (11°14'S, 75°49'W), 27-Fort Stanton Cave (33°18'N, 105°18'W), 28-Bells Cave (31°45'N, 110°45'W), 29-Pretoria Saltpan (25°50'S, 28°E), (Partridge et al., 1997), 30-Lake Tritrivakely, Madagascar (19°78'S, 46°S92'E), (Gasse and Van Campo, 2001), 31- MD96-2048 (26°10'S, 34°01'E), (Dupont et al., 2011), 32- Central Kenya Rift- Lake Naivasha (0°55'S 36°20'E), (Trauth et al., 2003),33-Eastern Mediterranean (ODP Site 968), (34°19.9'N, 32°45.0'E), (Ziegler et al., 2010), CD154 10-06P (31°S, 32° E), (this study). Arrows depict wind directions of the ISM, EASM, NASM, SASM and the Westerlies. Dashed lines show the modern position of the ITCZ in July and January, respectively.

A study based on pollen and diatom records in a 40 m sedimentary sequence from Lake Tritrivakely in the central highlands of Madagascar, provide evidence for climatic and environmental variability during the late Pleistocene and the Holocene (Fig. 6. 1), (Gasse

and Van Campo, 2001). The connection between warm Agulhas Current SSTs, increased rainfall and hinterland vegetation changes have been highlighted in a pollen-based reconstruction of vegetation, from a marine sediment core located ~120 km south of the Limpopo River mouth over the past 350 kyr (Fig. 6. 1), (Dupont et al., 2011). However, our knowledge of the large-scale hydrological changes in southernmost East Africa and its forcing remains limited due to the scarcity of continuous high-resolution records representing integrated signals of millennial- and orbital-scale regional climate variability from this area.

The purpose of this chapter is to extend the existing record of southeast African climate variability discussed in Chapter 5 further back in time. This will be based on the XRF-scanning derived Fe/K record of core CD154 10-06P offshore KwaZulu-Natal (KZN) Province over the past 270 kyr. By comparing this new time series with published reconstruction of the EASM, the synchronicity of past changes in these two components of the global monsoon will be assessed and the persistence of this anti-phased teleconnection will be explored. By doing so, the intention is to test the proposed concept of GPM on orbital timescales as well as rapid climate change over the past 270 kyr. Moreover, building upon the findings of Chapter 5 an attempt is made to evaluate the role of Agulhas Current's SST changes in influencing the long-term precipitation pattern on the southeast African continent.

6.2. Results and Discussion

6.2.1. Chronologies for core CD154 10-06P

In order to evaluate the orbital-scale climate variability in southeast Africa two different age model approaches for core CD154 10-06P will be presented here, one based on the tuning of the benthic δ^{18}O record of the core to the benthic global LR04 stack of Lisiecki and Raymo (2005) and another one based on matching common excursions within the Fe/K ratios of core CD154 10-06P to the speleothem records from Chinese Caves, Hulu (Wang et al., 2001) and Sanbao (Wang et al., 2008; Cheng et al., 2009).

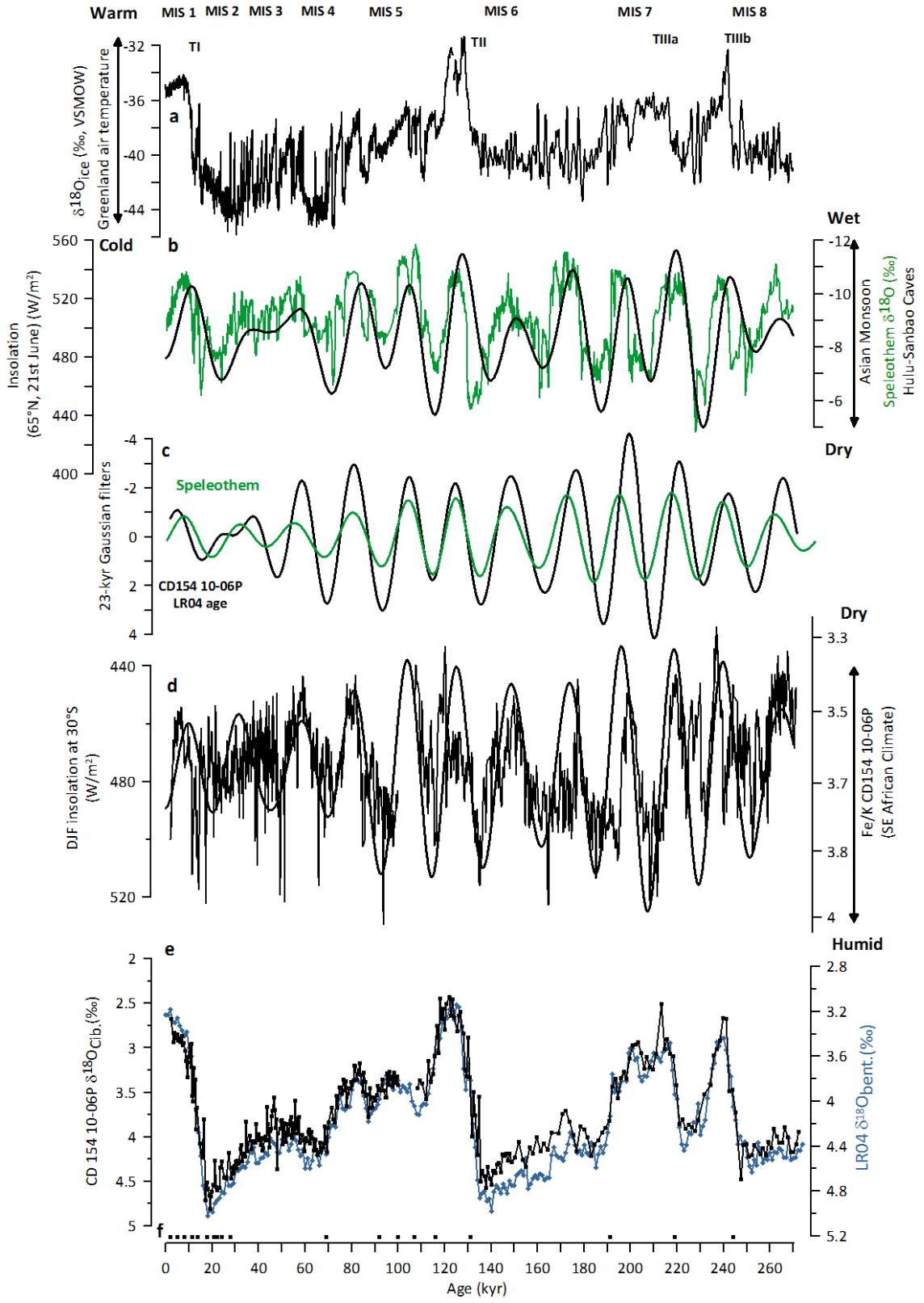

Fig. 6. 2 (a) $\delta^{18}O$ record from Greenland ice core NGRIP over the past 120 kyr displaying abrupt temperature variability in the North Atlantic (NGRIP, 2004), thereafter the synthetic record of Greenland climate variability was used (black, speleo-age model presented in Barker et al., (2011)) (b) $\delta^{18}O$ splice from Chinese speleothems (Wang et al., 2001; Wang et al., 2008; Cheng et al., 2009) as presented in Barker et al. (2011) showing synchronous variability of the EASM with Northern Hemisphere climate variability, Northern Hemisphere peak summer insolation record, 65 °N, 21st June (black) (c) 23-kyr

Gaussian filter of Chinese speleothem record (green) and Fe/K of CD 154 10-06P (black) (d) Fe/K ratios of CD 154 10-06P (5 point running mean) displayed with austral summer insolation at 30 °S (DJF) on top (black), (Laskar et al., 2004) (e) Benthic isotope record of CD154 10-06P (black) in comparison with benthic isotope stack LR04 (blue), (Lisiecki and Raymo, 2005) (f) Radiocarbon dates in the upper part of the record and tuning points based on LR04 comparison.

The former will allow to independently evaluate the timing of the long-term hydrological changes in the KZN province with respect to changes in the EASM as it is not subject to correlation imposed by the tuning method (as Ziegler et al., 2013b).

6.2.2. LR04 chronology

The LR04-based age model for core CD154 10-06P has been presented in Chapter 2, section 2.8.2 and Chapter 4. The LR04 stratigraphy, based on nine control points (Table 2.1) grants age control over the entire depth of the core, on orbital-scale, especially at times of prominent $\delta^{18}O$ shifts, like glacial terminations (Fig. 6. 2e). The resulting pattern emerging on the basis of this age model shows orbital-scale oscillations over the past 270 kyr of high Fe/K ratios indicating more humid conditions and low values pointing towards drier conditions in southeast Africa (Fig. 6. 2e). The Fe/K record of CD154-10-06P reveals highest spectral power in the 23-kyr band of precession (confidence level (CL) 99%), a), which is present throughout the past 270 kyr, however not consistently with the same power through time (Fig. 6. 3b). Periodicities centred around 23-kyr were found to stand out over the background noise with significant power (>75%) at above 90% CL but are limited to 150-240 ka as well as briefly between 90-70 ka (Fig. 6. 3b). This indicates that orbital timescale variations in the Fe/K records of CD154 10-06P can be linked to changes in Southern Hemispheres summer insolation (21st December till 21st of February, DJF) over South Africa (30°S), (Fig. 6. 2d) and reflect the 23-kyr periodicity of orbital precession which dominates local summer insolation changes at low latitudes (Fig. 6. 2c, Fig. 6. 3a), (Laskar et al., 2004). This assumption is confirmed when performing cross spectral analysis between the Fe/K record and the austral summer insolation (DJF) at 30 °S which shows an average in-phase relation (2.3 ° (± 17°). The long-term pattern in Fe/K data of core CD154 10-06P shows high similarity with the $\delta^{18}O$ in speleothems from Chinese Caves (Fig. 6. 2b) (Wang et al., 2008), however when compared directly the correlation between records is low (Pearson T= 0.142, CL 95% (0.07;0.34)). In general the EASM represents the composite effects of precipitation sources that vary with Northern Hemisphere summer insolation at 65 °N (Wang et al., 2008; Ziegler et al., 2010) apparently with a time lag (e.g., Clemens et

al., 2010; Cheng et al., 2012). It has been shown that the Chinese speleothem $\delta^{18}O$ record lags maximum Northern Hemisphere summer insolation (minimum precession) by ~2.9 ± 0.3 kyr at the precession cycle (Wang et al., 2008). While long-term changes to high Fe/K ratios in core CD154 10-06P indicate more humid conditions in southeast Africa simultaneous shifts towards high $\delta^{18}O$ values in the Chinese speleothems indicate less summer rainfall or monsoon weakening in the EASM regime. As expected, high spectral power in the 23-kyr band of precession (CL 99%) is also evident in the Chinese speleothems $\delta^{18}O$ records of the EASM (Fig. 6. 3a). Cross-spectral analysis between the two records shows significant coherence in the precession band (CL 95%), (Fig. 6. 3c) and reveals furthermore that the 23-kyr component of the CD154-10-06P Fe/K record on average leads the Chinese speleothem $\delta^{18}O$ records with a phase of 39 ° (± 22°) or ~2.5 kyr (Fig. 6. 3d). That is especially pronounced in the interval between 140-270 ka (Fig. 6. 2c) and is most likely related to the tuning approach employed in that interval which is based on only 3 age control points (Fig. 6. 2e). In summary, a LR04-based age model secures a solid stratigraphic framework for the CD154 10-06P Fe/K record however, a tuning directly to the speleothem record could be providing a more accurate and detailed chronology due to the higher fine-structure in the speleothem $\delta^{18}O$ record compared to the LR04 stack. Moreover, the findings presented in Chapter 5 support a direct tuning approach to the Chinese cave records.

6.2.3. Speleo-chronology

To establish a speleo-based age chronology for core CD154 10-06P beyond the range of the ^{14}C radiocarbon dates discussed in Chapter 5, common excursions within the Fe/K ratios have been used to match with the $\delta^{18}O$ speleothem record from Chinese Caves (Fig. 6. 4, Table 6. 1).

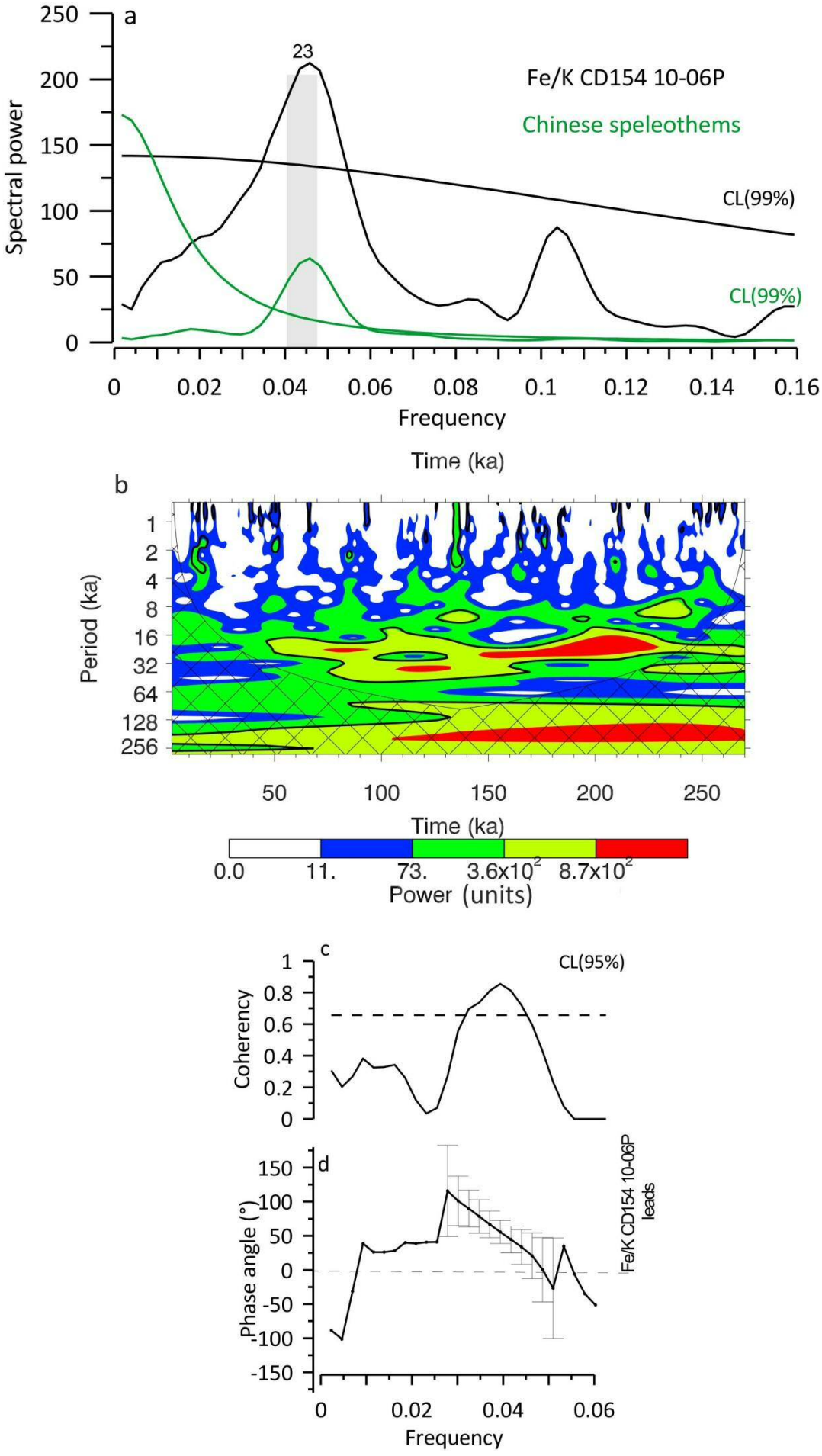
a
23
Fe/K CD154 10-06P
Chinese speleothems
CL(99%)
CL(99%)
Spectral power
Frequency
b
Time (ka)
Period (ka)
Time (ka)
Power (units)
c
CL(95%)
Coherency
d
Phase angle (°)
Fe/K CD154 10-06P leads
Frequency

Fig. 6. 3 (a) Power spectra calculated with the REDFIT-sofware (Schulz and Mudelsee, 2002) for Fe/K record of core CD154 10-06P (black) and Chinese speleothems $\delta^{18}O$ records (green), (red noise boundaries were estimated as upper 99% chi-squared limits of a fitted AR1 process. Bandwidth is 0.0186. Precession band (23-kyr) is highlighted (b) Wavelet analysis on the 150 year linear interpolated zero-padded Fe/K record from CD154 10-06P using Wavelet. White, blue, green, yellow and red colours denote power above red-noise of 0, 15, 25, 50 and 75% respectively. The black outline indicates confidence level of 90% assuming a red-noise model (c) Coherence levels from the cross-spectral analysis calculated with SPECTRUM software (Schulz and Stattegger, 1997) of the Fe/K record of core CD154 10-06P and Chinese speleothems $\delta^{18}O$ records. Strong coherence between records is found at the precession band (23-kyr) above 95% CL (d) Phase angle estimates between the two records showing the lead of the Fe/K record from CD154 10-06P at the precession band (23kyr).

Table 6. 1 Tuning points of Fe/k record of core CD154-10-06P to Chinese speleothem $\delta^{18}O$

Depth (cm)	Age (ka)
123	31
281	63
439	99.6
440	106
459	113
463	121
513.	129
518.	138.5
567.	152
631	178
675	192
702	199.5
736	211
761	227
776	229
807	239
818	246.5
847	249
911	266

The use of only 10 additional tuning points compared to the LR04 age model (9 in total), (Fig. 6. 4f) results in a good match between the Fe/K record and the Chinese speleothem record which improves the correlation between them, displayed by a Pearson T correlation coefficient of 0.35 with CL 95% (0.076; 0.55). The fine tuning leads to an in-phase relationship of both records in the 23-kyr precession band (Fig. 6. 4) which is confirmed by a significantly high Pearson T correlation coefficient of 0.87 with CL 95% (0.86; 0.88). Transferring the speleo-chronology of core CD 154 10-06P to the record of benthic $\delta^{18}O$ enables an evaluation of the discrepancies between a ^{230}Th-derived chronology and the LR04 isotopic stack which is widely used as tuning target for marine records.

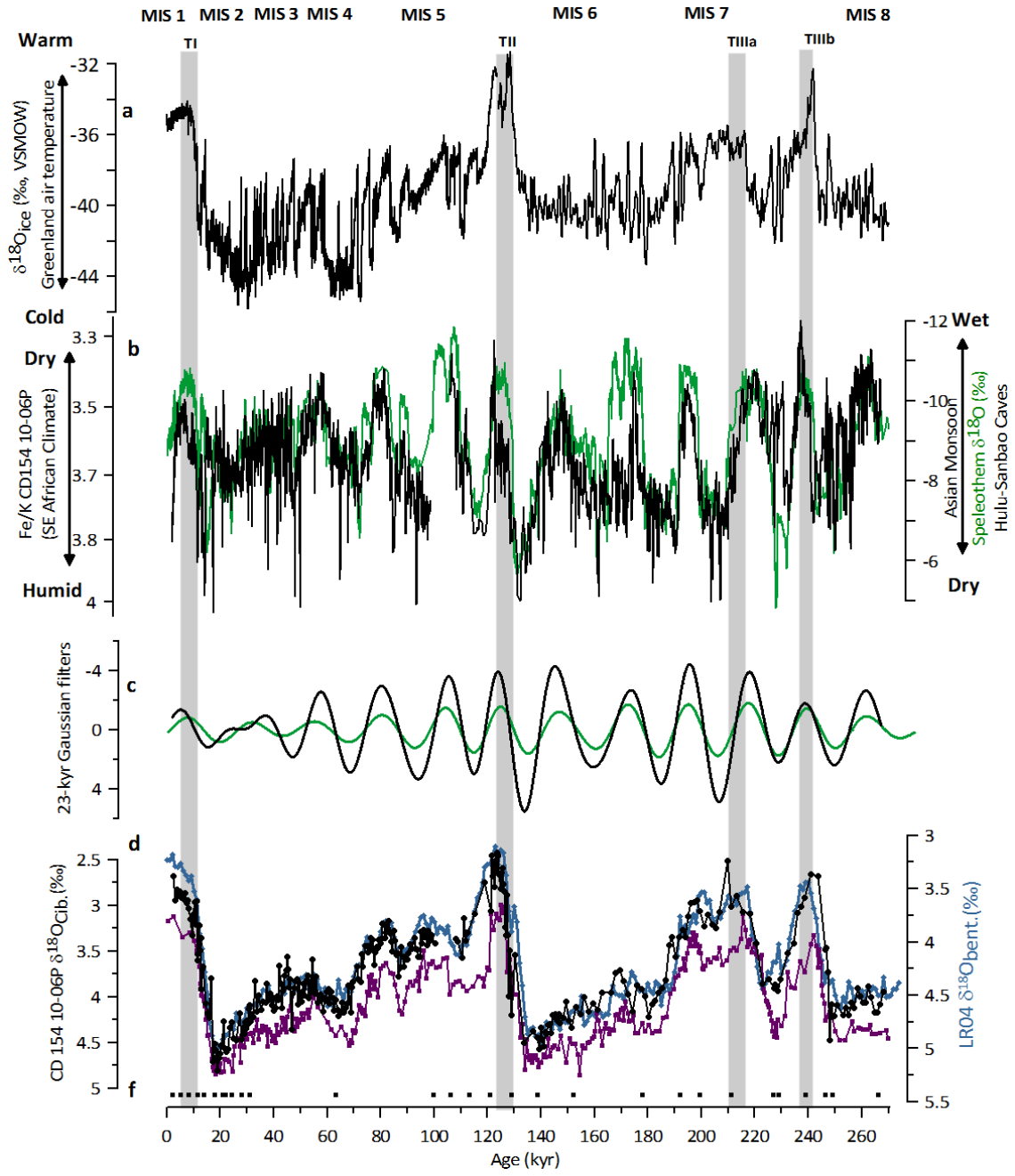

Fig. 6. 4 (a) $\delta^{18}O$ record from Greenland ice core NGRIP over the past 120 kyr displaying abrupt temperature variability in the North Atlantic (NGRIP, 2004), thereafter the synthetic record of Greenland climate variability was used (black, speleo-age model presented in Barker et al., (2011)). Grey bars indicate terminations (b) $\delta^{18}O$ splice from Chinese speleothems (green, Wang et al., 2001; Wang et al., 2008; Cheng et al., 2009) as presented in Barker et al. (2011) showing synchronous variability of the EASM with Northern Hemisphere climate variability and Fe/K ratios of CD 154 10-06P plotted on top (black, 5 point running mean) (c) 23-kyr Gaussian filter of Chinese speleothem record (green) and Fe/K of CD 154 10-06P (black) (d) Benthic isotope record of CD 154 10-06P (black) in comparison with benthic isotope stack LR04 (blue), (Lisiecki and Raymo, 2005) and benthic $\delta^{18}O$ record from the South China Sea (purple), also on a speleothem-derived chronology (Caballero-Gill et al., 2012) (f) Radiocarbon dates in the upper part of the record and tuning points based on speleothem derived age model for core CD154 10-06P.

The comparison shows that, despite the different tuning approach, a high level of synchronicity between the benthic $\delta^{18}O$ record of core CD154 10-06P and the LR04 record is achieved (Pearson T= 0.919; CL 95% (0.86; 0.95)). Recently, efforts have been made in order to derive a common chronological timeframe for marine isotope records and absolutely dated speleothems (Drysdale et al., 2009; Caballero-Gill et al., 2012) to tackle long-standing climatic questions, such as the timing of the climatic responses to Milanković parameters (Toggweiler and Lea, 2010; Berger, 2013). Caballero-Gill et al. (2012) recently endeavoured, with an approach based on temperature correspondence, to transfer the EASM chronology to marine benthic and planktonic records from the South China Sea.

A comparison of the here discussed benthic $\delta^{18}O$ record with their benthic curve reveals an overall good match with some notable timing disagreements in MIS 5d (Fig. 6. 4d). During this interval a better fit is achieved between the benthic $\delta^{18}O$ of CD154-10-06P and the LR04 stack compared to the South China Sea one (Fig. 6. 4d). In summary, using the speleo-chronology as outlined above results in a robust and more accurate age model for core CD154 10-06P as validated by the good agreement with the chronology derived from a marine isotopic stack (LR04).

6.2.4. Millennial-scale southeast African climate variability during the penultimate glacial-interglacial cycle

Chapter 5 highlighted that periods of more humid conditions in southernmost East Africa, resulting from higher palaeo-precipitation intensity, systematically corresponded to NHCS and to periods of weak EASM displaying an anti-phasing between monsoons (climate) in the two hemispheres most prominently over the last glacial cycle. To test if this pattern was a persistent feature also during the penultimate glacial-interglacial (G-I) cycle, the Fe/K record of core CD154 10-06P has been extended beyond the past 100 kyr to be evaluated for its millennial-scale variability during the entire stratigraphic range of the core spanning the past 270 kyr. With the aim to locate the timing of events when the EASM responded to NHCS the variability of the EASM record needs to be highlighted to this type of forcing, as opposed to the variability attributed to orbital forcing (Wang et al., 2008). For this, the insolation component of the EASM has been removed, i.e., 21 st of July at 65 °N, a procedure previously proposed by Barker et al. (2011). The same procedure has

been applied to the Fe/K record of core CD154 10-06P by subtracting the local austral summer insolation at 30 °S, as the southeast African records appear to be sensitive to Southern Hemispheres insolation at their specific latitude (Partridge et al., 1997; Trauth et al., 2003; Schefuß et al., 2011). For both the speleothem $\delta^{18}O$ and the insolation series, the mean value of the series was subtracted from each datum, and divided by the series' standard deviation. Then, the normalised values of insolation were subtracted from the coeval speleothem counterpart. This has been repeated for the Fe/K record of core CD154 10-06P.

By plotting the normalised Fe/K record of core CD154 10-06P on its speleothem-age model along with the normalised EASM speleothem record reveals that almost each abrupt weak EASM event between 100-270 ka can be matched with a humid interval in the southeast African record). It should be noted that although this age model is based on a speleo-tuning approach no fine-tuning on millennial timescales has been conducted. Heinrich Stadials, and shorter NHCS, testified by the ice rafted debris record of McManus et al. (1999), (Fig. 6. 5a) were shown to be strictly coupled with weak EASM conditions also during the penultimate G-I period (Wang et al., 2008; Barker et al., 2011). Especially evident are the marked more humid conditions in the KZN province evident in the normalised Fe/K record of core CD154 10-06P during each of the represented glacial terminations TIII b and TII (Fig. 6. 5d). These coincided with weak EASM intervals (Fig. 6. 5c). The current understanding is that during deglaciations, when large discharge of icebergs in the North Atlantic took place (McManus et al., 1999), freshwater induced reduction in North Atlantic open-ocean convection forcing the AMOC to weaken or even to collapse (McManus et al., 2004; Denton et al., 2010). Those changes were propagated to the tropical latitudes via rearrangements of atmospheric circulation (Toggweiler, 1999; Chiang and Bitz, 2005; Cheng et al., 2009). Both the Hadley cells and the ITCZ shifted southwards, and consequently, the distribution of rainfall over tropical latitudes was altered. Despite the recognition of these anti-phased intervals of continental climate variability in the EASM region and southeast Africa during the penultimate G-I cycle, other regions display similar pattern. This strengthens the assumption that these events had a global extent rather than a regional one alluding to the GPM concept on sub-orbital timescales. Speleothem records during TIII and TII suggest prevalent severe droughts in northern Borneo (Meckler et al., 2012) while Wang et al. (2004) identified increased rainfall over the Nordeste region of Brazil for TII and TI, when a more southern position of

the ITCZ carried Atlantic humidity more effectively over that region. NHCS dictated globally dry climate on the north side of the ITCZ and wetter conditions upon the southern side.

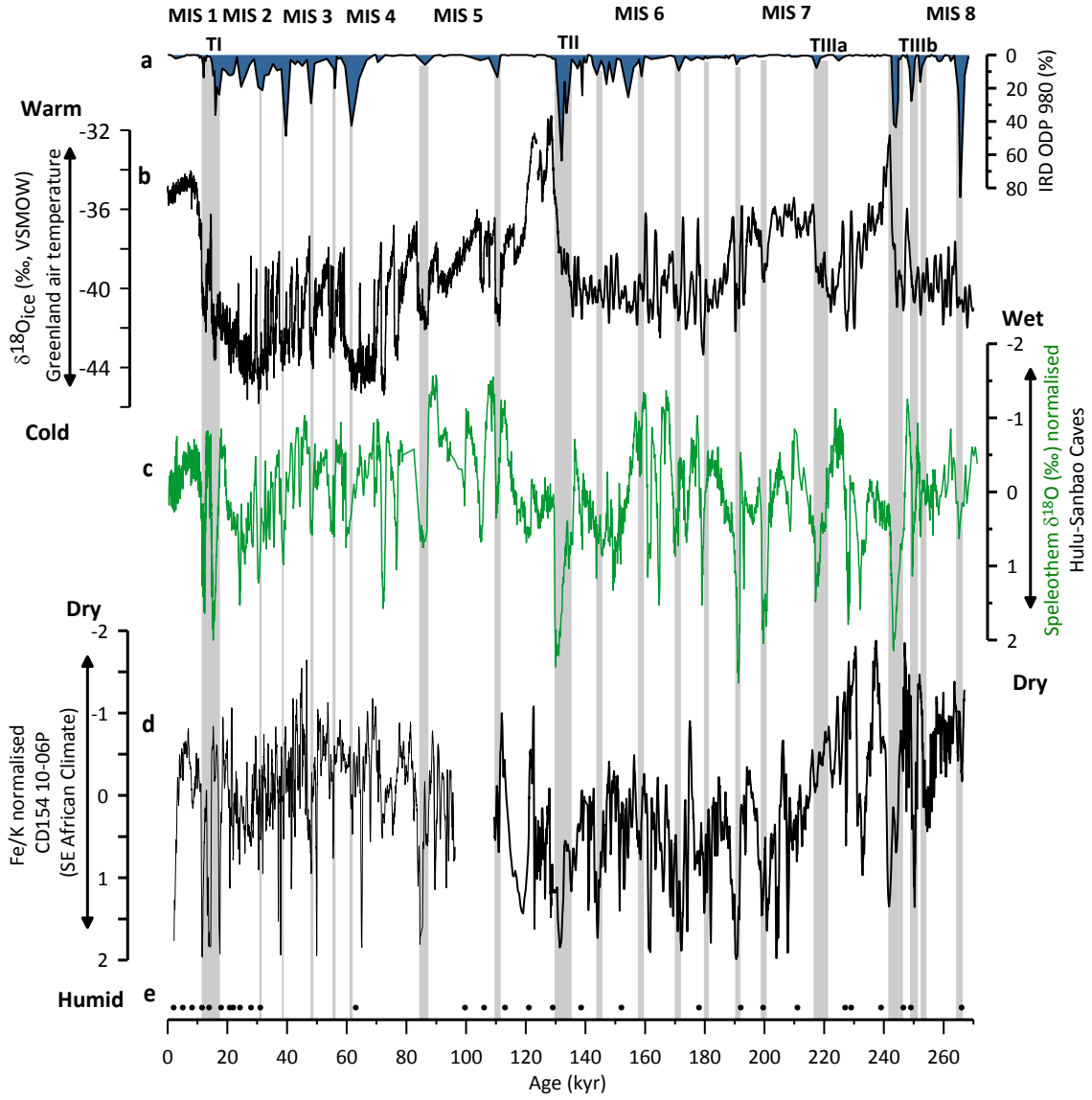

Fig. 6. 5 (a) Ice rafted debris record from North Atlantic core ODP 980 (McManus et al., 1999) (b)) $\delta^{18}O$ record from Greenland ice core NGRIP over the past 120 kyr displaying abrupt temperature variability in the North Atlantic (NGRIP, 2004), thereafter the synthetic record of Greenland climate variability was used (black, speleo-age model presented in Barker et al., (2011)) (c) Normalised $\delta^{18}O$ splice from Chinese speleothems (green, Wang et al., 2001; Wang et al., 2008; Cheng et al., 2009) as presented in Barker et al. (2011) showing synchronous variability of the EASM with Northern Hemisphere climate variability. Wide grey bars indicate terminations thinner bars synchronicity between North Atlantic IRD events, weak EASM intervals and humid phases in southeast Africa (d) Normalised Fe/K record of CD154 10-06P (7 point running mean) (e) Radiocarbon dates in the upper part of the record and tuning points based on speleothem derived age model for core CD154 10-06P.

6.2.5. Orbital-scale southeast African climate variability: Interhemispheric connection of precipitation belt shifts during the past 270 kyr

The inferred continental precipitation series from core CD154 10-06P display a direct relationship to Southern Hemisphere summer insolation at 30 °S during the past 270 kyr (Fig. 6. 2d). Stronger summer insolation intensifies atmospheric convection over the southeast African continent and due to enhanced land-sea thermal contrast which leads to higher rainfall. During the summer most of the moisture is brought by the easterlies, when a low pressure cell prevails over South Africa. Climate modelling studies support such a link between precession forcing and long-term changes in monsoonal climates (Kutzbach, 1981; Kutzbach et al., 2008; Ziegler et al., 2010). Earth's orbital precession affects the seasonal distribution of solar radiation resulting in precessional increase in northern tropical-subtropical summer insolation which is balanced by decreases in southern tropical-subtropical summer insolation and vice versa. The seesaw oscillations in solar radiation, alternating between tropics-subtropics of two hemispheres, results in an anti-phased relationship between monsoonal records in both sides of the globe, because the insolation forcing intensifies summer monsoon intensity.

Previous studies from South and East Africa have investigated the connection between precession induced insolation changes and climate variability and have equally noted an interhemispheric anti-phased relationship. South African rainfall variations reconstructed from the Pretoria Saltpan sedimentary record, South Africa (25°S), (Fig. 6. 1), (Partridge et al., 1997) have shown to closely track southern summer insolation changes, during the last 200 kyr. Changes in the NASM regime, as evident from fossil faunal assemblage variations in deep-sea sediment core RC24-07 (20 °N), (McIntyre et al., 1989), track northern tropical-subtropical summer insolation changes on orbital timescales and thus are opposed to the oscillations in South Africa. Lake level fluctuations of the equatorial Lake Niavasha in the Central Kenya Rift also demonstrate that periods of increased humidity in East Africa mainly follow maximum equatorial insolation during the past 175 kyr (Trauth et al., 2003). Records from Lake Tritrivakely, Madagaskar (Fig. 6. 1) (Gasse and Van Campo, 2001), also suggest a strong coupling between climate and Southern Hemisphere summer insolation and are out of phase with NASM indices (Street and Grove, 1979; Rossignol-Strick, 1983).

A direct comparison between the CD154 10-06P record, on the speleothem-tuned chronology, and the untuned Pretoria Saltpan time series of summer precipitation (Fig. 6. 6d,e), (Partridge et al., 1997) shows good correspondence between the two records with wet phases during high austral summer insolation (max precession) during the past 200 kyr (Fig. 6. 6b). This indicates that the southernmost East African region between (25 and 30 °S) was equally responding to local austral summer insolation changes but anti-phased with their Northern counterparts. High lake levels recorded in East Africa at around ~135 ka, ~110 ka and ~90 ka, which are also intervals of suggested increased humidity in the KZN province (regardless of the tuning approach) further strengthens the in-phase relationship among African regions in the vicinity or south of the ITCZ (Fig. 6. 1), (Trauth et al., 2003). The maximum highstands of Lake Naivasha at around ~135 ka correlate with highstands in other rift valley lakes (Hillaire-Marcel et al., 1986; Sturchio et al., 1993) as well as with more humid climate conditions in the KZN province which fall within NHCS Heinrich 11 (Fig. 6. 6d).

However, a southeast African vegetation reconstruction based on a pollen record from a marine core off the Limpopo River (Fig. 6. 1) does not reveal a precession paced pattern but rather display G-I fluctuations in the vegetation dynamics (Dupont et al., 2011). The terrestrial pollen assemblages indicate that during interglacials, the vegetation of eastern South Africa and southern Mozambique largely consisted of evergreen and deciduous forests whereas during glacials open mountainous scrubland vegetation was dominant (Dupont et al., 2011). The authors showed by comparing their record with SST estimates from the same core (Caley et al., 2011a) that the extension of the mountainous scrubland was apparently tightly coupled to the Agulhas Current system. The pattern was explained by the strong influence of western Indian Ocean surface temperatures on the summer precipitation in northern South Africa and southern Mozambique together with colder temperatures during glacial periods (Dupont et al., 2011). No SST record beyond 100 kyr exists in the core region of the Agulhas Current however the data of Caley et al. (2011a) located at the "precursor region" of the current (26 °S), (Fig. 6. 1) revealed a significant 41-kyr pattern in their SST record. That would imply that the southeast African climate variability recorded in the CD154 10-06P data offshore KZN province with a cyclicity of 23-kyr, was not immediately driven by variations in the Agulhas Current SSTs as those exhibited a different pacing (41-and 100-kyr cycles).

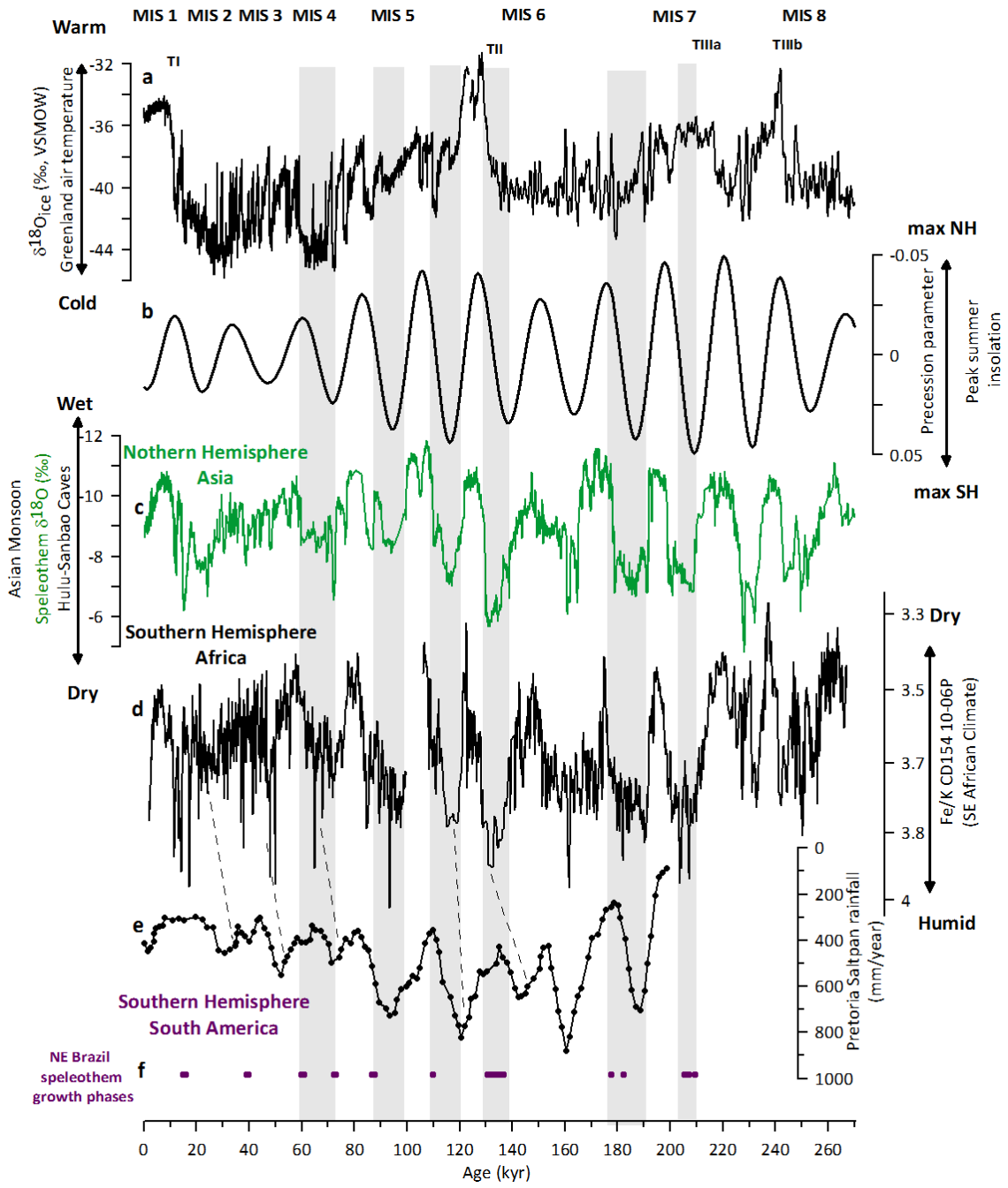

Fig. 6. 6 (a) $\delta^{18}O$ record from Greenland ice core NGRIP (NGRIP, 2004), (black, speleo-age model presented in Barker et al., (2011) displaying abrupt temperature variability in the North Atlantic (b) Orbital precession parameter (Laskar et al., 2004) (black) showing 23-kyr cycles and modulation by orbital eccentricity (100-kyr cycle). Precession maxima results in peaks in Southern Hemisphere summer insolation (c)) $\delta^{18}O$ splice from Chinese speleothems (green, Wang et al., 2001; Wang et al., 2008; Cheng et al., 2009) as presented in Barker et al. (2011) showing synchronous variability of the EASM with Northern Hemisphere climate variability (d) Fe/K ratios of CD 154 10-06P (black, 5 point running mean) (e) Pretoria Saltpan (untuned) time series of summer precipitation in South Africa 25 °S (Partridge et al., 1997) (f) Speleothem and travertine growth periods from the Nordeste caves, Brazil, South America (Wang et al., 2004).

A number of speleothem $\delta^{18}O$ records from tropical-subtropical South America have demonstrated that variations in the SASM track changes in Southern Hemisphere summer insolation on orbital timescale (Cruz et al. 2005, 2007; Wang et al. 2007a) and thus, exhibit an interhemispheric anti-phased relationship with ASMD records at precession bands (Fig. 6). Speleothem and travertine growth records from the Nordeste caves (Wang et al., 2004) indicate higher rainfall over the Nordeste region of Brazil simultaneously with increased humidity in southeast Africa during the past 210 kyr– a consistent pattern recurring every ~23-kyr paced by orbital precession (Fig. 6. 6d,f). The wet intervals displayed in records across South America (Wang et al., 2004; Cruz et al., 2005) and southeast Africa were times of dry conditions in the Northern Hemisphere as displayed by the NASM (Ziegler et al., 2010) and EASM records (Wang et al., 2008). In summary, the here presented comparison between regional and distal records confirms the GPM concept and suggests a coordinated response amongst regional monsoon systems, forced by the cycle of the differential hemispheric solar heating and associated ITCZ migration.

6.3. Conclusions

The Fe/K record of marine core CD154 10-06P from the southeast African continental margin presents a 270 kyr-long record of changes in the southeast African climate. This constitutes a unique and detailed time series of changes in the hydroclimate of the southernmost East African region, reflecting the intensity of summer precipitation. Moreover this sedimentary record offshore KZN province forms a new and important piece of information strengthening the concept of a GPM.

The intensity of the southeast African rainfall appears to have been sensitive to the forcing from NHCS, such as during Heinrich Stadials. Previous observations and model studies have indicated that cold Northern Hemisphere climate entails atmospheric circulation changes at tropical latitudes, with southern displacement of the ITCZ which seems to affect the ASMD and the South African climate systems. The extension of the CD154 10-06P Fe/K record beyond the past 100 kyr revealed that more humid intervals in southeast Africa corresponded to periods of weak EASM also during the penultimate G-I cycle. This synchronicity likely holds for sub-orbital Heinrich-type events, and appears most explicitly during cold Northern Hemisphere phases during deglaciations. It can therefore be

concluded that the EASM systems and the climate variability in southeast Africa were anti-phased during the last three glacial terminations, and the preceding glacials.

Periods of increased humidity in southernmost East Africa on orbital timescales were also likely linked to changes in peak summer insolation over southern Africa (30 °S) and reflect the 23-kyr periodicity of orbital precession which dominated local summer insolation changes at these latitudes confirming what was previously observed in shorter records from the nearby area (Partridge et al., 1997). Agulhas Current's SST changes did not seem to have influenced the long-term, precession paced, precipitation pattern on the southeast African continent. Instead, the southeast African hydrological balance varied synchronously with changes in the EASM regime during the late Pleistocene on orbital and sub-orbital timescales implying that the GPM was a persistent climatic feature of the last two G-I cycles.

7. Synthesis and Outlook

7.1. A Synthesis

This thesis provides reconstructions of palaeoclimate conditions at two locations in key points of the Agulhas Current within the broader Agulhas Current System. In this closing synthesis, the research questions formulated in the introductory, which overall motivated the studies contained in Chapter 3,4,5 and 6 will be re-examined. Based on the results an overview of the contribution of the presented work towards the better understanding of the Agulhas Current System will be provided.

7.1.1. Outcome of the studies on southwest Indian Ocean palaeocenography

Chapter 1 explained why the Agulhas Current system has emerged in the literature as a very important and influential area within the global climate system. **Chapter 2** provided a general overview as well as analytical details over all methods employed in this study.

In **Chapter 3** these questions were addressed: ***Did upstream Agulhas Current variability reflect inferred changes in Agulhas leakage and what did drive these variations?***

The findings of this work highlight three main **conclusions**:

- Interpretations of Agulhas leakage strengthening or weakening, as previously inferred from SST, ALF and $\delta^{18}O_{sw}$ variability observed in records from the IAOG (Peeters et al., 2004; Caley et al., 2012; Marino et al., 2013), may be a result of water mass property changes of the Agulhas Current.

- This would further imply that the actual amount of Agulhas leakage (volume transport) may have stayed the same, and rather its "signature" changed due to upstream modifications.

- Dynamics (e.g., strength of the Southern Hemisphere westerlies) impacting on Agulhas Current source waters exert major controls on the Agulhas leakage rather than migrations of the Subtropical Front as previously postulated (Bard and Rickaby, 2009; Zahn, 2009).

The study presented in **Chapter 4** focused on ***deep water inventory changes in the southwest Indian Ocean, their forcing and connection with the surface water variability***

of the Agulhas Current during the past 270 kyr. Potentially, the most intriguing question was if co-evolving changes in the surface and deep waters unravel whether Agulhas leakage had an active or passive role during glacial terminations?

The findings of this chapter highlight three **main conclusions**:

- The benthic stable isotope record from the southwest Indian Ocean indicates a persistent contribution of well-ventilated and nutrient-depleted ($\delta^{13}C$-enriched) NADW during interglacials/interstadial and a reduction during glacials/stadials. These variations might be linked to enhanced export of Southern Component Waters originating from the Southern Ocean and penetrating into the southwest Indian Ocean potentially substituted NADW during glacial conditions as its formation was potentially reduced in the North Atlantic open-ocean convection sites.

- During glacial terminations and NHCS, the NADW proportion steadily increased in the southwest Indian Ocean indicating a recovering ventilation of the area with Northern Component waters in the transition into interglacial/interstadial conditions.

- This, in conjunction with the surface records might potentially suggests an impact of Agulhas leakage on AMOC stability but need further investigations to exactly determine lead and lags between Agulhas leakage strengthening and NADW recovery in the Indian –Atlantic Ocean Gateway.

Taken the results of **Chapter 3** and **4** together, a couple of considerations arise which might challenge the current view on Agulhas leakage and its role during terminations:

The proposed maxima in Agulhas leakage at glacial terminations inferred from the ALF (Peeters et al., 2004) and *Globorotalia menardii* records (Caley et al., 2012) may have rather occurred as a consequence of increased local planktonic growth rate associated with global deglacial warming as species abundance and distribution in the world oceans is generally strongly related to SST (Kucera, 2007). Furthermore, counts of non-ALF planktonic foraminifera in the region also increase during deglaciations suggesting that warm water species abundance in the region behave similarly to the ALF, increasing upon terminations (Martínez-Méndez, G., personal communication, Barker et al., 2009). This might suggest that these species respond to a general deglacial Southern Hemisphere warming (EPICA, 2004) and may not be related to Agulhas leakage at all. In fact, new results from a fully coupled Earth system model (COSMOS) simulates decreased LGM SSTs

and an equatorward shift of the STF, in agreement with proxy data throughout the Agulhas region, however a significantly weak LGM Agulhas leakage water transport is not simulated (Purcell et al., in prep.). Similar preindustrial (~18 Sv) and LGM (~15 Sv) rates of Agulhas leakage water transport are at odds with the theory of decreased Agulhas leakage at the LGM as inferred from proxy data (Peeters et al., 2004; Caley et al., 2014).

The suggested Agulhas (salt)-leakage increase during terminations (Peeters et al., 2004; Marino et al., 2013) might be amplified through deglacial Heinrich Stadials which occurred at each termination (Barker et al., 2011). The Agulhas Current itself as well as the leakage area might simply respond with SST, ALF abundance and $\delta^{18}O_{sw}$ (salinity) increases to the bipolar thermal/salt seesaw mechanism (Lohmann, 2003; Stocker and Johnsen, 2003). This would imply that what has been interpreted previously as a change in Agulhas leakage (volume) might represent a passive responds of the broader Agulhas Current system to changes occurring during glacial terminations.

Moreover, a recent study by Broecker and Pena (2014) showed that the planktonic foraminifera *Globorotalia menardii*, often used as a proxy for Agulhas leakage transport, did not reappear in the Atlantic Ocean until ~7 ka, later than the AMOC transition to interglacial Holocene conditions had occurred (McManus et al., 2004; Gherardi et al., 2005; Negre et al., 2010). This could suggest that the proposed peaks of Agulhas leakage during glacial transitions may be unrelated to the hypothesised deglacial reinvigoration of the AMOC. Another set of sensitivity experiments employed with the COSMOS model investigating changes of Agulhas leakage and Drake Passage throughflow during freshwater induced AMOC mode shifts, reveals insignificant transport changes at the Agulhas leakage corridor during AMOC shifts on pre-industrial and Last Glacial Maximum background climate states (Purcell et al., in review). In contrast, a reduction of glacial sea ice cover in response to the thermal bipolar seesaw acts to modulate the wind forcing on the ocean surface, resulting in a ~35 % increased Drake Passage salt transport. This transport increase develops during the weak AMOC mode, and upon resumption of the AMOC to interstadial/interglacial conditions may have had a larger potential in acting as a positive feedback than the Agulhas leakage (Purcell et al., in review).

In summary, Agulhas leakage can be seen as one important component of the climate system with a relevant role during glacial terminations but not as a key player. Other factors (such as the right insolation forcing (Hays et al., 1976), supercritical size of

continental ice sheets as a possible precondition (Raymo, 1997) and ice albedo feedbacks (Clark et al., 1999), the CO_2 rise associated with an oscillation of the bipolar seesaw (Wolff et al., 2006; Barker et al., 2009; Cheng et al., 2009) in combination with the contribution of Agulhas leakage and the interplay of all these factors could provide the necessary additional forcing to promote deglaciation.

7.1.2. Outcome of the studies on southeast African climate variability

From previous studies it is known that the southeast African hydrological variability responded to two types of forcing: 1) high latitude Northern Hemisphere cooling and 2) low latitude insolation changes. Further, anti-phasing of the monsoon system of the Northern and Southern Hemispheres has been hypothesized, mediated by climatic forcing exerted by high-latitude Northern Hemisphere cooling. **Chapter 5** and **6** aimed to respond to the following questions: ***How did southernmost East African climate vary on different timescales, did Agulhas Current upper ocean temperature variability play a leading role in these shifts and are these hydrological shifts part of a bigger global monsoon system?***

The findings of these chapters highlight three main **conclusions**:

- Marine sediment cores in close vicinity to the southeast African continental margin are sensitive to terrestrial input and can be used to trace past climate variability on land.

- During the past 270 kyr the southeast African climate variability reflected both the effect of regional isolation and, more prominent, that of forcing by high-latitude Northern Hemisphere cold phases. These climatic oscillations seem to be coupled, and anti-phased with the EASM during the late Pleistocene which points to the Pleistocene persistence of a global-palaeo-monsoon.

- Agulhas Current upper ocean temperature variability may have been important as a source of moisture; however the observed hydrological changes in southeast Africa on orbital as well as sub-orbital timescales were not primarily driven by the regional Agulhas Current SST dynamics.

The observed oscillations in the southeast African hydrological balance over the late Pleistocene period may have had wider implications. Climate change and its effects on African ecosystems may have played a key role in human evolution (deMenocal, 2011).

Environmental hypotheses of African faunal evolution propose that major faunal speciation, extinction, and innovation events during the Pliocene-Pleistocene were mediated by changes in African climate or shifts in climate variability. The general assumption is that large-scale shifts in climate alter the ecological structure and resource availability of a given setting, which leads to selection pressures (Potts, 1998).

Comparing the history of hydrological changes in the Eastern Cape Province of South African with artifacts from the Middle Stone Age, a striking correspondence between the archaeological record of South Africa and the timing of the abrupt climate change as seen in a marine core has been discovered (Ziegler et al., 2013b). During the Middle Stone Age, humans developed the first symbolic art, like engraved pieces of red ochre and ostrich eggshell containers. Artifacts such as pierced shells, likely used for necklaces, and relatively complex stone and bone tools have also been dated within this time frame (Henshilwood et al., 2002; Jacobs et al., 2008). More humid conditions in southeast Africa all fell within periods of the archaeological evidence (Ziegler et al., 2013b). These findings are further supported by the new Fe/K record of core CD154 10-06P presented in this thesis (Chapter 5). Moreover, the longer stratigraphic range of that core might enable the correlation with dates from archaeological sites that are greater than the oldest samples from the CD154 17-17K record. For example the date of a 100,000-year-old ochre workshop at Blombos Cave has a relatively large uncertainty (Henshilwood et al., 2011) but appears to fall within a period of wet conditions in southeast Africa during the precession maximum of MIS 5b (Fig. 6.6b,d). Comparing the dates of occupational phases during the Later Stone Age with the Fe/k record again corroborates the overall relationship. Occupational phases of caves occurred at ~120 ka and ~165 ka again coincided with more humid conditions in South Africa as displayed by the Fe/k record from offshore KZN Province (Fig. 6.6b,d).

7.2. An outlook to future research

The studies presented in this thesis form the basis for potential future projects which might further improve our understanding of the Agulhas Current System.

7.2.1. Agulhas Current variability beyond the past 100 kyr

The reconstruction of surface water variability has been based on records of core CD154 17-17K and 10-06P however, these records only cover the past 100 kyr. The longer stratigraphic range of core CD154 10-06P offers the opportunity to extent the approach

applied in Chapter 3 over Termination II. An equivalent downstream record in the IAOG exists over that time interval (Marino et al., 2013) which could provide a new comparison between upstream and downstream dynamics. Moreover, Agulhas Current variability should be determined along the wider southeast African margin in order to proof that the findings presented here are a robust feature. Especially interesting are core location further to the North of 33 °S which should represent the Northern Agulhas Current, and locations further downstream near the western flank of the retroflection as part of the Southern Agulhas Current. It would be interesting to evaluate if these two parts of the current are displaying significant differences in their upper ocean hydrographic variability. In the modern system these two parts have distinctly different behaviours in terms of trajectory and volume flux (Lutjeharms, 2006). The Southern Agulhas is more vigorous, moreover it is determined by a higher volume flux, as it is fed by the recirculation off the Agulhas Return Current (Valentine et al., 1993). It has been shown in Chapter 3 that core locations situated at ~33 °S within the current are sensitive to the influence of the recirculation of the Return Current. Upper ocean dynamics in the Southern Agulhas Current area might be crucial in determining the final leakage signature as opposed to its Northern counterpart.

It has been shown that the marine sediments cores used in this study are sensitive to carbonate dissolution. Additional cores, recovered during RRS Charles Darwin Cruise 154 (Hall and Zahn, 2004) are available from a depth transect situated at ~29 °S from shallower depths between 1600 and 2600m. These cores sites would constitute an ideal case study to study the impact of carbonate dissolution on core material and provide potentially Mg/Ca-derived temperature estimates of the Northern Agulhas Current without any dissolution bias.

Moreover, the recently approved IODP 702 “Safari “ (Southern African Climates, Agulhas Warm Water Transports and Retroflection, and Interocean Exchanges) cruise targets a suite of drill sites on the southeast African margin and in the Indian-Atlantic ocean gateway going back as far as 5 Ma. This will enable to study the Agulhas Current variability under early Pliocene warm conditions, during the mid-Pliocene expansion of northern hemisphere ice sheets, and the Mid-Pleistocene Transition.

Shifting the focus away from the Agulhas Current system, the Warm Water Route (WWR), emphasis could be placed on a better understanding of the cold (Drake Passage) surface

water routes feeding the AMOC. The Cold Water Route (CWR) transports sub-Antarctic waters from the Pacific to the Atlantic Ocean via the Drake Passage, and has been presumed to be of secondary importance to the WWR, contributing just 25% of the latter's volume flux (Gordon, 1986). However, the recent model results mentioned above demonstrate that that might not be the case (Purcell et al., in review). Proxy based reconstruction of Drake Passage and CWR changes on millennial timescales is currently lacking. One potential future project could reconstruct the hydrographic variability from cores within the CWR which could be compared with their equivalent counterparts from the WWR to better understand the potential role of both areas on global climate change.

7.2.2. Reconstruction of deep water variability in the southwest Indian Ocean using radiogenic isotopes

Cores situated along the southeast African continental margin can be used to reconstruct deep-water variability in the southwest Indian Ocean which was linked to AMOC mode shifts (Chapter 4). The here presented record was the first to date from that area and is purely based on a benthic stable isotope record. Additional cores along the margin should be studied for their deep-water inventory changes especially over terminations in high-resolution; however additional proxies should be employed. Neodymium isotopes are an important proxy for reconstructing deep water sources and structure, because they vary between deep ocean water masses. The $^{143}Nd/^{144}Nd$ composition (usually given as εNd) of an authigenic marine phase should preserve the seawater composition from the past. Nd isotope analysis in the Fe-Mn oxide fraction of deep sea cores is advantageous because it is a direct proxy for changes in the water masses as compared to nutrient-based proxies such as benthic foraminiferal $\delta^{13}C$ and Cd/Ca. εNd values should not be affected by biological productivity, air–sea gas exchange or temperature (Goldstein and and Hemming, 2003).

7.2.3. (Southeast) African Climate and Human Evolution

It has been demonstrated in Chapter 5 and 6 that the marine cores along the southeast African margin are important archives preserving the history of the climate variability in South Africa. Linking the reconstructed climate shifts with archaeological evidence showed that these records constitute an important piece of information of the region and potentially contribute to one of the major questions of our species: Did climate change

shape human evolution? In this respect, the availability of additional cores along the southeast African margin should be used to backup and further develop the findings of this "trial" study. Further application of organic geochemical proxies which enable to reconstruct the terrestrial input from land in marine records should be applied more extensively and beyond the last deglaction (Chapter 5).

The provenance of terrigenous sediments can be identified using the radiogenic isotope compositions of strontium (Sr), Nd, Lead (Pb), hafnium (Hf), as well as their chemical compositions. Radiogenic isotopes in seawater reflect the balance of input from continental weathering against that from hydrothermal exchange at mid-ocean ridges (Frank, 2002). Prior studies have demonstrated the validity of using Sr-Nd isotopes ($^{87}Sr/^{86}Sr$ and εNd) of terrigenous detritus to infer their provenance and continental weathering states (Rhodes et al., 2002; Burton, 2006). Franzese et al. (2006) showed that sediment transported by the Agulhas Current has its own "fingerprint" with very high $^{87}Sr/^{86}Sr$ ratios derived from old continental terrains on the eastern coast of Africa. Climate-related changes in continental weathering can result in temporal changes in the composition of the sedimentary end-members (Franzese et al., 2009). Shifts between wet and dry climate regimes on the African continent could potentially change the provenance of sediment material derived from land and transported by the Agulhas Current downstream, which would be reflected by changes in the radiogenic isotope fingerprints. Core locations along the margin would be ideal to monitor the climate variability of the African terrain and the occurring wet-dry oscillations by measuring radiogenic isotopes in conjunction with organic geochemical tracers on bulk sediment material.

Hominin extinction, speciation, and behavioural events appear to be associated with changes in African climate in the past 5 million years (Trauth et al., 2005; deMenocal, 2011). One of the most famous examples would be the extinction of *Australopithecusafarensis* ("Lucy") near 2.9 Ma (Haviland et al., 2007). African climate changes during the past 5 million years bear the signatures of two separate processes: orbital precession forcing and a long-term trend toward increasing drier and more variable conditions is superimposed on these precessional wet-dry cycles, commencing after ~3 Ma and peaking near 1.8 to 1.6 Ma (deMenocal, 2004; Trauth et al., 2005; deMenocal, 2011). Most fossil discoveries are from East Africa: Ethiopia, Kenya, and Tanzania. East African Rift Valley Lake records severe as climate archives on those timescales to provide evidence of the East African climate variability (Trauth et al., 2005). The approved IODP 702 "Safari

"drill sites on the southeast African margin going back as far as 5 Ma would offer a unique opportunity to study climate variability and human evolution during the past 5 Myr in southernmost East Africa as no marine record exist from those areas documenting terrestrial climate change.

References

Adegbie, A.T., Schneider, R.R., Röhl, U., Wefer, G., 2003. Glacial millennial-scale fluctuations in central African precipitation recorded in terrigenous sediment supply and freshwater signals offshore Cameroon. Palaeogeography, Palaeoclimatology, Palaeoecology 197, 323-333.

Adkins, J.F., McIntyre, K., Schrag, D.P., 2002. The Salinity, Temperature, and $\delta^{18}O$ of the Glacial Deep Ocean. Science 298, 1769-1773.

Ahn, J., Brook, E.J., 2008. Atmospheric CO_2 and Climate on Millennial Time Scales During the Last Glacial Period. Science 322, 83-85.

Alley, R.B., Clark, P.U., 1999. The deglaciation of the Northern Hemisphere: A Global Perspective. Annual Review of Earth and Planetary Sciences 27, 149-182.

Alory, G., Wijffels, S., Meyers, G., 2007. Observed temperature trends in the Indian Ocean over 1960–1999 and associated mechanisms. Geophysical Research Letters 34, L02606.

Anand, P., Elderfield, H., Conte, M.H., 2003. Calibration of Mg/Ca thermometry in planktonic foraminifera from a sediment trap time series. Paleoceanography 18, 1050.

Anderson, R.F., Ali, S., Bradtmiller, L.I., Nielsen, S.H.H., Fleisher, M.Q., Anderson, B.E., Burckle, L.H., 2009. Wind-Driven Upwelling in the Southern Ocean and the Deglacial Rise in Atmospheric CO_2 Science 323, 1443-1448.

Anderson, R.F., Carr, M.-E., 2010. Uncorking the Southern Ocean's Vintage CO_2. Science 328, 1117-1118.

Arhan, M., Mercier, H., Park, Y.-H., 2003. On the deep water circulation of the eastern South Atlantic Ocean. Deep Sea Research Part I: Oceanographic Research Papers 50, 889-916.

Arz, H.W., Pätzold, J., Wefer, G., 1998. Correlated Millennial-Scale Changes in Surface Hydrography and Terrigenous Sediment Yield Inferred from Last-Glacial Marine Deposits off Northeastern Brazil. Quaternary Research 50, 157-166.

Asani, G.C., 2005. Tropical Meteorology. Praveen Printing Press, Pune.

Backeberg, B.C., Penven, P., Rouault, M., 2012. Impact of intensified Indian Ocean winds on mesoscale variability in the Agulhas system. Nature Clim. Change 2, 608–612.

Bahr, A., Schönfeld, J., Hoffmann, J., Voigt, S., Aurahs, R., Kucera, M., Flögel, S., Jentzen, A., Gerdes, A., 2013. Comparison of Ba/Ca and as freshwater proxies: A multi-species core-top study on planktonic foraminifera from the vicinity of the Orinoco River mouth. Earth and Planetary Science Letters 383, 45-57.

Bailey, G.W., Rogers, J., 1997. Chemical oceanography and marine geosciences off Southern Africa: past discoveries in the post-gilchrist era, and future prospects. Transactions of the Royal Society of South Africa 52, 51-79.

Bamber, J., van den Broeke, M., Ettema, J., Lenaerts, J., Rignot, E., 2012. Recent large increases in freshwater fluxes from Greenland into the North Atlantic. Geophysical Research Letters 39, L19501.

Bar-Matthews, M., Marean, C.W., Jacobs, Z., Karkanas, P., Fisher, E.C., Herries, A.I.R., Brown, K., Williams, H.M., Bernatchez, J., Ayalon, A., Nilssen, P.J., 2010. A high resolution and continuous isotopic speleothem record of paleoclimate and paleoenvironment from 90 to 53 ka from Pinnacle Point on the south coast of South Africa. Quaternary Science Reviews 29, 2131-2145.

Bard, E., 1988. Correction of accelerator mass spectrometry ^{14}C ages measured in planktonic foraminifera: Paleoceanographic implications. Paleoceanography 3, 635-645.

Bard, E., 2001. Comparison of alkenone estimates with other paleotemperature proxies. Geochemistry, Geophysics, Geosystems 2, 1002.

Bard, E., Rickaby, R.E.M., 2009. Migration of the subtropical front as a modulator of glacial climate. Nature 460, 380-383.

Bard, E., Rostek, F., Sonzogni, C., 1997. Interhemispheric synchrony of the last deglaciation inferred from alkenone palaeothermometry. Nature 385, 707-710.

Bard, E.M.A.a.D., J. C. , 1991. Reconciling the sealevel record of the last deglaciation with the $\delta^{18}O$ spectra from deep sea cores. Quat. Proc. 1, 67-73.

Barker, S., 2006. In Encyclopedia of Quaternary Science (ed. Elias, S. A.) Elsevier, 1711

Barker, S., Broecker, W., Clark, E., Hajdas, I., 2007. Radiocarbon age offsets of foraminifera resulting from differential dissolution and fragmentation within the sedimentary bioturbated zone. Paleoceanography 22, PA2205.

Barker, S., Cacho, I., Benway, H., Tachikawa, K., 2005. Planktonic foraminiferal Mg/Ca as a proxy for past oceanic temperatures: a methodological overview and data compilation for the Last Glacial Maximum. Quaternary Science Reviews 24, 821-834.

Barker, S., Diz, P., Vautravers, M.J., Pike, J., Knorr, G., Hall, I.R., Broecker, W.S., 2009. Interhemispheric Atlantic seesaw response during the last deglaciation. Nature 457, 1097-1102.

Barker, S., Elderfield, H., 2002. Foraminiferal Calcification Response to Glacial-Interglacial Changes in Atmospheric CO_2. Science 297, 833-836.

Barker, S., Greaves, M., Elderfield, H., 2003. A study of cleaning procedures used for foraminiferal Mg/Ca paleothermometry. Geochem. Geophys. Geosyst. 4, 8407.

Barker, S., Knorr, G., Edwards, R.L., Parrenin, F., Putnam, A.E., Skinner, L.C., Wolff, E., Ziegler, M., 2011. 800,000 Years of Abrupt Climate Variability. Science 334, 347-351.

Barker, S., Knorr, G., Vautravers, M.J., Diz, P., Skinner, L.C., 2010. Extreme deepening of the Atlantic overturning circulation during deglaciation. Nature Geosci 3, 567-571.

Bayon, G., German, C.R., Nesbitt, R.W., Bertrand, P., Schneider, R.R., 2003. Increased input of circumpolar deep water-borne detritus to the glacial SE Atlantic Ocean. Geochemistry, Geophysics, Geosystems 4, 1025.

Bé, A.W.H., and Tolderlund, D.S., 1971. Distribution and ecology of living planktonic foraminifera in surface waters of the Atlantic and Indian Oceans, in Funnel, B.M. and Riedel, W.R. (eds.). The Micropaleontology of Oceans, 105-149.

Beal, L.M., 2009. A Time Series of Agulhas Undercurrent Transport. Journal of Physical Oceanography 39, 2436-2450.

Beal, L.M., Bryden, H.L., 1997. Observations of an Agulhas Undercurrent. Deep Sea Research Part I: Oceanographic Research Papers 44, 1715-1724.

Beal, L.M., Bryden, H.L., 1999. The velocity and vorticity structure of the Agulhas Current at 32°S. J. Geophys. Res. 104, 5151-5176.

Beal, L.M., Chereskin, T.K., Lenn, Y.D., Elipot, S., 2006. The Sources and Mixing Characteristics of the Agulhas Current. Journal of Physical Oceanography 36, 2060-2074.

Beal, L.M., De Ruijter, W.P.M., Biastoch, A., Zahn, R., 2011. On the role of the Agulhas system in ocean circulation and climate. Nature 472, 429-436.

Begg, G.W., 1978. The Estuaries of Natal. Natal Town and Regional Planning Report 41.

Belkin, I.M., Gordon, A.L., 1996. Southern Ocean fronts from the Greenwich meridian to Tasmania. Journal of Geophysical Research: Oceans 101, 3675-3696.

Bender, M., Sowers, T., Brook, E., 1997. Gases in ice cores. Proceedings of the National Academy of Sciences of the United States of America 94, 8343-8349.

Benthien, A., Müller, P.J., 2000. Anomalously low alkenone temperatures caused by lateral particle and sediment transport in the Malvinas Current region, western Argentine Basin. Deep Sea Research Part I: Oceanographic Research Papers 47, 2369-2393.

Berger, A., 1978. Long-term variations of daily insolation and Quaternary climatic changes. J. Atmos. Sci. 35, 2362-2367.

Berger, A., 1989. Pleistocene climatic variability at astronomical frequencies. Quaternary International 2, 1-14.

Berger, A., and Loutre, M. F. , 1991. Insolation values for the climate of the last 10 million years. Quaternary Science Reviews 10, 297-317.

Berger, A.L., 1977. Support for the astronomical theory of climatic change. Nature 269, 44-45.

Berger, A.L., 1992. Astronomical theory of Paleoclimates and the last glacial-interglacial cycle. Quaternary Science Reviews 11, 571-581.

Berger, W.H., 1970. Planktonic Foraminifera: Selective solution and the lysocline. Marine Geology 8, 111-138.

Berger, W.H., 2013. On the Milankovitch sensitivity of the Quaternary deep-sea record. Clim. Past 9, 2003-2011.

Biastoch, A., Beal, L.M., Lutjeharms, J.R.E., Casal, T.G.D., 2009a. Variability and Coherence of the Agulhas Undercurrent in a High-Resolution Ocean General Circulation Model. Journal of Physical Oceanography 39, 2417-2435.

Biastoch, A., Böning, C.W., 2013. Anthropogenic impact on Agulhas leakage. Geophysical Research Letters 40, 1138-1143.

Biastoch, A., Böning, C.W., Getzlaff, J., Molines, J.-M., Madec, G., 2008a. Causes of Interannual–Decadal Variability in the Meridional Overturning Circulation of the Midlatitude North Atlantic Ocean. Journal of Climate 21, 6599-6615.

Biastoch, A., Boning, C.W., Lutjeharms, J.R.E., 2008b. Agulhas leakage dynamics affects decadal variability in Atlantic overturning circulation. Nature 456, 489-492.

Biastoch, A., Boning, C.W., Schwarzkopf, F.U., Lutjeharms, J.R.E., 2009b. Increase in Agulhas leakage due to poleward shift of Southern Hemisphere westerlies. Nature 462, 495-498.

Biastoch, A., Krauss, W., 1999. The Role of Mesoscale Eddies in the Source Regions of the Agulhas Current. Journal of Physical Oceanography 29, 2303-2317.

Bickert, T., Mackensen, A., 2003. Last Glacial to Holocene changes in South Atlantic deep water circulation.

Bickert, T., Wefer, G., 1996. Late Quaternary Deep Water Circulation in the South Atlantic: Reconstruction from Carbonate Dissolution and Benthic Stable Isotopes, The South Atlantic. Springer Berlin Heidelberg, pp. 599-620.

Birch, H., Coxall, H.K., Pearson, P.N., Kroon, D., O'Regan, M., 2013. Planktonic foraminifera stable isotopes and water column structure: Disentangling ecological signals. Marine Micropaleontology 101, 127-145.

Blackmon, P.D., and Todd, R., 1959. Mineralogy of some foraminifera as related to their classification and ecology. Journal of Paleontology 33, 1-15.

Blunier, T., Brook, E.J., 2001. Timing of Millennial-Scale Climate Change in Antarctica and Greenland During the Last Glacial Period. Science 291, 109-112.

Boebel, O., Rossby, T., Lutjeharms, J., Zenk, W., Barron, C., 2003. Path and variability of the Agulhas Return Current. Deep Sea Research Part II: Topical Studies in Oceanography 50, 35-56.

Bond, G., Broecker, W., Johnsen, S., McManus, J., Labeyrie, L., Jouzel, J., Bonani, G., 1993. Correlations between climate records from North Atlantic sediments and Greenland ice. Nature 365, 143-147.

Bond, G., Heinrich, H., Broecker, W., Labeyrie, L., McManus, J., Andrews, J., Huon, S., 1992. Evidence for massive discharges of icebergs into the North Atlantic ocean during the last glacial period. Nature.

Bond, G., Showers, W., Cheseby, M., Lotti, R., Almasi, P., deMenocal, P., Priore, P., Cullen, H., Hajdas, I., Bonani, G., 1997. A Pervasive Millennial-Scale Cycle in North Atlantic Holocene and Glacial Climates. Science 278, 1257-1266.

Bond, G.C., Lotti, R., 1995. Iceberg Discharges into the North Atlantic on Millennial Time Scales During the Last Glaciation. Science 267, 1005-1010.

Bosman, C., Uken, R., Leuci, R., Smith, A.M., Sinclair, D., 2007. Shelf sediments off the Thukela River mouth: complex interaction between fluvial and oceanographic processes. South African Journal of Science 103, , 490-492.

Bostock, H.C., Opdyke, B.N., Gagan, M.K., Fifield, L.K., 2004. Carbon isotope evidence for changes in Antarctic Intermediate Water circulation and ocean ventilation in the southwest Pacific during the last deglaciation. Paleoceanography 19, PA4013.

Boyd, E.S., Pearson, A., Pi, Y., Li, W.J., Zhang, Y.G., He, L., Zhang, C.L., Geesey, G.G., 2011. Temperature and pH controls on glycerol dibiphytanyl glycerol tetraether lipid composition in the hyperthermophilic crenarchaeon Acidilobus sulfurireducens. Extremophiles : life under extreme conditions 15, 59-65.

Boyle, E.A., 1983. Manganese carbonate overgrowths on foraminifera tests. Geochimica et Cosmochimica Acta 47, 1815-1819.

Boyle, E.A., Keigwin, L., 1987. North Atlantic thermohaline circulation during the past 20,000 years linked to high-latitude surface temperature. Nature 330, 35-40.

Bozzano, G., Kuhlmann, H., Alonso, B., 2002. Storminess control over African dust input to the Moroccan Atlantic margin (NW Africa) at the time of maxima boreal summer insolation: a record of the last 220 kyr. Palaeogeography, Palaeoclimatology, Palaeoecology 183, 155-168.

Braconnot, P., Otto-Bliesner, B., Harrison, S., Joussaume, S., Peterchmitt, J.Y., Abe-Ouchi, A., Crucifix, M., Driesschaert, E., Fichefet, T., Hewitt, C.D., Kageyama, M., Kitoh, A., Laîné, A., Loutre, M.F., Marti, O., Merkel, U., Ramstein, G., Valdes, P., Weber, S.L., Yu, Y., Zhao, Y., 2007. Results of PMIP2 coupled simulations of the Mid-Holocene and Last Glacial Maximum- Part 1: experiments and large-scale features. Clim. Past 3, 261-277.

Brassell, S.C., Eglinton, G., Marlowe, I.T., Pflaumann, U., Sarnthein, M., 1986. Molecular stratigraphy: a new tool for climatic assessment. Nature 320, 129-133.

Broecker, W., Clark, E., 2001. An evaluation of Lohmann's foraminifera weight dissolution index. Paleoceanography 16, 531-534.

Broecker, W., Pena, L.D., 2014. Delayed Holocene Reappearance of *G. menardii*. Paleoceanography, 2013PA002590.

Broecker, W.S., 1991. The Great Ocean Conveyor. Oceanography 4, 10.

Broecker, W.S., 1997. Thermohaline Circulation, the Achilles Heel of Our Climate System: Will Man-Made CO_2 Upset the Current Balance? Science 278, 1582-1588.

Broecker, W.S., 1998. Paleocean circulation during the Last Deglaciation: A bipolar seesaw? Paleoceanography 13, 119-121.

Broecker, W.S., Bond, G., Klas, M., Bonani, G., Wolfli, W., 1990. A salt oscillator in the glacial Atlantic? 1. The concept. Paleoceanography 5, 469-477.

Broecker, W.S., Clark, E., 2003. Holocene atmospheric CO_2 increase as viewed from the seafloor. Global Biogeochemical Cycles 17, 1052.

Broecker, W.S., Maier-Reimer, E., 1992. The influence of air and sea exchange on the carbon isotope distribution in the sea. Global Biogeochemical Cycles 6, 315-320.

Broecker, W.S., Thurber, D.L., Goddard, J., Ku, T.L., Matthews, R.K., Mesolella, K.J., 1968. Milankovitch hypothesis supported by precise dating of coral reefs and deep-sea sediments. Science 159, 297-300.

Broecker, W.S., van Donk, J., 1970. Insolation changes, ice volumes, and the $\delta^{18}O$ record in deep-sea cores. Reviews of Geophysics 8, 169-198.

Brown, S.J., Elderfield, H., 1996. Variations in Mg/Ca and Sr/Ca ratios of planktonic foraminifera caused by postdepositional dissolution: Evidence of shallow Mg-dependent dissolution. Paleoceanography 11, 543-551.

Bryden, H.L., Beal, L.M., 2001. Role of the Agulhas Current in Indian Ocean circulation and associated heat and freshwater fluxes. Deep Sea Research Part I: Oceanographic Research Papers 48, 1821-1845.

Bryden, H.L., Beal, L.M., Duncan, L.M., 2005a. Structure and Transport of the Agulhas Current and Its Temporal Variability. Journal of Oceanography 61, 479-492.

Bryden, H.L., Longworth, H.R., Cunningham, S.A., 2005b. Slowing of the Atlantic meridional overturning circulation at 25°N. Nature 438, 655-657.

Burrough, S.L., Thomas, D.S.G., Singarayer, J.S., 2009. Late Quaternary hydrological dynamics in the Middle Kalahari: Forcing and feedbacks. Earth-Science Reviews 96, 313-326.

Burton, K.W., 2006. Global weathering variations inferred from marine radiogenic isotope records. Journal of Geochemical Exploration 88, 262-265.

Caballero-Gill, R.P., Clemens, S.C., Prell, W.L., 2012. Direct correlation of Chinese speleothem $\delta^{18}O$ and South China Sea planktonic $\delta^{18}O$: Transferring a speleothem chronology to the benthic marine chronology. Paleoceanography 27, PA2203.

Caillon, N., Severinghaus, J.P., Jouzel, J., Barnola, J.-M., Kang, J., Lipenkov, V.Y., 2003. Timing of Atmospheric CO_2 and Antarctic Temperature Changes Across Termination III. Science 299, 1728-1731.

Caley, T., Giraudeau, J., Malaizé, B., Rossignol, L., Pierre, C., 2012. Agulhas leakage as a key process in the modes of Quaternary climate changes. Proceedings of the National Academy of Sciences 109, 6835-6839.

Caley, T., Kim, J.H., Malaizé, B., Giraudeau, J., Laepple, T., Caillon, N., Charlier, K., Rebaubier, H., Rossignol, L., Castañeda, I.S., Schouten, S., Damsté, J.S.S., 2011a. High-latitude obliquity forcing as a dominant forcing in the Agulhas current system. Clim. Past 7, 1285-1296.

Caley, T., Malaizé, B., Revel, M., Ducassou, E., Wainer, K., Ibrahim, M., Shoeaib, D., Migeon, S., Marieu, V., 2011b. Orbital timing of the Indian, East Asian and African boreal monsoons and the concept of a 'global monsoon'. Quaternary Science Reviews 30, 3705-3715.

Caley, T., Peeters, F.J.C., Biastoch, A., Rossignol, L., van Sebille, E., Durgadoo, J., Malaizé, B., Giraudeau, J., Arthur, K., Zahn, R., 2014. Quantitative estimate of the paleo-Agulhas leakage. Geophysical Research Letters 41, 2014GL059278.

Came, R.E., Oppo, D.W., Curry, W.B., Lynch-Stieglitz, J., 2008. Deglacial variability in the surface return flow of the Atlantic meridional overturning circulation. Paleoceanography 23, PA1217.

Carter, L., Cortese, G., Brigham-Grette, J., Powell, R., Newman, L., Kiefer, T., 2009. Change in the Southern Ocean: responding to Antarctica. PAGES News: change at the Poles, a paleoscience perspective, IGBP-PAGES (Past Global Changes), PAGES International Project Office 17, 30-32.

Casal, T.G.D., Beal, L.M., Lumpkin, R., Johns, W.E., 2009. Structure and downstream evolution of the Agulhas Current system during a quasi-synoptic survey in February&March 2003. J. Geophys. Res. 114, C03001.

Castañeda, I.S., Schefuß, E., Pätzold, J., Sinninghe Damsté, J.S., Weldeab, S., Schouten, S., 2010. Millennial-scale sea surface temperature changes in the eastern Mediterranean (Nile River Delta region) over the last 27,000 years. Paleoceanography 25, PA1208.

Charles, C.D., Lynch-Stieglitz, J., Ninnemann, U.S., Fairbanks, R.G., 1996. Climate connections between the hemispheres revealed by deep sea sediment core/ice core correlations. Earth and Planetary Science Letters 142, 19-27.

Charles, C.D., Wright, J.D., Fairbanks, R.G., 1993. Thermodynamic influences on the marine carbon isotope record. Paleoceanography 8, 691-697.

Chase, B.M., Meadows, M.E., 2007. Late Quaternary dynamics of southern Africa's winter rainfall zone. Earth-Science Reviews 84, 103-138.

Chave, K.E., 1954. Aspects of the biogeochemistry of magnesium 1. Calcareous marine organisms. Journal of Geology 62, 266-283.

Cheng, H., Edwards, R.L., Broecker, W.S., Denton, G.H., Kong, X., Wang, Y., Zhang, R., Wang, X., 2009. Ice Age Terminations. Science 326, 248-252.

Cheng, H., Sinha, A., Wang, X., Cruz, F., Edwards, R.L., 2012. The Global Paleomonsoon as seen through speleothem records from Asia and the Americas. Climate Dynamics 39, 1045-1062.

Chiang, J.H., Bitz, C., 2005. Influence of high latitude ice cover on the marine Intertropical Convergence Zone. Climate Dynamics 25, 477-496.

Clark, P.U., Alley, R.B., Pollard, D., 1999. Northern Hemisphere Ice-Sheet Influences on Global Climate Change. Science 286, 1104-1111.

Clark, P.U., Dyke, A.S., Shakun, J.D., Carlson, A.E., Clark, J., Wohlfarth, B., Mitrovica, J.X., Hostetler, S.W., McCabe, A.M., 2009. The Last Glacial Maximum. Science 325, 710-714.

Clark, P.U., Mix, A.C., 2002. Ice sheets and sea level of the Last Glacial Maximum. Quaternary Science Reviews 21, 1-7.

Clark, P.U., Pisias, N.G., Stocker, T.F., Weaver, A.J., 2002. The role of the thermohaline circulation in abrupt climate change. Nature 415, 863-869.

Clemens, S.C., Prell, W.L., Sun, Y., 2010. Orbital-scale timing and mechanisms driving Late Pleistocene Indo-Asian summer monsoons: Reinterpreting cave speleothem $\delta^{18}O$. Paleoceanography 25, PA4207.

Clement, A.C., and Cane, M.A., 1999. "Role for the tropical Pacific coupled ocean-atmosphere system on Milankovitch and millennial timescales. Part I: A modeling study of tropical Pacific variability," in Mechanisms of Global Climate Change at Millennial Timescales, eds. P. U. Clark et al. (Washington, DC: American Geophysical Union) 363-371.

Compton, J.S., Maake, L., 2007. Source of the suspended load of the upper Orange River, South Africa. South African Journal of Geology 110, 339-348.

Crowley, T.J., Hyde, W.T., 2008. Transient nature of late Pleistocene climate variability. Nature 456, 226-230.

Cruz, F.W., Burns, S.J., Karmann, I., Sharp, W.D., Vuille, M., Cardoso, A.O., Ferrari, J.A., Silva Dias, P.L., Viana, O., 2005. Insolation-driven changes in atmospheric circulation over the past 116,000 years in subtropical Brazil. Nature 434, 63-66.

Cunningham, S.A., Kanzow, T., Rayner, D., Baringer, M.O., Johns, W.E., Marotzke, J., Longworth, H.R., Grant, E.M., Hirschi, J.J.-M., Beal, L.M., Meinen, C.S., Bryden, H.L., 2007. Temporal Variability of the Atlantic Meridional Overturning Circulation at 26.5°N. Science 317, 935-938.

Cunningham, S.A., Marsh, R., 2010. Observing and modeling changes in the Atlantic MOC. Wiley Interdisciplinary Reviews: Climate Change 1, 180-191.

Curry, W.B., Duplessy, J.-C., Labeyrie, L., Shackleton, N.J., 1988. Changes in the distribution of $\delta^{13}C$ of deep water ΣCO_2 between the last glaciation and the Holocene. Paleoceanography 3.

Curry, W.B., Oppo, D.W., 2005. Glacial water mass geometry and the distribution of $\delta^{13}C$ of ΣCO_2 in the western Atlantic Ocean. Paleoceanography 20, PA1017.

Dansgaard, W., Johnsen, S.J., Clausen, H.B., Dahl-Jensen, D., Gundestrup, N.S., Hammer, C.U., Hvidberg, C.S., Steffensen, J.P., Sveinbjornsdottir, A.E., Jouzel, J., Bond, G., 1993. Evidence for general instability of past climate from a 250-kyr ice-core record. Nature 364, 218-220.

De Boer, A.M., Graham, R.M., Thomas, M.D., Kohfeld, K.E., 2013. The control of the Southern Hemisphere Westerlies on the position of the Subtropical Front. Journal of Geophysical Research: Oceans 118, 1-7.

De Deckker, P., Moros, M., Perner, K., Jansen, E., 2012. Influence of the tropics and southern westerlies on glacial interhemispheric asymmetry. Nature Geosci 5, 266-269.

de Oliveira, D.P.S., Cawthorn, R.G., 1999. Dolerite intrusion morphology at Majuba Colliery, northeast Karoo Basin, Republic of South Africa. International Journal of Coal Geology 41, 333-349.

de Ruijter, W.P.M., Biastoch, A., Drijfhout, S.S., Lutjeharms, J.R.E., Matano, R.P., Pichevin, T., Leeuwen, P.J.v., Weijer, W., 1999a. Indian-Atlantic interocean exchange: Dynamics, estimation and impact. Journal of Geophysical Research 104, 20,885-820,910, .

de Ruijter, W.P.M., Ridderinkhof, H., Lutjeharms, J.R.E., Schouten, M.W., Veth, C., 2002. Observations of the flow in the Mozambique Channel. Geophysical Research Letters 29, 140-141-140-143.

de Ruijter, W.P.M., van Leeuwen, P.J., Lutjeharms, J.R.E., 1999b. Generation and Evolution of Natal Pulses: Solitary Meanders in the Agulhas Current. Journal of Physical Oceanography 29, 3043-3055.

de Villiers, S., 2004. Optimum growth conditions as opposed to calcite saturation as a control on the calcification rate and shell-weight of marine foraminifera. Marine Biology 144, 45-49.

de Villiers, S., 2005. Foraminiferal shell-weight evidence for sedimentary calcite dissolution above the lysocline. Deep Sea Research Part I: Oceanographic Research Papers 52, 671-680.

Dekens, P.S., Lea, D.W., Pak, D.K., Spero, H.J., 2002. Core top calibration of Mg/Ca in tropical foraminifera: Refining paleotemperature estimation. Geochemistry, Geophysics, Geosystems 3, 1-29.

deMenocal, P., Ortiz, J., Guilderson, T., Adkins, J., Sarnthein, M., Baker, L., Yarusinsky, M., 2000. Abrupt onset and termination of the African Humid Period: rapid climate responses to gradual insolation forcing. Quaternary Science Reviews 19, 347-361.

deMenocal, P.B., 2004. African climate change and faunal evolution during the Pliocene–Pleistocene. Earth and Planetary Science Letters 220, 3-24.

deMenocal, P.B., 2011. Climate and Human Evolution. Science 331, 540-542.

deMenocal, P.B., Ruddiman, W.F., Pokras, E.M., 1993. Influences of High- and Low-Latitude Processes on African Terrestrial Climate: Pleistocene Eolian Records from Equatorial Atlantic Ocean Drilling Program Site 663. Paleoceanography 8, 209-242.

Denton, G.H., Anderson, R.F., Toggweiler, J.R., Edwards, R.L., Schaefer, J.M., Putnam, A.E., 2010. The Last Glacial Termination. Science 328, 1652-1656.

Denton, G.H., Hughes, T.J., 1983. Milankovitch theory of ice ages: Hypothesis of ice-sheet linkage between regional insolation and global climate. Quaternary Research 20, 125-144.

Dezileau, L., Bareille, G., Reyss, J.L., Lemoine, F., 2000. Evidence for strong sediment redistribution by bottom currents along the southeast Indian ridge. Deep Sea Research Part I: Oceanographic Research Papers 47, 1899-1936.

di Marco, S.F., Nowlin, W.D., Chapman, P., 1998. Properties and transport of the Mozambique Channel. 1998 US Woce report., 34-35.

Dickson, A.J., Leng, M.J., Maslin, M.A., Sloane, H.J., Green, J., Bendle, J.A., McClymont, E.L., Pancost, R.D., 2010. Atlantic overturning circulation and Agulhas leakage influences on southeast Atlantic upper ocean hydrography during marine isotope stage 11. Paleoceanography 25, PA3208.

Dijkstra, H.A., de Ruijter, W.P.M., 2001. On the Physics of the Agulhas Current: Steady Retroflection Regimes. Journal of Physical Oceanography 31, 2971-2985.

Dingle, R.V., Birch, G.V., Bremner, J.M., de Decker, R.H., du Plessis, A., Engelbrecht, J.A., Fincham, M.J., Fitton, T., Flemming, B.W., Gentle, R.I., Goodlad, S.H., Martin, A.K., Mills, E.G., Moir, G.J., ,, Parker, R.J., Robson, S.H., Rogers, J., Salmon, D.A., Sieser, W.G., Simpson, E.S.W., Summerhayes, C.P., Westall, F., Winter, A., Woodborne, M.W., 1997. Deep-sea environments around southern Africa (South-East Atlantic and South West Indian Oceans. Annals of the South African Museum 98, 1-2.

Dingle, R.V., Camden-Smith, F., 1979. Acoustic stratigraphy and current-generated bedforms in deep ocean basins off southeastern Africa. Marine Geology 33, 239-260.

Dirghangi, S.S., Pagani, M., Hren, M.T., Tipple, B.J., 2013. Distribution of glycerol dialkyl glycerol tetraethers in soils from two environmental transects in the USA. Organic Geochemistry 59, 49-60.

Dong, B.W., Sutton, R.T., 2002. Adjustment of the coupled ocean–atmosphere system to a sudden change in the Thermohaline Circulation. Geophysical Research Letters 29, 18-11-18-14.

Donohue, K.A., Firing, E., Beal, L., 2000. Comparison of three velocity sections of the Agulhas Current and Agulhas Undercurrent. Journal of Geophysical Research: Oceans 105, 28585-28593.

Driessen, P., Deckers, J., O. Spaargaren, Nachtergaele, F., 2001. Lecture Notes on the Major Soils of the World. Food and agriculture organization of the United Nations Rome.

Drysdale, R.N., Hellstrom, J.C., Zanchetta, G., Fallick, A.E., Sanchez Goni, M.F., Couchoud, I., McDonald, J., Maas, R., Lohmann, G., Isola, I., 2009. Evidence for obliquity forcing of glacial Termination II. Science 325, 1527-1531.

Duplessy, J.C., Shackleton, N.J., Fairbanks, R.G., Labeyrie, L., Oppo, D., Kallel, N., 1988. Deepwater Source Variations During the Last Climatic Cycle and Their Impact on the Global Deepwater Circulation. Paleoceanography 3, 343-360.

Duplessy, J.C., Shackleton, N.J., Matthews, R.K., Prell, W., Ruddiman, W.F., Caralp, M.H., Hendy, C.H., 1984. $\delta^{13}C$ record of benthic foraminifera in the last interglacial ocean: implications for the carbon cycle and the global deep water circulation. Quatern. Res. 21, 225-243.

Dupont, L.M., Caley, T., Kim, J.H., Castañeda, I., Malaizé, B., Giraudeau, J., 2011. Glacial-interglacial vegetation dynamics in South Eastern Africa coupled to sea surface temperature variations in the Western Indian Ocean. Clim. Past 7, 1209-1224.

Durgadoo, J.V., Loveday, B.R., Reason, C.J.C., Penven, P., Biastoch, A., 2013. Agulhas Leakage Predominantly Responds to the Southern Hemisphere Westerlies. Journal of Physical Oceanography 43, 2113–2131.

Elderfield, H., and Ganssen, G., 2000. Past temperature and $\delta^{18}O$ of surface ocean waters inferred from foraminiferal Mg/Ca ratios. Nature 405, 442-445.

Emiliani, C., 1955. Pleistocene Temperatures. Journal of Geology 63, 538-578.

EPICA, 2004. Eight glacial cycles from an Antarctic ice core. Nature 429, 623-628.

Epstein, S.R., Buchsbaum, R., Lowenstem, H.A., and Urey, H.C., 1953. Revised carbonate-water isotopic temperature scale. Geol. Soc. Am. Bull., 64, 1315-1326.

Erez, J., Honjo, S., 1981. Comparison of isotopic composition of planktonic foraminifera in plankton tows, sediment traps and sediments. Palaeogeography, Palaeoclimatology, Palaeoecology 33, 129-156.

Fairbanks, R.G., 1989. A 17,000-year glacio-eustatic sea level record: influence of glacial melting rates on the Younger Dryas event and deep-ocean circulation. Nature 342, 637-642.

Fairbanks, R.G., Wiebe, P.H., BÉ, A.W.H., 1980. Vertical Distribution and Isotopic Composition of Living Planktonic Foraminifera in the Western North Atlantic. Science 207, 61-63.

Falkowski, P., Scholes, R.J., Boyle, E., Canadell, J., Canfield, D., Elser, J., Gruber, N., Hibbard, K., Högberg, P., Linder, S., Mackenzie, F.T., Moore III, B., Pedersen, T., Rosenthal, Y., Seitzinger, S., Smetacek, V., Steffen, W., 2000. The Global Carbon Cycle: A Test of Our Knowledge of Earth as a System. Science 290, 291-296.

Fallet, U., Ullgren, J.E., Castañeda, I.S., van Aken, H.M., Schouten, S., Ridderinkhof, H., Brummer, G.-J.A., 2011. Contrasting variability in foraminiferal and organic paleotemperature proxies in sedimenting particles of the Mozambique Channel (SW Indian Ocean). Geochimica et Cosmochimica Acta 75, 5834-5848.

Feron, R.C.V., De Ruijter, W.P.M., Oskam, D., 1992. Ring shedding in the Agulhas Current System. Journal of Geophysical Research: Oceans 97, 9467-9477.

Fine, R.A., 1993. Circulation of Antarctic intermediate water in the South Indian Ocean. Deep Sea Research Part I: Oceanographic Research Papers 40, 2021-2042.

Flemming, B.W., 1981. Factors controlling shelf sediment dispersal along the southeast African continental margin. Marine Geology 42, 259-277.

Frank, M., 2002. Radiogenic Isotopes: Tracers of past ocean circulation and erosional input. Reviews of Geophysics 40, 1-1-1-38.

Franzese, A.M., Hemming, S.R., Goldstein, S.L., 2009. Use of strontium isotopes in detrital sediments to constrain the glacial position of the Agulhas Retroflection. Paleoceanography 24, PA2217.

Franzese, A.M., Hemming, S.R., Goldstein, S.L., Anderson, R.F., 2006. Reduced Agulhas Leakage during the Last Glacial Maximum inferred from an integrated provenance and flux study. Earth and Planetary Science Letters 250, 72-88.

Gaiero, D.M., Probst, J.L., Depetris, P.J., Bidart, S.M., Leleyter, L., 2003. Iron and other transition metals in Patagonian riverborne and windborne materials: geochemical control and transport to the southern South Atlantic Ocean. Geochimica et Cosmochimica Acta 67, 3603-3623.

Ganachaud, A., Wunsch, C., 2000. Improved estimates of global ocean circulation, heat transport and mixing from hydrographic data. Nature 408, 453-457.

Gasse, F., 1977. Evolution of lake Abhe (Ethiopia and TFAI), from 70 000 B.P. Nature 265, 47-45.

Gasse, F., 2000. Hydrological changes in the African tropics since the Last Glacial Maximum. Quaternary Science Reviews 19, 189-211.

Gasse, F., Chalié, F., Vincens, A., Williams, M.A.J., Williamson, D., 2008. Climatic patterns in equatorial and southern Africa from 30,000 to 10,000 years ago reconstructed from terrestrial and near-shore proxy data. Quaternary Science Reviews 27, 2316-2340.

Gasse, F., Van Campo, E., 2001. Late Quaternary environmental changes from a pollen and diatom record in the southern tropics (Lake Tritrivakely, Madagascar). Palaeogeography, Palaeoclimatology, Palaeoecology 167, 287-308.

Gebbie, G., 2014. How much did Glacial North Atlantic Water shoal? Paleoceanography 29, 190-209.

Gherardi, J.M., Labeyrie, L., McManus, J.F., Francois, R., Skinner, L.C., Cortijo, E., 2005. Evidence from the Northeastern Atlantic basin for variability in the rate of the meridional overturning circulation through the last deglaciation. Earth and Planetary Science Letters 240, 710-723.

Giulivi, C.F., Gordon, A.L., 2006. Isopycnal displacements within the Cape Basin thermocline as revealed by the Hydrographic Data Archive. Deep Sea Research Part I: Oceanographic Research Papers 53, 1285-1300.

Goldstein, S.L., and Hemming, S.R., 2003. Long-lived isotopic tracers in oceanography, paleoceanography, and ice-sheet dynamics. In: Treatise on Geochemistry. Elsevier, New York, 453-498.

Goodlad, S.W., 1986. Tectonic and sedimentary history of the mid-Natal Valley (SW Indian Ocean). J. Geol. Surv., Univ. Cape Town Bull 5, 625-630.

Gordon, A.L., 1985. Indian-Atlantic Transfer of Thermocline Water at the Agulhas Retroflection. Science 227, 1030-1033.

Gordon, A.L., 1986. Interocean Exchange of Thermocline Water. Journal of Geophysical Research 91, 5037-5046.

Gordon, A.L., 2001. Interocean exchange in Siedler, G., Church, J., Gould, J. (Eds.), Ocean Circulation and Climate. Academic Press, New York. 303-314.

Gordon, A.L., Lutjeharms, J.R.E., Gründlingh, M.L., 1987. Stratification and circulation at the Agulhas Retroflection. Deep Sea Research Part A. Oceanographic Research Papers 34, 565-599.

Govin, A., Holzwarth, U., Heslop, D., Ford Keeling, L., Zabel, M., Mulitza, S., Collins, J.A., Chiessi, C.M., 2012. Distribution of major elements in Atlantic surface sediments (36°N–49°S): Imprint of terrigenous input and continental weathering. Geochemistry, Geophysics, Geosystems 13, Q01013.

Graham, R.M., de Boer, A.M., Heywood, K.J., Chapman, M.R., Stevens, D.P., 2012. Southern Ocean fronts: Controlled by wind or topography? Journal of Geophysical Research: Oceans 117, C08018.

Grant, K.M., Rohling, E.J., Bar-Matthews, M., Ayalon, A., Medina-Elizalde, M., Ramsey, C.B., Satow, C., Roberts, A.P., 2012. Rapid coupling between ice volume and polar temperature over the past 150,000 years. Nature 491, 744-747.

Gründlingh, M.L., 1978. Drift of a satellite-tracked buoy in the southern Agulhas Current and Agulhas Return Current. Deep Sea Research 25, 1209-1224.

Gründlingh, M.L., 1980. On the volume transport of the Agulhas Current. Deep Sea Research Part A. Oceanographic Research Papers 27, 557-563.

Gründlingh, M.L., 1983. On the course of the Agulhas Current. South African Geographical Journal 65, 49–57.

Gyldenfeldt, A.B., Carstens, J.R., Meincke, J., 2000. Estimation of the catchment area of a sediment trap by means of current meters and foraminiferal tests. Deep- Sea Res. II :Top. Stud. Oceanogr 47, 1701-1717.

Hall, I.R., Becker, J., 2007. Deep Western Boundary Current variability in the subtropical northwest Atlantic Ocean during marine isotope stages 12–10. Geochemistry, Geophysics, Geosystems 8, Q06013.

Hall, I.R., Evans, H.K., Thornalley, D.J.R., 2011. Deep water flow speed and surface ocean changes in the subtropical North Atlantic during the last deglaciation. Global and Planetary Change 79, 255-263.

Hall, I.R., McCave, I.N., Shackleton, N.J., Weedon, G.P., Harris, S.E., 2001. Intensified deep Pacific inflow and ventilation in Pleistocene glacial times. Nature 412, 809-812.

Hall, I.R., Zahn, R., 2004. Cruise Report RRS Charles Darwin Cruise 154: 13/12/2003 - 10/01/2004, Durban to Cape Town, South Africa, Agulhas 'Leakage' and Abrupt Climate Change.

Hart, N.C.G., Reason, C.J.C., Fauchereau, N., 2010. Tropical–Extratropical Interactions over Southern Africa: Three Cases of Heavy Summer Season Rainfall. Monthly Weather Review 138, 2608-2623.

Haviland, W.A., Prins, H., E., L, Walrath, D., Mc Bride, B., 2007. Evolution And Prehistory: The Human Challenge.

Hays, J.D., Imbrie, J., Shackleton, N.J., 1976. Variations in the Earth's Orbit: Pacemaker of the Ice Ages. Science 194, 1121-1132.

Heinrich, H., 1988. Origin and consequences of cyclic ice rafting in the Northeast Atlantic Ocean during the past 130,000 years. Quaternary Research 29, 142-152.

Hemleben, C., Spindler, M., Erson, O.R., 1989. Modern planktonic foraminifera.

Hemming, S.R., 2004. Heinrich events: Massive late Pleistocene detritus layers of the North Atlantic and their global climate imprint. Reviews of Geophysics 42, RG1005.

Henshilwood, C.S., d'Errico, F., Yates, R., Jacobs, Z., Tribolo, C., Duller, G.A.T., Mercier, N., Sealy, J.C., Valladas, H., Watts, I., Wintle, A.G., 2002. Emergence of Modern Human Behavior: Middle Stone Age Engravings from South Africa. Science 295, 1278-1280.

Henshilwood, C.S., d'Errico, F., van Niekerk, K.L., Coquinot, Y., Jacobs, Z., Lauritzen, S.-E., Menu, M., García-Moreno, R., 2011. A 100,000-Year-Old Ochre-Processing Workshop at Blombos Cave, South Africa. Science 334, 219-222.

Herfort, L., Stefan Schouten, Jan P. Boon, Martijn Woltering, Marianne Baas, Johan W. H. Weijers, Damsté, J.S.S., 2007. Characterization of transport and deposition of terrestrial organic matter in the southern North Sea using the BIT index. Limnol. Oceanogr. 51, 2196-2205.

Herguera, J.C., Jansen, E., Berger, W.H., 1992. Evidence for a bathyal front at 2000-M depth in the glacial Pacific, based on a depth transect on Ontong Java Plateau. Paleoceanography 7, 273-288.

Hermes, J.C., Reason, C.J.C., Lutjeharms, J.R.E., 2007. Modeling the Variability of the Greater Agulhas Current System. Journal of Climate 20, 3131-3146.

Hesse, T., Butzin, M., Bickert, T., Lohmann, G., 2011. A model-data comparison of $\delta^{13}C$ in the glacial Atlantic Ocean. Paleoceanography 26, PA3220.

Hillaire-Marcel, C., Carro, O., Casanova, J., 1986. ^{14}C and Th/U dating of Pleistocene and Holocene stromatolites from East African paleolakes. Quaternary Research 25, 312-329.

Hodell, D.A., Venz, K.A., Charles, C.D., Ninnemann, U.S., 2003. Pleistocene vertical carbon isotope and carbonate gradients in the South Atlantic sector of the Southern Ocean. Geochemistry, Geophysics, Geosystems 4, 1004.

Hodgson, D.A., Sime, L.C., 2010. Palaeoclimate: Southern westerlies and CO_2. Nature Geosci 3, 666-667.

Holbourn, A., Kuhnt, W., Kawamura, H., Jian, Z., Grootes, P., Erlenkeuser, H., Xu, J., 2005. Orbitally paced paleoproductivity variations in the Timor Sea and Indonesian Throughflow variability during the last 460 kyr. Paleoceanography 20, PA3002.

Hönisch, B., Allen, K.A., Lea, D.W., Spero, H.J., Eggins, S.M., Arbuszewski, J., deMenocal, P., Rosenthal, Y., Russell, A.D., Elderfield, H., 2013. The influence of salinity on Mg/Ca in planktic foraminifers – Evidence from cultures, core-top sediments and complementary $\delta^{18}O$. Geochimica et Cosmochimica Acta 121, 196-213.

Hoogakker, B.A.A., Rohling, E.J., Palmer, M.R., Tyrrell, T., Rothwell, R.G., 2006. Underlying causes for long-term global ocean $\delta^{13}C$ fluctuations over the last 1.20 Myr. Earth and Planetary Science Letters 248,, 15.

Hopmans, E.C., Weijers, J.W.H., Schefuß, E., Herfort, L., Sinninghe Damsté, J.S., Schouten, S., 2004. A novel proxy for terrestrial organic matter in sediments based on branched and isoprenoid tetraether lipids. Earth and Planetary Science Letters 224, 107-116.

Huang, K.-F., Oppo, D.W., Curry, W.B., 2014. Decreased influence of Antarctic intermediate water in the tropical Atlantic during North Atlantic cold events. Earth and Planetary Science Letters 389, 200-208.

Huber, C., Leuenberger, M., Spahni, R., Flückiger, J., Schwander, J., Stocker, T.F., Johnsen, S., Landais, A., Jouzel, J., 2006. Isotope calibrated Greenland temperature record over Marine Isotope Stage 3 and its relation to CH_4. Earth and Planetary Science Letters 243, 504-519.

Huguet, C., Hopmans, E.C., Febo-Ayala, W., Thompson, D.H., Sinninghe Damsté, J.S., Schouten, S., 2006. An improved method to determine the absolute abundance of glycerol dibiphytanyl glycerol tetraether lipids. Organic Geochemistry 37, 1036-1041.

Huguet, C., Martrat, B., Grimalt, J.O., Sinninghe Damsté, J.S., Schouten, S., 2011. Coherent millennial-scale patterns in $U_{37}^{K'}$ and TEX_{86} temperature records during the penultimate interglacial-to-glacial cycle in the western Mediterranean. Paleoceanography 26, PA2218.

Huguet, C., Smittenberg, R.H., Boer, W., Sinninghe Damsté, J.S., Schouten, S., 2007. Twentieth century proxy records of temperature and soil organic matter input in the Drammensfjord, southern Norway. Organic Geochemistry 38, 1838-1849.

Hut, G., 1987. Consultants' Group Meeting on Stable Isotope Reference Samples for Geochemical and Hydrological Investigations. Rep. to Dir. Gen., Vienna, 16–18 September 1985, Int. At. Energy Agency, Vienna (1987), p. 42, 42.

Hutson, W.H., 1980. The agulhas current during the late pleistocene: analysis of modern faunal analogs. Science 207, 64-66.

Imbrie, J., 1985. A theoretical framework for the Pleistocene ice ages: William Smith Lecture. Journal of the Geological Society 142, 417-432.

Ingalls, A.E., Huguet, C., Truxal, L.T., 2012. Distribution of intact and core membrane lipids of archaeal glycerol dialkyl glycerol tetraethers among size-fractionated particulate organic matter in hood canal, puget sound. Appl Environ Microbiol 78, 1480-1490.

Jacobs, Z., Roberts, R.G., Galbraith, R.F., Deacon, H.J., Grün, R., Mackay, A., Mitchell, P., Vogelsang, R., Wadley, L., 2008. Ages for the Middle Stone Age of Southern Africa: Implications for Human Behavior and Dispersal. Science 322, 733-735.

Jenkins, R., 1999. X-Ray Fluorescence Spectroscopy. Second Edition. Wiley & Sons, New York, 207.

Johnsen, S.J., Dansgaard, W., Clausen, H.B., Langway, C.C., 1972. Oxygen Isotope Profiles through the Antarctic and Greenland Ice Sheets. Nature 235, 429-434.

Johnson, M.R., Van Vuuren, C.J., Hegenberger, W.F., Key, R., Show, U., 1996. Stratigraphy of the Karoo Supergroup in southern Africa: an overview. Journal of African Earth Sciences 23, 3-15.

Johnson, T.C., Brown, E.T., McManus, J., Barry, S., Barker, P., Gasse, F., 2002. A High-Resolution Paleoclimate Record Spanning the Past 25,000 Years in Southern East Africa. Science 296, 113-132.

Johnstone, H.J.H., Yu, J., Elderfield, H., Schulz, M., 2011. Improving temperature estimates derived from Mg/Ca of planktonic foraminifera using X-ray computed tomography–based dissolution index, XDX. Paleoceanography 26, PA1215.

Jouzel, J., Masson-Delmotte, V., Cattani, O., Dreyfus, G., Falourd, S., Hoffmann, G., Minster, B., Nouet, J., Barnola, J.M., Chappellaz, J., Fischer, H., Gallet, J.C., Johnsen, S., Leuenberger, M., Loulergue, L., Luethi, D., Oerter, H., Parrenin, F., Raisbeck, G., Raynaud, D., Schilt, A., Schwander, J., Selmo, E., Souchez, R., Spahni, R., Stauffer, B., Steffensen, J.P., Stenni, B.,

Stocker, T.F., Tison, J.L., Werner, M., Wolff, E.W., 2007. Orbital and Millennial Antarctic Climate Variability over the Past 800,000 Years. Science 317, 793-796.

Jungclaus, J.H., Keenlyside, N., Botzet, M., Haak, H., Luo, J.J., Latif, M., Marotzke, J., Mikolajewicz, U., Roeckner, E., 2006. Ocean Circulation and Tropical Variability in the Coupled Model ECHAM5/MPI-OM. Journal of Climate 19, 3952-3972.

Jury, M.R., Valentine, H.R., Lutjeharms, J.R.E., 1993. Influence of the Agulhas Current on Summer Rainfall along the Southeast Coast of South Africa. Journal of Applied Meteorology 32, 1282-1287.

Kallel, N., Labeyrie, L.D., Juillet-Leclerc, A., Duplessy, J.-C., 1988. A deep hydrological front between intermediate and deep-water, masses in the glacial Indian Ocean. Nature 333, 651-655.

Karner, M.B., DeLong, E.F., Karl, D.M., 2001. Archaeal dominance in the mesopelagic zone of the Pacific Ocean. Nature 409, 507-510.

Kasper, S., van der Meer, M.T.J., Mets, A., Zahn, R., Sinninghe Damsté, J.S., Schouten, S., 2014. Salinity changes in the Agulhas leakage area recorded by stable hydrogen isotopes of C_{37} alkenones during Termination I and II. Clim. Past 10, 251-260.

Katz, A., 1973. The interaction of magnesium with calcite during crystal growth at 25-90 °C and one atmosphere. Geochimica et Cosmochimica Acta 37, 1563-1586.

Keeling, R.F., Stephens, B.B., 2001. Antarctic sea ice and the control of Pleistocene climate instability. Paleoceanography 16, 112-131.

Keigwin, L.D., 1998. Glacial-age hydrography of the far northwest Pacific Ocean. Paleoceanography 13, 323-339.

Keigwin, L.D., Boyle, E.A., 1985. Carbon isotopes in deep-sea benthic foraminifera: Precession and changes in low-latitude biomass, The Carbon Cycle and Atmospheric CO_2: Natural Variations Archean to Present. AGU, Washington, DC, pp. 319-328.

Keigwin, L.D., Guilderson, T.P., 2009. Bioturbation artifacts in zero-age sediments. Paleoceanography 24, PA4212.

Key, R.M., Kozyr, A., Sabine, C.L., Lee, K., Wanninkhof, R., Bullister, J.L., Feely, R.A., Millero, F.J., Mordy, C., Peng, T.H., 2004. A global ocean carbon climatology: Results from Global Data Analysis Project (GLODAP). Global Biogeochemical Cycles 18, GB4031.

Kiefer, T., McCave, I.N., Elderfield, H., 2006. Antarctic control on tropical Indian Ocean sea surface temperature and hydrography. Geophys. Res. Lett. 33, L24612.

Kim, J.-H., Crosta, X., Michel, E., Schouten, S., Duprat, J., Sinninghe Damsté, J.S., 2009. Impact of lateral transport on organic proxies in the Southern Ocean. Quaternary Research 71, 246-250.

Kim, J.-H., S. Schouten, E. C. Hopmans, B. Donner, Damsté, J.S.S., 2008. Global sediment core-top calibration of the TEX_{86} paleothermometer in the ocean. Geochimica et Cosmochimica Acta, 72, 1154.

Kim, J.-H., Schouten, S., Buscail, R., Ludwig, W., Bonnin, J., Sinninghe Damsté, J.S., Bourrin, F., 2006. Origin and distribution of terrestrial organic matter in the NW Mediterranean (Gulf of Lions): Exploring the newly developed BIT index. Geochemistry, Geophysics, Geosystems 7, Q11017.

Kim, J.-H., van der Meer, J., Schouten, S., Helmke, P., Willmott, V., Sangiorgi, F., Koç, N., Hopmans, E.C., Damsté, J.S.S., 2010. New indices and calibrations derived from the distribution of crenarchaeal isoprenoid tetraether lipids: Implications for past sea surface temperature reconstructions. Geochimica et Cosmochimica Acta 74, 4639-4654.

Kim, J.-H., Zell, C., Moreira-Turcq, P., Pérez, M.A.P., Abril, G., Mortillaro, J.-M., Weijers, J.W.H., Meziane, T., Sinninghe Damsté, J.S., 2012. Tracing soil organic carbon in the lower Amazon River and its tributaries using GDGT distributions and bulk organic matter properties. Geochimica et Cosmochimica Acta 90, 163-180.

Kim, S.-T., O'Neil, J.R., 1997. Equilibrium and nonequilibrium oxygen isotope effects in synthetic carbonates. Geochimica et Cosmochimica Acta 61, 3461-3475.

Kim, S.J., Crowley, T.J., Stossel, A., 1998. Local orbital forcing of Antarctic climate change during the last Interglacial. Science 280, 728-730.

Kimoto, K., Takaoka, H., Oda, M., Ikehara, M., Matsuoka, H., Okada, M., Oba, T., Taira, A., 2003. Carbonate dissolution and planktonic foraminiferal assemblages observed in three piston cores collected above the lysocline in the western equatorial Pacific. Marine Micropaleontology 47, 227-251.

Kirst, G.J., Schneider, R.R., Müller, P.J., von Storch, I., Wefer, G., 1999. Late Quaternary Temperature Variability in the Benguela Current System Derived from Alkenones. Quaternary Research 52, 92-103.

Kitoh, A., Murakami, S., Koide, H., 2001. A simulation of the Last Glacial Maximum with a coupled atmosphere-ocean GCM. Geophysical Research Letters 28, 2221-2224.

Knorr, G., and Lohmann, G., 2004. The Southern Ocean as Flywheel of the oceanic conveyor belt circulation. . PAGES NEWS 12, 11-13.

Knorr, G., Lohmann, G., 2003. Southern Ocean origin for the resumption of Atlantic thermohaline circulation during deglaciation. Nature 424, 532-536.

Knorr, G., Lohmann, G., 2007. Rapid transitions in the Atlantic thermohaline circulation triggered by global warming and meltwater during the last deglaciation. Geochemistry, Geophysics, Geosystems 8, Q12006.

Knutti, R., Fluckiger, J., Stocker, T.F., Timmermann, A., 2004. Strong hemispheric coupling of glacial climate through freshwater discharge and ocean circulation. Nature 430, 851-856.

Kohfeld, K.E., Graham, R.M., Boer, A.M.d., Sime, L.C., Wolff, E.W., Quéré, C.L., Bopp, L., 2013. Southern Hemisphere Westerly Wind Changes during the Last Glacial Maximum: Paleo-data Synthesis. Quaternary Science Reviews 68, 76-95.

Kolla, V., Sullivan, L., Streeter, S.S., Langseth, M.G., 1976. Spreading of Antarctic Bottom Water and its effects on the floor of the Indian Ocean inferred from bottom-water potential temperature, turbidity, and sea-floor photography. Marine Geology 21, 171-189.

Kroopnick, P.M., 1985. The distribution of $\delta^{13}C$ of ΣCO_2 in the world oceans. Deep Sea Res. 32, 57-84.

Krueger, S., Leuschner, D.C., Ehrmann, W., Schmiedl, G., Mackensen, A., 2012. North Atlantic Deep Water and Antarctic Bottom Water variability during the last 200 ka recorded in an abyssal sediment core off South Africa. Global and Planetary Change 80-81.

Krueger, S., Leuschner, D.C., Ehrmann, W., Schmiedl, G., Mackensen, A., Diekmann, B., 2008. Ocean circulation patterns and dust supply into the South Atlantic during the last glacial cycle revealed by statistical analysis of kaolinite/chlorite ratios. Marine Geology 253, 82-91.

Kucera, M., 2007. Chapter Six Planktonic Foraminifera as Tracers of Past Oceanic Environments. In: Claude, H. M. & Anne D., V. (eds.) Developments in Marine Geology. Elsevier.

Kucera, M., Weinelt, M., Kiefer, T., Pflaumann, U., Hayes, A., Weinelt, M., Chen, M.-T., Mix, A.C., Barrows, T.T., Cortijo, E., Duprat, J., Juggins, S., Waelbroeck, C., 2005. Reconstruction of sea-surface temperatures from assemblages of planktonic foraminifera: multi-technique approach based on geographically constrained calibration data sets and its application to glacial Atlantic and Pacific Oceans. Quaternary Science Reviews 24, 951-998.

Kuhlbrodt, T., Griesel, A., Montoya, M., Levermann, A., Hofmann, M., Rahmstorf, S., 2007. On the driving processes of the Atlantic meridional overturning circulation. Reviews of Geophysics 45, RG2001.

Kutzbach, J.E., 1981. Monsoon Climate of the Early Holocene: Climate Experiment with the Earth's Orbital Parameters for 9000 Years Ago. Science 214, 59-61.

Kutzbach, J.E., Liu, X., Liu, Z., Chen, G., 2008. Simulation of the evolutionary response of global summer monsoons to orbital forcing over the past 280,000 years. Climate Dynamics 30, 567-579.

Kutzbach, J.E., Street-Perrott, F.A., 1985. Milankovitch forcing of fluctuations in the level of tropical lakes from 18 to 0 kyr BP. Nature 317, 130-134.

Lai, D., Springstead, J.R., Monbouquette, H.G., 2008. Effect of growth temperature on ether lipid biochemistry in Archaeoglobus fulgidus. Extremophiles : life under extreme conditions 12, 271-278.

Lambert, F., Delmonte, B., Petit, J.R., Bigler, M., Kaufmann, P.R., Hutterli, M.A., Stocker, T.F., Ruth, U., Steffensen, J.P., Maggi, V., 2008. Dust-climate couplings over the past 800,000 years from the EPICA Dome C ice core. Nature 452, 616-619.

Lamy, F., Hebbeln, D., Wefer, G., 1998. Late Quaternary precessional cycles of terrigenous sediment input off the Norte Chico, Chile (27.5°S) and palaeoclimatic implications. Palaeogeography, Palaeoclimatology, Palaeoecology 141, 233-251.

Lamy, F., Hebbeln, D., Wefer, G., 1999. High-Resolution Marine Record of Climatic Change in Mid-latitude Chile during the Last 28,000 Years Based on Terrigenous Sediment Parameters. Quaternary Research 51, 83-93.

Lamy, F., Kaiser, J., Arz, H.W., Hebbeln, D., Ninnemann, U., Timm, O., Timmermann, A., Toggweiler, J.R., 2007. Modulation of the bipolar seesaw in the Southeast Pacific during Termination 1. Earth and Planetary Science Letters 259, 400-413.

Lamy, F., Kaiser, J., Ninnemann, U., Hebbeln, D., Arz, H.W., Stoner, J., 2004. Antarctic Timing of Surface Water Changes off Chile and Patagonian Ice Sheet Response. Science 304, 1959-1962.

Large, W.G., Yeager, S.G., 2009. The global climatology of an interannually varying air–sea flux data set. Climate Dynamics 33, 341-364.

Laskar, J., Robutel, P., Joutel, F., Gastineau, M., Correia, A.C.M., Levrard, B., 2004. A long term numerical solution for the insolation quantities of the Earth. Astron. Astrophys 428, 261-285.

Le, J., Thunell, R.C., 1996. Modelling planktic foraminiferal assemblage changes and application to sea surface temperature estimation in the western equatorial Pacific Ocean. Marine Micropaleontology 28, 211-229.

Lea, D.W., Mashiotta, T.A., Spero, H.J., 1999. Controls on magnesium and strontium uptake in planktonic foraminifera determined by live culturing. Geochimica et Cosmochimica Acta 63, 2369-2379.

Leduc, G., Sachs, J.P., Kawka, O.E., Schneider, R.R., 2013. Holocene changes in eastern equatorial Atlantic salinity as estimated by water isotopologues. Earth and Planetary Science Letters 362, 151-162.

Leduc, G., Vidal, L., Tachikawa, K., Bard, E., 2009. ITCZ rather than ENSO signature for abrupt climate changes across the tropical Pacific? Quaternary Research 72, 123-131.

Leduc, G., Vidal, L., Tachikawa, K., Rostek, F., Sonzogni, C., Beaufort, L., Bard, E., 2007. Moisture transport across Central America as a positive feedback on abrupt climatic changes. Nature 445, 908-911.

Lee, K.E., Kim, J.-H., Wilke, I., Helmke, P., Schouten, S., 2008. A study of the alkenone, TEX_{86}, and planktonic foraminifera in the Benguela Upwelling System: Implications for past sea surface temperature estimates. Geochemistry, Geophysics, Geosystems 9, Q10019.

Lee, S.-Y., Chiang, J.C.H., Matsumoto, K., Tokos, K.S., 2011. Southern Ocean wind response to North Atlantic cooling and the rise in atmospheric CO_2: Modeling perspective and paleoceanographic implications. Paleoceanography 26, PA1214.

LeGrande, A.N., Schmidt, G.A., 2006. Global gridded data set of the oxygen isotopic composition in seawater. Geophysical Research Letters 33, L12604.

Levi, C., Labeyrie, L., Bassinot, F., Guichard, F., Cortijo, E., Waelbroeck, C., Caillon, N., Duprat, J., de Garidel-Thoron, T., Elderfield, H., 2007. Low-latitude hydrological cycle and rapid climate changes during the last deglaciation. Geochem. Geophys. Geosyst. 8, Q05N12.

Lewis, S.C., LeGrande, A.N., Kelley, M., Schmidt, G.A., 2010. Water vapour source impacts on oxygen isotope variability in tropical precipitation during Heinrich events. Clim. Past 6, 325-343.

Libes, S.M., 2009. Introduction to Marine Biogeochemistry. Elsevier, 2nd edition.

Lippold, J., Luo, Y., Francois, R., Allen, S.E., Gherardi, J., Pichat, S., Hickey, B., Schulz, H., 2012. Strength and geometry of the glacial Atlantic Meridional Overturning Circulation. Nature Geosci 5, 813-816.

Lisiecki, L.E., Raymo, M.E., 2005. A Pliocene-Pleistocene stack of 57 globally distributed benthic $\delta^{18}O$ records. Paleoceanography 20, PA1003.

Lisiecki, L.E., Raymo, M.E., Curry, W.B., 2008. Atlantic overturning responses to Late Pleistocene climate forcings. Nature 456, 85-88.

Locarnini, R.A., Mishonov, A.V., Antonov, J.I., Boyer, T.P., Garcia, H.E., Baranova, O.K., Zweng, M.M., Johnson, D.R., 2010. World Ocean Atlas 2009 Volume 1: Temperature In: Levitus, S. (Ed), NOAA Atlas NESDIS 68, U.S. Government Printing Office, Washington, D.C., 184 pp.

Lohmann, G., 2003. Atmospheric and oceanic freshwater transport during weak Atlantic overturning circulation. Tellus A 55, 438-449.

Lohmann, G.P., 1995. A model for variation in the chemistry of planktonic foraminifera due to secondary calcification and selective dissolution. Paleoceanography 10, 445-457.

Lopes dos Santos, R.A., Prange, M., Castañeda, I.S., Schefuß, E., Mulitza, S., Schulz, M., Niedermeyer, E.M., Sinninghe Damsté, J.S., Schouten, S., 2010. Glacial–interglacial variability in Atlantic meridional overturning circulation and thermocline adjustments in the tropical North Atlantic. Earth and Planetary Science Letters 300, 407-414.

Loveday, B.R., Durgadoo, J.V., Reason, C.J.C., Biastoch, A.a., Penven, P., in press. Decoupling of the Agulhas Current from the Agulhas Leakage. Journal of Physical Oceanography.

Lowe, J.J., and Walker, M.J.C., 1997. Reconstructing Quaternary Environments. Longman Ltd. , 446

Luthi, D., Le Floch, M., Bereiter, B., Blunier, T., Barnola, J.-M., Siegenthaler, U., Raynaud, D., Jouzel, J., Fischer, H., Kawamura, K., Stocker, T.F., 2008. High-resolution carbon dioxide concentration record 650,000-800,000 years before present. Nature 453, 379-382.

Lutjeharms, J.R.E., 1988. Remote sensing corroboration of retroflection of the East Madagascar Current. Deep Sea Research Part A. Oceanographic Research Papers 35, 2045-2050.

Lutjeharms, J.R.E., 2006. Three decades of research on the greater Agulhas Current. Ocean Sci. Discuss. 3, 939-995.

Lutjeharms, J.R.E., Ansorge, I.J., 2001. The Agulhas Return Current. Journal of Marine Systems 30, 115-138.

Lutjeharms, J.R.E., de Ruijter, W.P.M., 1996. The influence of the Agulhas Current on the adjacent coastal ocean: possible impacts of climate change. Journal of Marine Systems 7, 321-336.

Lutjeharms, J.R.E., Valentine, H.R., 1984. Southern ocean thermal fronts south of Africa. Deep Sea Research Part A. Oceanographic Research Papers 31, 1461-1475.

Lutjeharms, J.R.E., Van Ballegooyen, R.C., 1988. The Retroflection of the Agulhas Current. Journal of Physical Oceanography 18, 1570-1583.

Lutze, G.F., Thiel, H., 1989. Epibenthic foraminifera from elevated microhabitats; *Cibicidoides wuellerstorfi* and *Planulina ariminensis*. The Journal of Foraminiferal Research 19, 153-158.

Lynch-Stieglitz, J., Adkins, J.F., Curry, W.B., Dokken, T., Hall, I.R., Herguera, J.C., Hirschi, J.J.-M., Ivanova, E.V., Kissel, C., Marchal, O., Marchitto, T.M., McCave, I.N., McManus, J.F., Mulitza, S., Ninnemann, U., Peeters, F., Yu, E.-F., Zahn, R., 2007. Atlantic Meridional Overturning Circulation During the Last Glacial Maximum. Science 316, 66-69.

Lynch-Stieglitz, J., Schmidt, M.W., Gene Henry, L., Curry, W.B., Skinner, L.C., Mulitza, S., Zhang, R., Chang, P., 2014. Muted change in Atlantic overturning circulation over some glacial-aged Heinrich events. Nature Geosci 7, 144-150.

Lynch-Stieglitz, J., Stocker, T.F., Broecker, W.S., and Fairbanks, R.G.T., 1995. The influence of air-sea exchange on the isotopic composition of oceanic carbon - observations and modeling. Global Biogeochem. Cy., 9, 653-665.

Mackensen, A., 2001. Oxygen and carbon stable isotope tracers of Weddell Sea water masses: new data and some paleoceanographic implications. Deep Sea Research Part I: Oceanographic Research Papers 48, 1401-1422.

Mackensen, A., Bickert, T., 1999. Stable Carbon Isotopes in Benthic Foraminifera: Proxies for Deep and Bottom Water Circulation and New Production, in: Fischer, G., Wefer, G. (Eds.), Use of Proxies in Paleoceanography. Springer Berlin Heidelberg, pp. 229-254.

Mackensen, A., Hubberten, H.W., Bickert, T., Fischer, G., Fütterer, D., 1993. The $\delta^{13}C$ in benthic foraminiferal tests of *Fontbotia wuellerstorfi* (Schwager) relative to the $\delta^{13}C$ of dissolved inorganic carbon in southern ocean deep water: implications for glacial ocean circulation models. Paleoceanography 8, 587-610.

Mangerud, J., 1972. Radiocarbon dating of marine shells, including a discussion of apparent age of Recent shells from Norway. Boreas 1, 143-172.

Mann, M.E.a., Lees, J.M., 1996. Robust estimation of background noise and signal detection in climatic time series. Climatic Change 33, 409-445.

Marchal, O., François, R., Stocker, T.F., Joos, F., 2000. Ocean thermohaline circulation and sedimentary $^{231}Pa/^{230}Th$ ratio. Paleoceanography 15, 625-641.

Marchitto, T.M., Broecker, W.S., 2006. Deep water mass geometry in the glacial Atlantic Ocean: A review of constraints from the paleonutrient proxy Cd/Ca. Geochem. Geophys. Geosyst. 7, Q12003.

Marino, G., Zahn, R., Ziegler, M., Purcell, C., Knorr, G., Hall, I.R., Ziveri, P., Elderfield, H., 2013. Agulhas salt-leakage oscillations during abrupt climate changes of the Late Pleistocene. Paleoceanography 28, 599-606.

Marshall, B.J., Thunell, R.C., Henehan, M.J., Astor, Y., Wejnert, K.E., 2013. Planktonic foraminiferal area density as a proxy for carbonate ion concentration: A calibration study using the Cariaco Basin ocean time series. Paleoceanography 28, 363-376.

Marshall, J., Schott, F., 1999. Open-ocean convection: Observations, theory, and models. Reviews of Geophysics 37, 1-64.

Marsland, S.J., Haak, H., Jungclaus, J.H., Latif, M., Röske, F., 2003. The Max-Planck-Institute global ocean/sea ice model with orthogonal curvilinear coordinates. Ocean Modelling 5, 91-127.

Martínez-Méndez, G., Molyneux, E.G., Hall, I.R., Zahn, R., 2009. Variable water column structure of the South Atlantic on glacial–interglacial time scales. Quaternary Science Reviews 28, 3379-3387.

Martínez-Méndez, G., Zahn, R., Hall, I.R., Peeters, F.J.C., Pena, L.D., Cacho, I., Negre, C., 2010. Contrasting multiproxy reconstructions of surface ocean hydrography in the Agulhas Corridor and implications for the Agulhas Leakage during the last 345,000 years. Paleoceanography 25, PA4227.

Martínez-Méndez, G., Zahn, R., Hall, I.R., Pena, L.D., Cacho, I., 2008. 345,000-year-long multi-proxy records off South Africa document variable contributions of Northern versus Southern Component Water to the Deep South Atlantic. Earth and Planetary Science Letters 267, 309-321.

Martinez, J.I., Taylor, L., De Deckker, P., Barrows, T., 1998. Planktonic foraminifera from the eastern Indian Ocean: distribution and ecology in relation to the Western Pacific Warm Pool (WPWP). Marine Micropaleontology 34, 121-151.

Martrat, B., Grimalt, J.O., Shackleton, N.J., de Abreu, L., Hutterli, M.A., Stocker, T.F., 2007. Four Climate Cycles of Recurring Deep and Surface Water Destabilizations on the Iberian Margin. Science 317, 502-507.

Matsumoto, K., Lynch-Stieglitz, J., Anderson, R.F., 2001. Similar glacial and Holocene Southern Ocean hydrography. Paleoceanography 16, 445-454.

McCave, I.N., Crowhurst, S.J., Kuhn, G., Hillenbrand, C.D., Meredith, M.P., 2014. Minimal change in Antarctic Circumpolar Current flow speed between the last glacial and Holocene. Nature Geosci 7, 113-116.

McCave, I.N., Hall, I.R., 2006. Size sorting in marine muds: Processes, pitfalls, and prospects for paleoflow-speed proxies. Geochemistry, Geophysics, Geosystems 7, Q10N05.

McCorkle, D.C., Emerson, S.R., Quay, P.D., 1985. Stable carbon isotopes in marine pore waters. Earth and Planetary Science Letters 74, 13-26.

McCorkle, D.C., Heggie, D.T., Veeh, H.H., 1998. Glacial and Holocene stable isotope distributions in the southeastern Indian Ocean. Paleoceanography 13, 20-34.

McDonagh, E.L., Bryden, H.L., King, B.A., Sanders, R.J., 2008. The circulation of the Indian Ocean at 32 °S. Prog. Oceanogr. 79, 20-36.

McIntyre, A., Ruddiman, W.F., Karlin, K., Mix, A.C., 1989. Surface water response of the equatorial Atlantic Ocean to orbital forcing. Paleoceanography 4, 19-55.

McManus, J.F., Francois, R., Gherardi, J.M., Keigwin, L.D., Brown-Leger, S., 2004. Collapse and rapid resumption of Atlantic meridional circulation linked to deglacial climate changes. Nature 428, 834-837.

McManus, J.F., Oppo, D.W., Cullen, J.L., 1999. A 0.5-Million-Year Record of Millennial-Scale Climate Variability in the North Atlantic. Science 283, 971-975.

Meckler, A.N., Clarkson, M.O., Cobb, K.M., Sodemann, H., Adkins, J.F., 2012. Interglacial Hydroclimate in the Tropical West Pacific Through the Late Pleistocene. Science 336, 1301-1304.

Mekik, F., 2014. Radiocarbon dating of planktonic foraminifer shells: A cautionary tale. Paleoceanography 29, 2013PA002532.

Mekik, F., François, R., Soon, M., 2007. A novel approach to dissolution correction of Mg/Ca–based paleothermometry in the tropical Pacific. Paleoceanography 22, PA3217.

Michel, E., Labeyrie, L.D., Duplessy, J.-C., Gorfti, N., Labracherie, M., Turon, J.-L., 1995. Could deep subantarctic convection feed the world deep basins during the Last Glacial Maximum? Paleoceanography 10, 927-941.

Middelburg, J.J., van der Weijden, C.H., Woittiez, J.R.W., 1988. Chemical processes affecting the mobility of major, minor and trace elements during weathering of granitic rocks. Chemical Geology 68, 253-273.

Milanković, M., 1941. Kanon der Erdbestrahlung und seine Andwendung auf das Eiszeitenproblem. Royal Serbian Academy Special Publication, Belgrade, 633.

Milankovitch, M., 1930. Mathematische Klimalehre und Astronomische Theorie der Klimaschwankungen. Handbuch der Klimalogie, Borntrager Berlin Band 1

Mix, A.C., Le, J., Shackleton, N.J., 1995. Benthic foraminiferal stable isotope stratigraphy of Site 846: 0-1.8 Ma. Proc. Ocean Drill. Program Sci. Results 138, 839-854.

Mix, A.C., Pisias, N.G., Zahn, R., Rugh, W., Lopez, C., Nelson, K., 1991. Carbon 13 in Pacific Deep and Intermediate Waters, 0-370 ka: Implications for Ocean Circulation and Pleistocene CO_2. Paleoceanography 6, 205-226.

Mohtadi, M., Steinke, S., Groeneveld, J., Fink, H.G., Rixen, T., Hebbeln, D., Donner, B., Herunadi, B., 2009. Low-latitude control on seasonal and interannual changes in planktonic foraminiferal flux and shell geochemistry off south Java: A sediment trap study. Paleoceanography 24, PA1201.

Molyneux, E.G., Hall, I.R., Zahn, R., Diz, P., 2007. Deep water variability on the southern Agulhas Plateau: Interhemispheric links over the past 170 ka. Paleoceanography 22, PA4209.

Moura, A.D., Shukla, J., 1981. On the Dynamics of Droughts in Northeast Brazil: Observations, Theory and Numerical Experiments with a General Circulation Model. Journal of the Atmospheric Sciences 38, 2653-2675.

Mucci, A., 1987. Influence of temperature on the composition of magnesium calcite overgrowths precipitated from seawater. Geochimica et Cosmochimica Actaet 51, 1977-1984.

Mudelsee, M., 2003. Estimating Pearson's Correlation Coefficient with Bootstrap Confidence Interval from Serially Dependent Time Series. Mathematical Geology 35, 651-665.

Mulitza, S., Prange, M., Stuut, J.-B., Zabel, M., von Dobeneck, T., Itambi, A.C., Nizou, J., Schulz, M., Wefer, G., 2008. Sahel megadroughts triggered by glacial slowdowns of Atlantic meridional overturning. Paleoceanography 23, PA4206.

Müller, P.J., Kirst, G., Ruhland, G., von Storch, I., Rosell-Melé, A., 1998. Calibration of the alkenone paleotemperature index $U_{37}^{K'}$ based on core-tops from the eastern South Atlantic and the global ocean (60°N-60°S). Geochimica et Cosmochimica Acta 62, 1757-1772.

Murray, 1897. On the distribution of the pelagic Foraminifera at the surface and on the floor of the ocean. Journal of Natural Sciences 11, 17-27.

Naqvi, W.A., Charles, C.D., Fairbanks, R.G., 1994. Carbon and oxygen isotopic records of benthic foraminifera from the Northeast Indian Ocean: implications on glacial-interglacial atmospheric CO_2 changes. Earth and Planetary Science Letters 121, 99-110.

Negre, C., Zahn, R., Thomas, A.L., Masque, P., Henderson, G.M., Martinez-Mendez, G., Hall, I.R., Mas, J.L., 2010. Reversed flow of Atlantic deep water during the Last Glacial Maximum. Nature 468, 84-88.

NGRIP, 2004. High-resolution record of Northern Hemisphere climate extending into the last interglacial period. Nature 431, 147-151.

Nicholson, S.E., 2000. The nature of rainfall variability over Africa on time scales of decades to millenia. Global and Planetary Change 26, 137-158.

Niemi, T.M., Ben-Avraham, Z., Hartnady, C.J.H., Reznikov, M., 2000. Post-Eocene seismic stratigraphy of the deep ocean basin adjacent to the southeast African continental margin: a record of geostrophic bottom current systems. Marine Geology 162, 237-258.

Ninnemann, U.S., Charles, C.D., 2002. Changes in the mode of Southern Ocean circulation over the last glacial cycle revealed by foraminiferal stable isotopic variability. Earth and Planetary Science Letters 201, 383-396.

Noble, T.L., Piotrowski, A.M., Robinson, L.F., McManus, J.F., Hillenbrand, C.-D., Bory, A.J.M., 2012. Greater supply of Patagonian-sourced detritus and transport by the ACC to the Atlantic sector of the Southern Ocean during the last glacial period. Earth and Planetary Science Letters 317–318, 374-385.

Nof, D., Zharkov, V., Ortiz, J., Paldor, N., Arruda, W., Chassignet, E., 2011. The arrested Agulhas retroflection. Journal of Marine Research 69, 659-691.

Nürnberg, D., Bijma, J., Hemleben, C., 1996. Assessing the reliability of magnesium in foraminiferal calcite as a proxy for water mass temperatures. Geochimica et Cosmochimica Acta 60, 803-814.

Oomori, T., Kaneshima, H., Maezato, Y., 1987. Distribution coefficient of Mg^{2+} ions between calcite and solution at 10-50 °C. Marine Chemistry 20, 327-336.

Oppo, D.W., and Curry, W.B., 2012. Deep Atlantic Circulation During the Last Glacial Maximum and Deglaciation. Nature Education Knowledge 3.

Oppo, D.W., Horowitz, M., 2000. Glacial deep water geometry: South Atlantic benthic foraminiferal Cd/Ca and $\delta^{13}C$ evidence. Paleoceanography 15, 147-160.

Orsi, A.H., Whitworth, T., Nowlin, W.D., 1995. On the meridional extent and fronts of the Antarctic Circumpolar Current. Deep Sea Research Part I: Oceanographic Research Papers 42, 641-673.

Otto-Bliesner, B.L., Brady, E.C., Clauzet, G., Tomas, R., Levis, S., Kothavala, Z., 2006. Last Glacial Maximum and Holocene Climate in CCSM3. Journal of Climate 19, 2526-2544.

Pahnke, K., Goldstein, S.L., Hemming, S.R., 2008. Abrupt changes in Antarctic Intermediate Water circulation over the past 25,000 years. Nature Geosci 1, 870-874.

Pahnke, K., Zahn, R., 2005. Southern Hemisphere Water Mass Conversion Linked with North Atlantic Climate Variability. Science 307, 1741-1746.

Paillard, D., Labeyrie, L., Yiou, P., 1996. Macintosh Program performs time-series analysis. Eos, Transactions American Geophysical Union 77, 379-379.

Palastanga, V., van Leeuwen, P.J., de Ruijter, W.P.M., 2006. A link between low-frequency mesoscale eddy variability around Madagascar and the large-scale Indian Ocean variability. Journal of Geophysical Research: Oceans 111, C09029.

Parnell, A.C., Buck, C.E., Doan, T.K., 2011. A review of statistical chronology models for high-resolution, proxy-based Holocene palaeoenvironmental reconstruction. Quaternary Science Reviews 30, 2948-2960.

Partridge, T.C., de Menocal, P.B., Lorentz, S.A., Paiker, M.J., Vogel, J.C., 1997. Orbital forcing of climate over South Africa: A 200,000-year rainfall record from the pretoria saltpan. Quaternary Science Reviews 16, 1125-1133.

Pausata, F.S.R., Battisti, D.S., Nisancioglu, K.H., Bitz, C.M., 2011. Chinese stalagmite $\delta^{18}O$ controlled by changes in the Indian monsoon during a simulated Heinrich event. Nature Geosci 4, 474-480.

Pearson, P.N., 2012. Oxygen isotopes in foraminifera: Overview and Historical review. Paleontological Society Papers 18, 1-38.

Peeters, F.J.C., Acheson, R., Brummer, G.-J.A., de Ruijter, W.P.M., Schneider, R.R., Ganssen, G.M., Ufkes, E., Kroon, D., 2004. Vigorous exchange between the Indian and Atlantic oceans at the end of the past five glacial periods. Nature 430, 661-665.

Peeters, F.J.C., Brummer, G.-J.A., 2002. The seasonal and vertical distribution of living planktic foraminifera in the NW Arabian Sea. Geological Society, London, Special Publications 195, 463-497.

Peeters, F.J.C., Brummer, G.-J.A., Ganssen, G., 2002. The effect of upwelling on the distribution and stable isotope composition of Globigerina bulloides and Globigerinoides ruber (planktic foraminifera) in modern surface waters of the NW Arabian Sea. Global and Planetary Change 34, 269-291.

Pena, L.D., Calvo, E., Cacho, I., Eggins, S., Pelejero, C., 2005. Identification and removal of Mn-Mg-rich contaminant phases on foraminiferal tests: Implications for Mg/Ca past temperature reconstructions. Geochem. Geophys. Geosyst. 6, Q09P02.

Pena, L.D., Goldstein, S.L., Hemming, S.R., Jones, K.M., Calvo, E., Pelejero, C., Cacho, I., 2013. Rapid changes in meridional advection of Southern Ocean intermediate waters to the tropical Pacific during the last 30 kyr. Earth and Planetary Science Letters 368, 20-32.

Penven, P., Marchesiello, P., Debreu, L., Lefèvre, J., 2008. Software tools for pre- and post-processing of oceanic regional simulations. Environmental Modelling & Software 23, 660-662.

Peterson, L.C., Haug, G.H., Hughen, K.A., Röhl, U., 2000. Rapid Changes in the Hydrologic Cycle of the Tropical Atlantic During the Last Glacial. Science 290, 1947-1951.

Peterson, L.C., Prell, W.L., 1985. Carbonate dissolution in Recent sediments of the eastern equatorial Indian Ocean: Preservation patterns and carbonate loss above the lysocline. Marine Geology 64, 259-290.

Pflaumann, U., Duprat, J., Pujol, C., Labeyrie, L.D., 1996. SIMMAX: A modern analog technique to deduce Atlantic sea surface temperatures from planktonic foraminifera in deep-sea sediments. Paleoceanography 11, 15-35.

Pilcher, J.R., 1991. Radiocarbon dating for the Quaternary scientist. Quaternary Proceedings 1, 27-34.

Piotrowski, A.M., Galy, A., Nicholl, J.A.L., Roberts, N., Wilson, D.J., Clegg, J.A., Yu, J., 2012. Reconstructing deglacial North and South Atlantic deep water sourcing using foraminiferal Nd isotopes. Earth and Planetary Science Letters 357–358, 289-297.

Piotrowski, A.M., Goldstein, S.L., Hemming, S.R., Fairbanks, R.G., 2004. Intensification and variability of ocean thermohaline circulation through the last deglaciation. Earth and Planetary Science Letters 225, 205-220.

Piotrowski, A.M., Goldstein, S.L., Hemming, S.R., Fairbanks, R.G., 2005. Temporal Relationships of Carbon Cycling and Ocean Circulation at Glacial Boundaries. Science 307, 1933-1938.

Potts, R., 1998. Environmental hypotheses of hominin evolution. American journal of physical anthropology Suppl 27, 93-136.

Prahl, F.G., Wakeham, S.G., 1987. Calibration of unsaturation patterns in long-chain ketone compositions for palaeotemperature assessment. Nature 330, 367-369.

Pudsey, C.J., Howe, J.A., 1998. Quaternary history of the Antarctic Circumpolar Current: evidence from the Scotia Sea. Marine Geology 148, 83-112.

Purcell, C., Knorr, G., Hall, I.R., Lohmann, G., Stepanek, C., in review. Warm and cold water route gateway transport changes during abrupt climate shifts. Paleoceanography.

Purcell, C., Simon, M.H., Knorr, G., Hall, I.R., Stepanek, C., Ziegler, M., Lohmann, G., in prep. Similar pre-industrial and Last Glacial Maximum rates of Agulhas Leakage. .

Qian, W., Deng, Y., Zhu, Y., Dong, W., 2002. Demarcating the worldwide monsoon. Theor Appl Climatol 71, 1-16.

Rackebrandt, N., Kuhnert, H., Groeneveld, J., Bickert, T., 2011. Persisting maximum Agulhas leakage during MIS 14 indicated by massive Ethmodiscus oozes in the subtropical South Atlantic. Paleoceanography 26, PA3202.

Rahmstorf, S., 1995. Bifurcations of the Atlantic thermohaline circulation in response to changes in the hydrological cycle. Nature 378, 145-149.

Rahmstorf, S., 1996. On the freshwater forcing and transport of the Atlantic thermohaline circulation. Climate Dynamics 12, 799-811.

Rahmstorf, S., 2002. Ocean circulation and climate during the past 120,000 years. Nature 419, 207-214.

Raj, R.P., Peter, B.N., Pushpadas, D., 2010. Oceanic and atmospheric influences on the variability of phytoplankton bloom in the Southwestern Indian Ocean. Journal of Marine Systems 82, 217-229.

Ramsey, M.H., Potts, P.J., Webb, P.C., Watkins, P., Watson, J.S., Coles, B.J., 1995. An objective assessment of analytical method precision: comparison of ICP-AES and XRF for the analysis of silicate rocks. Chemical Geology 124, 1-19.

Rau, A.J., Rogers, J., Lutjeharms, J.R.E., Giraudeau, J., Lee-Thorp, J.A., Chen, M.T., Waelbroeck, C., 2002. A 450-kyr record of hydrological conditions on the western Agulhas Bank Slope, south of Africa. Marine Geology 180, 183-201.

Ravelo, A.C., Fairbanks, R.G., 1992. Oxygen Isotopic Composition of Multiple Species of Planktonic Foraminifera: Recorders of the Modern Photic Zone Temperature Gradient. Paleoceanography 7, 815-831.

Raven, J.A., Falkowski, P.G., 1999. Oceanic sinks for atmospheric CO_2. Plant, Cell & Environment 22, 741-755.

Raymo, M.E., 1997. The timing of major climate terminations. Paleoceanography 12, 577-585.

Raymo, M.E., Oppo, D.W., Flower, B.P., Hodell, D.A., McManus, J.F., Venz, K.A., Kleiven, K.F., McIntyre, K., 2004. Stability of North Atlantic water masses in face of pronounced climate variability during the Pleistocene. Paleoceanography 19, PA2008.

Reason, C.J.C., 2001. Evidence for the Influence of the Agulhas Current on Regional Atmospheric Circulation Patterns. Journal of Climate 14, 2769-2778.

Reason, C.J.C., Mulenga, H., 1999. Relationships between South African rainfall and SST anomalies in the Southwest Indian Ocean. International Journal of Climatology 19, 1651-1673.

Regenberg, M., Nürnberg, D., Steph, S., Groeneveld, J., Garbe-Schönberg, D., Tiedemann, R., Dullo, W.-C., 2006. Assessing the effect of dissolution on planktonic foraminiferal Mg/Ca ratios: Evidence from Caribbean core tops. Geochemistry, Geophysics, Geosystems 7, Q07P15.

Regenberg, M., Regenberg, A., Garbe-Schönberg, D., Lea, D.W., 2014. Global dissolution effects on planktonic foraminiferal Mg/Ca ratios controlled by the calcite-saturation state of bottom waters. Paleoceanography 29, 127-142.

Reid, J.L., 1989. On the total geostrophic circulation of the South Atlantic Ocean: Flow patterns, tracers, and transports. Progress in Oceanography 23 149-244.

Reimer, P.J., Baillie, M.G.L., Bard, E., Bayliss, A., Beck, J.W., Blackwell, P.G., Ramsey, C.B., Buck, C.E., Burr, G.S., Edwards, R.L., Friedrich, M., Grootes, P.M., Guilderson, T.P., Hajdas, I., Heaton,

T.J., Hogg, A.G., Hughen, K.A., Kaiser, K.F., Kromer, B., McCormac, F.G., Manning, S.W., Reimer, R.W., Richards, D.A., Southon, J.R., Talamo, S., Turney, C.S.M., van der Plicht, J., Weyhenmeyer, C.E., 2009. IntCal09 and Marine09 Radiocarbon Age Calibration Curves, 0-50,000 Years cal BP. Radiocarbon.

Renold, M., Raible, C.C., Yoshimori, M., Stocker, a.T.F., 2010. Simulated resumption of the North Atlantic meridional overturning circulation-Slow basin-wide advection and abrupt local convection. Quat. Sci. Rev. 29, 101-112.

Renssen, H., Seppä, H., Crosta, X., Goosse, H., Roche, D.M., 2012. Global characterization of the Holocene Thermal Maximum. Quaternary Science Reviews 48, 7-19.

Reznikov, M., Ben-Avraham, Z., Hartnady, C., Niemi, T.M., 2005. Structure of the Transkei Basin and Natal Valley, Southwest Indian Ocean, from seismic reflection and potential field data. Tectonophysics 397, 127-141.

Rhodes, M.K., Carroll, A.R., Pietras, J.T., Beard, B.L., Johnson, C.M., 2002. Strontium isotope record of paleohydrology and continental weathering, Eocene Green River Formation, Wyoming. Geology 30, 167-170.

Rial, J.A., 1999. Pacemaking the Ice Ages by Frequency Modulation of Earth's Orbital Eccentricity. Science 285, 564-568.

Richardson, P.L., 2007. Agulhas leakage into the Atlantic estimated with subsurface floats and surface drifters. Deep Sea Research Part I: Oceanographic Research Papers 54, 1361-1389.

Richardson, P.L., Lutjeharms, J.R.E., Boebel, O., 2003. Introduction to the ''Inter-ocean exchange around southern Africa''. Deep Sea Research Part II: Topical Studies in Oceanography 50, 1-12.

Richter, T.O., Van der Gaast, S., Koster, B., Vaars, A., Gieles, R., De Stigter, H., De Haas, H., vanWeering, T.C.E., 2006. The Avaatech XRF core scanner: technical description and applications to NE Atlantic sediments. In: Rothwell, R.G. (Ed.), New Techniques in Sediment Core Analysis. Special Publication,Geological Society, London, 267

39-50.

Rickaby, R.E.M., Bard, E., Sonzogni, C., Rostek, F., Beaufort, L., Barker, S., Rees, G., Schrag, D.P., 2007. Coccolith chemistry reveals secular variations in the global ocean carbon cycle. Earth and Planetary Science Letters 253, 83.

Ridderinkhof, H., van der Werf, P.M., Ullgren, J.E., van Aken, H.M., van Leeuwen, P.J., de Ruijter, W.P.M., 2010. Seasonal and interannual variability in the Mozambique Channel from moored current observations. Journal of Geophysical Research: Oceans 115, C06010.

Robinson, L.F., Adkins, J.F., Keigwin, L.D., Southon, J., Fernandez, D.P., Wang, S.-L., Scheirer, D.S., 2005. Radiocarbon Variability in the Western North Atlantic During the Last Deglaciation. Science 310, 1469-1473.

Roeckner, E., Brokopf, R., Esch, M., Giorgetta, M., Hagemann, S., Kornblueh, L., Manzini, E., Schlese, U., Schulzweida, U., 2006. Sensitivity of Simulated Climate to Horizontal and Vertical Resolution in the ECHAM5 Atmosphere Model. Journal of Climate 19, 3771-3791.

Rogers, J., 1987. Seismic, bathymetric and photographic evidence of widespread erosion and a manganese-nodule pavement along the continental rise of the Southeast Cape Basin. Marine Geology 78, 57-76.

Rohling, E.J., 2000. Paleosalinity: confidence limits and future applications. Marine Geology 163, 1-11.

Rojas, M., Moreno, P., Kageyama, M., Crucifix, M., Hewitt, C., Abe-Ouchi, A., Ohgaito, R., Brady, E., Hope, P., 2009. The Southern Westerlies during the last glacial maximum in PMIP2 simulations. Climate Dynamics 32, 525-548.

Roman, R.E., Lutjeharms, J.R.E., 2009. Red Sea Intermediate Water in the source regions of the Agulhas Current. Deep Sea Research Part I: Oceanographic Research Papers 56, 939-962.

Rosenthal, Y., Boyle, E.A., 1993. Factors controlling the fluoride content of planktonic foraminifera: An evaluation of its paleoceanographic applicability. Geochimica et Cosmochimica Acta 57, 335-346.

Rosenthal, Y., Boyle, E.A., Labeyrie, L., 1997. Last Glacial Maximum paleochemistry and deepwater circulation in the Southern Ocean: Evidence from foraminiferal cadmium. Paleoceanography 12, 787-796.

Rosenthal, Y., Lohmann, G.P., 2002. Accurate estimation of sea surface temperatures using dissolution-corrected calibrations for Mg/Ca paleothermometry. Paleoceanography 17, 1044.

Rosenthal, Y., Lohmann, G.P., Lohmann, K.C., Sherrell, R.M., 2000. Incorporation and preservation of Mg in Globigerinoides sacculifer: implications for reconstructing the temperature and $^{18}O/^{16}O$ of seawater. Paleoceanography 15, 135-145.

Rosenthal, Y., Perron-Cashman, S., Lear, C.H., Bard, E., Barker, S., Billups, K., Bryan, M., Delaney, M.L., deMenocal, P.B., Dwyer, G.S., Elderfield, H., German, C.R., Greaves, M., Lea, D.W., Marchitto, T.M., Pak, D.K., Paradis, G.L., Russell, A.D., Schneider, R.R., Scheiderich, K., Stott, L., Tachikawa, K., Tappa, E., Thunell, R., Wara, M., Weldeab, S., Wilson, P.A., 2004. Interlaboratory comparison study of Mg/Ca and Sr/Ca measurements in planktonic foraminifera for paleoceanographic research. Geochemistry, Geophysics, Geosystems 5, Q04D09.

Rossignol-Strick, M., 1983. African monsoons, an immediate climate response to orbital insolation. Nature 304, 46-49.

Rothwell, R.G.a.R., F.R., 2006. New techniques in sediment core analysis: an introduction. In: Rothwell, R.G. (Ed.), New Techniques in Sediment Core Analysis. Special Publication,. Geological Society, London. 267, 1-29.

Rouault, M., Lutjeharms, J., 2000. Air–sea exchange over an Agulhas eddy at the subtropical convergence. Global Atmos. Ocean Syst 7, 125-150.

Rouault, M., Penven, P., Pohl, B., 2009. Warming in the Agulhas Current system since the 1980's. Geophys. Res. Lett. 36, L12602.

Ruddiman, W.F., McIntyre, A., 1981. Oceanic Mechanisms for Amplification of the 23,000-Year Ice-Volume Cycle. Science 212, 617-627.

Rühs, S., Durgadoo, J.V., Behrens, E., Biastoch, A., 2013. Advective timescales and pathways of Agulhas leakage. Geophysical Research Letters 40, 3997-4000.

Ruiz, I., Martínez-Méndez, G., Hebbeln, D., Mohtadi, M., 2013. Evaluating the size effect on the stable isotopic composition of foraminifera *Fonbotia wuellerstorfi* and *Cibicidoides kullenbergi*. 11th INTERNATIONAL CONFERENCE ON PALEOCEANOGRAPHY 1-6 September, 2013. Sitges - Barcelona.

Russell, A.D., Emerson, S., Nelson, B.K., Erez, J., Lea, D.W., 1994. Uranium in foraminiferal calcite as a recorder of seawater uranium concentrations. Geochimica et Cosmochimica Acta 58, 671-681.

Rutberg, R.L., Hemming, S.R., Goldstein, S.L., 2000. Reduced North Atlantic Deep Water flux to the glacial Southern Ocean inferred from neodymium isotope ratios. Nature 405, 935-938.

Rutberg, R.L., Peacock, S.L., 2006. High-latitude forcing of interior ocean $\delta^{13}C$. Paleoceanography 21, PA2012.

Sabine, C.L., Feely, R.A., Gruber, N., Key, R.M., Lee, K., Bullister, J.L., Wanninkhof, R., Wong, C.S., Wallace, D.W.R., Tilbrook, B., Millero, F.J., Peng, T.-H., Kozyr, A., Ono, T., Rios, A.F., 2004. The Oceanic Sink for Anthropogenic CO2. Science 305, 367-371.

Saetre, R., Da Silva, A.J., 1984. The circulation of the Mozambique channel. Deep Sea Research Part A. Oceanographic Research Papers 31, 485-508.

Saher, M.H., Rostek, F., Jung, S.J.A., Bard, E., Schneider, R.R., Greaves, M., Ganssen, G.M., Elderfield, H., Kroon, D., 2009. Western Arabian Sea SST during the penultimate interglacial: A comparison of $U_{37}^{K'}$ and Mg/Ca paleothermometry. Paleoceanography 24, PA2212.

Schaetzl, R.J., and Anderson, S., 2005. Soils: Genesis and Morphology. Cambridge University Press, Cambridge.

Schefuß, E., Kuhlmann, H., Mollenhauer, G., Prange, M., Patzold, J., 2011. Forcing of wet phases in southeast Africa over the past 17,000 years. Nature 480, 509-512.

Schefuß, E., Schouten, S., Schneider, R.R., 2005. Climatic controls on central African hydrology during the past 20,000 years. Nature 437, 1003-1006.

Schlitzer, R., 2012. Ocean Data View, edited.

Schmid, C., Boebel, O., Zenk, W., Lutjeharms, J.R.E., Garzoli, S.L., Richardson, P.L., Barron, C., 2003. Early evolution of an Agulhas Ring. Deep Sea Research Part II: Topical Studies in Oceanography 50, 141-166.

Schmidt, G.A., 1999. Error analysis of paleosalinity calculations. Paleoceanography 14, 422-429.

Schmidt, M.W., and Hertzberg, J.E., 2011. Abrupt Climate Change During the Last Ice Age. Nature Education Knowledge 3(10):11.

Schouten, M.W., de Ruijter, W.P.M., van Leeuwen, P.J., 2002a. Upstream control of Agulhas Ring shedding. J. Geophys. Res. 107, 3109.

Schouten, S., Hopmans, E.C., Schefuß, E., Sinninghe Damsté, J.S., 2002b. Distributional variations in marine crenarchaeotal membrane lipids: a new tool for reconstructing ancient sea water temperatures? Earth and Planetary Science Letters 204, 265-274.

Schouten, S., Huguet, C., Hopmans, E.C., Kienhuis, M.V., Damsté, J.S., 2007. Analytical methodology for TEX_{86} paleothermometry by high-performance liquid chromatography/atmospheric pressure chemical ionization-mass spectrometry. Analytical chemistry 79, 2940-2944.

Schouten, S., Ossebaar, J., Schreiber, K., Kienhuis, M.V.M., Langer, G., Benthien, A., Bijma, J., 2006. The effect of temperature, salinity and growth rate on the stable hydrogen isotopic composition of long chain alkenones produced by *Emiliania huxleyi* and *Gephyrocapsa oceanica*. Biogeosciences 3, 113-119.

Schrag, D.P., Adkins, J.F., McIntyre, K., Alexander, J.L., Hodell, D.A., Charles, C.D., McManus, J.F., 2002. The oxygen isotopic composition of seawater during the Last Glacial Maximum. Quaternary Science Reviews 21, 331-342.

Schulz, M., Mudelsee, M., 2002. REDFIT: estimating red-noise spectra directly from unevenly spaced paleoclimatic time series. Computers & Geosciences 28, 421-426.

Schulz, M., Stattegger, K., 1997. Spectrum: spectral analysis of unevenly spaced paleoclimatic time series. Computers & Geosciences 23, 929-945.

Scussolini, P., Peeters, F.J.C., 2013. A record of the last 460 thousand years of upper ocean stratification from the central Walvis Ridge, South Atlantic. Paleoceanography 28, 426-439.

Scussolini, P., van Sebille, E., Durgadoo, J.V., 2013. Paleo Agulhas rings enter the subtropical gyre during the penultimate deglaciation. Clim. Past 9, 2631-2639.

Seager, R.a., Battisti, D.S., 2007. "Challenges to our understanding of the general circulation: Abrupt climate change," in The Global Circulation of the Atmosphere: Phenomena, Theory, Challenges, eds. T. Schneider & A. S. Sobel (Princeton, NJ: Princeton University Press. 331-371.

Shackleton, N., 1967. Oxygen Isotope Analyses and Pleistocene Temperatures Re-assessed. Nature 215, 15-17.

Shackleton, N.J., Opdyke, N.D., 1976. Oxygen-Isotope and Paleomagnetic Stratigraphy of Pacific Core V28-239 Late Pliocene to Latest Pleistocene. Geological Society of America Memoirs 145, 449-464.

Shchepetkin, A.F., McWilliams, J.C., 2005. The regional oceanic modeling system (ROMS): a split-explicit, free-surface, topography-following-coordinate oceanic model. Ocean Modelling 9, 347-404.

Shin, S.-I., Liu, Z., Otto-Bliesner, B.L., Kutzbach, J.E., Vavrus, S.J., 2003. Southern Ocean sea-ice control of the glacial North Atlantic thermohaline circulation. Geophysical Research Letters 30, 1096.

Shulmeister, J., Goodwin, I., Renwick, J., Harle, K., Armand, L., McGlone, M.S., Cook, E., Dodson, J., Hesse, P.P., Mayewski, P., Curran, M., 2004. The Southern Hemisphere westerlies in the Australasian sector over the last glacial cycle: a synthesis. Quaternary International 118–119, 23-53.

Sicre, M.A., Labeyrie, L., Ezat, U., Duprat, J., Turon, J.L., Schmidt, S., Michel, E., Mazaud, A., 2005. Mid-latitude Southern Indian Ocean response to Northern Hemisphere Heinrich events. Earth and Planetary Science Letters 240, 724-731.

Siegenthaler, U., Sarmiento, J.L., 1993. Atmospheric carbon dioxide and the ocean. Nature 365, 119-125.

Sigman, D.M., Boyle, E.A., 2000. Glacial/interglacial variations in atmospheric carbon dioxide. Nature 407, 859-869.

Sime, L.C., Kohfeld, K.E., Le Quéré, C., Wolff, E.W., de Boer, A.M., Graham, R.M., Bopp, L., 2013. Southern Hemisphere westerly wind changes during the Last Glacial Maximum: model-data comparison. Quaternary Science Reviews 64, 104-120.

Singleton, A.T., Reason, C.J.C., 2007. Variability in the characteristics of cut-off low pressure systems over subtropical southern Africa. International Journal of Climatology 27, 295-310.

Skinner, L.C., Fallon, S., Waelbroeck, C., Michel, E., Barker, S., 2010. Ventilation of the Deep Southern Ocean and Deglacial CO_2 Rise. Science 328, 1147-1151.

Skinner, L.C., Waelbroeck, C., Scrivner, A.E., Fallon, S.J., 2014. Radiocarbon evidence for alternating northern and southern sources of ventilation of the deep Atlantic carbon pool during the last deglaciation. Proceedings of the National Academy of Sciences 111, 5480-5484.

Smith, R.W., Bianchi, T.S., Li, X., 2012. A re-evaluation of the use of branched GDGTs as terrestrial biomarkers: Implications for the BIT Index. Geochimica et Cosmochimica Acta 80, 14-29.

Song, Q., Gordon, A.L., Visbeck, M., 2004. Spreading of the Indonesian Throughflow in the Indian Ocean. Journal of Physical Oceanography 34, 772-792.

Speich, S., Blanke, B., Madec, G., 2001. Warm and cold water routes of an O.G.C.M. thermohaline conveyor belt. Geophysical Research Letters 28, 311-314.

Srivastava, R., Ramesh, R., Jani, R.A., Anilkumar, N., Sudhakar, M., 2010. Stable oxygen, hydrogen isotope ratios and salinity variations of the surface Southern Indian Ocean waters Current Science 99, 1395–1399.

Stager, J.C., Ryves, D.B., Chase, B.M., Pausata, F.S.R., 2011. Catastrophic Drought in the Afro-Asian Monsoon Region During Heinrich Event 1. Science 331, 1299-1302.

Steinhardt, J., et al., 2012. Seasonal planktonic foraminifera assemblage changes in the Mozambique Channel Poster presentation at AGU Chapman, Stellenbosch, Western Cape, South Africa.

Stocker, T.F., Johnsen, S.J., 2003. A minimum thermodynamic model for the bipolar seesaw. Paleoceanography 18, 1087.

Stocker, T.F., Wright, D.G., 1991. Rapid transitions of the ocean's deep circulation induced by changes in surface water fluxes. Nature 351, 729-732.

Stouffer, R.J., Yin, J., Gregory, J.M., Dixon, K.W., Spelman, M.J., Hurlin, W., Weaver, A.J., Eby, M., Flato, G.M., Hasumi, H., Hu, A., Jungclaus, J.H., Kamenkovich, I.V., Levermann, A., Montoya,

M., Murakami, S., Nawrath, S., Oka, A., Peltier, W.R., Robitaille, D.Y., Sokolov, A., Vettoretti, G., Weber, S.L., 2006. Investigating the Causes of the Response of the Thermohaline Circulation to Past and Future Climate Changes. Journal of Climate 19, 1365-1387.

Stramma, L., Lutjeharms, J.R.E., 1997. The flow field of the subtropical gyre of the South Indian Ocean. J. Geophys. Res. 102, 5513-5530.

Street, F.A., Grove, A.T., 1979. Global maps of lake -level since 30,000 yr BP. Quat. Res. 12, 83-118.

Streeter, S., S., Shackleton, N.J., 1979. Paleocirculation of the Deep North Atlantic: 150,000-Year Record of Benthic Foraminifera and Oxygen-18. Science 203, 168-171.

Stuiver, M., 1998. INTCAL 98 radiocarbon age calibration, 24,000-0 cal BP. Radiocarbon 40, 1041-1083.

Stuiver, M., Braziunas, T.F., 1993. Sun, ocean, climate and atmospheric $^{14}CO_2$: an evaluation of causal and spectral relationships. The Holocene 3, 289-305.

Sturchio, N.C., Dunkley, P.N., Smith, M., 1993. Climate-driven variations in geothermal activity in the northern Kenya rift valley. Nature 362, 233-234.

Takahashi, K., Be´ , A.W.H., 1984. Planktonic foraminifera-factors controlling sinking speeds. Deep-Sea Res A31, 1477-1500.

Talley, L.D., Reid, J.L., Robbins, P.E., 2003. Data-Based Meridional Overturning Streamfunctions for the Global Ocean. Journal of Climate 16, 3213-3226.

Thomas, D.S.G., Bailey, R., Shaw, P.A., Durcan, J.A., Singarayer, J.S., 2009. Late Quaternary highstands at Lake Chilwa, Malawi: Frequency, timing and possible forcing mechanisms in the last 44 ka. Quaternary Science Reviews 28, 526-539.

Thomas, D.S.G., Shaw, P.A., 2002. Late Quaternary environmental change in central southern Africa: new data, synthesis, issues and prospects. Quaternary Science Reviews 21, 783-797.

Thornalley, D.J.R., Elderfield, H., McCave, I.N., 2011. Reconstructing North Atlantic deglacial surface hydrography and its link to the Atlantic overturning circulation. Global and Planetary Change 79, 163-175.

Tierney, J.E., Russell, J.M., Huang, Y., Damsté, J.S.S., Hopmans, E.C., Cohen, A.S., 2008. Northern Hemisphere Controls on Tropical Southeast African Climate During the Past 60,000 Years. Science 322, 252-255.

Tiwari, M., Nagoji, S.S., Kartik, T., Drishya, G., Parvathy, R.K., Rajan, S., 2013. Oxygen isotope–salinity relationships of discrete oceanic regions from India to Antarctica vis-à-vis surface hydrological processes. Journal of Marine Systems 113–114, 88-93.

Tjallingii, R., Claussen, M., Stuut, J.-B.W., Fohlmeister, J., Jahn, A., Bickert, T., Lamy, F., Rohl, U., 2008. Coherent high- and low-latitude control of the northwest African hydrological balance. Nature Geosci 1, 670-675.

Toggweiler, J.R., 1999. Variation of atmospheric CO_2 by ventilation of the ocean's deepest water. Paleoceanography 14, 571-588.

Toggweiler, J.R., Lea, D.W., 2010. Temperature differences between the hemispheres and ice age climate variability. Paleoceanography 25, PA2212.

Torrence, C., Compo, a.G.P., 1998. A Practical Guide to Wavelet Analysis. . Bulletin American Metereological Society 79, 61-78.

Trauth, M.H., Deino, A.L., Bergner, A.G.N., Strecker, M.R., 2003. East African climate change and orbital forcing during the last 175 kyr BP. Earth and Planetary Science Letters 206, 297-313.

Trauth, M.H., Maslin, M.A., Deino, A., Strecker, M.R., 2005. Late Cenozoic Moisture History of East Africa. Science 309, 2051-2053.

Trenberth, K.E., Stepaniak, D.P., Caron, J.M., 2000. The global monsoon as seen through the divergent atmospheric circulation. Journal of Climate 13.

Tsugawa, M., Hasumi, H., 2010. Generation and Growth Mechanism of the Natal Pulse. Journal of Physical Oceanography 40, 1597-1612.

Turner, J.V., 1982. Kinetic fractionation of carbon-13 during calcium carbonate precipitation. Geochim. Cosmochim. Ac., 46, , 1183-1191.

Tyson, P.D., Preston-Whyte, R.A., 2000. The Weather and Climate of Southern Africa. Oxford University Press: Cape Town.

Urey, H., C., 1947. The thermodynamic properties of isotopic substances. J. Chem. Soc., 562-581.

Valentine, H.R., Lutjeharms, J.R.E., Brundrit, G.B., 1993. The water masses and volumetry of the southern Agulhas Current region. Deep Sea Research Part I: Oceanographic Research Papers 40, 1285-1305.

van Aken, H.M., Ridderinkhof, H., de Ruijter, W.P.M., 2004. North Atlantic deep water in the south-western Indian Ocean. Deep Sea Research Part I: Oceanographic Research Papers 51, 755-776.

van Aken, H.M., van Veldhoven, A.K., Veth, C., de Ruijter, W.P.M., van Leeuwen, P.J., Drijfhout, S.S., Whittle, C.P., Rouault, M., 2003. Observations of a young Agulhas ring, Astrid, during MARE in March 2000. Deep Sea Research Part II: Topical Studies in Oceanography 50, 167-195.

van der Meer, M.T.J., Baas, M., Rijpstra, W.I.C., Marino, G., Rohling, E.J., Sinninghe Damsté, J.S., Schouten, S., 2007. Hydrogen isotopic compositions of long-chain alkenones record freshwater flooding of the Eastern Mediterranean at the onset of sapropel deposition. Earth and Planetary Science Letters 262, 594-600.

van der Meer, M.T.J., Benthien, A., Bijma, J., Schouten, S., Sinninghe Damsté, J.S., 2013. Alkenone distribution impacts the hydrogen isotopic composition of the C37:2 and C37:3 alkan-2-ones in Emiliania huxleyi. Geochimica et Cosmochimica Acta 111, 162-166.

van der Meer, M.T.J., Sangiorgi, F., Baas, M., Brinkhuis, H., Sinninghe Damsté, J.S., Schouten, S., 2008. Molecular isotopic and dinoflagellate evidence for Late Holocene freshening of the Black Sea. Earth and Planetary Science Letters 267, 426-434.

van Sebille, E., Beal, L.M., Johns, W.E., 2011. Advective Time Scales of Agulhas Leakage to the North Atlantic in Surface Drifter Observations and the 3D OFES Model. Journal of Physical Oceanography 41, 1026-1034.

van Sebille, E., Biastoch, A., van Leeuwen, P.J., de Ruijter, W.P.M., 2009. A weaker Agulhas Current leads to more Agulhas leakage. Geophysical Research Letters 36, L03601.

van Sebille, E., Johns, W.E., Beal, L.M., 2012. Does the vorticity flux from Agulhas rings control the zonal pathway of NADW across the South Atlantic? Journal of Geophysical Research: Oceans 117, C05037.

van Sebille, E., van Leeuwen, P.J., 2007. Fast Northward Energy Transfer in the Atlantic due to Agulhas Rings. Journal of Physical Oceanography 37, 2305-2315.

van Sebille, E., van Leeuwen, P.J., Biastoch, A., de Ruijter, W.P.M., 2010. On the fast decay of Agulhas rings. Journal of Geophysical Research: Oceans 115, C03010.

Vogel, J.C., Fuls, A., Ellis, R.P., 1978. The geographical distribution of Kranz grasses in South Africa. South African Journal of Science 74, 209-215.

Waelbroeck, C., Labeyrie, L., Michel, E., Duplessy, J.C., McManus, J.F., Lambeck, K., Balbon, E., Labracherie, M., 2002. Sea-level and deep water temperature changes derived from benthic foraminifera isotopic records. Quaternary Science Reviews 21, 295-305.

Waelbroeck, C., Paul, A., Kucera, M., Rosell-Melé, A., Weinelt, M., Schneider, R., Mix, A.C., Abelmann, A., Armand, L., Bard, E., Barker, S., Barrows, T.T., Benway, H., Cacho, I., Chen, M.T., Cortijo, E., Crosta, X., Vernal, A.d., Dokken, T., Duprat, J., Elderfield, H., Eynaud, F., Gersonde, R., Hayes, A., Henry, M., Hillaire-Marcel, C., Huang, C.C., Jansen, E., Juggins, S., Kallel, N., Kiefer, T., Kienast, M., Labeyrie, L., Leclaire, H., Londeix, L., Mangin, S., Matthiessen, J., Marret, F., Meland, M., Morey, A.E., Mulitza, S., Pflaumann, U., Pisias, N.G., Radi, T., Rochon, A., Rohling, E.J., Sbaffi, L., Schäfer-Neth, C., Solignac, S., Spero, H., Tachikawa, K., Turon, J.L., Waelbroeck, C., Paul, A., Kucera, M., Rosell-Melé, A., Weinelt, M., Schneider, R., Mix, A.C., Abelmann, A., Armand, L., Bard, E., Barker, S., Barrows, T.T., Benway, H., Cacho, I., Chen, M.T., Cortijo, E., Crosta, X., Vernal, A.d., Dokken, T., Duprat, J., Elderfield, H., Eynaud, F., Gersonde, R., Hayes, A., Henry, M., Hillaire-Marcel, C., Huang, C.C., Jansen, E., Juggins, S., Kallel, N., Kiefer, T., Kienast, M., Labeyrie, L., Leclaire, H., Londeix, L., Mangin, S., Matthiessen, J., Marret, F., Meland, M., Morey, A.E., Mulitza, S., Pflaumann, U., Pisias, N.G., Radi, T., Rochon, A., Rohling, E.J., Sbaffi, L., Schäfer-Neth, C., Solignac, S., Spero, H., Tachikawa, K., Turon, J.L., 2009. Constraints on the magnitude and patterns of ocean cooling at the Last Glacial Maximum. Nature Geoscience 2, 127-132.

Waelbroeck, C., Skinner, L.C., Labeyrie, L., Duplessy, J.C., Michel, E., Vazquez Riveiros, N., Gherardi, J.M., Dewilde, F., 2011. The timing of deglacial circulation changes in the Atlantic. Paleoceanography 26, PA3213.

Walker, N.D., Mey, R.D., 1988. Ocean/Atmosphere heat fluxes within the Agulhas Retroflection Region. J. Geophys. Res. 93, 15473-15483.

Walsh, J.E., 2013. Melting ice: What is happening to Arctic sea ice, and what does it mean for us? . Oceanography 26, 171-181.

Wang, B., and Ding , Q., 2008. The global monsoon: Major modes of annual variations in the tropics. Dynamics of Atmos. and Ocean, Special Issue 2.

Wang, B., Ding, Q., 2006. Changes in global monsoon precipitation over the past 56 years. Geophysical Research Letters 33, L06711.

Wang, L., 2000. Isotopic signals in two morphotypes of Globigerinoides ruber (white) from the South China Sea: implications for monsoon climate change during the last glacial cycle. Palaeogeography, Palaeoclimatology, Palaeoecology 161, 381-394.

Wang, P., 2009. Global monsoon in a geological perspective. Chinese Science Bulletin 54, 1113-1136.

Wang, X., Auler, A.S., Edwards, R.L., Cheng, H., Cristalli, P.S., Smart, P.L., Richards, D.A., Shen, C.-C., 2004. Wet periods in northeastern Brazil over the past 210 kyr linked to distant climate anomalies. Nature 432, 740-743.

Wang, Y., Cheng, H., Edwards, R.L., Kong, X., Shao, X., Chen, S., Wu, J., Jiang, X., Wang, X., An, Z., 2008. Millennial- and orbital-scale changes in the East Asian monsoon over the past 224,000 years. Nature 451, 1090-1093.

Wang, Y.J., Cheng, H., Edwards, R.L., An, Z.S., Wu, J.Y., Shen, C.C., Dorale, J.A., 2001. A High-Resolution Absolute-Dated Late Pleistocene Monsoon Record from Hulu Cave, China. Science 294, 2345-2348.

Weedon, G.P., 2003. Time-series analysis and cyclostratigraphy: examining stratigraphic records of environmental cycles. Cambridge University Press.

Wei, W., Lohmann, G., Dima, M., 2012. Distinct Modes of Internal Variability in the Global Meridional Overturning Circulation Associated with the Southern Hemisphere Westerly Winds. Journal of Physical Oceanography 42, 785-801.

Weijer, W., De Ruijter, W.P.M., Sterl, A., Drijfhout, S.S., 2002. Response of the Atlantic overturning circulation to South Atlantic sources of buoyancy. Global and Planetary Change 34, 293-311.

Weijer, W., van Sebille, E., 2013. Impact of Agulhas Leakage on the Atlantic overturning circulation in the CCSM4. Journal of Climate 27, 101-110.

Weijers, J.W.H., Schefuß, E., Schouten, S., Damsté, J.S.S., 2007a. Coupled Thermal and Hydrological Evolution of Tropical Africa over the Last Deglaciation. Science 315, 1701-1704.

Weijers, J.W.H., Schouten, S., Hopmans, E.C., Geenevasen, J.A.J., David, O.R.P., Coleman, J.M., Pancost, R.D., Sinninghe Damsté, J.S., 2006. Membrane lipids of mesophilic anaerobic bacteria thriving in peats have typical archaeal traits. Environmental Microbiology 8, 648-657.

Weijers, J.W.H., Schouten, S., van den Donker, J.C., Hopmans, E.C., Sinninghe Damsté, J.S., 2007b. Environmental controls on bacterial tetraether membrane lipid distribution in soils. Geochimica et Cosmochimica Acta 71, 703-713.

Weldeab, S., 2012. Bipolar modulation of millennial-scale West African monsoon variability during the last glacial (75,000–25,000 years ago). Quaternary Science Reviews 40, 21-29.

Weldeab, S., Lea, D.W., Schneider, R.R., Andersen, N., 2007. 155,000 Years of West African Monsoon and Ocean Thermal Evolution. Science 316, 1303-1307.

Weldon, D., Reason, C.J.C., 2014. Variability of rainfall characteristics over the South Coast region of South Africa. Theor Appl Climatol 115, 177-185.

Weltje, G.J., Tjallingii, R., 2008. Calibration of XRF core scanners for quantitative geochemical logging of sediment cores: Theory and application. Earth and Planetary Science Letters 274, 423-438.

White, F., 1983. The vegetation of Africa, Natural Rescourses Research. UNESCO, Paris, 20.

Whitfield, A.K., Harrison, T.D., 2003. River flow and fish abundance in a South African estuary. Journal of Fish Biology 62, 1467-1472.

Wolff, E.W., Fischer, H., Fundel, F., Ruth, U., Twarloh, B., Littot, G.C., Mulvaney, R., Röthlisberger, R., de Angelis, M., Boutron, C.F., Hansson, M., Jonsell, U., Hutterli, M.A., Lambert, F., Kaufmann, P., Stauffer, B., Stocker, T.F., Steffensen, J.P., Bigler, M., Siggaard-Andersen, M.L., Udisti, R., Becagli, S., Castellano, E., Severi, M., Wagenbach, D., Barbante, C., Gabrielli, P., Gaspari, V., 2006. Southern Ocean sea-ice extent, productivity and iron flux over the past eight glacial cycles. Nature 440, 491-496.

Wuchter, C., Schouten, S., Wakeham, S.G., Sinninghe Damsté, J.S., 2006. Archaeal tetraether membrane lipid fluxes in the northeastern Pacific and the Arabian Sea: Implications for TEX_{86} paleothermometry. Paleoceanography 21, PA4208.

Wyrtki, K., 1971. Oceanographic Atlas of the International Indian Ocean Expedition. National Science Foundation, Washington,DC, 531 pp.

Wyrwoll, K.-H., Dong, B., Valdes, P., 2000. On the position of southern hemisphere westerlies at the Last Glacial Maximum: an outline of AGCM simulation results and evaluation of their implications. Quaternary Science Reviews 19, 881-898.

Xie, R.C., Marcantonio, F., Schmidt, M.W., 2012. Deglacial variability of Antarctic Intermediate Water penetration into the North Atlantic from authigenic neodymium isotope ratios. Paleoceanography 27, PA3221.

Yarincik, K.M., Murray, R.W., Peterson, L.C., 2000. Climatically sensitive eolian and hemipelagic deposition in the Cariaco Basin, Venezuela, over the past 578,000 years: Results from Al/Ti and K/Al. Paleoceanography 15, 210-228.

Yu, E.-F., Francois, R., Bacon, M.P., 1996. Similar rates of modern and last-glacial ocean thermohaline circulation inferred from radiochemical data. Nature 379, 689-694.

Yu, J., Elderfield, H., 2007. Benthic foraminiferal B/Ca ratios reflect deep water carbonate saturation state. Earth and Planetary Science Letters 258, 73-86.

Zabel, M., Schneider, R.R., Wagner, T., Adegbie, A.T., de Vries, U., Kolonic, S., 2001. Late Quaternary Climate Changes in Central Africa as Inferred from Terrigenous Input to the Niger Fan. Quaternary Research 56, 207-217.

Zahn, R., 2009. Climate change: Beyond the CO_2 connection. Nature 460, 335-336.

Zahn, R., Stüber, A., 2002. Suborbital intermediate water variability inferred from paired benthic foraminiferal Cd/Ca and $\delta^{13}C$ in the tropical West Atlantic and linking with North Atlantic climates. Earth and Planetary Science Letters 200, 191-205.

Zahn, R., Winn, K., Sarnthein, M., 1986. Benthic foraminiferal $\delta^{13}C$ and accumulation rates of organic carbon: *Uvigerina Peregrina* group and *Cibicidoides Wuellerstorfi*. Paleoceanography 1, 27-42.

Zarriess, M., Mackensen, A., 2011. Testing the impact of seasonal phytodetritus deposition on $\delta^{13}C$ of epibenthic foraminifer *Cibicidoides wuellerstorfi:* A 31,000 year high-resolution record from the northwest African continental slope. Paleoceanography 26, PA2202.

Zell, C., Kim, J.-H., Abril, G., Sobrinho, R., Dorhout, D., Moreira-Turcq, P., Sinninghe Damsté, J., 2013. Impact of seasonal hydrological variation on the distributions of tetraether lipids along the Amazon River in the central Amazon basin: Implications for the MBT/CBT paleothermometer and the BIT index. Frontiers in Microbiology 4.

Zhang, X., Lohmann, G., Knorr, G., Purcell, C., 2014. Abrupt glacial climate shifts controlled by ice sheet changes. Nature 512, 290-294.

Zhang, X., Lohmann, G., Knorr, G., Xu, X., 2013. Different ocean states and transient characteristics in Last Glacial Maximum simulations and implications for deglaciation. Clim. Past 9, 2319-2333.

Zhou, J., Lau, K.M., 1998. Does a Monsoon Climate Exist over South America? Journal of Climate 11, 1020-1040.

Ziegler, M., Diz, P., Hall, I.R., Zahn, R., 2013a. Millennial-scale changes in atmospheric CO_2 levels linked to the Southern Ocean carbon isotope gradient and dust flux. Nature Geosci 6, 457-461.

Ziegler, M., Simon, M.H., Hall, I.R., Barker, S., Stringer, C., Zahn, R., 2013b. Development of Middle Stone Age innovation linked to rapid climate change. Nat Commun 4, 1905.

Ziegler, M., Tuenter, E., Lourens, L.J., 2010. The precession phase of the boreal summer monsoon as viewed from the eastern Mediterranean (ODP Site 968). Quaternary Science Reviews 29, 1481-1490.

Zinke, J., Loveday, B.R., Reason, C.J.C., Dullo, W.C., Kroon, D., 2014. Madagascar corals track sea surface temperature variability in the Agulhas Current core region over the past 334 years. Sci. Rep. 4.

Zonneveld, K.A.F., Ganssen, G., Troelstra, S., Versteegh, G.J.M., Visscher, H., 1997. Mechanisms forcing abrupt fluctuations of the indian ocean summer monsoon during the last deglaciation. Quaternary Science Reviews 16, 187-201.